

1982

# The Effects Of Deafferentiation Of The Cerebellar Cortex In The Rat

William Athen Anderson

Follow this and additional works at: <https://ir.lib.uwo.ca/digitizedtheses>

---

## Recommended Citation

Anderson, William Athen, "The Effects Of Deafferentiation Of The Cerebellar Cortex In The Rat" (1982). *Digitized Theses*. 2733.  
<https://ir.lib.uwo.ca/digitizedtheses/2733>

This Dissertation is brought to you for free and open access by the Digitized Special Collections at Scholarship@Western. It has been accepted for inclusion in Digitized Theses by an authorized administrator of Scholarship@Western. For more information, please contact [tadam@uwo.ca](mailto:tadam@uwo.ca), [wlsadmin@uwo.ca](mailto:wlsadmin@uwo.ca).

The author of this thesis has granted The University of Western Ontario a non-exclusive license to reproduce and distribute copies of this thesis to users of Western Libraries. Copyright remains with the author.

Electronic theses and dissertations available in The University of Western Ontario's institutional repository (Scholarship@Western) are solely for the purpose of private study and research. They may not be copied or reproduced, except as permitted by copyright laws, without written authority of the copyright owner. Any commercial use or publication is strictly prohibited.

The original copyright license attesting to these terms and signed by the author of this thesis may be found in the original print version of the thesis, held by Western Libraries.

The thesis approval page signed by the examining committee may also be found in the original print version of the thesis held in Western Libraries.

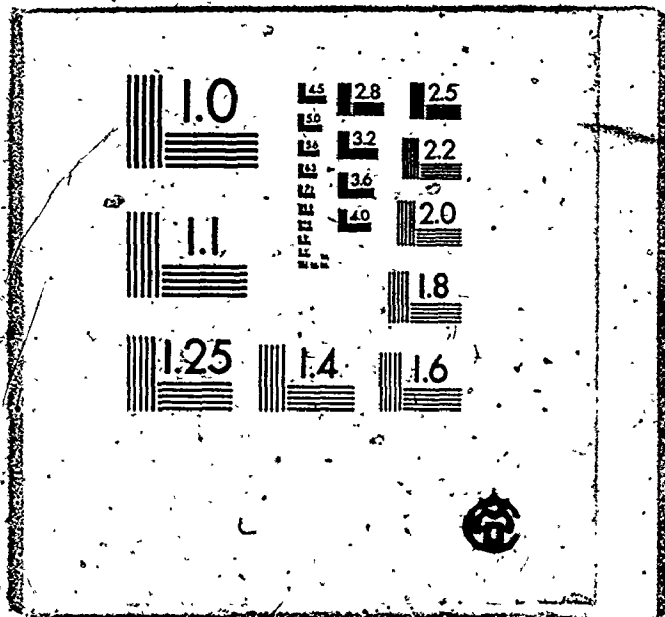
Please contact Western Libraries for further information:

E-mail: [libadmin@uwo.ca](mailto:libadmin@uwo.ca)

Telephone: (519) 661-2111 Ext. 84796

Web site: <http://www.lib.uwo.ca/>

# 1



## NOTICE

The quality of this microfiche is heavily dependent upon the quality of the original thesis submitted for microfilming. Every effort has been made to ensure the highest quality of reproduction possible.

If pages are missing, contact the university which granted the degree.

Some pages may have indistinct print especially if the original pages were typed with a poor typewriter ribbon or if the university sent us a poor photocopy.

Previously copyrighted materials (journal articles, published tests, etc.) are not filmed.

Reproduction in full or in part of this film is governed by the Canadian Copyright Act, R.S.C. 1970, c. C-30. Please read the authorization forms which accompany this thesis.

**THIS DISSERTATION  
HAS BEEN MICROFILMED  
EXACTLY AS RECEIVED**

## AVIS

La qualité de cette microfiche dépend grandement de la qualité de la thèse soumise au microfilmage. Nous avons tout fait pour assurer une qualité supérieure de reproduction.

S'il manque des pages, veuillez communiquer avec l'université qui a conféré le grade.

La qualité d'impression de certaines pages peut laisser à désirer, surtout si les pages originales ont été dactylographiées à l'aide d'un ruban usé ou si l'université nous a fait parvenir une photocopie de mauvaise qualité.

Les documents qui font déjà l'objet d'un droit d'auteur (articles de revue, examens publiés, etc.) ne sont pas microfilmés.

La reproduction, même partielle, de ce microfilm est soumise à la Loi canadienne sur le droit d'auteur, SRC 1970, c. C-30. Veuillez prendre connaissance des formules d'autorisation qui accompagnent cette thèse.

**LA THÈSE A ÉTÉ  
MICROFILMÉE TELLE QUE  
NOUS L'AVONS REÇUE**

THE EFFECTS OF DEAFFERENTATION OF  
THE CEREBELLAR CORTEX IN THE RAT

VOLUME I

by  
William Athen. Anderson

Department of Anatomy

Submitted in partial fulfillment  
of the requirements for the degree of  
Doctor of Philosophy

Faculty of Graduate Studies  
The University of Western Ontario  
London, Ontario  
December, 1981

© William Athen Anderson 1981.

DEDICATION

This thesis is dedicated to my parents, Nora and John,  
my son, Athen and especially to my wife, Edith.

## ABSTRACT

The trilaminar structure of the cerebellar cortex provides a unique opportunity to investigate the effects of (specific) deafferentation in the central nervous system. Its inner and outer layers possess different extrinsic afferent connections which can be readily distinguished by their physiological and ultrastructural characteristics. It was therefore undertaken in the present study to investigate the effects of selective deafferentation (climbing fibers, mossy fibers and parallel fibers) of both the weanling and the adult cerebellar cortex with a view to determining the remodeling capabilities of the mature cerebellum.

Using the horseradish peroxidase technique (HRP), an area of the cerebellar cortex was identified which receives the majority of its mossy fibers from one center. Retrograde labeling showed that the ansiform lobule receives a massive mossy fiber input from the basilar pontine gray and a substantial climbing fiber projection from the principal nucleus of the inferior olive.

The climbing fiber input to the ansiform lobule was eliminated using both electrolytic (dorsal and ventral parapharyngeal approaches) and chemical (3-acetylpyridine) lesions. The effects of 3-acetylpyridine (3AP) intoxication on the inferior olivary complex and cerebellar cortex of weanling and adult rats were examined at both the light and electron microscopic level. Following the intraperitoneal injection of 65 mg of 3AP per kg body weight, the inferior olivary

neurons of the adult rat underwent a rapid form of electron-dense degeneration. A complete bilateral involvement of the nuclear complex was well advanced by 12 hours following injection. By the end of the second week, all cytoplasmic and nuclear debris was removed. Concurrently, degenerative changes were evident in the cerebellar cortex from 12 hours onwards. All climbing fiber varicosities were observed to be degenerative as early as 24 hours following treatment. Electron microscopic observations revealed that these electron-dense fragments were largely phagocytized and cleared by Bergmann glial cells by 7 days. A similar time course for climbing fiber degeneration was found following electrolytic ablation of the adult inferior olivary complex.

An investigation of the effects of 3AP on the inferior olivary complex of the weanling rat revealed that it possesses a much higher tolerance to 3AP than the adult. Injections containing 90 mg per kg body weight of 3AP were necessary to produce a total bilateral olivary ablation in the weanling rat.

In contrast to the more conventionally used electrolytic methods 3AP causes a complete bilateral ablation of all olivary neurons while avoiding the problems inherent to electrolytic procedures, such as incomplete destruction of the nucleus and involvement of fibers of passage. A total loss of the climbing fiber input to the ansiform lobule was found following 3AP treatment and it suggests that the inferior olive is the sole source of the climbing fiber input.

Electrolytic lesions placed in the basilar pontine gray resulted in the degeneration of nearly the entire population of mossy



fiber rosettes within the ansiform lobule. The degenerating rosettes represented two distinct populations with respect to their time course of degeneration. The majority of them (simple and complex dispersed terminals) underwent a slow course of electron-dense degeneration. As a result, most glomeruli contained debris from degenerating mossy fiber varicosities during the first 57 days. A second, small population of mossy fiber rosettes of the simple clustered variety underwent a rapid course of electron-dense degeneration (by the 5th day). Since many of the electrolytic lesions of the basilar pontine gray also included the nucleus reticularis tegmenti pontis, this center may be the source of the simple clustered variety of mossy fiber rosette. All glomeruli were denervated by 80 days following pontine lesions. Morphological evidence is provided which suggests that the mossy fiber varicosities play an active role in the removal of the granule cell digitiform dendrite.

Parallel fiber-deafferentation of the ansiform lobule was accomplished using superficial parasagittal cuts in the lateral cerebellar hemisphere. A short-term (3-4.5 days) electron microscopic examination confirmed that the only neuronal elements affected following cerebellar cuts (medial to the lesion) were the axons of the granule cells, the parallel fibers. These axons and their terminals underwent a rapid course of electron-dense degeneration and their debris was cleared by the 5th day. Evidence is provided which suggests that Bergmann glial cells play an active role in the phagocytic removal of parallel fibers and Purkinje cell dendritic spines.

The possibility of synaptic remodeling in the cerebellar

cortex following deafferentation of both the weanling and the adult rat was investigated over a period of time ranging from 12 hours to 380 days following surgery. In the short-term cases (12 hours to 12 days) the sequence and time course of changes was examined during the degeneration of the various fiber types and the distribution and synaptic localization of the degenerating terminals was determined. At a later stage (three months onward), after adequate time had passed for removal of the degenerative debris and remodeling to take place, a second lesion or an injection of tritiated leucine was made in an intact afferent system to investigate the possibility of synaptic reorganization of either the climbing or the mossy fiber systems. Short-term (24-48 hours) observations were made and compared to those obtained with animals processed following only a single lesion. Although several experimental methods were employed, including silver impregnation, autoradiography and electron microscopy, no evidence was found to suggest sprouting of either the climbing or the mossy fibers. The synaptic specificity of the cerebellar cortex is therefore maintained following mossy or climbing fiber-deafferentation.

Evidence is provided, however, which suggests that basket axons, and in particular, the parallel fiber system possess some capabilities for sprouting following climbing or parallel fiber-deafferentation. An ectopic formation of dendritic spines occurred following climbing fiber-deafferentation of the weanling rat, but not the adult. Ultrastructural examination revealed, furthermore, that these ectopic spines were synaptically innervated by either the parallel fiber system or basket axons.

Although a loss of dendritic spines occurred along the terminal branchlets following mossy or parallel fiber-deafferentation, many of the existing spines underwent marked changes in form. Morphological evidence is provided which suggests that denervated Purkinje cell dendritic spines elongate to acquire a new synaptic input.

While the cerebellar cortex of the weanling or adult rat possesses some potential for synaptic reorganization, the primary response to deafferentation was transneuronal degeneration. Image analysis of the Golgi impregnated Purkinje cell indicated significant losses in both smooth branch and spiny branchlet numbers following the loss of climbing fibers, mossy fibers or parallel fibers. The loss of smooth branches and spiny branchlets which occurred following climbing fiber-deafferentation of the weanling rat was due to a reduction in postnatal branching, rather than transneuronal degeneration. Ultrastructural evidence for transneuronal degeneration which supports the quantitative findings is provided. In addition, transneuronal degenerative changes are reported in the population of molecular layer interneurons following climbing fiber-deafferentation of both weanling and adult rats. These changes are evidence for a direct climbing fiber input to these cells. Degeneration of the molecular layer interneurons following mossy fiber-deafferentation, on the other hand, is secondary to the transneuronal loss of the granule cell system.

## ACKNOWLEDGEMENTS

I am pleased to acknowledge with sincere appreciation the assistance provided me by several individuals during the preparation of this thesis. The author is deeply indebted to Dr. A.W. Hrycyshyn for his patience, understanding and helpful criticisms during the course of this study. I would also especially like to thank Mrs. Judy Sholdice for her invaluable technical assistance and editorial suggestions.

My appreciation is also extended to Miss Olive Donaldson and Mrs. Linda Manning for their typing of this thesis.

I am especially indebted to Dr. B.A. Flumerfelt for his direction and supervision which he provided during the course of this study. I offer him my appreciation and gratitude. I would also like to thank Dr. J.A. Kiernan and Dr. A.H. Martin who served as members of my supervisory committee.

Finally, I would like to express my sincerest appreciation to my wife, Edith, who has sacrificed in countless ways during the course of this degree. For her support and encouragement, I will always be grateful. I only hope a time will come when I can serve her as loyally.

This research was supported by a grant to Dr. B.A. Flumerfelt from the Medical Research Council of Canada. The author wishes to express his appreciation to this organization for their support.

# TABLE OF CONTENTS

	Page
CERTIFICATE OF EXAMINATION . . . . .	ii
DEDICATION . . . . .	iii
ABSTRACT . . . . .	iv
ACKNOWLEDGEMENTS . . . . .	ix
TABLE OF CONTENTS . . . . .	x
LIST OF FIGURES . . . . .	xvii
LIST OF TABLES . . . . .	xxiv
LIST OF APPENDICES . . . . .	xxvi
CHAPTER 1 - INTRODUCTION . . . . .	1
CHAPTER 2 - HISTORICAL REVIEW . . . . .	7
2.1 The Cerebellar Cortex . . . . .	7
A. Normal Cytoarchitecture . . . . .	7
1. Cerebellar Afferents . . . . .	10
a) Climbing Fiber Origin . . . . .	10
(1) Olivocerebellar . . . . .	12
b) Mossy Fiber Origin . . . . .	14
(1) Ceruleocerebellar . . . . .	15
(2) Pontocerebellar . . . . .	15
(3) Reticulocerebellar . . . . .	17
(4) Spinocerebellar . . . . .	18
(a) Dorsal and Ventral Tracts . . . . .	18
(b) Rostral and Cuneocerebellar Tracts . . . . .	19
(5) Trigemino-cerebellar . . . . .	20
(6) Vestibulocerebellar . . . . .	21
(a) Primary Afferents . . . . .	21
(b) Secondary Afferents . . . . .	21
2.2 3-Acetylpyridine: A Neurotoxin . . . . .	22
2.3 Evidence for Transneuronal Degeneration . . . . .	24
A. The Central Nervous System . . . . .	24
1. Somal Alterations . . . . .	25
2. Immature Systems . . . . .	27
3. Species Variations . . . . .	28
4. Dendritic Alterations . . . . .	29
5. Secondary and Tertiary Atrophy . . . . .	32

	Page
2.4 Abnormal Cerebellar Development . . . . .	33
A. Parallel Fiber Removal . . . . .	35
1. The Effect on Purkinje Cell Development . . . . .	35
a) Dendritic Spines . . . . .	38
B. Climbing Fiber Removal . . . . .	39
1. The Effect on Purkinje Cell Development and Maintenance . . . . .	39
a) Dendritic Spines . . . . .	40
C. Mossy Fiber Removal . . . . .	42
1. The Effect on Granule Cell Dendrites . . . . .	42
2.5 Synaptic Remodeling within the Central Nervous System . . . . .	42
2.6 Heterologous Synaptogenesis within the Cerebellar Cortex . . . . .	51
CHAPTER 3 - MATERIALS AND METHODS . . . . .	55
3.1 Perfusion Apparatus and Technique . . . . .	55
3.2 Operative Procedures . . . . .	56
A. Inferior Olivary Nucleus . . . . .	56
1. 3-Acetylpyridine . . . . .	56
2. Electrolytic Lesions and Injections . . . . .	57
a) Ventral Approach . . . . .	57
b) Dorsal Approach . . . . .	60
B. Pontine Nucleus . . . . .	61
C. Lateral Cerebellar Hemisphere . . . . .	62
1. Parasagittal Cuts . . . . .	62
2. Horseradish Peroxidase (HRP) Injections . . . . .	63
3.3 Light Microscopic Methods . . . . .	64
A. Preparation of Tissue for Normal Cytoarchitecture . . . . .	64
1. Horseradish Peroxidase Technique . . . . .	65
2. Golgi-Cox Technique . . . . .	68
a) Analysis of Golgi-stained cells . . . . .	68
b) Quantitative Analysis . . . . .	70
3. Modified Fink-Heimer and De Olmos-Ingram Technique . . . . .	71
4. Autoradiographic Technique . . . . .	72
5. Photographic Procedures . . . . .	73

	Page
3.4 Preparation of Tissue for Electron Microscopy . . . . .	73
A. Perfusion . . . . .	73
B. Tissue Dissection . . . . .	74
C. Processing and Embedding . . . . .	75
D. Quantitative Analysis . . . . .	75
CHAPTER 4 - RESULTS . . . . .	77
4.1 Horseradish Peroxidase Injections within the Lateral Cerebellar Hemisphere . . . . .	77
A. Cerebellar Afferents . . . . .	78
1. Pontocerebellar . . . . .	78
2. Olivocerebellar . . . . .	80
3. Reticulocerebellar . . . . .	82
4. Trigemino-cerebellar . . . . .	83
5. Vestibulocerebellar . . . . .	85
6. Ceruleocerebellar . . . . .	87
7. Cuneocerebellar . . . . .	87
8. Spinocerebellar . . . . .	87
9. Reticular Formation (gigantocellularis) . . . . .	88
4.2 The Inferior Olivary Complex . . . . .	88
A. Electrolytic Ablation . . . . .	88
1. Lesion Site within the Adult . . . . .	88
B. 3-Acetylpyridine (3AP) Intoxication . . . . .	89
1. Lesion Site within the Adult . . . . .	90
a) Short- and Long-Term Changes Following 3AP Treatment . . . . .	90
2. Lesion Site within the Weanling . . . . .	95
a) Short- and Long-Term Changes Following 3AP Treatment . . . . .	95
4.3 The Ansiform Lobule of the Cerebellum . . . . .	97
A. Electrolytically or Chemically Lesioned (3AP) Adult Rats . . . . .	97
1. Short-Term Changes Following Climbing Fiber-Deafferentation . . . . .	98
4.4 Synaptic Remodeling within the Deafferentated Adult or Weanling Cerebellar Cortex . . . . .	100

	Page
4.5 The Ansiform Lobule of the Cerebellum . . . . .	104
A. Chemically Lesioned (3AP) Adult Rats . . . . .	104
1. Long-Term Changes Following Olivocerebellar- Deafferentation . . . . .	107
a) Golgi-Cox Technique . . . . .	107
(1) The Purkinje Cell Dendritic Tree . . . . .	107
(2) Spine Morphology and Distribution . . . . .	108
b) Electron Microscopy . . . . .	109
(1) Transneuronal Degeneration . . . . .	109
B. Chemically Lesioned (3AP) Weanling Rats . . . . .	112
1. Long-Term Changes Following Olivocerebellar- Deafferentation . . . . .	113
a) Golgi-Cox Technique . . . . .	113
(1) The Purkinje Cell Dendritic Tree . . . . .	113
(2) Spine Morphology and Distribution . . . . .	114
b) Electron Microscopy . . . . .	115
(1) Transneuronal Degeneration . . . . .	115
(2) Ectopic Spine Formation . . . . .	115
(3) Heterotypical Reinnervation . . . . .	116
C. Chemically Lesioned (3AP) Weanling and Adult Rats . . . . .	118
1. Long-Term Changes Following Olivocerebellar- Deafferentation . . . . .	119
a) Transneuronal Changes within Cerebellar Interneurons . . . . .	119
4.6 Lesion Site within the Adult Basilar Pontine Gray . . . . .	121
4.7 The Ansiform Lobule of the Cerebellum . . . . .	121
A. Short-Term Changes Following Pontine Ablation . . . . .	121
1. Electron Microscopy . . . . .	121
a) The Mossy Fiber Glomerulus . . . . .	121
b) The Granule Cell Dendrite . . . . .	128
B. Long-Term Changes Following Pontine Ablation . . . . .	129
1. Golgi-Cox Material . . . . .	129
a) The Purkinje Cell Dendritic Tree . . . . .	129
b) Spine Morphology and Distribution . . . . .	130



	Page
2. Electron Microscopy . . . . .	130
a) The Mossy Fiber Glomerulus . . . . .	130
b) The Granule Cell Dendrite . . . . .	134
c) The Granule Cell Soma . . . . .	135
d) The Granule Cell Axon . . . . .	137
e) The Purkinje Cell Dendritic Tree . . . . .	139
f) The Dendritic Arborization of the Cerebellar Interneuron . . . . .	141
4.8 Lesion Site within the Adult or Weanling Lateral Cerebellar Hemisphere . . . . .	142
4.9 The Ansiform Lobule of the Cerebellum . . . . .	143
A. Short-Term Changes Following Parallel Fiber- Deafferentation of the Adult or Weanling Rat . . . . .	143
B. Long-Term Changes Following Parallel Fiber- Deafferentation of the Adult Rat . . . . .	145
1. Golgi-Cox Material . . . . .	145
a) The Purkinje Cell Dendritic Tree . . . . .	145
b) Spine Morphology and Distribution . . . . .	146
C. Long-Term Changes Following Parallel Fiber- Deafferentation of the Weanling Rat . . . . .	147
1. Golgi-Cox Material . . . . .	147
a) The Purkinje Cell Dendritic Tree . . . . .	147
b) Spine Morphology and Distribution . . . . .	148
D. Long-Term Changes Following Parallel Fiber- Deafferentation of the Adult and/or Weanling Rat . . . . .	149
1. Electron Microscopy . . . . .	149
a) Transneuronal Degeneration . . . . .	149
(1) The Granule Cell Layer . . . . .	149
(2) The Purkinje Cell Dendritic Tree . . . . .	150
(3) The Stellate Cell . . . . .	152
b) Spine Morphology and Distribution . . . . .	153
E. Comparisons Between Experimental Groups Following Long-Term Climbing, Mossy or Parallel Fiber-Deafferentation of the Adult or Weanling Rat . . . . .	154

	Page
1. The Purkinje Cell Dendritic Tree . . . . .	154
a) Climbing Fiber Loss in the Adult Versus the Weanling . . . . .	154
b) Parallel Fiber Loss Versus Climbing Fiber Loss . . . . .	155
c) Parallel Fiber Removal Versus Mossy Fiber Removal . . . . .	156
d) Parallel Fiber Deafferentation in the Adult Versus the Weanling . . . . .	157
 CHAPTER 5 - "DISCUSSION" . . . . .	 158
5.1 The Topography of the Afferents to the Lateral Cerebellar Hemisphere . . . . .	158
5.2 3-Acetylpyridine: A Neurotoxin Specific for the Climbing Fiber Projection . . . . .	160
5.3 The Origin of Climbing Fiber Afferents . . . . .	167
5.4 Do Climbing Fiber Glomerular Collaterals Exist? . . . . .	169
5.5 Recurrent Climbing Fiber Collaterals to the Inferior Olive . . . . .	172
5.6 Regional Sparring Following 3-Acetylpyridine Intoxication . . . . .	174
5.7 Climbing Fiber Suppression of Spine Growth . . . . .	177
5.8 Purkinje Cell Growth Beyond the 21st Postnatal Day . . . . .	179
5.9 Characterization of Pontocerebellar Rosettes . . . . .	181
5.10 Deafferentation of the Cerebellum Following Parasagittal Cuts . . . . .	184
5.11 Transneuronal Degeneration of the Purkinje Cells and Granule Cells . . . . .	185
A. Climbing Fiber Deafferentation . . . . .	185
B. Parallel Fiber Deafferentation . . . . .	187
C. Mossy Fiber Deafferentation . . . . .	190
5.12 Hypertrophied Purkinje Cell Spines . . . . .	193
5.13 Transneuronal Degeneration of the Molecular Layer Interneurons . . . . .	195
A. Climbing Fiber Deafferentation . . . . .	195
B. Parallel Fiber Deafferentation . . . . .	196

	Page
5.14 The Cerebellum: Its Potential to Remodel . . . . .	198
A. Climbing Fiber Deafferentation . . . . .	198
B. Mossy Fiber Deafferentation . . . . .	200
C. Parallel Fiber Deafferentation . . . . .	201
CHAPTER 6 - PART I - SUMMARY . . . . .	203
PART II - CONCLUSIONS . . . . .	209
BIBLIOGRAPHY . . . . .	211
VITA . . . . .	260
FIGURES . . . . .	264
TABLES . . . . .	412
APPENDICES . . . . .	428

LIST OF FIGURES

Figure	Description	Page
1	Photomicrographs of an HRP injection within the lateral cerebellar hemisphere and retrogradely labeled fibers within the corpus medullaris	265
2	A diagrammatic representation of an HRP injection site within the ansiform lobule and the resulting distribution of retrogradely labeled somata within the rostral portion of the hindbrain	267
3	Typical HRP-labeled cells in the basilar pontine gray; the inferior olivary complex and the lateral reticular nucleus following cerebellar injections	269
4	A diagrammatic representation of an HRP injection site within the lobulus simplex and the resultant distribution of retrogradely labeled somata within the rostral portion of the hindbrain	271
5	A diagrammatic representation of an HRP injection site within Crus I and the medial portion of Crus II and the subsequent distribution of retrogradely labeled somata within the rostral portion of the hindbrain	273
6	A diagrammatic representation of an HRP injection site within Crus I and the lateral portion of Crus II and the resulting distribution of retrogradely labeled somata within the rostral portion of the hindbrain	275
7	A diagrammatic representation of the distribution of retrogradely labeled somata within the caudal portion of the medulla oblongata following an HRP injection of the ansiform lobule	277
8	A diagrammatic representation of the distribution of retrogradely labeled somata within the caudal portion of the medulla oblongata following an HRP injection of lobulus simplex	279
9	A diagrammatic representation of the distribution of retrogradely labeled somata within the caudal portion of the medulla oblongata following an HRP injection of Crus I and the medial portion of Crus II	281

Figure	Description	Page
10	A diagrammatic representation of the resulting distribution of retrogradely labeled somata within the caudal portion of the medulla oblongata following an HRP injection of Crus I and the lateral portion of Crus II	283
11	A diagrammatic representation of the distribution of retrogradely labeled somata within the rostral portion of the medulla oblongata following an HRP injection of Crus I and the lateral portion of Crus II	285
12	Typical HRP-labeled cells in the spinal nucleus of the trigeminal nerve, the medial vestibular nucleus, the nucleus reticularis gigantocellularis and the locus ceruleus following cerebellar injections	287
13	A diagrammatic representation of the distribution of retrogradely labeled somata within the rostral portion of the medulla oblongata following an HRP injection of the ansiform lobule	289
14	A diagrammatic representation of the distribution of retrogradely labeled somata within the rostral portion of the medulla oblongata following an HRP injection of Crus I and the medial portion of Crus II	291
15	A photomicrograph and a series of line drawings representing transverse sections through the rostrocaudal extent of a lesion within the inferior olivary nucleus of an adult rat	293
16	Light micrographs of the inferior olivary complex from control and short-term 3AP treated rats following Nissl body staining	295
17	Light micrographs of the inferior olivary complex from control and short-term 3AP treated rats following hematoxylin and eosin or silver staining	297
18	Electronmicrographs of a normal and a 3AP intoxicated (12 hours following treatment) inferior olivary neuron	299
19	Electronmicrographs of the inferior olivary complex at 24 and 60 hours following 3AP treatment	301

Figure	Description	Page
20	An electronmicrograph of a microglia-like cell 60 hours following 3AP treatment	303
21	Electronmicrographs of a reactive microglia-like cell and an inferior olivary neuron 72 hours following 3AP treatment	305
22	Electronmicrographs of inferior olivary neurons 7 days following 3AP treatment	307
23	Electronmicrographs of degenerative olivary dendrites (14 days following 3AP treatment) and a normal climbing fiber tendril branch	309
24	Photomicrographs of the medulla oblongata from control and 3AP treated rats showing the cellular configuration of the inferior olivary complex	312
25	Electronmicrographs of the medial accessory olive following long-term 3AP treatment of the weanling rat	314
26	Electronmicrographs of the normal Purkinje cell dendritic tree and climbing fiber varicosities	316
27	Electronmicrographs of degenerating climbing fiber varicosities following 3AP treatment	318
28	Photomicrographs of Golgi-Cox preparations of control Purkinje cells	320
29	A camera lucida drawing of a Golgi-Cox preparation of an adult control Purkinje cell	322
30	Photomicrographs of Golgi-Cox preparations of Purkinje cells following long-term climbing fiber-deafferentation of the adult rat	324
31	Camera lucida drawings of Golgi-Cox preparations of Purkinje cells following long-term climbing fiber-deafferentation of the adult rat	326
32	A histogram of the length and number of Purkinje cell dendritic segments in the experimental groups or W CONT expressed as a percentage of the A CONT	330
33	A histogram of the length and number of Purkinje cell dendritic segments in the experimental group expressed as a percentage of the W CONT	332

Figure	Description	Page
34	Electronmicrographs of the smooth portion of the Purkinje cell dendritic tree following long-term climbing fiber-deafferentation of the adult rat	334
35	Electronmicrographs of terminal branchlets of the Purkinje cell dendritic tree following long-term climbing fiber-deafferentation	336
36	Photomicrographs of Golgi-Cox preparations of Purkinje cells following long-term climbing fiber-deafferentation of the weanling rat	338
37	Camera lucida drawings of Golgi-Cox preparations of Purkinje cells following long-term climbing fiber-deafferentation of weanling rats	340
38	Electronmicrographs of dendritic appendages along the smooth portion of the Purkinje cell dendritic tree following long-term climbing fiber-deafferentation of the weanling rat	342
39	Electronmicrographs of cerebellar interneurons within the molecular layer following long-term climbing fiber-deafferentation in the adult rat	343
40	Electronmicrographs of dendrites of cerebellar interneurons following long-term climbing fiber-deafferentation	346
41	A photomicrograph and a series of line drawings representing transverse sections through the rostrocaudal extent of a lesion within the ventral pontine gray of an adult rat	348
42	Electronmicrographs of the cytoarchitecture of the simple mossy fiber rosette of the adult cerebellar cortex	350
43	Electronmicrographs of the complex mossy fiber rosette of the adult cerebellar cortex	352
44	Electronmicrographs of mossy fibers following short-term pontine ablation	354
45	Electronmicrographs of cerebellar glomeruli following short-term (3.5-4 days) pontine ablation	356

Figure	Description	Page
46	Electronmicrographs of cerebellar glomeruli following short-term (5 days) pontine ablation	358
47	Photomicrographs of a Golgi-Cox preparation of a Purkinje cell following long-term mossy fiber ablation of the adult	360
48	Camera lucida drawings of a Golgi-Cox preparation of a Purkinje cell following long-term mossy fiber ablation of the adult	362
49	Electronmicrographs of cerebellar glomeruli following long-term (35-40 days) pontine ablation	364
50	Electronmicrographs of cerebellar glomeruli following long-term (35-40 days) pontine ablation	366
51	Electronmicrographs of cerebellar glomeruli following long-term (57 days) pontine ablation	368
52	Electronmicrographs of cerebellar glomeruli following long-term (80 days) pontine ablation	370
53	Electronmicrographs of cerebellar granule cells following long-term pontine ablation	372
54	Electronmicrographs of a control Purkinje cell primary dendrite and spiny branchlet	374
55	Electronmicrographs of the cerebellar molecular layer following long term (40-57 days) pontine ablation	376
56	Electronmicrographs of the cerebellar molecular layer following long-term (57 days) pontine ablation	378
57	Electronmicrographs of the cerebellar molecular layer following long-term (80 days) pontine ablation	380
58	A photomicrograph and a series of drawings representing coronal sections through the rostrocaudal extent of a parasagittal lesion within the lateral cerebellar hemisphere	382



Figure	Description	Page
59	Electronmicrographs of the granule cell layer	384
60	Electronmicrographs of the molecular layer of the cerebellar cortex following short-term parallel fiber transection	386
61	Photomicrographs of Golgi-Cox preparations of Purkinje cells following long-term parallel fiber deafferentation	388
62	Camera lucida drawings of a Golgi-Cox preparation of a Purkinje cell following long-term parallel fiber-deafferentation in an adult rat	390
63	Camera lucida drawings of a Golgi-Cox preparation of a Purkinje cell following long-term parallel fiber-deafferentation of a weanling rat	392
64	Electronmicrographs of large caliber Purkinje cell dendrites within the molecular layer of the cerebellar cortex following long-term (57-93 days) parallel fiber-deafferentation of the adult rat	394
65	Electronmicrographs of small caliber Purkinje cell dendrites within the molecular layer of the cerebellar cortex following long-term (57-93 days) parallel fiber-deafferentation of the adult rat	396
66	Electronmicrographs of the molecular layer following long-term (55-57 days) parallel fiber-deafferentation	398
67	Electronmicrographs of stellate cells following long-term parallel fiber-deafferentation	400
68	Electronmicrographs of dendritic spines along Purkinje cell terminal branchlets following long-term parallel fiber-deafferentation	402
69	A histogram of the length and number of Purkinje cell dendritic segments in experimental groups expressed as a percentage of the A 3AP	404

Figure	Description	Page
70	A histogram of the length and number of Purkinje cell dendritic segments in experimental groups expressed as a percentage of the W 3AP	406
71	A histogram of the length and number of Purkinje cell dendritic segments in experiment groups expressed as a percentage of the A CERB L	408
72	A histogram of the length and number of Purkinje cell dendritic segments in A PONT L expressed as a percentage of the W CERB L	410

LIST OF TABLES

Table	Description	Page
1	A working table of a 2 x 3 factorial ANOVA for the length and number of Purkinje cell dendritic segments in control and experimental groups	413
2	A working table of two separate one way ANOVAS for the length and number of Purkinje cell dendritic segments in control and experimental groups	414
3	A working table of a one way ANOVA for the length and number of Purkinje cell dendritic segments in control and experimental groups	415
4	Significant values for the length and number of Purkinje cell dendritic segments in experimental groups or W-CONT compared with the A-CONT.	416
5	Significant values for the length and number of Purkinje cell dendritic segments in experimental groups compared with the W-CONT	417
6	Significant values for the length and number of Purkinje cell dendritic segments in experimental groups compared with the A-3AP	418
7	Significant values for the length and number of Purkinje cell dendritic segments in experimental groups compared with the W-3AP	419
8	Significant values for the length and number of Purkinje cell dendritic segments in experimental groups compared with the A-CERB L	420
9	Significant values for the length and number of Purkinje cell dendritic segments in A-PONT L compared with the W-CERB L	420

Table	Description	Page
10	A working table of a one way ANOVA for the length of Purkinje cell dendritic appendages in the W 3AP compared with the A CONT	422
11	Significant values for the length of Purkinje cell dendritic appendages in the W 3AP group compared with the A CONT	423
12	A working table of a one way ANOVA for the length of spines along the Purkinje cell terminal branchlets in the A and W CERB L groups compared with the A CONT	424
13	Significant values for the length of spines along the Purkinje cell terminal branchlets in the A and W CERB L groups compared with the A CONT	425

## LIST OF APPENDICES

Appendix	Description	Page
APPENDIX I	A tilted data graph for the dependent variable MLPT	429
APPENDIX II	A tilted data graph for the dependent variable MLSB	431
APPENDIX III	A tilted data graph for the dependent variable MLSpB	433
APPENDIX IV	A tilted data graph for the dependent variable MNPT	435
APPENDIX V	A tilted data graph for the dependent variable MNSB	437
APPENDIX VI	A tilted data graph for the dependent variable MNSpB	439
APPENDIX VII	A tilted data graph for the dependent variable TLPT	441
APPENDIX VIII	A tilted data graph for the dependent variable TLSB	442
APPENDIX IX	A tilted data graph for the dependent variable TLSpB	445

## CHAPTER 1

### INTRODUCTION

It is well established that the regenerative<sup>5</sup> properties of the central nervous system are poorly developed in comparison with the peripheral nervous system, becoming progressively more limited during the course of phylogenetic and ontogenetic development (Raisman, 1969) and being least developed in adult mammals (Clemente, 1964; Bernstein, 1967). Damage to axons within the central nervous system does not generally result in their regeneration, but rather, the potential for central regeneration is limited particularly to specific adrenergic and cholinergic systems. However, in most instances a loss of axon terminals induces sprouting of collaterals from adjacent intact axon systems. This collateral sprouting often leads to a heterotypical reinnervation of vacated synaptic sites, a process which has been termed synaptic remodeling or neuronal plasticity (Raisman, Cowan and Powell, 1965; Goodman and Horel, 1966; Raisman, 1969; Bernstein and Bernstein, 1973; Nah and Leong, 1976a,b). It is apparent, therefore, that the central nervous system is not as

refractory to reinnervation as was commonly believed, although the new afferents are often heterotypical in origin.

The trilaminar structure of the cerebellar cortex provides a unique opportunity to investigate the effects of deafferentation in the central nervous system. It is well known that the cerebellum receives two main types of extrinsic afferents: the climbing fibers and mossy fibers which terminate in the outer and inner layers of the cortex respectively. It has been established that climbing fibers synapse directly with the Purkinje cells and originate largely from the inferior olivary complex (Desclin, 1974; Palay and Chan-Palay, 1974). The mossy fibers, on the other hand, arise from multiple sources throughout the brain stem and spinal cord and terminate as "rosette formations" within the granule cell layer where they synapse with the dendrites of the granule cell neurons (Snider, 1936; Grant, 1962; Szentagothai, 1962; Chan-Palay and Palay, 1971). The latter cells send their axons into the molecular layer where they bifurcate and form synapses with the spiny branchlets of the Purkinje cell dendritic tree.

While the effects of various experimental influences (x-irradiation, neurotoxins, viral infections and neurological mutations) on cerebellar development have been well documented (Altman, 1976a,b,c, 1973; Hirano, Dembitzer and Jones, 1972; Llinas, Hillman and Precht, 1973), little information is available concerning the potential for synaptic reorganization in the mature cerebellum (post neurogenesis). Convincing evidence now exists which suggests that the cerebellar cortex of the rat possesses a potential for

synaptic reorganization or remodeling prior to the completion of postnatal neurogenesis (between the 5th and 21st postnatal days). The proposed study is designed to extend our knowledge of the response to deafferentation in the cerebellum by investigating its remodeling capabilities following neurogenesis.

Since the likelihood of inducing reorganization is greater if a majority of the fibers are eliminated an area of the cerebellar cortex which receives as pure a mossy fiber input as possible must be identified to facilitate their surgical removal. The retrograde tracing method employing horseradish peroxidase histochemistry will be used for that purpose.

The methods which will be employed to induce deafferentation in the cerebellum include electrolytic, surgical and chemical lesions. With each of these methods observations will be made over a period of time ranging from 12 hours to 1 year following surgery. The short-term cases will be used to examine the exact localization of each fiber type and the sequence of changes which occur during their degeneration. In the later stages, from three months onward, changes in the organization which result from long-term deafferentation will be examined.

Following long-term deafferentation, the image analysis of Golgi impregnated Purkinje cells will be employed primarily to study the localization of dendritic appendages and alterations in the three dimensional orientation of the Purkinje cell dendritic tree. The elements which are most likely to undergo change during deafferentation are the dendrites, particularly the



4

dendritic appendages (thorns and spines) and these features will be quantified using the Image Analysis System. The entire question of spine loss following deafferentation is an important consideration in terms of eventual reorganization since spine formation and axonal sprouting are thought to be related (Lynch, Brecha, Cotman and Globus, 1974). Evidence has been provided to suggest that the pattern of dendritic branching also undergoes distinct alterations following deafferentation (Colonnier, 1969; Kawaguchi, Yamamoto, Mizuno and Iwahori, 1975; Altman, 1976a,c; Desclin and Colin, 1980). Image analysis will therefore be employed to examine the mean length and number of the various segments of the Purkinje cell dendritic tree following specific deafferentation.

A limited number of ultrastructural studies have employed degeneration methods to study the cerebellar cortex and only a few of these investigations have examined the long-term changes in organization which occur as a result of deafferentation (Colonnier, 1969; Desclin and Colin, 1980). Electron microscopy will therefore be employed extensively throughout this study to investigate the ultrastructural changes that occur both during the initial degenerative phase and following long-term deafferentation.

Degeneration and autoradiographic techniques will also be employed to examine the possibility of remodeling or plastic reorganization in the mature cerebellum. Initially, the removal of either the mossy fiber or the climbing fiber input will be performed. After a predetermined survival period which will

allow for degeneration and subsequent reorganization, a short-term lesion or injection ( $^3\text{H}$ -leucine) will be made in the nucleus of the other input. In that way, changes in the pattern or organization of mossy and climbing fiber inputs in response to selective deafferentation will be examined.

Various types of reorganization are possible following each type of proposed lesion. Normally, mossy fibers do not ascend beyond the infraganglionic plexus and thus do not synapse directly with the Purkinje cell. The presence of mossy fiber terminals in the molecular layer would therefore represent a major change in organization. The climbing fibers, on the other hand, synapse solely with the Purkinje cells so that a climbing fiber input to the granule cells would be readily distinguished as aberrant. Any alteration in the distribution of the parallel fiber input should be easily determined because of its specific localization on the spiny branchlet system of the Purkinje cell dendritic tree.

Histochemical experiments have indicated that axon sprouting in general may begin as early as 5 to 7 days after lesioning (Moore, Bjorklund and Stenevi, 1971; Lynch, Matthews, Mosko, Parks and Cotman, 1972). In the hippocampus, it has been shown that functional synaptic contacts are established by 14 days (Lynch et al., 1974). Initially, then, observations will be made at frequent intervals during the first 6 weeks following surgery. After that period, animals will be sacrificed at wider intervals up to one year post-operatively to ascertain the long-term effects of deafferentation and to determine if the early changes are

transient in nature.

It has not yet been undertaken in any species to compare the response to deafferentation in the mature cerebellar cortex following the removal of mossy, climbing and parallel fibers. The cerebellar cortex is particularly well suited for such a study because of its unique organization and the wealth of available data concerning its normal structure and function. The proposed investigation promises to provide fundamental information concerning the means by which the cerebellum deals with afferent loss. An understanding of its response to injury and its potential for recovery should thereby be provided.

## CHAPTER 2

### HISTORICAL REVIEW

#### 2.1 The Cerebellar Cortex

##### A. Normal Cytoarchitecture

In their recent text entitled "Cerebellar Cortex, Cytology and Organization" Palay and Chan-Palay state: "Probably no other part of the central nervous system has been so thoroughly investigated and is so well known as the cerebellar cortex. For nearly a century all of its cell-types have been recognized, and the course and terminations of their processes have been described countless times by numerous authors" (Palay and Chan-Palay, 1974). This statement, which refers to the structure and morphology of the cerebellar cortex, is no less true concerning physiological investigations (see Eccles, Ito and Szentagothai, 1967).

The trilaminar structure of the mammalian cerebellar cortex is well known. It consists of an outer molecular layer, an intermediate Purkinje cell layer and an inner granule cell layer. The Purkinje cell layer consists of a sheet of large, flask-shaped cells, one cell layer thick. These Purkinje cells possess a flat

dendritic tree which ascends into the molecular layer and branches extensively in the sagittal plane. The small caliber dendrites which make up the peripheral portion of the Purkinje cell dendritic tree are studded with numerous dendritic spines and represent the terminal (spiny) branchlet system. In addition, however, ultrastructural investigations have recently reported a small population of stubby appendages along the smooth portion of these cells which have been more accurately described as dendritic thorns (Palay and Chan-Palay, 1974; Desclin and Escubi, 1976). The Purkinje cell axons descend through the underlying granular layer, become myelinated, and project primarily to the deep cerebellar nuclei as the efferent outflow of the cerebellar cortex. The postnatal neurogenesis of the internal granular layer is complete by about 20 days post-partum in the rat (Addison, 1911; Altman, 1969). This layer consists largely of numerous granule cells which are 5-8  $\mu$  in diameter and lack a Nissl body content. The axons of these cells ascend vertically into the molecular layer where each bifurcates into two branches that run parallel to the long axis of the folium to form the parallel fibers. It has been postulated that these fibers complete their growth prior to the downward migration of the granule cell somata to form the future internal granule cell layer (Altman, 1972a, c). Each Purkinje cell dendritic tree makes contact with thousands of parallel fibers which run orthogonal to the plane of the dendritic arborization and make synaptic contact with spines covering the spiny branchlets of the dendritic tree (Gray, 1961; Palkovits, Magyor and Szentagothai, 1971). Most neuroanatomists agree that all extrinsic afferents to

the cerebellar cortex terminate as either mossy or climbing fibers (Brodal and Grant, 1962). The mossy fibers enter the granule cell layer, branch repeatedly and terminate as lobulated enlargements called rosettes (Smith, Hudgens and O'Leary, 1966). These rosettes enter into complex synaptic arrangements, called glomeruli, with granule cell dendrites and the axon and dendrites of another cell type termed a Golgi cell (Palay and Chan-Palay, 1974). The second type of afferent, the climbing fiber, originates principally or entirely in the contralateral inferior olivary nucleus (Brodal, 1940; Scheibel, 1954; Szentagothai and Rajkovits, 1959; Desclin, 1974). These fibers pass through the granule and Purkinje cell layers where they climb along the dendritic arbor of the Purkinje cells and ultimately make contact with stubby thorns projecting from the main dendritic branches (Kirsche, David, Winklemann and Marx, 1964; Chan-Palay and Palay, 1970; Kornguth and Scott, 1972). Recently, the olivocerebellar system has been postulated to give rise to branches, called glomerular collaterals, within the granule cell layer which form mossy fiber-like rosettes (Chan-Palay and Palay, 1971). Anterograde transport of <sup>35</sup>S methionine following inferior olive injections has provided further evidence for these collaterals within the granule cell layer (Chan-Palay, Palay, Brown and Van Itallie, 1977). Subsequent autoradiographic and chemical lesion studies of the olivocerebellar system have failed to confirm their existence, (Groenewegen and Voogd, 1977) although climbing fiber terminals have been reported to degenerate within the molecular layer (Desclin and Colin, 1980).

## 1. Cerebellar Afferents

### a) Climbing Fiber Origin

The adult cerebellum has not been used widely in studies of plasticity because of the difficulties encountered until recently in demonstrating afferent projections and intrinsic fibers within the cerebellar cortex (climbing, mossy and parallel fibers) using routine degeneration methods. These difficulties were reported by both Szentagothai and Voogd as late as 1969. Szentagothai and Rajkovits (1959) used the Nauta-Gygax method to demonstrate olivocerebellar fibers within the molecular layer of the cerebellum and suggested that they were climbing fibers, although their terminal arborizations were not impregnated. Miskolczy (1931) and Carrea, Reissig and Mettler (1947) suggested, on the basis of electrolytic lesions of the inferior olive, that its projection was mossy in nature. O'Leary, Dunsker, Smith, Inukai and O'Leary (1970) and Murphy, O'Leary and Cornblath (1973) reported both degenerating climbing and mossy fibers following olivary lesions, while Hamori and Szentagothai (1964) maintained that the olivocerebellar tract is comprised solely of climbing fibers. Confusion persisted as to the nature of the olivary projection until Desclin and Escubi's work in 1974 which involved the use of a specific olivocerebellar tract toxin 3-Acetylpyridine (3AP) and the development of a new suppressive silver method (modified Fink-Heimer and De Olmos-Ingram technique).

The question of extra-olivary climbing fibers has intrigued many investigators since Cajal's early work in 1911, which suggested that climbing fibers could arise from both the pontocerebellar

and vestibulocerebellar systems. Carréa et al. (1947) reported climbing fiber degeneration in the molecular layer of the cerebellar cortex following lesions in the deep cerebellar nuclei. Szentagothai and Rajkovits (1959) reported degeneration resembling that of climbing fibers in the contralateral flocculus after lesioning the brachium conjunctivum. Batini and Pumain (1968) found that climbing fiber excitatory postsynaptic potentials (EPSP) were still recorded in 58% of the Purkinje cells tested following midline lesioning of the crossed olivocerebellar pathways, a finding which they interpreted to suggest that half of the climbing fibers arose from extra-olivary sources. Silver impregnation methods have failed to detect a numerical change in the terminal field of the climbing fibers following olivocerebellar transection within the medulla (Rivera-Dominguez, Mettler and Noback, 1974). Autoradiographic injections of the inferior olivary complex (Courville, Faraco-Cantin and Diakiv, 1974; Courville, 1975; Groenewegen and Voogd, 1976, 1977; Chan-Palay et al., 1977), anterograde degeneration of the olivocerebellar system (Rivera-Dominguez, Mettler and Noback, 1974) and electrophysiological recordings (Armstrong, Harvey and Schild, 1974) have failed to show a projection to the entire cerebellar cortex; instead a sagittal banding pattern occurred, which suggested that the empty bands might be innervated by an extra-olivary source of climbing fibers (Courville et al., 1974; Courville, 1975). Later studies have reported that this banding pattern is lost following total olivary injections (Courville and Faraco-Cantin, 1978). In fact, recent studies have described a small ipsilateral counterpart to this system (Matsushita and Ikeda, 1970; Eller and Chan-Palay, 1976; Chan-Palay et al., 1977). While



many authors are convinced that the inferior olivary complex is the sole source of climbing fibers to the cerebellum (Bell and Dow, 1967; Grant, 1970; Desclin, 1974, 1976; Batini, Corvisier, Destombes, Gioanni and Everett, 1976), controversy exists among others as to both their course and origin (Matsushita and Ikeda, 1970; Batini et al., 1976; Eller and Chan-Palay, 1976; Chan-Palay et al., 1977; Courville and Faraco-Cantin, 1978). More recently, silver impregnation methods have been used with varying success to demonstrate climbing, mossy and parallel fibers (Grant, 1970; Desclin, 1974; Sotelo, Hillman, Zamora and Llinas, 1975; Brand, Dahl and Mugnaini, 1976; Desclin, 1976; Meria, 1976; Matsushita and Ikeda, 1976; Groenewegen and Voogd, 1977).

With the advent of the retrograde tracing method of horseradish peroxidase histochemistry (LaVail and LaVail, 1972; Kristensson and Olsson, 1976) and the anterograde tracing method of tritiated amino acid autoradiography (Cowan, Gottlieb, Hendrickson, Price and Woolsey, 1972), demonstration of both the cells of origin and their terminal fields has become possible for various systems enabling a fresh approach to the investigation of cerebellar afferents.

#### (1) Olivocerebellar

Retrograde degeneration studies suggested a topological arrangement within the olivocerebellar projection following extirpation of specific cerebellar loci (Brödal, 1940, 1954) and these findings have been confirmed using electrophysiological methods (Van Gilder and O'Leary, 1970; Groenewegen and Voogd, 1977). The medial and dorsal accessory nuclei were found to generate orthodromic volleys within

the cerebellar vermis and pars intermedia of the anterior lobe following excitation, while the hemispheric regions of the cerebellum were stimulated following excitation of the principal olive (Groenewegen and Voogd, 1977). More specifically, the dorsal lamella appeared to project to Crus I, while Crus II received an innervation from the ventral lamella (Brodal, 1940; Groenewegen and Voogd, 1977). However, horseradish peroxidase (HRP) injections have not entirely agreed with this topography (Kotchabhakdi, Walberg and Brodal, 1978). The advent of a retrogradely transported protein marker (HRP) has enabled the detailed mapping of the olivocerebellar projection for the entire cerebellar cortex. As a result, the ansiform lobule has been shown to receive olivocerebellar fibers originating mainly from the dorsal and ventral lamellae of the principal olive (specifically, Crus I from the medial parts of the two lamellae and Crus II from the lateral portions and the bend) although a minor projection from the accessory nuclei has also been reported (Kotchabhakdi et al., 1978). On the contrary, Kimoto et al. (1978) have suggested that all inferior olivary neurons except those within the caudal part of the medial accessory olive are responsible for supplying climbing fibers to the ansiform lobule of the cerebellum. The paramedian lobule, on the other hand, has been found to receive its climbing fiber input from the caudal half of the ventral and dorsal lamellae of the principal olive, along with a small projection from the dorsal accessory and rostral half of the medial accessory olive (Brodal, Walberg and Hoddevik, 1975). A later study, however, failed to show labeled cells within the ventral lamella when injections

were restricted to the caudal third of the paramedian lobule (Brodal and Walberg, 1977b). The cerebellar visual cortex (Lobules VI, VIIA, A, VIIIA and B) has been shown to receive an olivocerebellar input from an area within the caudal portion of the medial accessory olive (Batini et al., 1976; Hoddevik, Brodal and Walberg, 1976), while the archicerebellum (flocculonodular lobe) receives its olivary projection from the dorsal cap of Kooy, the rostral tip of the medial accessory olive and the adjoining portion of the dorsomedial cell column (Hoddevik and Brodal, 1977). The uvula, on the other hand, receives its climbing fiber projection from two discrete subnuclei of the olivary complex, the nucleus  $\beta$  and the dorsomedial cell column (Brodal, 1976). Retrograde labeling from the anterior lobe of the cerebellar cortex indicates an olivocerebellar input from the dorsal and medial accessory olives (Brodal and Walberg, 1977a), except for its most lateral portion which is innervated by an area in the dorsal lamella of the principal olive.

#### b) Mossy Fiber Origin

The new tracing methods have shown that the cerebellar cortex receives mossy fibers from a variety of brain centers which include the pons (Burne, Eriksson, Saint-Cyr and Woodward, 1978), the lateral reticular nucleus (Brodal, 1975), the sensory nuclei of the trigeminal nerve (Ikeda, 1979), the cuneate and external cuneate nuclei (Rinvik and Walberg, 1975), the lateral vestibular nucleus

(Kotchabhakdi and Walberg, 1978; Korte and Mugnaini, 1979), the nucleus locus ceruleus (Kimoto et al., 1978) and the spinal cord (Matsushita, Hosoya and Ikeda, 1979). The current state of knowledge regarding the topographical organization of these various projections to the cerebellum is presented below.

#### (1) Ceruleocerebellar

Cerebellectomies have been shown to produce retrograde degenerative changes within the noradrenergic neurons of the dorsolateral locus ceruleus (Olson and Fuxe, 1971). Lesions which involve the collaterals of these neurons to the cerebral cortex (dorsal noradrenergic pathway) have been used to increase the intraneuronal amine content of the noradrenergic cerebellar plexus and have indicated a sparse histochemical localization throughout the cerebellar cortex. Fluorescence histochemistry and autoradiographic localization of [<sup>3</sup>H] noradrenaline have localized the afferent projection from the nucleus locus ceruleus in direct association with major Purkinje cell dendritic trunks and occasionally with their associated stubby spines (Bloom, Höffer and Siggins, 1971). While the nucleus locus ceruleus has been considered the sole source of the noradrenergic input to the cerebellar cortex, recent investigations have suggested that at least one other center (nucleus subceruleus) may also be involved (Kimoto et al., 1978).

#### (2) Pontocerebellar

The pontocerebellar afferents constitute a bilateral system having a contralateral predominance (Höddevik, 1975; Burne et

al., 1978). Retrograde labeling (HRP) has revealed a massive pontocerebellar mossy input to the lobulus simplex, the ansiform lobule (Crus I and Crus II) and the paramedian lobule of the cerebellar cortex. The input to lobulus simplex has been shown to arise from an area of the contralateral pontine nuclei ventral to the peduncle (ventral pontine nuclei). Moreover, injections restricted to the ansiform lobule have resulted in labeling within two discrete zones (medial and lateral pontine nuclei) located immediately adjacent and dorsal to the lobulus simplex output (Hoddevik, 1975; Burne et al., 1978). This finding contrasts with other experiments which have labeled pontine neurons within an intermediate zone of this nuclear complex (Kimoto et al., 1978). Studies employing discrete injections of various cerebellar lobules have attempted to elucidate the topographical arrangement of the pontocerebellar projection. The vermal region of the anterior lobe has been shown to receive a projection from the lateral pontine nucleus of the caudal half of the contralateral pons; while the intermediate-lateral region was found to be innervated by pontine fibers from this nucleus and the medial pontine nucleus (Brodal and Walberg, 1977a; Brodal, 1979). The posterior vermal input has been localized within two zones located dorsomedially and dorsolaterally throughout the extent of the pons (Brodal, 1979), although micro-injections within sublobule "a" of the uvula have indicated a projection from a distinct dorsointermediate column within the caudal pons (Eisenman and Noback, 1980). The pontocerebellar afferents to Crus I originate from a dorsomedial cell column in the rostral third of the pons,

while the pontocerebellar afferents to Crus II arise from the medial pontine nucleus caudally and an intermediate region of the ventral pontine nucleus at rostral levels. In addition, the nucleus reticularis tegmenti pontis (reticulo-tegmental nucleus) projects heavily to the neocerebellum (Kimoto et al., 1978). Recent horseradish peroxidase studies have shown that the pontine projection to the paramedian lobule originates within the lateral pontine nucleus (Brodal, 1979) while the input to the cerebellar visual cortex (Lobules VI, VIIA, B, VIIIA and B) occurs via four discrete longitudinal cell columns (the dorsolateral, peduncular, lateral and paramedian pontine nuclei) situated throughout the pons (Hoddevik, Brodal, Kawamura and Hashikawa, 1977).

### (3) Reticulocerebellar

Using retrograde chromatolysis Brodal (1943) reported that the projection from the lateral reticular nucleus was restricted to the ipsilateral cerebellar cortex and described a topographical organization for its various subnuclei (parvocellular-vermis, magnocellular-lateral hemisphere and subtrigeminal-flocculonodular lobe). In later studies, which have involved anterograde degeneration methods, a bilateral reticulocerebellar projection has been described within specific cerebellar lobules (Voogd, 1964; Matsushita and Ikeda, 1976). Autoradiography and silver impregnation have confirmed the ipsilateral predominance of this system and have localized these terminals within the cerebellar granule cell layer (Kunzle, 1975; Matsushita and Ikeda, 1976;

Chan-Palay et al., 1977). These reticulocerebellar fibers have been reported within the vermal, paravermal and lobulus simplex regions while the ansiform and paramedian lobules appear to lack a reticular input. Electrophysiological recordings have suggested a reticulocerebellar projection to the classical spinal receiving zones (the anterior lobe, pyramis and the paramedian lobule) (Clendenin, Ekerot, Oscarsson and Rosen, 1974a, b) and the retrograde marker HRP has confirmed a reticulocerebellar projection to these areas (Brodal, 1975). Anterograde labeling methods (tritiated amino acids and orthograde degeneration) have indicated additional projections to lobulus simplex and the medial portion of the ansiform and paramedian lobule (Kunzle, 1975; Matsushita and Ikeda, 1976).

#### (4) Spinocerebellar

The spinocerebellar system has been shown to consist of four major tracts: the ventral, dorsal, rostral and cuneocerebellar tracts (Matsushita et al., 1979).

##### (a) Dorsal and Ventral Tracts

Extensive cerebellar injections of HRP have revealed heavy labeling within Clark's column, the central cervical nucleus, the main cuneate and external cuneate nuclei and the dorsolateral border of the ventral horn between lumbar (L)<sub>3</sub> and L<sub>5</sub> (spinal border cells), in addition to scattered labeling throughout the spinal grey (Snyder, 1977; Matsushita et al., 1979). Retrograde chromatolytic changes have been observed within perikarya in the

lumbosacral segments (dorsolateral portion of the ventral grey) following hemocerebellectomy and appear to correspond to the group of spinal border cells in the ventrolateral gray of the lumbar spinal cord of monkeys described by Cooper and Sherrington (1940). Subsequent ablation of these neurons has resulted in degenerative fibers confined to the ventral spinocerebellar tract (Ha and Liu, 1968; Burke, Lundberg and Weight, 1971; Matsushita et al., 1979). Similarly, it has been established that the dorsal spinocerebellar tract arises from the neurons within Clark's column (Matsushita et al., 1979). Following HRP injections, these systems have been found to project to the anterior lobe, the vermis of the posterior lobe and the paramedian lobule (Matsushita et al., 1979).

#### (b) Rostral and Cuneocerebellar Tracts

Anatomical and physiological data suggest that the cuneocerebellar and rostral spinocerebellar tracts represent the forelimb equivalent of the dorsal and ventral spinocerebellar tracts (Jansen and Brodal, 1958; Grant, 1962; Holmqvist, Oscarsson and Rosen, 1963; Oscarsson, 1973). Electrophysiological data has suggested that the rostral spinocerebellar tract originates from the contralateral central cervical nucleus of the spinal cord (Matsushita and Ikeda, 1975; Matsushita et al., 1979). Localization of the external cuneate afferents (cuneocerebellar input), using retrograde chromatolysis, has suggested a terminal distribution within the vermis and intermediate part of the anterior lobe, the pyramis and the uvula of the ipsilateral cerebellum (Brodal, 1941).



Anterograde degeneration (Grant, 1962) and physiological studies (Cook, Larson, Oscarsson and Sjolund, 1977) have confirmed the projection to the forelimb areas of the anterior lobe (Larsell's lobule V, pars intermedia and the anterior part of lobule VI) and have suggested an additional input to the anterior portion of the paramedian lobule. As expected, horseradish peroxidase injections within the intermediate portion of Larsell's lobule V and the paramedian lobule of the same side have provided an extensive labeling within the external and main cuneate nuclei.

#### (5) Trigemino-cerebellar

Using the Nauta technique, Carpenter and Hanna (1964) demonstrated an ipsilateral projection to the vermal cortex of Lobules V and VI from the spinal nucleus of the trigeminal nerve. Horseradish peroxidase injections have confirmed its ipsilateral course and have indicated a much larger field of termination which includes the rostral folia of the paramedian lobule, the posterior folia of Crus II, the intermediolateral portion of lobulus simplex, the medial portion of the crura and the rostral folia of lobule IX (Ikeda and Matsushita, 1977, 1978; Somana, Kotchabhakdi and Walberg, 1980). Ikeda (1979) was unable to identify a trigemino-cerebellar input to the anterior portion of the anterior lobe, Crus I, the anterior folia of Crus II, the paraflocculus, the flocculus or the ventral portion of the paramedian lobule. However, Komoto et al. (1978) have reported a few labeled cells within various nuclei of the trigeminal nerve following injections within the

lateral cerebellar hemispheres. Most of the labeled cells were localized within the nucleus interpolaris and oralis of the spinal trigeminal nerve, although the principal sensory nucleus has been postulated to reach the region of the crura adjoining the paramedian lobule and lobule IX (Somana et al., 1980).

#### (6) Vestibulocerebellar

##### (a) Primary Afferents

Using the Nauta-Laidlaw technique, primary vestibular afferents were traced to the cortex of the ipsilateral paraflocculus, the lingula, and the parvocellular portion of the dentate nucleus following vestibular nerve transections (Brodal and Hovik, 1964). The primary vestibulocerebellar projection was re-examined using newly developed silver methods and was found to be localized within the ipsilateral flocculonodular lobe and the uvula. Confirmation of the labeling within the dentate, paraflocculus and lingula was not found (Korte and Mugnaini, 1979).

##### (b) Secondary Afferents

Early mappings of degeneration suggested a bilateral secondary vestibulocerebellar system within the nodulus, the adjoining folia of the uvula, the flocculus and the fastigial nucleus (Dow, 1936). A later study, which examined retrograde cellular changes following cerebellar cortical lesions, found that the majority of the secondary vestibulocerebellar afferents originate from the caudal portion of the inferior vestibular nucleus and cell group f

(Brodal and Torvik, 1957), although recent HRP injections into lobules V and VI have labeled cells in the dorsal part of the medial and inferior vestibular nuclei (Precht, Volkind and Blanks, 1977). Retrograde HRP labeling from the cerebellar vermis, the fastigial nucleus and the anterior and posterior interpositus nuclei suggested a bilateral projection from the medial, inferior and cell groups f and x of the vestibular nuclear complex, while the superior and lateral vestibular nuclei were bilaterally labeled following injections into the nodulus, the flocculus, the vermal region and the fastigial nucleus (Kotchabhakdi and Walberg, 1978). A note of importance to Kotchabhakdi and Walberg (1978) was the absence of vestibular labeling following injections into Crus I and II, the paramedian lobule, the paraflocculus and the lateral dentate nucleus. In addition, labeled cells were observed in the vestibular complex following HRP injections in the fastigial nucleus (Ruggiero, Batton and Jayarama, 1977) but not following injections into the nucleus interpositus anterior (McCrea, Bishop and Kitai, 1977) or the dentate nucleus. (Eller and Chan-Palay, 1976; Chan-Palay, 1977).

In addition, the facial nucleus, the dorsal part of the nucleus ambiguus, the prepositus hypoglossal and the dorsal raphe nuclei have shown a sparse bilateral labeling of HRP following injections within the neocerebellum (Kimoto et al., 1978).

## 2.2 3-Acetylpyridine: A Neurotoxin

The introduction of chemical lesioning methods that

employ toxic agents such as 6-hydroxydopamine and kainic acid has represented a significant advance in the experimental investigation of the central nervous system organization. The search for lesion inducing substances has revealed that certain vitamin analogues may also involve specific centers selectively. One such agent is the nicotinamide antagonist, 3-Acetylpyridine (3AP), the toxic effects of which are the result of competition between it and nicotinamide for incorporation into NAD. The pathological changes induced by this substance are thus a reflection of the inhibition of the nicotinamide-dependent metabolic pathways (Desclin, 1975).

Several regions of gray matter undergo selective degeneration following the intraperitoneal administration of 3AP. Histological investigators employing Nissl preparations (Denk, Haider, Kovak and Studynka, 1968) and suppressive silver methods (Desclin, 1974; Desclin and Escubi, 1974) have suggested a partial degeneration of facial, hypoglossal and ambiguous nuclei. Desclin (1974) has also demonstrated discrete lesions in the pars compacta of the substantia nigra, areas CA<sub>3</sub> and CA<sub>4</sub> of the hippocampus, the supra-optic nucleus of the hypothalamus, and the nucleus dorsalis of the raphe in the midbrain.

The area that is reportedly most affected by 3AP administration is the inferior olivary nucleus, although there is less than universal agreement on this point. Denk et al. (1968) reported subtotal ablations of the inferior olivary complex following 3AP treatment, while Koikegami and Fuse (1961) found argyrophilic bodies in both facial and hypoglossal nuclei but failed to perceive

any degenerative changes in the inferior olivary neurons. More recently, Desclin and Escubi (1974) have employed suppressive silver methods to demonstrate a total bilateral ablation of the inferior olivary complex. It is also noteworthy that the susceptibility of olivary neurons to 3AP has been shown to be age-dependent (Woodhams, Rodd and Balazs, 1978). In addition to an extensive necrosis of the inferior olivary neurons, degeneration has also been observed within their axons, the climbing fibers of the cerebellar cortex (Desclin, 1974; Desclin and Escubi, 1974; Sotelo et al., 1975; Simantov, Snyder and Oster-Granite, 1976; Desclin and Colin, 1980). The chemical induction of discrete lesions using toxins such as 3AP may prove valuable as a complementary method to conventional electrolytic procedures, which involve passing fibers and adjacent nuclei indiscriminately. Thus far, however, a detailed examination of the inferior olivary nucleus following 3AP administration has not been undertaken at the ultrastructural level.

### 2.3 Evidence for Transneuronal Degeneration

#### A. The Central Nervous System

As early as the first half of this century, transneuronal changes were postulated to occur following afferent fiber transection (Winkler, 1918; Cook, Walker and Barr, 1951; Hamlyn, 1954; Goldby, 1957), but until recently few have appreciated the extent and magnitude of such changes. The first reports of transneuronal degeneration described it in the dorsal nucleus of the lateral geniculate body following eye enucleation (Minkowski, 1913), the anterior horn cells following pyramidal tract transections (Barron, 1933) and the cuneate nucleus following damage to the posterior fasciculus (Foerster and Gagel, 1934),

while transneuronal atrophy was described in the pyramidal cells of the prepyriform cortex of rabbits following olfactory peduncle transection (Winkler, 1918), and the spinal cord of monkey and man following posterior root rhizotomy (Foerster, Gagel and Sheehan, 1933). Torvik (1956) believed that these changes in mature brains might be peculiar to the visual system (lateral geniculate body and superior colliculus) and questioned their existence in other centers.

#### 1. Somal Alterations

It has clearly been shown that a loss of Nissl granules occurs during transneuronal atrophy (Allison, 1953, 1954; Hamlyn, 1954; Goldby, 1957; Glees, 1961; Matthews, 1964). In addition, Glees, Hasan and Tischner (1967) have shown a marked depletion in the cytoplasmic organelles and the nuclear and cytoplasmic content during the early stages of transneuronal atrophy. These authors also found that cytoplasmic vacuolation was a prominent feature of the long-term effects of deafferentation. Transneuronal changes have been reported in the lateral geniculate body of the monkey, cat, rabbit and man following optic nerve transection (Minkowski, 1920; LeGros Clark, 1932, LeGros Clark and Penman, 1934; Glees and LeGros Clark, 1941; Matthews, Cowan and Powell, 1960). The first attempt at quantifying such changes came in a study of the lateral geniculate nucleus following enucleation in the cat and rabbit (Cook et al., 1951). Between the second and tenth postoperative month, the mean cross-sectional area of the cells in lamina A showed a reduction of between 16.0% and 30.0%. Over the same time period, a significant reduction of 8.6% - 18.4% and 16.7% - 26.1% was reported in the diameter of the nucleus and nucleolus respectively. In animals which

survived for longer periods (between 210 - 213 days) a marked cytoplasmic vacuolation occurred within the lateral geniculate nucleus. Measurements of perikarya taken 130 days following olfactory nerve transection recorded a 50% and a 40% reduction in the size of the mitral and tufted cells respectively (Matthews and Powell, 1962). The time course and degree of neuronal shrinkage was similar for the superior cervical ganglion in adult rabbits following deafferentation (Hamlyn, 1954).

The possibility of cell death occurring as a result of deafferentation has intrigued several investigators. A loss of perikarya following deafferentation was initially reported by Hechst (1933) and Tsang (1937) and was later confirmed in the lateral geniculate body of the immature monkey (Polyak, 1957), the pontine and inferior olivary nuclei of the kitten (Torvik, 1956) and the superior colliculus of both the fetal and the adult guinea pig (Hess, 1957). A lack of neuronophagia has been reported in the lateral geniculate nucleus of the adult cat, rabbit and monkey (Cook et al., 1951; Matthews et al., 1960) and the auditory and vestibular nuclei of the cat (Powell and Erulkar, 1962). However, Penman and Smith (1950), Goldby (1957) and Kupfer (1965) have reported a significant cell loss (50%) in the adult human lateral geniculate body following retinal macular lesions. In a cytochemical study of the deafferentated lateral geniculate body of the monkey, Kupfer and Downer (1967) reported decreased RNA levels (68%) as early as 48 hours following deafferentation. In a later study, Matthews (1964) re-investigated cell loss following deafferentation of the lateral geniculate nucleus in mature monkeys and observed a loss of between 14 - 20% for the neurons in the affected laminae. The mean cross-sectional area of the surviving cells in lamina 1 and 2 was also reduced by 57.0%.

while the small celled laminae incurred a 60% reduction.

## 2. Immature Systems

Using conventional histological techniques, early workers (Berger, 1900; Goodman, 1932; Chow, 1955) failed to demonstrate anatomical changes in the lateral geniculate body of immature animals (kitten, rabbit and monkey) following visual deprivation (lid suturing). However, several authors have reported alterations in the retinal ganglion cells following light deprivation. These changes ranged from a reduction in the level of retinal proteins (Brattgard, 1952) to retinal ganglion cell degeneration (Chow, Riesen and Newell, 1957; Riesen, 1960, 1962; Rasch, Swift, Riesen and Chow, 1961). The importance of a normal sensory stimulation in the development and maintenance of neuronal systems has been convincingly demonstrated by Wiesel and Hubel (1963, 1965). They showed that visual deprivation from birth in young kittens resulted in a significant decrease (25 - 40%) in the mean cross sectional area of cells in laminae A and B. They also found a direct correlation between the degree of transneuronal atrophy and the age at which visual deprivation occurred. In adult cats (> 3 months), eyelid closure failed to produce transneuronal changes in the lateral geniculate body. DeLong and Sidman (1962) have speculated that if axonal deprivation occurs prior to normal synaptic development, then cellular dissolution occurs. However, if deafferentation is postponed beyond normal synaptic development it induces shrinkage rather than neuronal cell death.

The suggestion that transneuronal atrophy occurs in immature animals was met with skepticism, since many believed that the resulting changes could be explained on the grounds of arrested postnatal



growth (Wiesel and Hubel, 1963; Cowan, 1979). A study by Wiesel and Hubel (1965) did little to dispel such criticism, but did provide additional morphological data supporting transneuronal atrophy in the mature visual system. Furthermore, the histological and cytochemical work of Kupfer and Palmer (1964) did not support the occurrence of transneuronal atrophy following visual deprivation in younger animals. Following analysis of cytoplasmic volume, Nissl body content and several enzyme systems, they concluded that the normal metabolic activity of lateral geniculate neurons remained unaltered. They suggested further that the most important effect of eyelid closure was the retardation of normal postnatal growth.

### 3. Species Variations

Species differences in the reaction to deafferentation has been suggested in several reports. Tsang (1937), Hess (1957), DeLong and Sidman (1962) and Terry, Roland and Race (1962) have observed a marked hypoplasia in the superior colliculus of rats, fetal guinea pigs and mice following enucleation, with little effect on the lateral geniculate body. At variance with this, carnivores and primates have shown little indication of transneuronal alterations within the superior colliculus, while marked changes have been reported within the lateral geniculate body (Glees and LeGros Clark, 1941; Torvik, 1956; Goldby, 1957; Matthews, Cowan and Powell, 1960; Wiesel and Hubel, 1963; Kupfer and Palmer, 1964; Kupfer, 1965). Torvik (1956) noted a wide variation in the speed and intensity of degeneration in the lateral geniculate nucleus of different animals. Primates showed marked transneuronal changes within seven days of deafferentation while no visible signs were detected in cats for 60

days, and rabbits appeared normal for five or six months following deafferentation. Similar findings have been reported in the olfactory system (Pinching and Powell, 1971). Polyak (1957) attempted to explain such species variations anatomically, suggesting a change in the ratio of retino-collicular and retino-geniculate fibers as the basis for such variations in higher mammals. Torvik (1956) claimed that the differences were based on the existence of association neurons in the lateral geniculate body of certain species.

#### 4. Dendritic Alterations

Little attention, however, was focused on the effect of deafferentation on the maintenance and development of the normal dendritic pattern of these neurons. Only recently has it become apparent that the effect of deafferentation is shared by both the perikaryon and its dendrites. The Golgi method has been used by several groups to demonstrate alterations in the impregnation of neurons following deafferentation (Jones and Thomas, 1962; Matthews and Powell, 1962; White and Westrum, 1964; Globus and Scheibel, 1966; Powell, 1967; Valverde, 1967; Coleman and Riesen, 1968). Jones and Thomas (1956, 1962) were the first to observe transneuronal changes within the dendritic arbors of adult animals. Deafferentation caused a marked reduction in the dendritic segments of pyramidal cells in the piriform cortex following removal of the olfactory bulb or transection of the olfactory peduncle, a finding which was supported in a later study by Powell (1967). Combining the information obtained from Nissl, Bodian and Golgi-Cox preparations, LeGros Clark (1957) and Matthews and Powell (1962) noted such changes in the principal dendrites of mitral, tufted and periglomerular cells

associated with degenerating olfactory nerve fibers. White and Westrum (1964) found that persisting dendrites were often devoid of their normal spine population, although a corresponding electron microscope study (Westrum, 1966) provided no evidence regarding their phagocytic removal.

Other investigations (Globus and Scheibel, 1966, 1967 and Valverde, 1967) attempted to monitor transneuronal changes in the striate cortex. Using the Golgi-Cox technique, Valverde (1967) reported a reduction in the dendritic length and the branching pattern of stellate cells in the visual cortex of cats raised from birth in total darkness. In an earlier study, Globus and Scheibel (1966) demonstrated a marked reduction in the number of spines along the apical dendrites of pyramidal cells following either eye enucleation or ipsilateral lesions of the lateral geniculate nucleus (LGN). These authors felt that the pattern of loss of dendritic spines was a direct reflection of the localization of the presynaptic terminals. In a companion study on mice, Valverde (1971) reported identical findings in the visual cortex following decreased sensory stimulation. This author felt that subsequent spine loss was a direct consequence of a diminished visual input from the corticopetal fibers. Similarly, entorhinal lesions have been shown to produce a 30% reduction in the number of spines within the outer molecular layer of the dentate gyrus (Lynch, Brecha, Cotman and Globus, 1974). Reinnervation of this layer by commissural and cross temporoammonic fibers (Lynch, Mosko, Parks and Cotman, 1973; Steward, Cotman and Lynch, 1973) occurs simultaneously with a restoration of a normal spine complement (Lynch et al., 1974). Identical findings have been reported in the septal nuclear complex following fimbrial lesions (Raisman and Field, 1973). Provided a sufficient number of afferents exist, neurons appear capable of generating

their normal complement of spines independent of the type of afferent fibers (Lynch et al., 1974).

Few investigations have attempted an ultrastructural analysis of the dendritic alterations following deafferentation. Benes, Parks and Rubel (1977) reported a reduction in the density of dendritic profiles (85%) following dorsal cochlear tract transection in young chickens. Glees et al. (1967) and Ghetti, Horoupian and Wisniewski (1975) studied the Lateral geniculate nucleus (LGN) in the monkey following enucleation and reported dendritic profiles having a watery appearance (electron-lucent) or containing tubulovesicular-complexes from 7 days following enucleation. LeVay (1971) and Berger (1973) reported similar changes in the lateral geniculate body and olfactory system of the cat and rabbit respectively as late as 29 months following deafferentation. The most recent examination has reported transneuronal changes in the Purkinje cell dendrites of the cerebellar cortex following long-term survival from 3-acetylpyridine intoxication (Desclin and Colin, 1980). Along with the electron-dense appearance typical of degenerating profiles, Purkinje cell dendrites devoid of their climbing fiber input showed an abnormal accumulation of mitochondria and the development of an extensive tubulovesicular system.

Various studies have investigated the effects of deafferentation of postsynaptic structures. Gutman and Young (1944) suggested that a loss of the postsynaptic membrane thickening occurred following deafferentation. In a later study, Gray and Hamlyn (1962) reported similar findings following deafferentation of the optic tectum in adult chickens. McMahan (1967) suggested that deafferentation in the lateral geniculate nucleus of rats caused a disruption of the subsynaptic

formation (a dense band localized on the cytoplasmic side of the postsynaptic differentiation); however, Sotelo (1968) reported no change in the postsynaptic differentiation (the layer of amorphous dense material found apposed to the postsynaptic plasmalemma) or the subsynaptic formation following preganglionic deafferentation of the VII and IX abdominal sympathetic ganglia. Many studies have indicated that degenerating terminals can be removed from their postsynaptic site without interfering with the integrity of the postsynaptic membrane (Gray and Hamlyn, 1962; Westrum, 1966; Pinching, 1969; Lund and Lund, 1970; Pinching and Powell, 1971; Westrum and Black, 1971; Lund, 1972). Others have suggested that phagocytic cells (both astrocytes and microglia) remove both the pre- and postsynaptic membranes following deafferentation (Colonnier, 1964; Ghetti and Wisniewski, 1972; Wisniewski, Ghetti and Horoupian, 1972). The role of dendrites in phagocytizing degenerating terminals was first observed by Walberg (1963) in a study of the olivary nucleus of the adult cat and has subsequently been reported to occur in the spinal cord (Conradi, 1969), the ventral cochlear nucleus (Gentshev and Sotelo, 1973), the nucleus gracilis (Rustioni and Sotelo, 1974) and the visual system (Ghetti and Wisniewski, 1972; Wisniewski et al., 1972; Ghetti et al., 1975).

##### 5. Secondary and Tertiary Atrophy

Powell and Erulkar (1962) and Matthews and Powell (1962) were among the first to suggest that the transneuronal degenerative effect could be transmitted successfully across several successive synaptic junctions. Until recently, few reports have described such changes beyond the site of afferent removal. Powell and Erulkar (1962)

found unexpected secondary transneuronal changes in several of the auditory relay nuclei (lateral superior olive and medial trapezoid nucleus) following destruction of the spiral ganglion, and suggested from the overall appearance of the contralateral lateral lemniscus and the ipsilateral preolivary nuclei that these auditory relay nuclei might subsequently undergo similar changes. The findings obtained from their quantitative studies clearly suggest that the time-course and severity of degeneration within the primary and secondary relay nuclei are similar, although the changes within the second order nuclei must be consequent to those in the cochlear nuclei. Following the examination of thionin-stained preparations, secondary transneuronal changes have been suggested in the granule cells of the olfactory bulb following surgical destruction of the nasal mucosa (Matthews and Powell, 1962). Likewise, Hamori (1969) has found transneuronal degeneration of the granule cell dendritic digits following extensive neocortical ablation and Valverde and Esteban (1968) have found tertiary anterograde transneuronal changes within the visual cortex of mice. Enucleation at birth was found to result in a significant loss of spines along the apical dendrites in layer III of the ipsilateral peristriate cortex (that portion of the tree receiving contralateral fibers from the striate cortex) within 24-48 days. As pointed out by Cowan (1970), these changes suggest that the original effect of deafferentation may not be confined to cells of direct innervation, and subsequent second and third order neurons may also become involved.

#### 2.4 Abnormal Cerebellar Development

Although little information is available on the synaptic

reorganization of the adult cerebellum, the effects of various experimental influences on cerebellar development have been well documented. In neonatal studies, lesions have been introduced to establish the influences exerted by the affected elements on normal cerebellar development. In altricial mammals, synaptogenesis and the acquisition of a cerebellar microneuronal population are a postnatal phenomenon which occurs during the first three weeks (Altman, 1976; Altman and Das, 1966). The majority of microneurons are generated between the second and third postnatal week (Altman, 1969, 1972c).

The maturation of the Purkinje cell soma and the dendritic arborization was described in the early work of Ramon Y Cajal and has since been examined in several different species (Larramendi, 1969; Mugnaini, 1969; O'Leary et al., 1970; Altman, 1972b; Berry and Bradley, 1976c). Tissue culture studies (Privat and Drian, 1974, 1976; Privat, 1975) have shown an inherent growth potential within Purkinje cells for the elaboration of a dendritic system, although their plane of orientation and localization of dendritic specializations appear to be dependent upon the presence of the afferent input (Kawaguchi, Yamamoto, Mizuno and Iwahori, 1975; Bradley and Berry, 1975, 1978; Privat and Drian, 1976; Berry and Bradley, 1976b,c).

Using specific schedules of low-level x-irradiation during postnatal development, Altman and Anderson prevented the acquisition of specific cerebellar microneurons (basket, stellate or granule cells). The monolaminar dispersion of Purkinje cells has been shown to be dependent upon an adequate cell proliferation within the external germinal layer (Altman and Anderson, 1973). X-irradiation schedules, which selectively prevent basket cell formation, have shown that these cells

are important for the maturation of the Purkinje stem (main) dendrites since their absence has resulted in the formation of twisted and entangled dendrites (Altman, 1976a). The postponement of x-irradiation beyond basket cell acquisition (Altman, 1976b), while ensuring the proper formation of the stem dendrites, has been found to prevent both stellate cell formation and the growth of the smooth branches of the Purkinje cell dendritic arborization. Altman has postulated that their outgrowth was dependent upon an interaction with the maturing stellate cell axon during postnatal neurogenesis.

#### A. Parallel Fiber Removal

##### 1. The Effect on Purkinje Cell Development

The finding that synapses can occur on dendritic growth cones and their filopodial extensions suggested a morphological basis for the afferent control of dendritic growth (Morest, 1968, 1969a,b). It has been hypothesized more recently that dendritic growth and branching are controlled by a synaptogenic interaction between the filopodia of dendritic growth cones and the afferent input (Skoff and Hamburger, 1974; Vaughn, Henrikson and Frieshaber, 1974; Berry and Bradley, 1976a). Once a filopodium is engaged synaptically, the growth cone is transposed beyond the synapse and a definitive dendritic branch results. Contact with more than one filopodium from the same growth cone initiates various degrees of branching (Bradley and Berry, 1976b). This theory suggests that dendritic development occurs as a result of an interaction between growing dendrites and their afferent input (Bradley and Berry, 1978) and that the number of dendritic segments and the degree of branching is directly related to the available synaptic input (Berry and Bradley,



1976a,c). Further, in the absence of sufficient afferent input, dendritic growth and branching is greatly reduced due to a lack of synaptically engaged filopodia (Bradley and Berry, 1978).

The sensitivity of the external germinal layer to various agents during postnatal neurogenesis has been demonstrated by a loss of the precursors of cerebellar microneurons, thereby depriving the adult cerebellar cortex of its normal complement of intrinsic neurons. The effects of parallel fiber-deafferentation on the development of the Purkinje cell dendritic tree have been examined in various types of agranular cerebella produced as a result of chemical toxins such as cycasin (Hirano, Dembitzer and Jones, 1972), cyclophosphamide (Nathanson, Cole and Van der Loos, 1969) and fluxuridine (Langman, Schimade and Rodier, 1972), postnatal x-irradiation (Schmidt, 1962; Altman, Anderson and Wright, 1968; Hamori, 1969; Altman, 1972a,b,c, 1973, 1976a,b,c; Altman and Anderson, 1971, 1972, 1973), parvovirus infection (Kilham and Margolis, 1964, 1965, 1966a,b; Herndon, Margolis and Kilham, 1971a,b; Llinas, Hillman and Precht, 1973), the neurological mutants staggerer and weaver (Sidman, 1968; Rezai and Yoon, 1972; Hirano and Dembitzer, 1973; Sotelo and Changeux, 1974; Herndon and Oster-Granite, 1975; Hirano and Dembitzer, 1975; Sotelo, 1975a,b; Rakic, 1975; Sotelo and Privat, 1978) or the surgical removal of the embryonic rhombic lip (Forstronen, 1963). The reduction in Purkinje cell dendritic growth associated with the agranular cerebella has been suggested as a result of parallel fiber depletion (Altman and Anderson, 1971, 1972, 1973; Herndon et al., 1971b; Bradley and Berry, 1975, 1976a; Berry and Bradley, 1976c; Privat and Drihan, 1976). Many of the Purkinje cell dendritic arborizations in degranulating experiments were characterized by massive primary dendritic

trunks and a sparse complement of secondary and tertiary branches and spiny branchlets (Herndon et al., 1971b, Altman and Anderson, 1972, 1973; Berry and Bradley, 1976c; Privat and Drian, 1976). Recently, the proliferation of the Purkinje cell spiny branchlets has been shown to be dependent upon the presence of the parallel fiber milieu (Sidman, 1968; Rakic, 1971, 1974; Altman, 1973; Mirano and Dembitzer, 1975; Rakic, 1975; Sotelo, 1975). In addition, several studies have suggested that the plane of orientation of the cerebellar dendritic trees (Purkinje, basket and stellate) is guided by the parallel fiber system (Altman, 1973; Llinas et al., 1973; Altman, 1976a,c; Bradley and Berry, 1976b).

Although spiny branchlets are rare in degranulating experiments, several studies have described the ectopic development of two distinct types of spines along the surface of large caliber Purkinje cell dendrites. The first type has morphological characteristics similar to those found on normal spiny branchlets (Herndon et al., 1971b; Hirano and Jones, 1972; Privat and Drian, 1976; Berry and Bradley, 1976c; Bradley and Berry, 1978), while the second type has been described as a "giant spine" (Bradley and Berry, 1976a,c). The configuration of the degranulated Purkinje cell dendritic tree often has a "weeping willow" appearance which is consistent with the filopodial synaptogenic hypothesis (Bradley and Berry, 1975, 1976a). Bradley and Berry have suggested that the lack of parallel fiber acquisition at the surface of the molecular layer in degranulated cerebella would force Purkinje cell dendrites to grow downward in the direction of the Purkinje cell layer in an attempt to seek out the few parallel fibers which would be added to the molecular layer through continued axonal growth of existing parallel fibers (Bradley and Berry, 1976a).

## a) Dendritic Spines

The development and persistence of Purkinje cell dendritic spines following parallel fiber-deafferentation had been shown in agranular cerebella following x-irradiation (Altman and Anderson, 1972, 1973; Altman, 1976b,c) and in neurological mutants (Sidman, 1968; Sotelo, 1975a; Rakic and Sidman, 1973c; Mariani, Crepel, Mikoshiba, Changeux and Sotelo, 1977). This finding contrasted sharply with their reported loss following surgical transection of the parallel fiber input (Hamori, 1966; Mourén-Mathieu and Colonnier, 1969). More recently, observations on cerebellar tissue cultures treated with methylazoxymethanol (MAM) have suggested that spine formation may be genetically controlled (Priyat and Drian, 1974, 1976). In addition, postsynaptic membrane specializations are abundant in degranulated cerebella (Herndon et al., 1971b; Altman and Anderson, 1972; Hirano et al., 1972; Llinas et al., 1973; Rakic and Sidman, 1973c; Rakic, 1975; Altman, 1976b), a finding which Rakic (1975) has interpreted to suggest that postsynaptic membrane specializations are not regulated by a presynaptic influence.

In weaver cerebella the postsynaptic spines remain asynaptic, even in the vicinity of climbing, stellate and basket cell axons which normally establish synaptic contacts along the smooth portion of the Purkinje cell soma and dendritic shaft (Rakic and Sidman, 1973c; Rakic, 1975). Judging from the analysis of both weaver and reeler mutants, Purkinje cell dendritic spines display little affinity for heterologous contacts. Afferent fibers contacting Purkinje cells are highly selective as to their postsynaptic surface (Rakic, 1975). At the present time, most researchers believe that Purkinje cell dendritic spines develop autonomously, independent of any direct presynaptic

influence (Hirano and Dembitzer, 1973, 1974, 1975; Rakic and Sidman, 1973a,b,c; Sotelo, 1973, 1975a,b; Sotelo and Arsenio-Nunes, 1976; Landis and Reese, 1977). However, it has been suggested that asynaptic Purkinje cell dendritic spines induce parallel fiber sprouting in weaver mutant material (Herndon et al., 1971b) and following cerebellar folial transections (Mouren-Mathieu and Colonnier, 1969).

Hamori (1973) has postulated that the climbing fiber input is responsible for spine induction and maintenance, although tissue culture studies (Seil and Herndon, 1970) have clearly shown spine formation in the absence of an afferent input. Because degranulating techniques fail to eliminate all parallel fiber contacts, the suggestion has been made that a one-to-one relationship with dendritic spines may not be essential for parallel induction. Instead, a small proportion of parallel fiber contacts may be sufficient to trigger spine formation over the entire dendritic tree (Hirano and Dembitzer, 1974). Likewise, the production of postsynaptic receptor protein is thought to be an autonomous process which may depend on its regulation from the granule cell - Purkinje spine synapse (Sotelo, 1975a). In the degranulated mutant, weaver, which lacks this neuronal circuit, an overproduction of postsynaptic differentiation generally occurs.

#### B. Climbing Fiber Removal

##### 1. The Effect on Purkinje Cell Development and Maintenance

As a result of the intimate association between the climbing fiber and the Purkinje cell dendritic tree during maturation, Kornuth and Scott (1972) and Berry and Bradley (1976c) anticipated a possible trophic influence. Destruction of the inferior olivary nucleus in newborn kittens

suggested a possible trophic influence from the olivocerebellar system (Kawaguchi et al., 1975). These findings revealed a reduced dendritic branching pattern following olivocerebellar deafferentation. Many of the main stem dendrites were reported to extend unbranched through the molecular layer. Several other studies have supported such a reduction in the size of the dendritic tree following climbing fiber deafferentation in immature animals (Privat, 1975; Bradley and Berry, 1976b; Privat and Drian, 1976; Sotelo and Arsenio-Nunes, 1976). While electron microscopic observations have suggested a transneuronal degeneration of Purkinje cell dendrites following a loss of the olivocerebellar input (Desclin and Colin, 1980), network analysis of Golgi preparations has challenged its existence in the adult (Bradley and Berry, 1976c).

a) Dendritic Spines

It has been suggested that presynaptic afferents exert an important trophic influence on spine formation, following an examination of maturing brain tissue (Scheibel and Scheibel, 1971) and tissue cultures (Kruger, Hamori, Miller, Varon and Maxwell, 1970). Recent tissue culture experiments (in the absence of extracerebellar afferents) on newborn cerebellum have suggested that somatic and dendritic spines have an autonomous origin (Calvet, Drian and Privat, 1974; Privat and Drian, 1974). In fact, an ectopic development of spines has been shown along the main dendritic shafts of rat Purkinje cells (Seil and Herndon, 1970; Privat, 1975). Developmental studies in mice have revealed an absorption of dendritic spines along the smooth portion of the Purkinje cell dendritic tree upon climbing fiber contact (Larramendi and Victor, 1966) although many of these spines have been reported to have contacts with parallel fiber varicosities (Meller and Glees, 1969; Mugnaini, 1969;

Altman, 1972b).

Desclin and Colin's findings (1980) support an earlier interpretation of Hamori (1973) that climbing fiber deafferentation results in a significant loss of Purkinje cell dendritic spines following climbing fiber-deafferentation of adult rats. In unpublished findings, Zabersky and Hamori have estimated this loss to exceed 40% of the total spine population and have suggested an indirect heterotopic induction by olivocerebellar afferents. Several recent studies have failed to confirm these findings and instead support a redistribution of dendritic spines following climbing fiber-deafferentation (Bradley and Berry, 1975, 1976b, c; Sotelo and Arsenio-Nunes, 1976). Contrary to earlier reports, climbing fiber-deafferentation prior to Purkinje cell dendritic development has been found to result in the production of large ectopic spines along previously smooth portions of the Purkinje cell dendritic tree (Bradley and Berry, 1975, 1976b). Likewise, in adult rats Sotelo et al. (1975) have found that climbing fiber removal results in an increase in spines along secondary and tertiary Purkinje cell dendrites. The neonatal studies suggest that spine resorption may not occur along the main dendrites in the absence of climbing fibers (Bradley and Berry, 1975, 1976b).

The reported increases in dendritic spines emerging from the tertiary and secondary dendritic branches following olivocerebellar deafferentation of adult rats have been confirmed with the electron microscope (Desclin and Colin, 1980). In addition, parallel fiber varicosities have recently been shown to form synaptic contacts with ectopic spines, and a sprouting of these parallel fibers has been suggested as a result of their increased multiple synaptic contact with

the dendritic spines (Sotelo and Arsenio-Nunes, 1976): Axon terminals of stellate cells and ascending collaterals of basket cells have also been found to innervate these ectopic spines (Sotelo and Arsenio-Nunes, 1976).

The ectopic spines, on the distal portions of the main stem dendrites following 3AP treatment in adult rats (Bradley and Berry, 1976c) contrast with the dendritic and somatic distribution of ectopic spines from Purkinje cells deafferentated from birth (Sotelo and Arsenio-Nunes, 1976).

### C. Mossy Fiber Removal

#### 1. The Effect on Granule Cell Dendrites

Few studies have been published concerning the effects of mossy fiber-deafferentation on the adult or weanling cerebellar cortex. Short-term lesions have yielded two distinct forms of degeneration (an electron-dense and an electron-lucent type) within the mossy fiber glomeruli of the cat following peduncular transections (Smith et al., 1966). Mugnaini (1972) and Palay and Chan-Palay (1974) have examined the time course of the degenerative changes within the spinocerebellar afferents of the cat and rat following cervical hemisection. In neonatal cerebella permanently deprived of their pontocerebellar input the postsynaptic granule cell dendritic microspines failed to develop (Hamori, 1969). Furthermore, under identical experimental conditions Purkinje cell dendritic spines were found to undergo anterograde tertiary transneuronal atrophy, becoming altered in shape and significantly reduced in size (Uzunova and Hamori, 1974).

#### 2.5 Synaptic Remodeling Within the Central Nervous System

It is now well established that the mammalian central

nervous system has a substantial capacity for synaptic reorganization following localized lesions despite its poorly developed regenerative properties (Clement, 1964; Bernstein, 1967). However, several authors have reported sprouting of intact afferent systems adjacent to the deafferentated zones which often results in heterotypical reinnervation of vacated synaptic sites. This type of reinnervation appears to constitute the major form of reconstruction within most parts of the central nervous system.

Under normal circumstances the effects of nerve fiber transection within the mammalian central nervous system are irreversible and regeneration does not occur. However, recent observations have suggested that central adrenergic fibers are capable of regeneration following axonal transection (Bjorklund and Stenevi, 1971; Bjorklund, Katzman, Stenevi and West, 1971; Katzman, Bjorklund, Owan, Stenevi and West, 1971; Stenevi, Bjorklund and Moore, 1973). Denervated irides transplanted within the medial forebrain bundle were densely innervated by sprouts from transected adrenergic axons (Bjorklund and Stenevi, 1971), a result which has been enhanced following nerve growth factor administration (Bjorklund and Stenevi, 1971; Bjerre, Bjorklund and Stenevi, 1973). In addition, cholinergic axons from the septo-hippocampal pathway have also been shown to sprout into iris transplants (Stenevi et al., 1973; Svenggaard, Bjorklund and Stenevi, 1976). A marked increase in the adrenergic input to the molecular layer of the cerebellar cortex has been reported following incomplete damage to the afferents from locus ceruleus (Pickel, Krebs and Bloom, 1973). Devor (1976) has reported similar activity upon pruning the distal branches of axons in the lateral olfactory tract. Anterograde transport of tritiated proline has suggested



a regeneration of corticospinal tract connections at lower spinal cord levels following complete mid-thoracic spinal cord transections in rats (Feringa, Shuer, Vählsing and Davis, 1977).

An investigation into the possibility of axonal sprouting within the central nervous system was not conducted until the 1950's. The first indication that such a form of remodeling exists came following spinal cord deafferentations (Liu and Chambers, 1958). Intact dorsal roots were found to sprout extensively into denervated areas of the cord following dorsal root and corticospinal tract transections. At about that time, intact preganglionic fibers were also shown to sprout and reinnervate denervated superior cervical ganglion cells (Murray and Thompson, 1957; Guth and Bernstein, 1961). Barnes and Worrall (1968) have suggested that axons of lower motor neurons regenerate into the dorsal horn of the spinal cord if anastomosed to a dorsal root. Tritiated leucine labeling and acetylcholinesterase staining (Burgin and Chipman, 1951; Snell, 1961; Koelle, 1963) have indicated that these axons regenerate centrally along the dorsal root pathways (Ochs and Barnes, 1969). One of the most significant studies to suggest the existence of axonal sprouting involved an examination of the deafferented rat septal nuclear complex (Raisman, 1969). Long-term removal of hippocampal afferents by means of fimbrial lesions revealed a marked increase in the multiple synaptic index of healthy hypothalamic afferents (control material has shown the majority of the hypothalamic axon terminals to be in synaptic contact with only one postsynaptic profile). Raisman (1969) suggested that the sites left vacant by the removal of degenerating endings were reinnervated by adjacent healthy terminals and thus acquired more than one synaptic contact. More recently, Moore, Bjorklund and

Stenevi (1971) have re-examined this question using a fluorescence histochemical approach. The catecholamine terminals of the medial forebrain bundle were monitored following fimbrial lesions using the Falck-Hillarp fluorescence technique. The increased density of the adrenergic innervation to those septal nuclei which normally receive a significant hippocampal projection was suggestive of a sprouting within the norepinephrine input to the septal nuclear complex. The data collected thus far indicates that adrenergic neurons have the capacity for both regeneration and collateral sprouting.

The precise lamination of afferent projections to the dentate gyrus has prompted several workers to investigate its capabilities for plastic change. Silver degeneration studies have shown that the septo-hippocampal fibers from the medial septal nucleus form two distinct zones within the dentate gyrus, one immediately below the commissural terminals (among the superficial granule cells) and the other just below the granule cell layer (Raisman, Cowan and Powell, 1965). Shute and Lewis (1961), reported a high concentration of acetylcholinesterase (AChE) in the septal fibers and terminals of the septo-hippocampal tract. This prompted Lynch and his colleagues to employ AChE histochemistry as a measure of septal fiber innervation. An increase in the level of acetylcholinesterase and choline acetyltransferase was reported in the outer molecular layer of the dentate gyrus following perforant path lesions in adult rats (Lynch, Matthews, Mosko, Parks and Cotman, 1972; Storm-Mathisen, 1974) and immature rats (Cotman, Matthews, Taylor and Lynch, 1973; Nadler, Cotman and Lynch, 1973) and was localized with the electron microscope within axon terminals which innervate the denervated portion of the molecular layer. Electrolytic lesions of the medial

septal nucleus have revealed that this increase in AChE in the outer molecular layer is dependent on the integrity of the septo-hippocampal fibers (Storm-Mathisen, 1974). It was therefore suggested by Storm-Mathisen (1974) that the loss of entorhinal terminals initiated a massive growth of septal fibers which reinnervated regions vacated by the entorhinal lesions. Unilateral entorhinal lesions denervated the outer three quarters of the dentate gyrus molecular layer and eliminated approximately 90% of the synaptic terminals (Matthews, Cotman and Lynch, 1976). The subsequent denervation of this granule cell domain in both immature and adult rats has resulted in an ectopic reinnervation by commissural fibers (Lynch et al., 1973; Lynch, Stanfield and Cotman, 1973), ipsilateral associational fibers (Lynch, Gall, Rose and Cotman, 1976) contralateral entorhinal fibers (Steward, Cotman and Lynch, 1974; Steward, White, Cotman and Lynch, 1976; Steward and Vinsant, 1978) and septo-hippocampal fibers (Lynch et al., 1972; Storm-Mathisen, 1974). All of these systems have been interpreted as expanding their axonal domains by collateral sprouting. In addition, several of these newly sprouted systems have been shown to form electrophysiologically viable projections, e.g. the crossed perforant path (Steward et al., 1976) and the commissural expansion (Lynch, Deadwyler and Cotman, 1973). Although axonal sprouts from several different afferent centers frequently reinnervate an area, this process under certain circumstances can be rather selective with regards to the afferent type (Lynch, Stanfield, Park and Cotman, 1974). For instance, following commissural/associational deafferentation of the inner molecular layer of the dentate gyrus, adjacent septal and entorhinal projections were not able to sprout and reoccupy the vacated synaptic sites. A commissural/association zone

which is unreceptive to either septal or entorhinal fibers has been postulated for the granule cell dendritic tree, even though temporal factors make these fibers the most appropriate terminals for reinnervation (Lynch et al., 1974). Likewise, the spinal nucleus of the trigeminal nerve (Kerr, 1971) and the medial superior olive (Liu and Liu, 1971) appear refractory either to forming sprouts or to accepting new ones. Beech and Raisman (1980) have reported an ectopic sprouting of fibers within the medial mammillary nucleus following either long-term fimbrial or dorsal fornical lesions in adult rats.

Quantification of the electron microscopic observations has provided unequivocal support for axonal sprouting of the commissural and ipsilateral associational afferents following specific deafferentation (Lee, Stanford, Cotman and Lynch, 1977; McWilliams and Lynch, 1978). Following perforant path lesions, the middle molecular layer of the hippocampus showed a gradual restoration in its synaptic bouton density which could not be attributed to an increase in the multiple synaptic index or an enlargement of the presynaptic terminals. Rather, these findings suggested that the generation of an entirely new collateral system had occurred (Lee et al., 1977). Likewise, unilateral hippocampectomies, which resulted in a loss of contralateral commissural fibers, were found to cause a temporary reduction in the synaptic bouton density (36%) of the inner molecular layer of the dentate gyrus, although normal bouton levels had returned by 75 days post-lesioning (McWilliams and Lynch, 1978). The formation of a new fiber tract (crossed perforant path) has recently been described following unilateral entorhinal lesions in both immature (Steward et al., 1973) and adult rats (Steward et al., 1974). These fibers have been found to terminate in the

region denervated by contralateral entorhinal lesions and are capable of monosynaptically activating the contralateral dentate gyrus (Steward et al., 1974). The extensive growth of the contralateral entorhinal fibers and accompanying synapse formation has not been previously shown in the mature central nervous system.

In adult systems, light and electron microscopic studies have shown a time lag of 5 days prior to the expansion of the commissural/associational system into the deafferentated outer molecular layer (Lee et al., 1977; Lynch, Gall and Cotman, 1977), an innervation which usually involves only the adjacent 50  $\mu$ m of the denervated zone (Gall and Lynch, 1978). On the other hand, if perforant path lesions were performed within the first two postnatal weeks the commissural/associational system was found to innervate the entire width of the denervated zone within 48 hours following deafferentation (Lynch et al., 1973; Zimmer, 1973; Gall and Lynch, 1978). These findings would seem to suggest that the maturation of neuronal systems limits both the speed and extent to which axonal sprouting can occur within the central nervous system. Devor (1975) has suggested that the extent of axonal growth is genetically predetermined (Devor, 1975). The axonal growth (sprouting) which frequently occurs following deafferentation, then, might be subsequent to an equivalent absorption of its axon terminal field in another area. Several authors have investigated this possibility and have reported no change in the terminal field projection as a result of axonal sprouting (Gall, McWilliams and Lynch, 1979).

The evidence favoring synaptic reinnervation suggests some form of cytochemical recognition between the postsynaptic membrane and its afferent input. Gottleib and Cowan (1972) attempted to test this

possibility in the dentate gyrus, where ipsilateral associational and commissural fibers terminate in the same region and on identical segments of the dentate dendrite. Their autoradiographic studies suggested that a complex interaction occurs between these two afferent systems and that their final distribution is dependent upon the relative numbers of each during synaptogenesis. In view of these findings, Gottlieb and Cowan postulated that immature axons may be cytochemically marked in a general way to form connections with a limited portion of their target neurons, but that their final distribution depends upon a competitive interaction for the available synaptic membrane.

That terminal field projections often depend upon complex interactions between corresponding fiber systems has been suggested in the developing systems which supply bilateral structures (Hicks and D'Amato, 1970; Leong and Lund, 1973; Lund, Cunningham and Lund, 1973). Retinal lesions have demonstrated that decussation through the optic chiasm depends upon such an interaction. A partial loss of retinal projections resulted in a modified growth pattern for the corresponding retinotectal fibers which had not yet reached the optic chiasm. These fibers were often prevented from decussating and thereby induced an anomalous ipsilateral projection. Unilateral ablation of the corticofugal pathway (Leong and Lund, 1973) or transection of the corticospinal tract (Hicks and D'Amato, 1970) has resulted in the formation of anomalous bilateral projections to the pons, superior colliculus and spinal cord in immature rats. In each case, the anomalous pathways were thought to form as a result of a re-routing of axons due to a lack of the normal "guidance factors", which depend on an interaction with the contralateral pathway. Similarly, the retinohypothalamic projection has shown an

anomalous ipsilateral projection pattern following neonatal eye removal (Stanfield and Cowan, 1976). Unfortunately, this finding could be explained as the result of either collateral sprouting or the re-routing of fibers at the optic chiasm.

Goodman and Horel (1967) studied axonal sprouting of the optic tract projections as a consequence of occipital cortex removal. Sprouting was observed in the ventral lateral geniculate nucleus, the lateral nucleus of the optic tract and the pretectal nucleus, all of which are regions of convergence of the occipitofugal and retinofugal projections. Ralston and Chow (1973) and Stelzner, Baisden and Goodman (1976) have also reported axonal sprouting in the lateral geniculate nucleus after visual cortex removal.

Plasticity in the red nucleus has been demonstrated by both anatomical and physiological methods (Tsukahara, Hultborn, Murakami and Fujito, 1975; Nah and Leong, 1976a,b). Following neonatal sensorimotor cortical lesions in the rat, a contralateral corticorubral projection has been shown to develop from a corresponding region of the intact hemisphere (Nah and Leong, 1976a). This sprouting of a crossed projection gives rise to axon terminals which terminate synaptically in a manner similar to the normal corticorubral projection (Nah and Leong, 1976b). Similarly, Lim and Leong (1975) have demonstrated aberrant ipsilateral projections from the dentate and interposed nuclei to the red nucleus after neonatal lesions of the contralateral cerebellar nuclei. An ectopic localization of corticorubral terminals following a bilateral ablation of the interposed nuclei also suggests a sprouting of these fibers into the magnocellular portion of the red nucleus (Nakamura, Mizuno, Konishi and Sato, 1974).

Collateral sprouting within the hemisected spinal cord has frequently been described (McCouch, Austin, Liu and Liu, 1958; Bernstein and Bernstein, 1973) and its possible significance concerning functional recovery has recently been considered by Murray and Goldberger (1974). The results of this study suggest that collateral sprouting in the spinal cord after subtotal hemisection may have an adaptive significance in the mediation of recovery of certain movements. A re-occupation of vacated postsynaptic densities by inhibitory interneurons has been suggested within the deafferented nucleus gracilis following lumbo-sacral rhizotomy (Rustioni and Sotelo, 1974). Physiological studies have suggested an altered tactile receptive field within the nucleus ventralis lateralis posterior as a result of cuneate fiber sprouting following ablation of the nucleus gracilis (Wall and Egger, 1971).

It becomes apparent, therefore, that the central nervous system is not as refractory to reinnervation as previously suggested. The new afferents, however, are often ectopic in nature and in certain regions are restricted to specific afferent types.

## 2.6 Heterologous Synaptogenesis Within the Cerebellar Cortex

Several studies have reported a normal development of postsynaptic structures in the absence of afferent input, especially in agranular cerebella induced by x-irradiation (Altman and Anderson, 1972; Altman, 1976b) or other causative factors (toxins and neurological mutants) (Herridon et al., 1971b; Hirano et al., 1972; Llinas et al., 1973; Rakic and Sidman, 1973c; Sotelo, 1973, 1975a). Thus a condition might exist which would allow for the formation of heterologous or ectopic



Collateral sprouting within the hemisectioned spinal cord has frequently been described (McCouch, Austin, Liu and Liu, 1958; Bernstein and Bernstein, 1973) and its possible significance concerning functional recovery has recently been considered by Murray and Goldberger (1974). The results of this study suggest that collateral sprouting in the spinal cord after subtotal hemisection may have an adaptive significance in the mediation of recovery of certain movements. A re-occupation of vacated postsynaptic densities by inhibitory interneurons has been suggested within the deafferentated nucleus gracilis following lumbo-sacral rhizotomy (Rustioni and Sotelo, 1974). Physiological studies have suggested an altered tactile receptive field within the nucleus ventralis lateralis posterior as a result of cuneate fiber sprouting following ablation of the nucleus gracilis (Wall and Egger, 1971).

It becomes apparent, therefore, that the central nervous system is not as refractory to reinnervation as previously suggested. The new afferents, however, are often ectopic in nature and in certain regions are restricted to specific afferent types.

#### 2.6 Heterologous Synaptogenesis Within the Cerebellar Cortex

Several studies have reported a normal development of postsynaptic structures in the absence of afferent input, especially in agranular cerebella induced by x-irradiation (Altman and Anderson, 1972; Altman, 1976b) or other causative factors (toxins and neurological mutants) (Herndon et al., 1971b; Hirano et al., 1972; Llinas et al., 1973; Rakic and Sidman, 1973c; Sotelo, 1973, 1975a). Thus a condition might exist which would allow for the formation of heterologous or ectopic

synapses.

Several instances of heterologous synaptogenesis have been reported following postnatal x-irradiation. X-irradiation schedules which deafferentate either the Purkinje cell soma (Altman and Anderson, 1972, 1973; Altman, 1976a) or its main dendritic arborizations (Altman and Anderson, 1972, 1973; Altman, 1976b) have suggested that mossy fibers are capable of forming heterologous synapses with the synaptic surface vacated by basket and stellate cells. Mossy fibers have not been reported to extend beyond the Purkinje cell layer in normal animals. The possibility of a translocation of mossy fiber terminals occurring within the cerebellar cortex has been suggested following an examination of weaver mutant mice (Rakic and Sidman, 1973c) and x-irradiated cerebella (Altman, 1973; 1976b). Hypertrophied dendritic digits of ectopically positioned granule cells (located in the molecular layer) have been frequently contacted by mossy fibers (Rakic and Sidman, 1973c).

The greatest degree of non-specific synaptic receptiveness was expressed by the Purkinje cell dendritic thorns, which in addition to their normal climbing fiber synapses formed synaptic contacts with mossy fiber terminals (Altman and Anderson, 1973). Antimitotic agents which interfere with granule cell formation (Hirano et al., 1972) have induced the formation of similar atypical synapses. In methylazoxymethanol (MAM) treated cerebellar cultures, recurrent collaterals of Purkinje cell axons are capable of ectopically innervating Purkinje cell spiny branchlets (Calvet et al., 1974; Privat and Drian, 1974). Mossy fibers have been found to innervate Purkinje cell dendritic spines in weaver cerebellum (Sotelo, 1973), irradiated cerebellum (Altman and Anderson, 1972) and feline panleukopenia virus infected cerebellum (Llinas et al., 1973).

Since the main postsynaptic partner of the mossy fiber terminal is the granule cell dendrite, the loss of the target cell in agranular cerebella appears to be rectified by an increased postsynaptic contact with Golgi cell dendrites (Kilham and Margolis, 1966a,b; Rakic and Sidman, 1973c; Sotelo, 1975a, 1977; Sotelo and Privat, 1978). The persistence of mossy terminals despite granule cell depletion has suggested that their contact with Golgi cell dendrites is sufficient to prevent retrograde degeneration (Herndon et al., 1971a). Furthermore, a direct mossy fiber input to the inhibitory interneurons (stellate cells) has been demonstrated following feline panleukopenia virus infection (Llinas et al., 1973).

The most important difference between the cerebellar circuitry of mutants and those exposed to x-irradiation concerns the Golgi cell. If the x-irradiation schedule has prevented basket and stellate cell acquisition (loss of the inhibitory input to the Purkinje cell), the morphological development of presynaptic vesicular grids has been shown to occur in the Golgi cell soma and dendrites (Sotelo, 1977). A large proportion of these grids have been shown to form somato-dendritic and dendro-dendritic synapses with Purkinje cell dendritic spines. In agranular cerebella (weaver and reeler) in which a sufficient population of inhibitory cerebellar interneurons has not been maintained, the granule cells have been found to undergo identical morphological changes and synapse on similar portions of the Purkinje cell dendritic tree (Sotelo, 1975a; Mariani et al., 1977). However, when stellate and basket cells are present, mossy fibers have been found to establish heterologous synapses with the perikarya and dendrites of these interneurons (Llinas et al., 1973; Sotelo and Privat, 1978).

While the effects of various experimental influences

on cerebellar development in neonates have been well studied, these findings relate to plasticity in the mature cerebellum only indirectly since, in the mature cerebellum all of the cortical elements have completed growth, migration and differentiation. In the neonatal studies, the various treatments prevent the acquisition or migration of specific cell types during postnatal neurogenesis and they have thus been able to examine the influences exerted by these elements on the other components of the cerebellar cortex during development. A natural progression of the current state of knowledge is to employ those neuroanatomical and histochemical methods that have been used to study plasticity elsewhere in the central nervous system to examine the effects of deafferentation on the mature cerebellum.

## CHAPTER 3

### MATERIALS AND METHODS

Male Wistar rats both adult and weanling, were used as the experimental species in this investigation. The weanling rats ranged in weight from 40 to 55 gms while the adults registered between 250 and 490 gms in body weight. The animals were watered and fed a standard diet (Purina rat chow) ad libitum and were housed in individual cages both pre- and post-operatively.

#### 3.1 Perfusion Apparatus and Technique

The perfusion apparatus consisted of a gravity-fed system having two 1 litre I.V. bottles and two drip sets (Flexitron solution administration set - Baxter Laboratories, Malton, Ontario). The two I.V. bottles were suspended about 1.5 m above the animal and each was fitted to a drip set which was joined distally to the other drip set by a plastic Y joint. A single tubing then connected the Y joint to a cannula. The rate of flow of the perfusate was regulated by an adjustable clamp around each of the tubes above the Y joint.

All animals were secured in the supine position to a wire mesh-topped dissecting stage. The rats were then anaesthetized with sodium pentobarbital (0.06 ml/100 gms/body weight) (Nembutal, Abbot Laboratories, Montreal) administered intraperitoneally. A midline incision through the skin and superficial fascia was extended from the sternal angle to the level of the umbilical region. The skin and fascia were reflected exposing the upper portion of the abdomen and the thoracic rib-cage. A transverse incision through the anterior abdominal wall was made immediately inferior to the thoracic diaphragm. The thoracic cavity was then opened bilaterally, cutting through the costal margin, the ribs and intercostal muscles on either side. The xiphoid process was then clamped with a haemostat and reflected rostrally to expose the mediastinum. The pericardial sac was incised and iridectomy scissors were used to slit the apex of the left ventricle. A cannula was then inserted into the ascending aorta by way of the left ventricle and clamped with haemostatic forceps. The right atrium was severed to permit egress of blood and perfusate. Each rat was perfused with 500 ml of perfusate over a period of about 30 minutes.

### 3.2 Operative Procedures

#### A. Inferior Olivary Nucleus.

Olivocerebellar-deafferentation of the rat cerebellar cortex was achieved using both chemical and electrolytic lesions.

##### 1. 3-Acetylpyridine

The neurotoxin 3-Acetylpyridine (3AP), a nicotinamide

antagonist, was used to induce degeneration of the inferior olivary complex. Sixty-five adult male Wistar rats were given a single intraperitoneal injection of 1.5%–2.0% 3AP (Sigma Chemical Co.) diluted in physiological saline using a dosage level of 65 mg/kg body weight (Desclin and Escubi, 1974). These concentrations produced a mortality rate of 50% (L.D.<sub>50</sub>). A similar pattern of olivary degeneration was incurred in weanling rats (forty) only following injections using a dosage level 50% more concentrated (95 mg/kg body weight) than that employed for adults.

## 2. Electrolytic Lesions and Injections

### a) Ventral Approach

Ten adult rats were anaesthetized by an intraperitoneal injection of sodium pentobarbital (0.06 ml/100 gms body weight). Their ventral aspects were shaved from the mental protuberance to the level of the sternal angle and swabbed with an antiseptic and germicidal agent (Zephiran chloride or iodine solution). The rats were then mounted on a stereotaxic frame (David Kopf Industries) whose upper incisor bar was placed 5.0 mm above the interaural line to accommodate full extension of the neck. With the rat in a stable position, the stereotaxic frame was rotated 180° to accommodate a parapharyngeal approach to the brain stem. A midline incision was made through the skin, extending from a point 0.5 cm rostral to the hyoid bone to the superior border of the pectoralis major muscle. The skin and superficial fascia were reflected exposing the supra- and infrahyoid muscles. The sternohyoid and omohyoid muscles were separated and

retracted exposing the more deeply lying infrahyoid muscles (the sternothyroid and thyrohyoid). Unilateral removal of these muscles was necessary to obtain direct access to the prevertebral layer of muscles. The carotid sheath, containing the common carotid artery, lies immediately anterior to these muscles and poses a major obstacle in the parapharyngeal approach to the inferior olivary complex. Following removal of the prevertebral layer of muscles, the space existing between the pharynx and carotid sheath was widened using retractors. At the inferior border of the hyoid bone, the pharynx and carotid sheath appear to run in close association to one another. Directly dorsal to this lies the atlanto-occipital joint which consists of an articulation between the lateral facets of the atlas and the condyles of the occipital bone. Using Ash burs (round 3) in a Robbins Dermasurgical drill, a small hole was made in the ventral aspect of the occipital condyle and atlas to expose the ventral surface of the medulla oblongata. In order to facilitate entry and prevent deflection of the electrode or the micropipette, the dura and arachnoid were incised.

Electrolytic lesions were made using stainless steel microelectrodes (Fredrick Haer & Co.) having an exposed tip length of 25  $\mu$ m and a shank diameter of 0.254 mm. A D.C. current intensity of 1.5 milliamperes was applied using a Stoelting Lesion Maker (G.H. Stoelting Co., Chicago, Ill.) for 10 seconds to create a lesion which was restricted to the inferior olivary complex in its dorso-ventral extent. Four separate co-ordinates, approximately 0.5 mm apart were used to obtain a complete but discrete ablation of the inferior



olivary complex.

Anatomically, the inferior olivary complex lies immediately dorsal to the pyramidal tract. Unless the electrode was angled, its placement necessitated passage through the pyramidal tract fibers. Any attempt at lesioning caused a firing of pyramidal tract fibers and thus violent skeletal muscle contractions. Because the inferior olivary complex lies behind the interaural line, muscular contractions frequently resulted in undesired dorsoventral movement which offset the stereotaxic lesion. In an attempt to eliminate this, neuromuscular blocking agents (succinylcholine 0.25 mg/kg/.1 ml and D-Tubocurarine 0.06 mg/kg/.1 ml) were administered intravenously via the external jugular vein immediately following the tracheal intubation of the animals on a respirator (Model 607 Harvard Apparatus Co., Inc.). Prior to tracheal intubation, atropine was administered through the saphenous vein to avoid excess mucus accumulation within the tracheal and broncheal passages.

Injections of [<sup>3</sup>H]-leucine (4,5-[<sup>3</sup>H]L-leucine, Amersham Corp., Oakville, Ontario) were made using a 5 µl Hamilton syringe fitted with a finely drawn glass micropipette with a tip diameter of about .25 mm. The tritiated amino acid was evaporated in a vacuum centrifuge and reconstituted in normal saline to give a solution with an activity of about 50 µCi/µl. The micropipette was then filled by capillary action and fitted onto the Hamilton syringe. An injection of 0.5 µl of the reconstituted tritiated amino acid solution was made over a period of 20 to 30 minutes. The micropipette was then left in place for at least 15 minutes after the injection was

completed in order to reduce the spread of the label along the micropipette tract.

Gelfoam, an absorbable gelatin sponge, was placed over the exposed brainstem for protection and to control hemorrhaging. Several tiers were cut to replace the extracted infrahyoid muscles. The suprahyoid muscles were then sutured back into place with Ethicon 000 plain catgut and the skin was drawn together and closed with either surgical clips or cotton sutures. As a precaution, the skin was then sprayed with an antibiotic solution (Sprayband antibiotic) and the animal was placed in a separate cage and allowed to recover.

B) Dorsal Approach

Fifteen adult Wistar rats were anaesthetized and the dorsal aspect of the cranium and cervical region shaved and sterilized as described (above). The rats were then mounted on a Kopf stereotaxic frame using the deGroot reference planes (1959). A midline incision was made through the skin and superficial fascia extending from bregma to the level of the superior angle of the scapula. The skin was retracted and the skull scraped free of membranous periosteum. The muscles over the dorsal cervical region which attach to the external occipital crest and occipital bone were detached using a double ended dissector (Sklar) and retracted with a haemostat. This approach provided a direct access to the atlanto-occipital joint. Using Ash burs (round 8) in a dermasurgical drill, a semilunar opening was made in the occipital bone immediately rostral to the atlanto-occipital joint. At this time, the dura and arachnoid membranes were stripped from the

caudal surface of the cerebellum so that the obex and dorsal median sulcus could be clearly visualized. Using this approach, the electrode could be placed within the inferior olivary complex without encroaching upon cerebellar tissue by orientating it at a 30° angle to the long axis of the medulla oblongata. Once placed correctly, a D.C. current of 2.0 milliamperes for 15 seconds was sufficient to create a suitable lesion to ablate the entire inferior olivary complex, unilaterally. Post-operative care was similar to that described (above).

#### B. Pontine Nuclei

Unilateral lesions were placed within the basilar pontine gray of 23 adult rats using the deGroot system (1959). A midline incision following the sagittal suture was extended caudally from bregma to the external occipital crest. The skin and superficial fascia were reflexed exposing the parietal portion of the cranium. The site of entry through the parietal bone was determined by extrapolating the stereotaxic co-ordinates to the skull surface.

Co-ordinates for the lesions were obtained by consulting the stereotaxic atlases for the rat provided by König and Klippel (1963) and by Pellegrino and Cushman (1967). Routinely, three co-ordinates 0.5 mm apart using a D.C. current intensity of 2.0 milliamperes for 10 seconds were used to obtain a unilateral pontine ablation.

Injections of [<sup>3</sup>H]-leucine were made stereotaxically with a 5 µl Hamilton syringe using the co-ordinates determined from the lesion experiments. The injection protocol followed was similar to

that described in the previous section for olivary injections. Post-operative care was similar to that described above.

### C. Lateral Cerebellar Hemisphere

#### 1. Parasagittal Cuts

Unilateral parasagittal cuts were made in the lateral cerebellar hemisphere of 23 rats. Parallel fiber transection was performed in twelve adult and eleven weanling rats. A midline incision following the sagittal suture was extended from bregma rostrally to the external occipital crest caudally. The skin and superficial fascia were reflected exposing the parietal and interparietal portions of the calvarium. Using a dermasurgical drill, a small hole was made in the cranium at the junction of parietal-interparietal suture and the external occipital crest. Rongeurs were used to remove the interparietal bone and portions of the occipital bone covering the caudal folia of the cerebellum, unilaterally. The dura and arachnoid were stripped from the surface of the cerebellum being careful not to damage the transverse sinus running along the attached border of the tentorium cerebelli.

Parasagittal cuts were performed using stainless steel razor blades which were pretrimmed to a triangular shape and clamped to a pair of forceps. Parasagittal cuts, traversing several folia in the lateral aspect of the cerebellar cortex (mainly Crus I, Crus II and Lobus simplex) were carried out on both weanling and adult rats. In

the adult rats parasagittal cuts were placed 5.0 mm lateral to the mid-vermal line, while in the weanlings folial transections were made approximately 4.0 mm lateral to this line. In either case, the lesions were standardized to the most lateral 2.0 mm of the cerebellar hemisphere. In the transverse plane, lesions varied between 1.5 and 2.5 mm in depth. Because of the planar organization of the perikarya of the molecular layer (parasagittal orientation) and the angular course of the climbing fiber and Purkinje cell axons within the white matter, these neuronal elements were found to be free of degenerative change in the area immediately medial to the parasagittal cut. As a result, tissue sampled in this area was found to contain primarily degenerating parallel fibers.

The opening within the cranium was closed with Hygienic Repair Acrylic (The Hygienic Dental Mfg. Co., Akron, Ohio). The skin was drawn together with either surgical clips or cotton sutures and sprayed with an antibiotic solution (Sprayband antibiotic). Postoperative care was similar to that described above.

## 2. Horseradish Peroxidase (HRP) Injections

Initially, an investigation of the topographical organization of the afferent systems to the cerebellar cortex was undertaken. Although the climbing fiber input to the cerebellar cortex has recently been shown to originate entirely within the inferior olivary nucleus, several centers are recognized as providing contributions to the mossy fiber system. Since the primary objective was to examine the short- and long-term effects of deafferentation on the cerebellar cortex, the

localization of a cortical area which received its mossy fiber afferent input from only one source would greatly simplify the procedure of deafferentation.

The dorsal surface of the cerebellar cortex was exposed as previously described for the parasagittal lesions. In these experiments, it was only necessary to remove the interparietal portion of the calvarium. Upon removal of the dura and arachnoid, the intercrural sulcus could be seen demarcating the boundary between the two crura of the ansiform lobule. Horseradish peroxidase (HRP Sigma, type VI) injections (0.3  $\mu$ l, 10-20% solution) were made into the intercrural sulcus of adult rats weighing 290 to 440 gms. The HRP was dissolved in saline and drawn up into a fine glass micropipette (tip diameter of about 0.25 mm) by capillary action. The micropipette was then sealed by wax to the needle of a 5.0  $\mu$ l Hamilton syringe (Reno, Nevada). All HRP injections were made using a stereotaxic holder. Injection sites were located within 2.0 mm of the lateral border of the cerebellum and approximately 0.5 mm deep to the intercrural sulcus. The peroxidase was slowly injected over a period of about 15-30 minutes.

### 3.3. Light Microscopic Methods

#### A. Preparation of Tissue for Normal Cytoarchitecture

Perfused brains were allowed to fix in situ during the first 24 hours, after which they were carefully dissected out and immersed in fresh fixative (10% formalin) for at least four weeks. The normal cytoarchitecture of the cerebellum, the inferior olive and the pons were investigated using both paraffin and frozen sections. Material for paraffin embedding was dehydrated in methyl alcohols, cleared in

terpineol and benzene, infiltrated through a series of paraffin changes and embedded. All paraffin blocks were sectioned transversely at 8  $\mu$ m and serially mounted on gelatin coated slides (Culling, 1963). Tissue which was to be cut on the freezing microtome was washed in running water for 2-4 hours prior to sectioning to remove the excess formalin. The tissue blocks were then cut transversely or parasagittally on a Leitz freezing microtome at 30  $\mu$ m and mounted on gelatin coated slides. The brainstems and cerebella were stained with cresyl violet or thionine (Davenport, 1960) then counter stained with Harris's hematoxylin and eosin (Drury and Wallington, 1967).

#### 1. Horseradish Peroxidase Technique

Following survival times of from 48-60 hours, the brains and spinal cords [levels cervical (C)<sub>8</sub>-thoracic (T)<sub>2</sub>, T<sub>12</sub>-lumbar (L)<sub>2</sub>, and sacral (S)<sub>3</sub>-S<sub>4</sub>] of 12 adult rats were processed for HRP histochemically using three different chromogens: DAB (3,3'-diaminobenzidine), BDHC (benzidine dihydrochloride) and TMB (3,3', 5,5'-tetramethyl benzidine). In the first series of rats (consisting of 7 animals) alternate sections of the brains and spinal cords were processed using DAB or BDHC as the chromogen. The animals were fixed by vascular perfusion with 1.0% paraformaldehyde and 1.25% glutaraldehyde in 0.1 M phosphate buffer (pH 7.2). The heads and spinal cords were immersed in fresh fixative overnight at 4°C and dissected out the following morning. The tissues were then transferred to 0.1M phosphate buffer (pH 7.3) with 5% sucrose for at least

overnight (4°C). The material was then transferred to a solution of 30% sucrose in 0.1M phosphate buffer (4°C) until the brains and spinal cords sank.

The tissues were cut on a freezing microtome (Leitz Kryomat) at 40 µm and collected at room temperature in a 0.1M phosphate buffer containing 5% sucrose. All sections were rinsed in distilled water prior to incubating. Two sections from every five serial sections through the brain and two sections from every ten serial sections through the spinal cord were processed using either DAB or BDHC as the chromogen. Half of the sections were incubated for 10 minutes in a freshly prepared bath containing 50 mg of 3,3'-diaminobenzidine (DAB) in 100 ml of phosphate buffer to which 3 ml of a 0.2% hydrogen peroxide solution was added (La Vail, 1975). The sections were then washed in 0.1M phosphate buffer and stored until mounted.

The remaining sections were processed according to the benzidine dihydrochloride (BDHC) method (Mesulam, 1976). The tissues were first processed for 20 minutes in a pre-reaction soak containing 50 mg of BDHC, 100 mg sodium nitroferricyanide, 5 ml of 0.2M acetate buffer (pH 5.0), 65 ml of distilled water and 30 ml of absolute ethanol. The enzymatic reaction was initiated by the addition of 4.0 ml of fresh 0.3% hydrogen peroxide (H<sub>2</sub>O<sub>2</sub>) per 100 ml of presoak solution. The tissues were then placed in this mixture and incubated for 25 minutes. Following incubation, the tissues were placed in cold stabilizer (4°C) containing 9 gms of sodium nitroferricyanide, 5 ml of 0.2M acetate buffer (pH 5.0), 45 ml of distilled water and 50 ml of absolute alcohol. The sections were then washed in 0.1M phosphate buffer and stored until mounted.

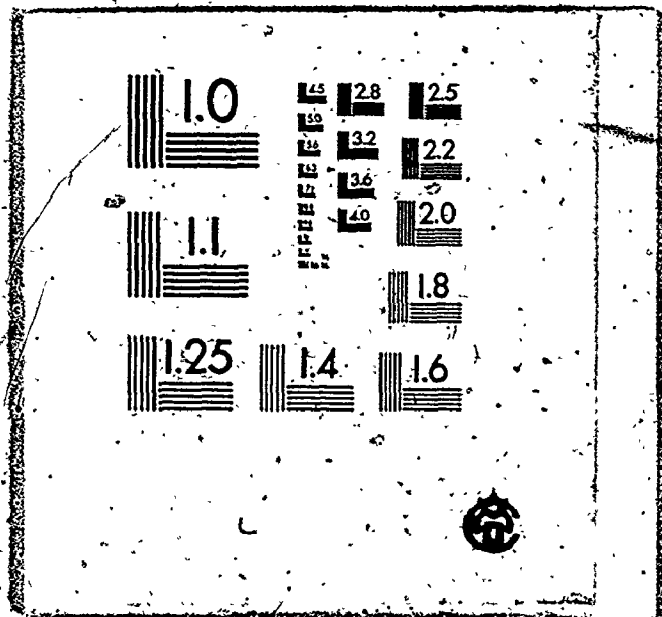


A second series (consisting of 5 animals), having similar survival times (48-60 h), was processed using the chromogen TMB (Mesuiam, 1978). In this series, the rats were initially exsanguinated with 50 ml. of physiological saline (0.9%) solution. Immediately following, the animals were fixed by vascular perfusion with 1.25% glutaraldehyde and 1% paraformaldehyde in 0.1M phosphate buffer at pH 7.4 for a period of 30 minutes. Excess fix was promptly removed by a second perfusion of 0.1M phosphate buffer solution containing 10% sucrose (4°C) for a similar time period. All tissues were removed and placed in the sucrose-buffer solution at 4°C for 12-24 hours. The brains and spinal cord segments were cut at 40 µm and collected in 0.1M phosphate buffer without sucrose. Tissue sections were stored at 4°C in the phosphate buffer for 9-48 h prior to incubation. Following a brief wash in distilled water, sections were soaked for 20 minutes at 19-23°C in a mixture of pre-reaction solution. The tissue was then removed from the solution and 4.0-8.0 ml of 0.3% H<sub>2</sub>O<sub>2</sub> was added. The tissue was then returned to this mixture and incubated for 20 minutes and subsequently transferred to cold stabilizer solution (4°C) as described for the BDHC method.

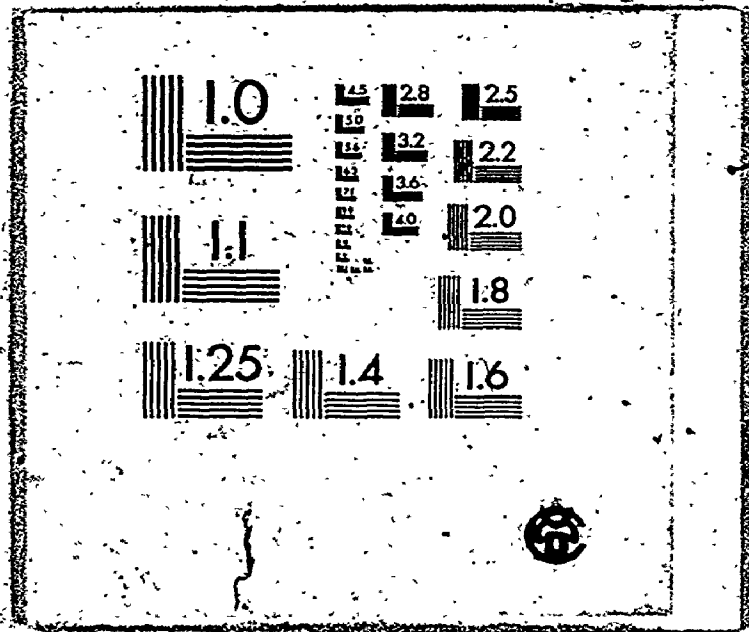
All sections were mounted on gelatin coated slides, dried and counterstained for 3 minutes in a 1% aqueous solution of neutral red (buffered at pH 4.8 with acetate buffer). The slides were then briefly washed in water (10 seconds), differentiated in graded alcohols (approximately 10 seconds in each concentration), cleared in xylene and coverslipped with Pro-texx mounting medium:

The localization of the injection site within the lateral cerebellar cortex was recorded and every twentieth section

# 1



2



through the brain and spinal cord was mapped for retrogradely labeled neurons under bright field optics with a camera lucida.

## 2. Golgi-Cox Technique

The cerebella of control, 3AP treated and mossy and parallel fiber-deafferentated animals were impregnated using Ramon-Moliner's modification of the Golgi-Cox technique (1970). Following Nembutal anaesthesia, fresh cerebella were removed and placed in a solution of mercuric chloride for 20<sup>±</sup> 30 days (19-23°C). Each tissue was rinsed briefly in distilled water and subsequently dehydrated in absolute alcohol-ether (1:2) for a period of 24 hours. The tissue blocks were infiltrated through a graded series of parlodion solutions (3%, 5% and 8%), embedded in a 10% solution of celloidin and solidified by immersion in cold chloroform (-10°C). Prior to sectioning, the tissue blocks were attached to wooden stubs and stored in 70% alcohol for 24 hours (-10°C). Serial sections (450 µm) were cut transversely along the longitudinal axis of the cerebellar folia (parasagittal plane). The sections were dehydrated, cleared, softened in a mixture of methyl benzoate and benzyl alcohol (1:4) on gelatinized slides and rehardened by immersion in toluene for subsequent alkalization steps. The mercuric impregnation was stabilized following alkalization in alcoholic ammonia. Sections were dehydrated, cleared in toluene and mounted under cover glass using Pro-Texx mounting medium.

### a) Analysis of Golgi-stained Cells

The Golgi-Cox material was used to provide information about the dendritic arborizations and spines on Purkinje cells following

climbing, mossy and parallel fiber-deafferentation. In 3AP treated and mossy fiber-deafferentated animals, impregnated Purkinje cells were selected from the contralateral ansiform lobule. A control series of Purkinje cells was taken from the same lobule of the cerebellar cortex. In parallel fiber-deafferentated animals, a zone 1.5 mm in width was sampled medial to the parasagittal transection within the ansiform lobule.

The following criteria were used to select suitable cells for quantification: (a) the orientation of the dendritic tree had to be parallel to the plane of section and (b) the impregnation had to be interpreted as complete. Measurements were taken from those Purkinje cells which possessed an impregnated soma and at least one representative branch from each of the three portions of the Purkinje cell dendritic tree (primary trunk, smooth branches and spiny branchlets). For the purpose of this study, the Purkinje cell dendritic tree was divided into three portions. The primary trunk system was defined as that segment of the Purkinje cell dendritic tree which extended from the soma to the first major dendritic division. The small, spine-rich branches were designated as the spiny (terminal) branchlets while the spine-free segments, lying between the primary trunk and the spiny branchlets, were referred to as the "smooth branches" of the Purkinje cell dendritic tree.

Two hundred and sixteen Purkinje cells were analyzed with a Leitz - A.S.A. Image Analysis System in combination with a camera lucida (Leitz) using a X25 objective lens. Several of these cells were drawn using a camera lucida at the magnification 1,429 X.

Measurements of the following parameters (dependent variables) of each cell were recorded: mean length, mean number, and mean total length for the primary trunk, smooth branches (spine free dendritic segments between the primary trunk and spiny branchlets) and spiny branchlets.

#### b) Quantitative Analysis

The SPSS (Statistical Package for Social Sciences) system of computer programs was used in the present study for the analysis of descriptive statistics, one-way (involving more than two population means) and two-way analysis of variance (ANOVA). All statistics, excluding the F-test for two population means and the post-hoc Dunnett test were computed with a PRIME 400 computer.

Composite mean values were derived for the control, 3AP treated, mossy and parallel fiber-deafferentated animals for each of the nine dependent variables described above. Statistical assessments of the differences between these means were carried out for each variable. In those experiments where six groups were compared, a two-way ANOVA was applied followed by post-hoc testing with the Dunnett test (for comparisons made directly with the control group) and the Newman-Keuls test (for multiple comparisons). The two independent variables of interest in this two-way ANOVA were the type of lesion and the time of deafferentation.

Initially a tilted data graph was drawn for each dependent variable to determine if an interaction existed between the independent variables (Tukey, 1977). For those dependent variables where an interaction was not found, the two-way ANOVA was broken down into two one-way ANOVAS to determine the main effect of

each independent variable and followed by post-hoc testing with the Dunnett and Newman-Keuls tests. In experiments that compared seven groups, a one-way ANOVA was used followed by similar post-hoc testing. Upper and lower confidence limits for each significant comparison were calculated to estimate the relative difference between the two groups as described by Ambrose and Donner (1973). The above statistical methods, particularly post-hoc testing, are discussed in detail in "Experimental Design" by Kirk (1968). The .10 level was adopted as the minimal criterion for statistical significance.

### 3. Modified Fink-Heimer and DeOlmos-Ingram Technique

After post-operative survival times of 24, 48 hours, 7 days, 2 weeks and 3 months, 3AP treated adult and weanling rats were sacrificed under sodium pentobarbital anaesthesia by intracardiac perfusion with 10% formalin in 4% sucrose. On the following day, the medulla oblongata and cerebella were dissected out and immersed in fresh fixative for at least 15 days. Prior to paraffin embedding, the medullas and cerebella were placed in a 10% formalin solution containing 33% sucrose for 24 hours. The tissues were then embedded in paraffin, sectioned (25  $\mu$ m) and mounted as described above. One section in three through the inferior olivary complex and cerebellar cortex was subsequently stained according to the modified Fink-Heimer and DeOlmos-Ingram technique (Desclin and Escubi, 1975) for degenerating somata and fibers respectively. Another section was stained with either cresyl violet or thionin to assist in the

identification of the borders of the inferior olivary complex and the laminar structure of the cerebellar cortex. Transverse sections through the inferior olivary complex were examined to determine the extent of olivary degeneration and the possible recovery of olivary neurons following 3AP treatment. Parasagittal sections of the cerebellum were examined to localize the exact areas of climbing fiber terminal degeneration within the cortex.

#### 4. Autoradiographic Technique

Following post-operative survival times of from 2 to 5 days, rats were perfused intracardially with 10% formalin. The pons, medulla oblongata and cerebella were removed and fixed in 10% formalin for at least 1 week. Frozen serial sections through the cerebellum and the injection site (pons or inferior olivary complex) were then cut in the parasagittal and transverse planes respectively at a thickness of 20  $\mu\text{m}$ . Every third section was mounted on a glass slide and treated for autoradiography according to the method of Cowan et al. (1972). The slides were dipped in Kodak NTB2 nuclear track emulsion (Eastman Kodak, Rochester, New York) and then dried for 1 to 3 hours in an incubator. They were next placed in light-tight boxes containing a desiccant (silica gel) and stored at 4°C for an exposure period of from 6 to 12 weeks. After this period had elapsed, the coated slides were removed from the light-tight boxes and developed in Kodak D-19 developer at 14° or 15°C for 3 minutes, washed briefly and then fixed for 10 minutes in a rapid fixer (Kodak Ektaflo). They were washed again in gently running tap water for about 30 minutes, then stained



through the emulsion with thionin.

The injection sites were examined using both bright and dark field optics. Terminal projection fields within the cerebellum were identified by their higher concentration of silver grains in comparison to background levels.

### 5. Photographic Procedures

All light photomicrographs were taken with a Leitz Orthomat camera mounted on a Leitz Orthoplan microscope. Kodak Panatomic-X and Ilford Pan-F 35 mm film were used and the negatives were developed using Kodak Microdol-X and Ilford ID-11 developers.

### 3.4 Preparation of Tissue for Electron Microscopy

#### A. Perfusion

All rats processed for electron microscopy were fasted for 24 hours prior to exsanguination. The animals were placed under Nembutal anaesthesia by an intraperitoneal injection of 0.06 ml/100 gms body weight. To ensure an adequate perfusion, a vasodilator (1.0 ml of 1.0% sodium nitrite) and an anticoagulant (0.1 ml of 50 units of heparin per ml in isotonic sodium sulphate) were administered via the inferior vena cava approximately 5-10 minutes prior to perfusion with at least 500 ml of a freshly prepared mixture of 1% glutaraldehyde and 1% paraformaldehyde in 0.12 M phosphate buffer containing 0.02 mM calcium chloride ( $\text{CaCl}_2$ ) (Palay and Chan-Palay, 1974). Following perfusion, the animals were decapitated and the heads were left in fresh fixative overnight for up to 18 hours. The brains were dissected out and placed in 0.12 M phosphate buffer until the following morning.

B. Tissue Dissection

Transverse slabs of cerebellum, each about 0.5 mm in thickness, were cut using the posterior superior fissure and the ansoparamedian fissure as the rostro-caudal landmarks respectively. In that way, the cerebellum was routinely divided into seven transverse slabs, including a median slab which corresponded in level to the intercrural sulcus (designated ICS), three rostral segments (R#1, R#2, R#3) and three caudal segments (C#1, C#2, and C#3).

Within each of these transverse areas, a rectangular piece of tissue involving the most dorso-lateral folia was removed. Each of these rectangular pieces was then placed in a mounting mold which allowed the cerebellum to be sectioned in the transverse plane of the folium.

In a similar manner, the inferior olivary complex was routinely sliced into five transverse segments (two rostral and two caudal to the median segment) which incorporated the entire rostro-caudal extent of the nucleus. Each of these transverse sections was briefly osmicated to identify the outline of the inferior olivary complex and subsequently trimmed. These pieces were then orientated in B.E.E.M. capsules which allowed the inferior olive to be sectioned in the transverse plane.

In parasagittally cut cerebella, transverse slabs of cerebellum were cut from the ansiform lobule as described above. Rectangular areas were sampled immediately adjacent to the lesion (medially) and embedded in flat molds and capsules to permit

sectioning of the cerebellum in both the parasagittal and transverse planes of the folium.

C. Processing and Embedding

Each slab of tissue was processed individually in disposable glass vials. Each tissue was washed in rinse solution containing 0.12 M phosphate buffer and 0.02 mM CaCl<sub>2</sub> and 8% dextrose to remove excess aldehyde. All tissues were post-fixed in 2% osmium tetroxide (OsO<sub>4</sub>) in 0.12 M phosphate buffer containing 7% dextrose under continuous agitation for 2-3 hours, rinsed in 0.1 M sodium acetate (4°C) and subsequently stained en bloc in cold (4°C) saturated aqueous uranyl acetate for 4-5 hours (Palay and Chan-Palay, 1974). The blocks were again rinsed in 0.1 M sodium acetate solution, dehydrated in methyl alcohols, cleared in propylene oxide, passed through propylene oxide and resin mixtures and finally embedded in Epon-Araldite (3:1). The embedding mixture was polymerized at 60°C for at least 24 hours. Then sections were cut with a Reichert OmU<sub>3</sub> ultramicrotome using a diamond knife (Dupont Instruments) and mounted on 200 mesh copper grids. The sections were subsequently stained with lead citrate (0.075%) and examined with an A.E.I. E.M. 6B electron microscope operating at 60 k.V. Electron micrographs were taken on Kodalith 70 mm LR 2562 Estar base film which was developed in Kodak D-19 developer for two minutes at 20-22°C.

D. Quantitative Analysis

The lengths of thorns, spines and spine-like

appendages of control, 3AP treated and parallel fiber-deafferentated Purkinje cells were measured from an extensive sampling of electron micrographs. Composite mean values were obtained for each group and statistical assessments were made of the differences between these means and the control. In these experiments where two groups were compared, an F-test for two population means was used (Ambrose and Donner, 1973). The .05 level was adopted as the minimal criterion for statistical significance.

## CHAPTER 4

### RESULTS

#### 4.1 Horseradish Peroxidase Injections within the Lateral Cerebellar Hemisphere

Following injections of 0.3 - 1.0  $\mu$ l of HRP into the lateral cerebellar hemisphere of ten adult rats, coronal sections through the brain and spinal cord were studied to determine the distribution of labeled somata whose axons project to the neocerebellum. Coronal and transverse sections were likewise examined through the cerebellum to localize the area of HRP staining in the injection site. The staining of the cerebellar injection sites as a rule involved both the cortex and small portions of the underlying white matter, but did not encroach upon the deep cerebellar nuclei (Fig. 1a). Both a region of intense HRP deposit and a surrounding zone of lighter staining were localized in the cerebella, following exposure to either the chromogen diaminobenzidine (DAB) or benzidine dihydrochloride (BDHCl). The remaining cerebellar injection sites were identified using a more sensitive chromogen, tetramethylbenzidine (Figs. 2, 4, 6). The afferents which project to the zone of HRP staining were found to be retrogradely labeled in the

vicinity of the injection site (Fig. 1b) and deep within the white matter of the cerebellum (Fig. 1c) 24 hours following HRP injection.

#### A. Cerebellar Afferents

##### 1. Pontocerebellar

Following an injection which involved the ansiform lobule (Crura I and II) and the lateral extremity of both the lobulus simplex and the paramedian lobule, the pontocerebellar projection was found to be bilateral with a predominantly contralateral representation (Fig. 2). On the contralateral side the somata which gave rise to this projection was most heavily labeled within the area of the pontine gray (Fig. 3a - c) below the peduncular fibers (corticospinal projection) and were localized within two longitudinal cell columns located ventromedial and ventrolateral to the cortical peduncle (Fig. 2B - E). In addition, the dorsal pontine nuclei (i.e. the region of the pontine gray located immediately above the corticospinal fibers) of the caudal half of the pons and the nucleus reticularis tegmenti pontis (NRTP) were heavily labeled following an injection of the ansiform lobule (Fig. 2D - F). The bilateral nature of the pontocerebellar system was especially evident within the caudal third of the pons where the ipsilateral and contralateral systems persisted in approximately equal proportions (Fig. 2E, F) and were localized within similar areas of the pontine gray.

Following an injection into the lateral part of lobulus simplex and a small intermediate portion of the rostral folium of Crus I, HRP positive somata were found mainly contralaterally within a central region of the pontine gray immediately

ventral to the corticospinal fibers (Fig. 4B-F). These somata were found to occupy the exact area of the ventral pontine gray left unlabeled following an injection into the ansiform lobule (i.e. the area between the two ventral longitudinal cell columns). The pontocerebellar projection to lobulus simplex was bilateral, although predominantly contralateral in origin. The majority of the labeled somata formed a single longitudinal cell column in the ventral pontine gray which extended throughout the caudal five-sixths of the pons. The smaller ipsilateral projection was formed from regions of the ventral pontine gray which were shown to be responsible for the formation of the contralateral system (Fig. 4A-F).

The discrete labeling of longitudinal cell columns which occurred following injections into either the lobulus simplex or the ansiform lobule did not prevail following injections which involved Crus I and the medial portion of the rostral folium of Crus II. Instead, a heavier more generalized distribution of labeled somata encompassed virtually all portions of the ventral pontine gray (Fig. 5A-F). In fact, the distribution of these somata resembled a pattern which combined the somata that projected to both the lobulus simplex (Fig. 4) and the ansiform lobule (Fig. 2). A comparison of the pattern of distribution of somata shown in Figs. 2 and 5 suggested that the medial portion of the ansiform lobule received its afferent projection from the same region of the ventral pontine gray as that which projected to the lobulus simplex (Fig. 4). While the pontocerebellar input to this region was bilateral, the ipsilateral projection; especially in its caudal half, was small. The large numbers of labeled somata which project from the nucleus reticularis tegmenti

pontis, on the other hand, were localized bilaterally and were of equal proportions (Fig. 5D - F).

The pattern of retrograde labeling following an injection of HRP into Crus I and the lateral portion of the rostral folium of Crus II resembled the distribution reported above following an injection of the ansiform lobule (compare Figs. 2, 6). Although, less obvious, two longitudinal cell columns were visualized within several levels of the ventral pontine gray; one lying ventromedially and the other ventrolaterally. It appeared that the larger the injection site was within the lateral cerebellar hemisphere, the greater the number of labeled somata were within these two longitudinal columns (compare Figs. 2C - E, 6C - E).

2. Olivocerebellar

Following an injection into the ansiform lobule, HRP labeled somata were found within both the dorsal and ventral lamellae of the principal olive throughout its rostrocaudal extent (Figs. 3d - f, 7A - C). In addition, the rostral tip of the dorsal accessory olive and the medial portion of the medial accessory olive were retrogradely labeled (Fig. 7A - F). While the olivocerebellar projection to the ansiform lobule consisted primarily of a contralateral projection from the principal and discrete portions of both the medial and dorsal accessory olives, a small afferent projection was localized within the genu of the ipsilateral caudal principal olive (Fig. 7D).

Following an injection into lobulus simplex, retrogradely labeled somata were confined to several discrete cell



groups (Fig. 8). HRP-containing cells were found in the ventral lamella of the mid-portion of the principal olive, the medial border of the middle half of the dorsal accessory olive and along the medial border of the caudal third of the medial accessory olive (Fig. 8B-F). It appears, therefore, that the lobulus simplex receives a major proportion of its olivocerebellar afferents from the medial border of both accessory olives while obtaining a relatively small projection from the ventral lamella of the principal olivary nucleus.

Following an injection into Crus I and the medial portion of the rostral folium of Crus II, HRP labeling within the principal olive was distributed contralaterally, primarily within the genu and the dorsal lamella of the principal olive (Fig. 9A-D). The ventral lamella of the principal olive, on the other hand, was noticeably devoid of label except for its most rostral limit (Fig. 9A-C). However, a substantial projection was found from both the dorsal and medial accessory olives throughout the mediolateral and rostrocaudal extent of both nuclei (Fig. 9A-G).

Following an injection into Crus I and the lateral portion of the rostral folium of Crus II, a similar pattern of labeling to that reported in Fig. 9 was found within the principal olive (Fig. 10). The afferents which arose from the principal olive and projected to Crus I and the lateral two-thirds of the rostral folium of Crus II originated mainly from the genu and the dorsal lamella of the principal olive (Fig. 10A-D). This injection site showed less involvement of the pars intermedia and the pars vermis of the cerebellar cortex than those described above in Figs. 2 or 5 and

subsequently less retrograde labeling within the contralateral accessory olivary nuclei (Fig. 4A-H). Moreover, an examination of the distribution of somata in Figs. 5 and 10 suggests that the olivocerebellar afferents to the caudal folia of Crus II arise from the ventral lamella of the principal olive.

### 3: Reticulocerebellar

The pattern of retrograde labeling following injections into the ansiform lobule confirmed the existence of a bilateral projection to the cerebellum from the lateral reticular nuclei (LRN) (Fig. 7). The rostral tip of the LRN, specifically the subtrigeminal and magnocellular divisions, was shown to be responsible for the small contralateral projection (Fig. 7C, D). The larger ipsilateral projection that supplies the major portion of the reticulocerebellar afferents to the ansiform lobule originated from the rostrocaudal extent of the subtrigeminal division (Figs. 3g-1, 7B-F) and from a small column of cells along the medial border of the magnocellular portion of the LRN (Fig. 7B-G).

The reticulocerebellar afferents to the lobulus simplex originated both ipsilaterally and contralaterally although a marked ipsilateral predominance prevailed. In contrast with the ansiform lobule, the ipsilateral projection to the lobulus simplex from the subtrigeminal division of the LRN originated from within its caudal half rather than its rostrocaudal extent (Fig. 8E-G). In addition, a mossy fiber input from the principal LRN was found to originate caudal to the rostral third of the nucleus, beginning as a horizontal band of cells ventromedially, passing caudally along the medial border of

the principal LRN and finally terminating dorsomedially within the caudal pole of the principal LRN (Fig. 8E-I). The contralateral projection, on the other hand, originated within the middle third of the magnocellular division of the principal LRN (Fig. 8E, F) and contrasted in origin (rostral third) with the reticular input to the ansiform lobule (Fig. 7C, D). Somata within the principal LRN that projected to the lobulus simplex were localized within the caudal two-thirds of the principal LRN originating from both the magno- and parvocellular subdivisions contralaterally (Fig. 8E-I).

#### 4. Trigemincerebellar

Following an injection into Crus I and the lateral portion of the rostral folium of Crus II, HRP labeled neurons were found exclusively within the ipsilateral sensory nucleus of the trigeminal nerve (NST) (Fig. 11). Retrogradely filled somata appeared within discrete groups at the rostral and caudal limits of the NST (Fig. 12A, C). Two groups of cells were localized within the central portion of the NST; one at its rostral limit (Fig. 11A) and the other at its caudal pole (Fig. 11C). A third group was isolated along the ventromedial border of the NST within its rostral pole (Fig. 11A). More caudally, labeling was found within the spinal nucleus of the trigeminal nerve (NTST) and was localized specifically in the pars oralis (NTST(o)) and the pars interparalis (NTST(i)) subdivisions ipsilaterally (Fig. 12a-c). On rare occasions labeled cells were also observed on the contralateral side (Figs. 10E, 11E). The distribution of somata of the trigemincerebellar afferents within the

NTST(o) and the NTST(i) formed two fairly discrete longitudinal cell columns, one situated dorsally and the other lying more ventrally within the NTST (Fig. 10A-E). This distribution was apparent caudally as far as the rostral half of the NTST(i). No labeling of neurons was found caudal to this region.

The distribution of cells that project to the ansiform lobule was found to be similar to that described in Figs. 10 and 11 for Crus I and the lateral portion of Crus II, although a substantial increase in the number of retrogradely labeled somata was found in several areas (Figs. 7, 13). A larger number of neurons that were retrogradely filled were found along the ventromedial border of the rostral pole of the NST (Fig. 13A). Similarly, the projection from the NTST was larger. While the dorsal cell column appeared less distinct (Fig. 7A-E), a ventral cell column formed a well developed cell group localized within the caudal half of the NTST(o) and the rostral two-thirds of the NTST(i) (Fig. 7A-F). The small group of cells found near the caudal limit of the NST was labeled following either injection (Figs. 11C, 13B). Using a subtractive approach, it would appear that the posterior folium of Crus II receives the major source of its afferents from the enlarged ventral cell column within the NTST and the ventromedial border of the rostral pole of the NST.

Labeled neurons in the NST were localized within its rostral pole along the ventrolateral border following HRP injections into Crus I and the medial portion of the rostral folium of Crus II (Fig. 14A). This was in direct contrast with their ventromedial distribution following injections of Crus I and the lateral portions

of Crus II (Fig. 11A). In a manner reminiscent of the labeling in the NTST following injections into Crus I and the lateral portions of Crus II, HRP injections into Crus I and the medial portion of the rostral folium of Crus II showed retrograde filling of somata within the ipsilateral pars oralis (caudal half) and pars interpolaris (rostral half) (Fig. 9A-E).

Following an injection into lobulus simplex, no HRP labeled somata were found within the NST or the NTST(o) except for the most caudal tip of the ipsilateral NTST(o) where a few retrogradely filled cells were found centrally (Fig. 8B). The origin of the afferent projection from the NTST(i), however, was localized specifically within its dorsal region and extended throughout its rostral half (Fig. 8C-F). Below this level and within the pars caudalis of the NTST no retrograde labeling was found. In summary, the trigeminocerebellar afferents to the lobulus simplex originate from cells within the rostral half of the dorsal NTST(i) as opposed to the ventrally distributed somata that project to the ansiform lobule.

#### 5. Vestibulocerebellar

Following an injection into the ansiform lobule retrogradely transported HRP was visualized within all of the nuclei of the vestibular nuclear complex except the spinal nucleus (Fig. 13). Firstly, contralateral labeling was found within the ventrolateral aspect of the caudal portion of the superior vestibular nucleus (Fig. 13D). Secondly, a bilateral projection was observed from the medial vestibular nucleus (NVM) (Figs. 12d-f, 13). The major portion

of the projection, however, originated from the caudal pole of the NVM along its ventrolateral aspect (Fig. 13D-F).

The retrograde labeling within the vestibular nuclear complex following an injection into Crus I and the medial portion of the rostral folium of Crus II was identical to that reported following HRP staining of the entire ansiform lobule (compare Figs. 14C-F, 13C-F). In addition, both injection sites lacked an afferent projection from the spinal vestibular nucleus (NVSP).

Following an injection into Crus I and the lateral portion of the rostral folium of Crus II, labeled cells within the medial vestibular nucleus were confined solely to its ventral aspect throughout its rostrocaudal extent bilaterally (Fig. 11C-F). By comparison with the labeled somata reported following an injection of the ansiform lobule, a reduced number of retrogradely labeled somata were present within the lateral vestibular nucleus as a result of the more lateral placement of the injection site. The NVSP was labeled bilaterally following injections into that area. An ipsilateral projection was formed from a small group of cells within the ventrolateral aspect of the rostral portion of the NVSP (Fig. 11C), while the contralateral cerebellar projection was shown to originate from a small locus of cells within the ventral aspect of the caudal portion of the NVSP (Fig. 11D, E).

Retrogradely labeled somata were not found within the vestibular nuclear complex following injections into lobulus simplex.

## 6. Ceruleocerebellar

While a small number of retrogradely labeled somata were localized within the caudal portion of the contralateral locus ceruleus following large injections into the ansiform lobule (Fig. 12j-1, 13B), because no retrograde labeling was found within the locus ceruleus following smaller HRP injections of the ansiform lobule, the exact area of afferent fiber termination was difficult to localize (Figs. 8, 11, 14).

## 7. Cuneocerebellar

Although several HRP injections of the cerebellar cortex failed to provide evidence to support the existence of a cuneocerebellar projection to the ansiform lobule or the lobulus simplex (Figs. 7A-H, 8A-H), in two instances a small ipsilateral system from the rostral pole of the nucleus gracilis (GR) was shown to project to the ansiform lobule (Figs. 9D, 10D). In both cases, however, the labeled somata were relatively sparse by comparison to the projection from other centers.

## 8. Spinocerebellar

Injections which involved the ansiform lobule did not provide evidence to indicate the existence of a spinocerebellar projection to the neocerebellum. However, single retrogradely filled somata were localized within lamina II and IV at the level of the twelfth thoracic and third lumbar spinal nerves respectively following injections into lobulus simplex.

## 9. Reticular Formation (nucleus reticularis gigantocellularis)

Following an injection into the ansiform lobule, a bilateral projection was mapped from an area of the reticular formation (gigantocellularis) dorsal to the rostral third of the inferior olivary complex (Figs. 12g-i, A-C). HRP injections which involved only Crus I and the medial portion of the rostral folium of Crus II had labeled a few neurons in the same region of the reticular formation bilaterally (Fig. 9C). In contrast, injections of the lobulus simplex resulted in a unilateral labeling of the ipsilateral reticular formation dorsal to the caudal pole of the medial accessory olive (Fig. 8F).

### 4.2 The Inferior Olivary Complex

#### A. Electrolytic Ablation

##### Lesion Site within the Adult

The removal of the olivocerebellar input to the contralateral cerebellar hemisphere was performed electrolytically using either a dorsal or a ventral (parapharyngeal) approach. Serial sections of thionine-stained material were examined throughout the rostrocaudal extent of the medulla oblongata to determine the location of the lesion site. Animals having lesions which involved the portion of the inferior olivary complex found in this study to project to the ansiform lobe (specifically the dorsal and ventral lamellae of the principal olive) were subsequently used in investigations of the short- and long-term effects of olivocerebellar deafferentation (Fig. 15).



## B. 3-Acetylpyridine (3AP) Intoxication

### General

Within a few hours of 3AP administration in adult rats (84 days), several functional disorders became apparent. Within the first ten hours, all rats were observed to undergo a period of forced breathing which was accompanied by severe problems in swallowing. Over the following 18 hours, all of the rats were characteristically docile. At the dosage level employed (65 mg/kg body weight) a mortality rate of approximately 60% was found, with the majority of deaths occurring between 18 and 40 hours following treatment. By the second day, however, many of the rats began to show signs of renewed activity. An examination of their gait revealed several abnormal patterns. The hind limbs extended laterally, effecting a wide stance which appeared to support the animal's weight with difficulty. Any attempt to initiate motion was accompanied by an uncontrollable motoric tremor throughout the trunk and limbs, which persisted and magnified until the attempt at movement was terminated. In most cases when movement did occur, not only was it tremor associated, but it also tended to be rotary in nature. In all cases examined, the forelimbs appeared to be unaffected and showed normal signs of coordination and function. The earlier symptoms related to breathing and swallowing tended to alleviate over the following few days while the problems with gait and tremor were still evident following survival times as long as six months.

Weanling rats injected intraperitoneally with 3AP on the 21st postnatal day displayed many of the functional disorders

that occurred following 3AP administration, in adult rats. However, mortality rates were found to be 10% higher in the weanling counterparts, involving an overall loss in numbers of 70%.

#### 1. Lesion Site within the Adult

##### a) Short- and Long-Term Changes Following 3AP Treatment

###### Light microscopy

The appearance of the normal inferior olivary nucleus in Nissl preparations revealed a complex consisting of a highly folded band of gray matter which lay immediately dorsal to the pyramidal tract. This complex occupied a combined rostral to caudal distance of approximately 3 mm and was composed of three prominent nuclei: a principal olivary nucleus which was formed by dorsal and ventral lamellae, a medial accessory nucleus (Fig. 16a) and a dorsal accessory nucleus. Other cytoarchitectural subdivisions within these nuclei have recently been described in the adult Wistar rat and include the nucleus  $\beta$ , the dorsal cap of Kooy and the ventrolateral cell column (Fig. 24c, d) (Gwyn, Nicholson and Flumerfelt, 1977). The cellular composition of the inferior olivary complex was characterized predominantly by small neurons with a high content of Nissl substance, as indicated by the intense basophilic staining of their cytoplasm (Fig. 16a).

An examination of the inferior olivary nucleus with the light microscope suggested an early onset of degenerative change following 3AP treatment. By 24 hours, thionine-stained material showed a complete absence of staining for Nissl substance (Fig. 16b), and hematoxylin and eosin-stained material revealed a substantial

loss in the eosinophilia of the neuronal cytoplasm (Fig. 17b). Using silver impregnation methods, the inferior olivary somata were found to be darkly argyrophilic suggesting a marked neuronal regression of these cells (Fig. 17f).

No apparent signs of recovery in the staining of Nissl material or cytoplasmic protein were observed at later stages (7 or 14 days) (Fig. 16c, d, 17c, d). Furthermore, an examination of corresponding silver preparations gave unequivocal support to these findings and revealed that 3AP caused a total bilateral destruction of the inferior olivary complex. The prominent, dense, argyrophilic bodies present at 24 hours became much reduced in size by 8 days (Fig. 17g) and almost inconspicuous by the end of the 2nd week (Fig. 17h). In addition to staining degenerative neurons darkly, these silver preparations (modified De Olmos-Ingram technique) stained the cytoplasm and nuclei of normal neurons lightly. It was therefore possible to ascertain the relative number of degenerating olivary neurons at all stages examined. As late as 86 days following 3AP treatment, the inferior olivary complex remained aneuronic with no apparent recovery within any portion of the inferior olivary complex. In all of the long-term cases examined, the olivary neurons appeared to be irreversibly affected following 3AP administration. Regional variations were not observed with any of the three staining methods, although on rare occasions the inferior olivary complex on one side remained unaffected following 3AP administration. In such instances there were no apparent signs of degeneration on that side, whereas all of the olivary neurons on the contralateral side appeared

necrotic. The results therefore suggest that olivary neurons are either totally destroyed or unaffected following 3AP treatment, and that sparing is an uncommon occurrence at appropriate dosage levels.

#### Electron microscopy

The normal inferior olivary neuron is found to possess an oval or round profile which measures approximately 12 - 23  $\mu\text{m}$  in diameter. Its Nissl bodies and rod shaped mitochondria are randomly scattered throughout the neuronal cytoplasm. Axonal and dendritic profiles of the neuropil normally lie adjacent to the somatic surface of the olivary neurons although axo-somatic contacts are only occasionally observed (Fig. 18a).

By 12 hours following 3AP injection, electron microscopic findings noted marked degenerative changes within the inferior olivary complex (Fig. 18b). All cells showed extensive condensation of their nuclear chromatin resulting in large irregular masses of heterochromatin throughout the nucleus. The nuclear envelope appeared distended and fragmented while severe shrinkage in both the nuclear and cytoplasmic mass increased the overall electron density of the cell. Mitochondrial profiles frequently showed signs of swelling and the neuronal plasmalemma appeared highly discontinuous at this stage. Along the periphery of the degenerating neuronal mass, several dendritic profiles which displayed synaptic junctions were found in a marked stage of regression. The mitochondria of these dendritic profiles appeared enlarged and their longitudinally orientated cristae were discontinuous, swollen and highly irregular in form. In most instances the dendritic plasmalemma appeared intact

but irregular in outline. Even at this early stage, glial profiles had already made direct contact with extensive regions of the somatic surface. In many cases, the glial processes were found intruding considerable distances into the neuronal cytoplasm, often as far as the nuclear envelope.

The appearance of the inferior olivary neurons at 24 and 48 hours following 3AP treatment was similar to that reported previously for the 12 hour period (Fig. 19a). Both nuclear shrinkage and cytoplasmic fragmentation were more advanced. Glial profiles resembling astrocytes were greatly hypertrophied and penetrated and fragmented extensive areas of the neuronal cytoplasm. Scattered throughout the neuropil were several dendritic profiles which were highly shrunken in appearance and accommodated little more than a few necrotic mitochondria.

By 60 hours, the cytoplasmic matrix of many of the olivary neurons was reduced to a thin, necrotic osmiophilic rim (Fig. 19b). Astrocytic involvement was still predominant, but for the first time glial elements having the characteristic appearance of microglial profiles were evident at the periphery of the degenerating mass (Fig. 20). These microglia-like profiles were distinguished from the astrocytic elements by a darker, more homogeneously granulated cytoplasm, prominent cell outlines and an absence of bundles of cytoplasmic filaments. These cells often contained phagocytic vacuoles engorged with osmiophilic debris that probably represented remnants of degenerating olivary neurons (Fig. 21a).

By 72 hours, continued astrocytic hypertrophy

resulted in isolation of the nucleus from the surrounding fragmented cytoplasm (Fig. 21b). As a result, the pyknotic nucleus in many cases became completely ensheathed by astrocytic profiles. Astrocyte and microglia-like activity were primarily restricted to the cytoplasm, while nuclear regression was characterized largely by coagulation and shrinkage of chromatin.

It became apparent that the early infiltration by glial processes involved the astrocytes, while the darker, more highly phagocytic glial elements which appeared at later stages represented microglia-like activity. Direct evidence for phagocytosis by astrocytic processes was not convincing and their function appeared to be related instead to the invagination and fragmentation of olivary neurons. The enhanced microglia-like activity from 60 hours onwards suggested a phagocytic removal of degenerating cellular fragments beyond this stage.

By 7 days, hypertrophied astrocytic sheaths were often found engulfing the surface of the pyknotic nuclei (Fig. 22a). Extensive microglia-like activity occurred throughout the remainder of the cell with frequent sites of cytoplasmic engulfment. Little of the original cytoplasmic content persisted and in some cases only a small pyknotic nucleus remained engulfed by an inner sheath of astrocytic processes, which in turn were surrounded by microglia-like profiles (Fig. 22b).

By the end of the second week, only small degenerative profiles continued to persist in the neuropil (Fig. 23a). Many of these profiles showed persisting synaptic contacts which suggested

that they were actually degenerating dendrites and that all the olivary perikarya had since been resorbed.

Although degenerating myelinated axons, interpreted as part of the olivocerebellar system, were frequently observed in the neuropil adjacent to the inferior olivary complex, the neuropil of the inferior olivary complex was conspicuously absent of any axon terminal degeneration. Contrasting with the degenerative loss of the olivary somata and their dendritic profiles, the numerous presynaptic terminals converging upon the dendritic arborization of the necrotic olivary neurons appeared unaffected during the two weeks following 3AP treatment. An electron microscopic examination confirmed that a total loss of the cellular component of the inferior olivary complex occurred following long-term (123 days) 3AP treatment in the adult.

## 2. Lesion Site within the Weanling

### a) Short- and Long-Term Changes Following 3AP Treatment

#### Light microscopy

As in the adult rat, the cellular composition of the inferior olivary complex of the weanling rat was characterized predominantly by small perikarya which stained intensely basophilically as a result of their high Nissl content. Nissl staining revealed a laminar organization within this nucleus which was similar to that described for the adult (Fig. 24c, d). The inferior olivary complex even at this early postnatal stage (21 days) can be divided into the three main nuclei (the principal olivary nucleus, the medial accessory

nucleus and the dorsal accessory nucleus) and the various subnuclei which are characteristic of the adult (Fig. 24a, b). The only detectable difference in the inferior olivary complex of the weanling rat was the shorter rostrocaudal length of the nucleus. In the weanling rat, the complex begins rostrally just caudal to the facial nucleus and extends approximately 2.2 mm to terminate at the mid-level of the lateral reticular nucleus.

Climbing fiber-deafferentation of the weanling rat was performed by means of the intraperitoneal administration of the 3AP protocol described previously for obtaining a bilateral destruction of the inferior olivary complex in the adult rat (Desclin, 1976). While a higher mortality rate among weanling rats suggested a greater sensitivity to 3AP, a light microscopic examination 120 days after administration revealed a selective sparing within two of the olivary nuclei (Fig. 24e, f). In all cases examined, sparing occurred within specific areas of the inferior olivary complex. The regions most resistant to 3AP were located within the medial accessory and the principal olivary nuclei. More specifically, a column of cells was found bilaterally within the medial aspect of the caudal pole of the medial accessory olive and the nucleus  $\beta$  (Fig. 24e). Furthermore, smaller areas of sparing were found bilaterally within the main lamina of the medial accessory olive and the genu of the principal olivary nuclei (Fig. 25e, f).

In an attempt to procure a total olivocerebellar (climbing fiber) deafferentation of the cerebellar cortex, a dosage of 90 mg/kg of 3AP was administered to weanling rats. Mortality rates,



as expected, were noticeably increased (to 85%), but the sparing which was prominent following the administration of the adult dosage was largely eliminated. In all cases examined, the sparing noted previously within the nucleus  $\beta$ , the genu of the principal olivary nuclei and the medial portion of the medial accessory nuclei was no longer evident (Fig. 24g, h). On rare occasions, however, small islands of olivary neurons were found within the medial and lateral extremities of the main lamina of the caudal portion of the medial accessory nuclei (Fig. 24g).

#### Electron microscopy

The above findings were confirmed and extended next in an electron microscopic study of the inferior olivary complex following long-term (120 days) 3AP treatment. Following the injection of the lower dose of 3AP, several areas within the inferior olivary complex were found to have normal morphology. In particular, the inferior olivary perikarya and the neuropil within the medial aspect of the medial accessory olive showed no signs of degeneration following long-term 3AP treatment (Fig. 25a, b), although the lateral portions of this nucleus were found to have an acellular appearance. In contrast, however, the injection of the higher dose of 3AP resulted in a total loss of the inferior olivary neurons throughout the rostrocaudal extent of the nucleus.

### 4.3 The Ansiform Lobule of the Cerebellum

#### A. Electrolytically or Chemically Lesioned (3AP) Adult Rats

##### Normal cytoarchitecture

### The climbing fiber

The normal cytology of the climbing fiber has received considerable attention (Hamori and Szentagothai, 1966a; O'Leary et al., 1971; Palay and Chan-Palay, 1974). Upon entering the molecular layer, the climbing fiber becomes unmyelinated and ascends the Purkinje cell dendritic tree, giving rise to a number of fine tendril-like branches (0.1  $\mu$ m in diameter). These collaterals are characterized by bulbous enlargements along their course which represent the synaptic varicosities. The climbing fiber varicosity exhibits several distinguishing features: a dense population of spherical synaptic vesicles, a prominent microtubular core and a synaptic association with stubby thorns which project from the smooth portion of the Purkinje cell dendritic tree (Figs. 23b, 26b-f).

## 2. Short-term Changes Following Climbing Fiber-Deafferentation

### Electron microscopy

Since the degenerative changes reported within the cerebellar cortex and the time-course for their onset were found to be comparable irrespective of the type of lesion (electrolytic or chemical), the subsequent description will deal entirely with the short-term changes which occurred following 3AP treatment.

Although the majority of the climbing fiber terminals appeared normal at 12 hours post-treatment (3AP), some early signs of degeneration were detected (Fig. 27a). During these early stages of degeneration, the synaptic vesicles frequently underwent changes in shape and size, becoming swollen or pleomorphic in appearance.

Concurrently the axoplasmic matrix underwent a moderate darkening. In

many cases, Bergmann glial processes were already engaged in active phagocytosis of the degenerating terminals.

Between 24 and 60 hours all climbing fiber varicosities were found to undergo an electron-dense form of degeneration (Fig. 27b), whereas all other elements within the cerebellar cortex appeared unaffected. The climbing fiber terminals showed marked degenerative changes as evidenced by the increased electron density of the mitochondrial profiles and axoplasmic matrix. Most of these terminals displayed an irregular outline, were highly shrunken in appearance and were surrounded by Bergmann glial cytoplasm. In spite of this, their synaptic junctions were still intact regardless of the advanced degenerative changes taking place in the terminal. Within this time period, normal climbing fiber varicosities could not be found along the major dendritic shafts of Purkinje cells.

At 72 hours, the first post-synaptic sites (dendritic thorns) denuded of their normal axonal contacts (climbing fiber varicosities) were found to be completely surrounded by Bergmann glial processes (Fig. 27c).

By 7 days, the vast majority of degenerating terminals had disappeared (Fig. 27d). Only occasionally could small, dark, degenerating fragments be found in Bergmann glial profiles along the shafts of Purkinje cell dendrites.

Although relatively few in number, collaterals have been described by several authors which arise from the main stem of the climbing fiber within the granular layer and terminate in synaptic association with the granule cells (Palay and Chan-Palay, 1974; Desclin, 1976). An extensive search throughout the ansiform lobule

failed to substantiate the existence of these glomerular collaterals. Electron microscopically, all the glomeruli examined within the first two weeks following 3AP treatment appeared normal. These preliminary findings suggest that, at least in the ansiform lobe, few if any glomerular collaterals arise from climbing fibers.

In summary, 3AP intoxication was found to cause a rapid form of electron-dense degeneration in climbing fiber afferents to the cerebellar cortex. Several climbing fiber varicosities showed distinct degenerative signs as early as 12 hours following treatment. By 24 hours, marked degenerative changes were characteristic of all climbing fibers. During the degenerative stage, Bergmann glial cells were instrumental in the phagocytic removal of climbing fibers, with their subsequent clearing taking place by the end of the first week following treatment.

#### 4.4 Synaptic Remodeling within the Deafferentated Adult or Weanling Cerebellar Cortex

Using the cerebellar cortex of the rat as an experimental model, it was proposed to investigate plastic changes (remodeling) in its synaptic organization following selective removal of climbing fibers, mossy fibers (extrinsic afferents) and parallel fibers (intrinsic afferents) using chemical and electrolytic lesions in weanling and adult animals. The cerebellar cortex of the rat, being a precisely laminated structure, consists of three uniquely organized layers. The inner and outer layers (granular and molecular) possess different extrinsic afferent connections (primarily mossy and climbing fibers respectively) which can be readily distinguished by

both physiological and ultrastructural characteristics. Any reorganization by axonal sprouting into these layers can therefore readily be demonstrated.

Since a number of centers give rise to mossy fibers projecting to the cerebellar granular layer, a cortical region receiving its mossy fiber input from as few centers as possible would prove more appropriate for extrinsic deafferentation. HRP injections of the cerebellar cortex in the present study have revealed that the lateral part of the ansiform lobule is characterized by a nearly pure mossy fiber input from the basilar pontine gray (pontocerebellar fibers). In addition, the short-term electron microscopic investigation undertaken in this study has supported the view that the inferior olivary nucleus in the rat is the sole source of climbing fibers. An extensive deafferentation of the mossy or climbing fiber projections to the lateral ansiform lobule is therefore possible by ablating a single nuclear complex.

Removal of the olivocerebellar fibers was performed using two approaches: (1) electrolytic lesions by either a dorsal or a ventral parapharyngeal approach or (2) a chemical lesion using the metabolic poison, 3AP. The sensitivity of the olivocerebellar system to 3AP (as shown in this study) thus provides a convenient and selective means of eliminating all the inferior olivary neurons and their axons, i.e. the climbing fibers of the cerebellar cortex in both weanling and adult rats. In contrast to the more conventionally used electrolytic methods, 3AP causes a complete bilateral ablation of all olivary neurons while avoiding problems inherent in electrolytic

procedures, such as incomplete destruction of the nucleus and involvement of fibers of passage. Removal of the pontocerebellar fibers was performed electrolytically using a dorsal approach since their location is rostral enough to avoid involvement of other cerebellar afferents.

Reorganization of the cerebellar cortex was studied by means of several neuroanatomical techniques including silver impregnation, (DeOlmos-Ingram modification of the Fink-Heimer method), autoradiography and electron microscopy. A number of double-lesion experiments were also undertaken which included an ablation of both the inferior olive and the pons. Lesions were first placed in either the inferior olive or the basilar pontine gray. After a predetermined survival period of sufficient duration to allow for the degeneration and removal of the first projection and subsequent remodeling, a (short-term) lesion or injection ( $^3\text{H}$  leucine) was made which involved the other center. Degeneration and autoradiographic techniques were then used to map the topography of the second system (olivocerebellar or pontocerebellar terminals) to determine whether remodeling or plastic reorganization had occurred.

In several long-term 3AP treated or inferior olivary lesioned animals, tritiated leucine was injected into the basilar pontine gray, or short-term pontine lesions were made to investigate the possibility of mossy fiber sprouting into the molecular layer. The animals were processed for autoradiography, silver impregnation or electron microscopy. Although several experimental methods were employed, no evidence was found to suggest that mossy fibers might

relocate or sprout beyond the confines of the granular layer in either the adult or weanling rat.

Concurrently, in several long-term pontine lesioned cases, tritiated leucine was injected into the inferior olivary complex, or short-term olivary lesions were made and the hind-brain was processed for autoradiography, silver impregnation or electron microscopy. Each case was designed to provide information concerning the possibility of climbing fiber sprouting in the granular layer following mossy fiber-deafferentation. An examination of the climbing fiber distribution, however, has failed to provide any evidence which would suggest a sprouting or possible reinnervation of denervated mossy fiber glomeruli. In fact, climbing fiber glomerular collaterals have not been observed within the ansiform lobule in this study and therefore their existence remains questionable. Furthermore, the local axonal milieu of the molecular layer (climbing fibers, stellate, basket and recurrent Purkinje cell axons) showed no indication of reinnervating deafferentated spiny branchlets (asynaptic spines) or Purkinje cells during the subsequent transneuronal degeneration of the parallel fiber system following long-term mossy fiber-deafferentation (below). Moreover, the cerebellar cortex underwent a marked decrease in the density of dendritic spines.

In summary, the synaptic specificity of the cerebellar cortex appears to be maintained even following extensive deafferentation. While the parallel fiber system and ascending basket axon collaterals has been shown to retain some capabilities of sprouting or remodeling (below), the primary reaction of the

cerebellar cortex to deafferentation appears to be one of transneuronal degeneration.

#### 4.5 Ansiform Lobule of the Cerebellum

##### A. Chemically Lesioned (3AP) Adult Rats

###### Normal cytoarchitecture

###### The Purkinje cell

The normal cytology of the Purkinje cells has been extensively described (Palay and Chan-Palay, 1974). In the present study, their cell bodies measured 21-25  $\mu\text{m}$  in diameter and formed a single sheet of cells which lay between the molecular and granule cell layer. The cytoplasmic organelles of these cells are commonly arranged in a circular fashion around the nuclear envelope (Fig. 26a). The soma of the Purkinje cell has a highly developed agranular endoplasmic reticulum which extends throughout the cell, in contrast to its granular counterpart, the Nissl body, which is localized mainly within the Purkinje cell soma (Palay and Chan-Palay, 1974). Immediately below the plasmalemma of the Purkinje cell, and parallel to it, the agranular endoplasmic reticulum forms a broad discontinuous cisterna. This specialization of the agranular endoplasmic reticulum (the hypolemmal cisterna) forms a distinct characteristic of the Purkinje cell soma (Fig. 26a), dendritic tree (Fig. 26b,c,e,h) and axon. While the hypolemmal cisterna system is highly discontinuous in the rat, it nevertheless forms a characteristic membranous boundary secondary to the Purkinje cell plasmalemma (Palay and Chan-Palay, 1974).

The dendritic arborization of the adult Purkinje cell has been found to arise from one or several primary trunks which



project from the apical pole of the soma (Figs. 28a, 29A). The Purkinje cell dendritic tree spreads out (300 - 400  $\mu\text{m}$ ) in the vertical plane perpendicular to the longitudinal axis of the folium, its width rarely exceeding 20  $\mu\text{m}$  (Berry and Bradley, 1976b). While the branching pattern of the Purkinje cell dendritic tree has most frequently been described as dichotomous (Palay and Chan-Palay, 1974; Berry and Bradley, 1976; Weiss and Pysch, 1978), many branches throughout the arborization have been shown to give rise to more than two divisions (Figs. 28a, 29A). Usually, the primary trunks branch to form two or more secondary dendrites that frequently run a course parallel to the pial surface. Subsequent branching results in the formation of tertiary and higher-order branches.

For the purpose of this study, the primary trunk system was defined as that portion of the dendritic tree which arose from the soma and extended to the first major dendritic division. The small, spine-rich branches (1 - 2  $\mu\text{m}$  in diameter) which correspond to the final branch orders were specified as the terminal or spiny branchlets (Figs. 28b, e, 28c) while the spine-free segments, lying between the primary trunk and the spiny branchlets (including secondary, tertiary and higher order branches) were designated as the "smooth branches" of the Purkinje cell dendritic tree (Figs. 28c, g, 29B). The small terminal branchlets were confirmed to have a rich complement of long slender appendages (the dendritic spines) with the electron microscope (Fig. 26g inset).

Measurements (mean number, length and total branch length) of the primary trunks, smooth branches and spiny branchlets

from control Purkinje cells (150 days) were made with a Leitz A.S.M. Image Analysis System using a camera lucida (as described in Materials and Methods, p. 70). The average length of the adult control primary trunk was determined to be 41.06  $\mu\text{m}$  while the number per soma was estimated to be slightly greater than one (1.22) (Table 4). The smooth branches of the Purkinje cell dendritic tree averaged 59.6  $\mu\text{m}$  in length. The mean number for each cell was 5.22 accounting for a mean total smooth branch length of 298.97  $\mu\text{m}$ . Each Purkinje cell dendritic tree was found to have a mean number of 186.18 spiny branchlets. Their mean branch length was determined to be 21.29  $\mu\text{m}$ , while the total spiny branchlet length per cell was estimated as 3,969.46  $\mu\text{m}$ . In absolute terms, the dendritic tree of the control Purkinje cell averaged 4,310.26  $\mu\text{m}$  in length.

#### Spine morphology and distribution

While they are considered the highest dendritic order, the spiny branchlets were found to originate from various dendritic segments (tertiary, secondary and even primary dendrites) (Fig. 28c). Regardless of their origin, however, they were found to possess a rich complement of dendritic spines. Furthermore, it has been documented that these dendritic spines are restricted solely to the spiny branchlets (Figs. 28c,g,29B) (Eccles et al., 1967). The major trunks and higher order non-spiny branches are considered to be "smooth" because they lacked the dendritic spines characteristic of the terminal or spiny branchlet (Figs. 28b,29c). A second category of dendritic appendage has been identified on the "smooth" portion of the Purkinje cell dendritic tree with the electron microscope. This

appendage has a localization which is different from the dendritic spine covering of the terminal branchlet and, furthermore, has been shown to be morphologically different from the dendritic spines (Palay and Chan-Palay, 1974). Due to its shorter stem length and larger head, it has more appropriately been termed a "dendritic thorn" (Hamori and Szentágothai, 1966a; O'Leary et al., 1971). These thorns have been localized along the "smooth" portion of the Purkinje cell dendritic tree and are believed to serve as the exclusive postsynaptic site of the climbing fiber varicosity (Fig. 26c,f) (Palay and Chan-Palay, 1974).

#### 1. Long-Term Changes Following Olivocerebellar Deafferentation

##### a) Golgi-Cox Technique

The inferior olivary complex of the adult rat was chemically destroyed following the intraperitoneal administration of 3AP. These animals were allowed to survive for 123-131 days.

##### (1) The Purkinje Cell Dendritic Tree

Purkinje cells deafferentated of their climbing fiber input in the adult were not found to be significantly different from the adult controls with regards to the mean length of the primary trunks, smooth branches and spiny branchlets (Fig. 32, Table 4). These dendritic arborizations, however, were characterized by a marked decrease in the number of smooth branches and spiny branchlets when compared to the adult controls (Figs. 30a,c,e,31A,B,32, Table 4). More specifically, the smooth branches and spiny branchlets were significantly decreased in number by 44% and by 61% respectively

following climbing fiber-deafferentation. The decrease in the number of smooth branches was responsible for a 31% decrease in the mean total smooth branch length while the loss of spiny branchlets resulted in a 58% reduction in the mean total spiny branchlet length. While the number of smooth branches and spiny branchlets was significantly reduced from adult control levels following climbing fiber-deafferentation (Fig. 32; Table 4), these losses, in addition, represented a 14% decrease in the number of smooth branches and a 40% reduction in spiny branchlet numbers from the weanling control values (Fig. 33; Table 5). Climbing fiber-deafferentation of the adult Purkinje cell dendritic tree, therefore, appears to result in a transneuronal degeneration of both smooth branches and spiny branchlets.

## (2) Spine Morphology and Distribution

The distribution of spines along the Purkinje cell dendritic tree following climbing fiber-deafferentation in the adult showed little change from the normal pattern. Although the number of spiny branchlets was significantly reduced (Figs. 30a, c, e, 31A,B), those which persisted were covered with a normal complement of dendritic spines (Fig. 30b, d, h). The loss of the spiny branchlets appeared to account for the total loss of spines. More importantly, the smooth portion of the Purkinje cell dendritic tree (primary trunks and smooth branches) remained non-spiny in appearance (Fig. 30b, f), although stubby thorn-like appendages were more frequently visualized along this segment following climbing fiber-

deafferentation (Fig. 30g). This finding is in direct contrast to the extensive distribution of ectopic spines found following climbing fiber-deafferentation of weanling rats. (see below).

#### b) Electron Microscopy

The inferior olivary complex of the adult rat was electrolytically lesioned using a ventral (parapharyngeal) approach or was chemically destroyed (as described above) by means of intraperitoneal administration of 3AP. In cases in which the olivocerebellar input was electrolytically destroyed animals were perfused 125 days following an inferior olivary ablation. Chemically lesioned animals were perfused 123-296 days following treatment. Since the changes reported within the cerebellar cortex were found to be comparable following either electrolytic or chemical lesions, the following description will deal mainly with the changes observed following long-term 3AP treatment.

##### (1) Transneuronal Degeneration

An examination of the cerebellar cortex following long-term climbing fiber-deafferentation of the adult has revealed marked degenerative changes within several of the neuronal elements. The Purkinje cell dendritic tree, in particular, showed definite signs of transneuronal degeneration. While the spiny branchlets were the most severely affected, the smooth branches showed degenerative changes following long-term climbing fiber-deafferentation (Fig. 34a, b, c). Electron-dense laminated bodies were a common feature within the dendritic matrix of these branches. While the origin of these

bodies is unknown, their formation appeared to coincide with the decrease in the number of mitochondrial profiles. The persisting agranular endoplasmic reticulum, in particular the profiles of hypolemmal cisternae, were highly swollen and irregular in outline. Although both the covering of Bergmann glia and the afferent input to the smooth branches of the Purkinje cell dendritic tree appeared normal, a small population of electron-dense profiles were found along the shafts of these smooth branches and are thought to represent recurrent axons of transneuronally degenerating Purkinje cells (Fig. 34a).

The changes found within the smooth branches of the Purkinje cell dendritic tree, however, appeared minor with respect to the alterations within the spiny branchlets. These branches were easily identified by their rich complement of mitochondria, dendritic spines and the presence of a system of hypolemmal cisternae. This portion of the Purkinje cell dendritic tree showed two distinct changes following long-term (123 days) climbing fiber-deafferentation. Firstly, large segments of the dendritic matrix were occupied by swollen profiles of the agranular endoplasmic reticulum. These profiles were frequently grouped into circular clusters giving the dendritic matrix a honeycombed appearance (Fig. 35a, d). Secondly, electron-dense laminated bodies were a prominent feature of the Purkinje cell dendritic matrix. In advanced terminal branchlet degeneration, many of the dendritic spines remained intact and appeared unaffected by the degenerative changes which had occurred within the shaft of the terminal branchlet (Figs. 35a, d). Along with the dendritic spine, a thin rim of dendritic matrix remained

associated with the plasmalemma of the spiny branchlet (Fig. 35d): The mitochondria and the hypolemmal cisternae were frequently the only organelles that persisted within this attenuated layer of dendritic matrix.

Within the cerebellar cortex 296 days following 3AP intoxication, the Purkinje cell terminal branchlets were in an advanced state of degeneration. By that time, the terminal branchlets were largely replaced by hypertrophied glial (Bergmann-like) processes. In many areas of the molecular layer, portions of the Purkinje cell dendritic tree appeared to be replaced by long linear profiles of glial elements. In other instances, these glial profiles contained long, thin, attenuated strands of electron-dense material which appeared to resemble the final remnants of spiny branchlet degradation (Fig. 35e, f).

These findings suggest that both the smooth branches and spiny branchlets undergo transneuronal degeneration following long-term climbing fiber-deafferentation. Furthermore, the extensive domain which these branches occupy within the normal cerebellar cortex appears to be subsequently filled by Bergmann glia-like profiles.

An examination of the granular layer following long-term climbing fiber-deafferentation in the adult has revealed a small population of degenerative profiles. These electron-dense profiles, although partially ensheathed by glia, were frequently in synaptic contact with an outer covering of granule cell dendrites (Fig. 35c). While these terminals could not be positively identified, the time

course for their removal would seem to exclude their being mossy fibers, leaving either recurrent Purkinje cell axons or glomerular collaterals of climbing fibers as possible alternatives.

#### B. Chemically Lesioned (3AP) Weanling Rats

##### Normal cytoarchitecture

##### The Purkinje cell

The Purkinje cell of the weanling control displayed a dendritic arborization at 21 days which was similar to that of the adult (Fig. 28d). Following Golgi impregnation, the weanling Purkinje cell dendritic tree was measured for the mean length, total length and number of primary trunks, smooth branches and spiny branchlets. By comparing the weanling value with the adult value, the amount of postnatal growth between the 21st and 150th day was estimated for each of the above parameters. The findings show that the majority of the primary trunks form and become fully mature in size prior to the 21st postnatal day (Table 4; Fig. 32). However, the mean length and the number of smooth branches were found to increase by 10% and 20% respectively and accounted for a 47% increase in the mean total smooth branch length over this period. Similarly, a postnatal growth within the spiny branchlet system was suggested by a 12% increase in the mean length and a 54% increase in the mean number of spiny branchlets between the 21st and the 150th postnatal day.

##### Spine morphology and distribution

The distribution of spines in the weanling rat was identical to that in the adult. The terminal branchlets possessed



a profuse studding of spines (Fig. 28f) while the primary trunks and smooth branches were characteristically smooth at the light microscopic level. The somatic spines that have been reported during the first two postnatal weeks (Larramendi, 1965) were not evident at the 21st postnatal day in the present study.

#### 1. Long-Term Changes Following Olivocerebellar Deafferentation

At the end of the 3rd postnatal week, the cerebellar cortex of the weanling rat was selectively deafferentated of its climbing fiber input following the intraperitoneal administration of 3AP (90 mg/kg body weight). These animals were allowed to survive for a period of from 131-380 days and their deafferentated cerebella were subsequently examined following Golgi impregnation or preparation for electron microscopy.

##### a) Golgi-Cox Material

##### (1) The Purkinje Cell Dendritic Tree

Linear measurements of the primary trunks, smooth branches and spiny branchlets were taken from the deafferentated weanling Purkinje cells as described previously. Adult Purkinje cells which had been deafferentated of their climbing fiber input as weanlings showed no change in the mean length or number of their primary trunks when compared with the adult controls (Fig. 32; Table 4). While the mean length of the smooth branches was similarly unchanged, the number of these branches was significantly reduced by 27% when compared to the adult control value. Due to a significant interaction between the two variables (lesion and time) a separation of the main effects could not be determined (Table 1, Appendix V). In

addition, both the mean length and number of spiny branchlets were found to undergo a significant decrease of 13% and 47% respectively from the adult controls (Fig. 32). The decreased mean spiny branchlet length which occurred following climbing fiber removal was dependent on the time of deafferentation (Table 1; Appendix III) and is expressed as a loss of postnatal growth (compare Figs. 32, 33). The decreased number of spiny branchlets, however, was the result of an interaction between both variables (Appendix VI). The dendritic arborization of these cells underwent a 37% decrease in the mean total smooth branch length and a 55% loss in the mean total spiny branchlet length. The loss of smooth branch and spiny branchlet numbers which occurs following climbing fiber-deafferentation in weanling rats appears to be the result of a loss of postnatal branching rather than transneuronal degeneration (compare Figs. 32, 33; Tables 4, -5).

## (2) Spine Morphology and Distribution

Light micrographs and corresponding camera lucida tracings of adult Purkinje cells deafferentated of climbing fibers as weanlings are represented in Figs. 36a,d and 37A,B. The long-term effect of weanling climbing fiber-deafferentation on the distribution of spines in the adult included an ectopic formation of spines along the smooth portion of the Purkinje cell dendritic tree (Fig. 36c). These spines resembled the dendritic appendages which characterize the spiny branchlets of adult control Purkinje cells (Fig. 28b,e). In several instances, these ectopic spines covered segments of major branches (secondary) as well as smaller preterminal branches within the "smooth portion" of the Purkinje cell dendritic arborization

(Figs. 36b, e, 37C, D). Although the number of spiny branchlets was significantly reduced, the distribution of spines along persisting branches appeared unchanged following long-term deafferentation of the climbing fiber input to the smooth portion of the Purkinje cell dendritic tree (compare Fig. 28b with 36b, e).

#### b) Electron Microscopy

##### (1) Transneuronal Degeneration

In contrast to the findings reported following long-term climbing fiber-deafferentation of the adult, olivocerebellar-deafferentation of the weanling rat did not produce significant degenerative changes in the dendritic tree of the Purkinje cell. Although a few spiny branchlets were found which appeared to have undergone degenerative changes (Fig. 35b), the dendritic arborizations of these cells appeared normal.

##### (2) Ectopic Spine Formation

While the dendritic tree of the Purkinje cell appeared normal following long-term climbing fiber-deafferentation of the weanling rat, there was an ectopic formation of dendritic spines along the "smooth branches" of these cells (Fig. 38f). Although the population of dendritic appendages along the "smooth branches" of the Purkinje cell dendritic tree in the control animal has been categorized by several authors as being comprised solely of dendritic thorns (Hamori and Szentagothai, 1966a; Palay and Chan-Palay, 1974; Desclin, 1976), the appendages found along this portion of the Purkinje cell dendritic arbor following long-term climbing fiber-

deafferentation of the weanling rat consisted of two distinct types. The first type averaged  $0.64 \mu\text{m}$  in length and corresponded morphologically to the dendritic thorn (Fig. 38a-c). These appendages had an enlarged head portion that was connected to the dendritic plasmalemma by a comparatively short neck piece. Occasionally, they lacked an obvious neck portion and took the form of an elevation of the dendritic plasmalemma (Fig. 38a inset). This population of dendritic appendages was not significantly different in length from the dendritic thorns of the control Purkinje cell (Tables 10, 11). In addition, many dendritic appendages which appeared structurally distinct from the dendritic thorns were found along the smooth portion of the Purkinje cell dendritic tree. This second type of dendritic appendage averaged  $0.9 \mu\text{m}$  in length and was 34% longer than the control dendritic thorn. It possessed an elongated neck piece that gave rise to an enlarged head portion (Fig. 38d, e, g, h). While these appendages were significantly longer than the dendritic thorns, they were not found to be significantly different from the dendritic spines on the terminal branchlets of the control Purkinje cell dendritic tree (Tables 10, 11).

### (3) Heterotypical Reinnervation

While climbing fiber varicosities were not observed within the molecular layer of the long-term 3AP treated weanling rat, many dendritic appendages, which structurally resembled the thorn processes, were found. It appeared, however, that many of these thorns had become heterotypically reinnervated and in several instances an axon bouton resembling a parallel fiber varicosity was found in

synaptic association with these dendritic thorns (Fig. 38a,c). Most often parallel fiber profiles adjacent to the smooth portion of the Purkinje cell dendritic tree are passing fibers en route to their postsynaptic target, the dendritic spines of the terminal branchlets. Unless a dendritic spine from an adjacent Purkinje cell terminal branchlet is found in the immediate vicinity of the smooth portion of the Purkinje cell dendritic tree, these fibers are not found to display synaptic specializations. The parallel fiber varicosities found in synaptic contact with the dendritic thorns might represent existing terminals or en passant boutons having a synaptic contact in a different plane with a dendritic spine. However, an examination of the varicosities of parallel fiber-dendritic thorn synapses has not shown the existence of a second synaptic specialization. It is equally possible that the postsynaptic element, the dendritic thorn, is capable of inducing the formation of an entirely new parallel fiber varicosity rather than simply being reinnervated by a pre-existing formation (Fig. 38a,c).

The dendritic spine-like processes (the second type of dendritic appendage) found along the smooth portion of the Purkinje cell dendritic tree were frequently observed to have a synaptic input. In most situations, the afferent input to these ectopic spines originated from a parallel fiber varicosity (Fig. 38e,g,h). In addition, however, axons of an inhibitory nature (basket axons) were found in synaptic contact with the dendritic spine-like processes (Fig. 38d). Within the same plane of section these boutons were found making synaptic contact with both the smooth portion of the Purkinje

cell dendritic tree and dendritic spine-like appendages. Thus, these findings would suggest that the dendritic spine-like appendages are also capable of inducing a sprouting or an enlargement of pre-existing basket boutons.

C. Chemically Lesioned (3AP) Weanling  
and Adult Rats

Normal cytoarchitecture

Cerebellar interneurons

Localized within the lower third of the molecular layer, the basket cell is most commonly found orientated in the sagittal plane with the long axis of its nucleus lying parallel to the Purkinje cell layer. The somata of these cells are occupied largely by their nuclei which are often deeply invaginated. The dendritic arborization of the basket cell, which fans out in the vertical plane, has been shown in rapid-Golgi preparations to be relatively sparse (Chan-Palay and Palay, 1970). The dendrites are highly irregular in caliber and contorted in appearance. Unlike the Purkinje cell, the basket cell has been found to lack a neuroglial sheath. Despite this, synaptic contacts are infrequent on the soma and dendrites of these cells as compared to the Purkinje cell (Palay and Chan-Palay, 1974).

Within more superficial levels of the molecular layer (particularly its outer two-thirds) a different perikaryal profile appears to predominate. Like the basket cell, the somata of these cells are occupied primarily by their nuclei, however, the cytoplasm usually appears even less voluminous (Fig. 68a). Their nuclei are

simple in outline and have a homogeneous dispersed content of heterochromatin. Under low magnification, mitochondria and Golgi complexes are the most prominent organelles within the cytoplasm. Although the dendrites of these cells lie along the parasagittal plane, they are not restricted to a fan-shaped distribution. The dendrites of these cells follow a course and possess a caliber which is even more variable than that shown by the basket cell. As a result, electron microscopic sections rarely follow the longitudinal axis of these dendrites (Fig. 68b). As neither the perikaryon nor its dendritic arborization possess a Bergmann glial covering, these profiles are readily distinguished from Purkinje cells. Their localization within more superficial portions of the molecular layer and their paucity of axosomatic and axodendritic contacts are the main features that distinguish the soma and dendrites of the stellate cell from the morphologically similar basket cell.

1. Long-Term Changes Following Olivocerebellar Deafferentation

- a) Transneuronal Changes within Cerebellar Interneurons

- ✓ Electron microscopy

A most unexpected finding of the present study was the presence of transneuronally degenerating perikarya within the molecular layer of both climbing fiber-deafferentated weanling and adult rats which were clearly not Purkinje cells (Fig. 39a,b). The somata of these cells were localized throughout all levels of the molecular layer and under high magnification they were found to lack a neuroglial covering (Fig. 39c,d). By virtue of their

location and shape, and their lack of a neuroglial covering, these profiles were identified as degenerating somata of both basket and stellate cells. Those degenerating somata within the lower third of the molecular layer generally possessed voluminous cytoplasm, an irregular nuclear envelope (Fig. 39a) and a high percentage of axosomatic contacts, and were therefore identified as deafferentated basket cells (Fig. 39c). The remaining degenerating somata were found to possess a simple nuclear outline, a thinner layer of cytoplasm and relatively few axosomatic contacts, which are all characteristics of stellate cells (Fig. 39d).

The degenerative changes of both the basket and stellate somata were accompanied by a large number of smaller electron-dense profiles within the molecular layer of both weanling and adult rats (Fig. 40). These profiles represented dendrites which had undergone an electron-dense form of degeneration. While these dendrites were rarely cut parallel to their longitudinal axis, transverse sections through them often displayed several synaptic contacts with parallel fiber varicosities (Fig. 40b,f). The dendritic matrix of these profiles appeared homogeneously electron opaque, thus concealing most of the cytoplasmic contents. By 180 days following 3AP treatment, the mitochondrial profiles were frequently the only distinguishable organelle.

By 296 days following climbing fiber-deafferentation, the dendrites of both basket and stellate cells were at an advanced stage of electron-dense degeneration. On occasion, sections were cut along the longitudinal axis of a degenerating dendrite (Fig. 40e). In



such instances, thin attenuated strands of electron-dense material (which often still maintained an afferent input) were found projecting through the molecular layer. While astrocyte-like elements were occasionally found to engulf large fragments of degenerative debris (Fig. 40d), most of the dendritic profiles did not appear to have an association with glial elements even though they were in an advanced stage of degeneration (Fig. 40a-c,f,g). Although at least a partial loss of the basket and stellate cell population occurred following climbing fiber-deafferentation, the afferent input to these transneuronally degenerating profiles (largely parallel fibers) appeared unaffected (Fig. 40b,e).

#### 4.6 Lesion Site within the Adult Basilar Pontine Gray

Removal of the pontocerebellar input to the contralateral cerebellar hemisphere was performed electrolytically using a dorsal approach. Serial sections of thionine-stained material were examined throughout the rostrocaudal extent of the pons to determine the location of the lesion. Animals with pontine lesions involving a major portion of the basilar pontine gray were used in investigations of the short- and long-term effects of pontocerebellar-deafferentation (Fig. 41).

#### 4.7 The Ansiform Lobule of the Cerebellum

##### A. Short-Term Changes Following Pontine Ablation

##### 1. Electron Microscopy

##### a) The Mossy Fiber Glomerulus

Although Golgi methods have been used to impregnate

the axonal plexus of pontine neurons, the synaptic details of these fibers within the granular layer were poorly documented until recently (Palay and Chan-Palay, 1974). The inadequacies of the Golgi method usually have precluded the simultaneous infiltration of both pre- and postsynaptic elements of the synapse (Cajal, 1909; Scheibel and Scheibel, 1954). As a result, many of the early reports of interneuronal connections relied primarily upon speculation about the proximity of specific fibers. Until the advent of high resolution electron microscopy the complexities of the interneuronal contacts of the cerebellar glomeruli were pure conjecture.

Within the granular layer, the preterminal portion of the mossy fiber is found to be a thinly myelinated axon. As the mossy fiber approaches its synaptic portion the myelin sheath terminates, allowing the axon to distend and form a tuberos enlargement which is variable in form, called the mossy fiber varicosity. The synaptic portion, which gives the mossy fiber its name, may form along the course of the fiber, within its branching points or as the terminal arborization of the axon. Three types of mossy fiber varicosities have been described based on the presence or absence and the arrangement of filopodia-like extensions over their surface (Palay and Chan-Palay, 1974). The first type, the simple mossy fiber varicosity, is a simple fusiform enlargement which is smooth in form and has no filopodial projections (Fig. 42a-c, e). The second type, the complex mossy fiber varicosity, is more complicated in form and has several angular profiles which project from the surface of the varicosity (Fig. 43a, b, e). The third variety, the filigree type, which most frequently

represents the terminal expansion of the mossy fiber, has a cone shaped varicosity which terminates into a "flower-spray figure". In addition, a variation exists in the concentration of synaptic vesicles, which necessitates a further classification of mossy fiber terminals as either dispersed (Fig. 42a-c, 43a,b,e,) or clustered (Fig. 42e) for all three forms of mossy fiber varicosities.

A careful examination of the population of mossy fiber varicosities within the ansiform lobule of the cerebellum revealed that the majority of the terminals resembled either the simple dispersed (60%) or the complex dispersed (26%) variety. While fewer in number, mossy fiber varicosities were identified which structurally corresponded to either the simple clustered (12%) or the complex clustered (2) varieties. The existence, however, of the filigree type of mossy fiber terminal within the ansiform lobule was not confirmed.

Since extensive descriptions of the normal cytological characteristics of the mossy fiber glomerulus in the rat already exist; only the structural features which are pertinent to the findings reported following short- and long-term mossy fiber deafferentation will be described (Hamori and Szentagothai, 1966a; Palay and Chan-Palay, 1974).

The mossy fiber varicosity was confirmed as the central component of the cerebellar glomerulus (Figs. 42b, 43b). The varicosity of the mossy fiber has been shown to contain three overlapping layers of organelles (Palay and Chan-Palay, 1974). The first layer, a central core of neurofilaments, is surrounded by the

second layer, an adjacent stratum of elongated mitochondria. The third layer, the outer "cortical zone" has been shown to contain the vesicular component of the mossy fiber varicosity (Figs. 42a, 43a). These varicosities are completely ensheathed by the profiles of granule cell dendrites which frequently lodge in shallow grooves along the outer surface (Figs. 42b, 43a). Oblique sections through dendritic profiles of granule cells have confirmed an extensive area of approximation between these dendrites and the mossy fiber varicosity. These dendritic profiles (granule cell digitiform branches) are commonly found to be several rows deep around the periphery of the mossy fiber varicosity, forming a thick dendritic covering. Granule cell digitiform branches, which are cut transversely, are found to contain a single mitochondrial profile and a few tubules of smooth endoplasmic reticulum (Fig. 42f). The synaptic cleft between the granule cell digitiform dendrite and the mossy fiber terminal is a widened intercellular space filled with dark filamentous material that results from a slight concavity in the surface of the postsynaptic dendrite (Fig. 42d). On the cytoplasmic side of the postsynaptic element there is a thickened filamentous plaque, which contrasts sharply with the small tufts of filamentous material which project into the mossy fiber varicosity and form the presynaptic plaque. Generally a small cluster of round synaptic vesicles is associated with the presynaptic plaque. The synaptic contact between the mossy fiber varicosity and the granule cell dendrite corresponds closely to the Gray's type 1 junctional complex.

Recently, the axonal arborization of the Golgi cell has been shown to contribute to the mossy fiber glomerular complex.

Distributed along the periphery of the glomerulus, these terminals have been shown to make synaptic contact with the outer surface of the granule cell digitiform dendrites opposite to the synapses made with the mossy fiber varicosity (Fig. 42f) (Mugnaini, 1972).

#### Anterograde degeneration

At the end of the 12th postnatal week, the mossy fiber input (the pontocerebellar projection) to the lateral cerebellar cortex of the rat was destroyed by electrolytically lesioning the contralateral basilar pontine gray. These deafferentated animals were permitted to survive from 3-4 days.

An electron microscopic examination of both the contralateral and ipsilateral ansiform lobule was undertaken. The distribution of degenerative debris following pontine ablation confirmed a large pontocerebellar input to the ansiform lobule. The degeneration, heaviest on the contralateral side, was restricted to the granular layer and confirmed to be mossy fiber in nature. Although the percentage of degenerating mossy fiber varicosities was not calculated following pontine ablation, few normal-appearing mossy fiber varicosities were found within the ansiform lobule. Furthermore, the majority of the degenerating mossy fiber terminals resembled either the simple dispersed or the complex dispersed variety of varicosity. On occasion, however, mossy fiber varicosities were found which appeared to correspond structurally to either the simple clustered or the complex clustered varieties.

As early as 3 days following pontine ablation, the

myelinated portions of the pontocerebellar fibers were found in an advanced stage of degeneration (Fig. 44a,b). The axoplasmic content of these fibers was frequently clumped, forming small fragments of electron-dense material. The mitochondrial profiles contributed to the electron opacity of the axoplasmic content through the increased staining of their intercrystal matrix and the loss of their cristae.

Concurrently, degenerative changes were observed within the synaptic portions of the pontocerebellar fibers. Most of the mossy fiber varicosities showed early signs of degeneration within 3 days of pontine ablation. Two distinct axonal reactions were apparent. A large proportion of the mossy fiber varicosities were found to undergo an electron-lucent type of degeneration while a much smaller group followed a course of electron-dense degeneration. The pontocerebellar varicosities which underwent an initial electron-lucent type of degeneration showed two distinct degenerative changes. Firstly, these varicosities were found to contain a number of double membrane bound organelles with clear centers. Secondly, the vesicular component of the varicosity was frequently clumped, forming discrete islands of clustered synaptic vesicles (Figs. 44c,e, 45a,b). The formation of these clear organelles and synaptic vesicle clusters resulted in an overall loss of electron-density within the mossy fiber varicosity. These organelles were considered to be profiles of mitochondria which had lost their cristae and intercrystal matrix. The mossy fiber varicosities which had undergone an electron-lucent type of degeneration appeared to correspond either to the simple or the complex variety of mossy fiber varicosity and had a dispersed

synaptic vesicle population.

By the end of the 3rd day, a small population of mossy fiber varicosities (15.3%) were found which appeared to have undergone an electron-dense form of degeneration (Fig. 45d,e). In each instance, these electron-dense varicosities had a simple outline and possessed a dense synaptic vesicle population. The axoplasm and mitochondrial matrix of these pontocerebellar varicosities were markedly electron-dense. Their synaptic vesicles were found to vary both in shape and size, and were thought to be more densely clustered than the vesicle population of control pontocerebellar varicosities. Cytologically and numerically, these varicosities appeared to correspond to the simple clustered variety of mossy fiber terminal.

By the end of the 4th day, small fragments of necrotic debris were occasionally encountered within the granular layer. This debris was interpreted as representing the remains of pontocerebellar varicosities of the simple clustered type (Fig. 46a-d). Frequently, these profiles were found completely ensheathed by glial membranes and were separated from their normal postsynaptic contacts, the granule cell digitiform branches. However, just as often these degenerating mossy fiber varicosities were found to maintain a synaptic contact with their postsynaptic element even during the final stages of pontocerebellar degeneration. In many instances, microglia-like profiles were associated with degenerating pontocerebellar varicosities and contained dense globular fragments which resembled necrotic mossy fiber terminals (Fig. 46d). These pontocerebellar varicosities appeared to represent the degenerative

remains of the simple clustered variety of mossy fiber terminal because of their similarities in shape, number and vesicle population density.

b) The Granule Cell Dendrite.

Normal cytoarchitecture

The soma of the granule cell has been shown to give rise to 3-5 dendritic trunks which remain unbranched until they are within the vicinity of a mossy fiber varicosity. At that point, each of the main dendrites divides and forms a number of digitiform branches which eventually ensheath a mossy fiber varicosity. The main dendritic branches contain a complement of microtubules, smooth endoplasmic reticulum and mitochondria, all of which are orientated along the longitudinal axis of the dendrite. Recent observations have shown that these organelles continue within the smaller digitiform branches (Palay and Chan-Palay, 1974). At the electron microscopic level, these branches are conspicuous by their peripheral localization about the mossy fiber varicosity and their mitochondrial content (Fig. 42c).

Transneuronal degeneration

The dendrites of granule cells which ensheathed either the simple or the complex dispersed forms of mossy fiber varicosities appeared normal following short-term pontine ablation (Figs. 44d, 45c). Even within the glomeruli which underwent a rapid form of electron-dense degeneration, the granule cell digitiform branches appeared normal. Their postsynaptic plaques remained intact and were found



associated with small fragments of degenerating pontocerebellar varicosities (Fig. 46a). In such instances, the digitiform branches frequently appeared less oval and more pyramidal in shape as a result of the subsequent degeneration and shrinkage of the pontocerebellar varicosity. However, their cytological components appeared normal. The profiles of Golgi cell axons, on the other hand, were occasionally found containing membrane bound profiles which may be indicative of early transneuronal changes (Fig. 46a).

## B. Long-Term Changes Following Pontine Ablation

### 1. Golgi-Cox Material

At the end of the 12th postnatal week, the cerebellar cortex was selectively deafferentated of its mossy fiber input.

These deafferentated animals were permitted to survive from 125 - 130 days.

#### a) The Purkinje Cell Dendritic Tree

Purkinje cells, from cerebella deafferentated of their mossy fiber input in the adult, were not found to be significantly different from the adult controls with regards to the mean length of their primary trunks, smooth branches and spiny branchlets (Fig. 32, Tables 3,4). Their dendritic arborizations, however, were characterized by a marked decrease in the number of smooth branches and spiny branchlets when compared to the adult control values (compare Figs. 47a, 48A with Figs. 28a, 29A). More specifically, both the smooth branches and spiny branchlets were significantly decreased in number by 51% and 55% respectively following mossy fiber-deafferentation. The decrease

in the number of smooth branches was responsible for a 50% decrease in the mean total smooth branch length while the loss of spiny branchlets resulted in a 64% reduction in the mean total spiny branchlet length. These decreases have been interpreted as a result of transneuronal degeneration following mossy fiber-deafferentation. In addition, these losses represented a 25% reduction in the number of smooth branches and a 32% loss in the number of spiny branchlets as compared to the values obtained for the weanling controls (Fig. 33, Table 5).

#### b) Spine Morphology and Distribution

While a loss of spines occurred following mossy fiber-deafferentation, it took place primarily as a result of the reduction in the number of spiny branchlets (Figs. 47a, 48A). More importantly however, these spines were found to undergo marked changes in form. Purkinje cells from mossy fiber-deafferentated cerebella were found to possess a dendritic spine population along their spiny branchlets which appeared markedly hypertrophied (elongated) (Figs. 47b, 48B). While these alterations were not found in all Purkinje cells, nor were they homogenous within the dendritic tree of a single Purkinje cell, a considerable number of the dendritic spines were involved.

## 2. Electron Microscopy

### a) The Mossy Fiber Glomerulus

At the end of the 12th postnatal week, the mossy fiber input to the lateral cerebellar cortex was electrolytically

destroyed following a lesion of the contralateral basilar pontine gray. These deafferentated animals were permitted to survive from 34 - 93 days.

Examination of the granular layer of the ansiform lobule revealed the presence of degenerating pontocerebellar fibers following long-term (34 - 40 days) pontine ablation. Degenerating myelinated pontocerebellar fibers were found coursing through the granular layer (Fig. 49a). Cytologically, these fibers resembled the degenerative fibers found on the 3rd day following pontine ablation. Removal of the myelinated pontocerebellar debris appears to be a very slow process. Even more unexpectedly, a large number of degenerating pontocerebellar varicosities were found to persist following long-term (40 days) pontine ablation. At this stage, all pontocerebellar varicosities were in an advanced form of electron-dense degeneration and contrasted sharply with their appearance following short-term pontine ablation (Figs. 49c, e, 50a, d). The electron-density of both the axoplasm and the mitochondrial intercrystal matrix of the pontocerebellar varicosities increased between the 3rd and the 34th day following pontine ablation. Many of the synaptic vesicles had become pleomorphic in shape while others had undergone dissolution. In general, the vesicles were less easily discerned from the background axoplasmic matrix.

The removal of this second group of pontocerebellar varicosities (simple and complex dispersed mossy fiber varicosities) appears to be a much slower process than that reported for the first type of pontocerebellar terminal (simple clustered type of mossy

fiber varicosity). Reactive glial elements resembling those described during the removal of the simple clustered type of mossy fiber varicosity, were not found in association with the second group of degenerating pontocerebellar varicosities and may explain their persistence.

Between 40 and 57 days following pontine ablation, the pontocerebellar varicosities appeared to undergo a substantial reduction in size with a further increase in electron opacity (Fig. 51a-c). For the first time, glial elements which had the appearance of astrocytic profiles were found adjacent to the necrotic debris of mossy fiber varicosities (Fig. 51a, b). In spite of this, the irregular and necrotic profiles of these mossy fiber varicosities were found to maintain their synaptic contacts with the postsynaptic element, the granule cell dendrite. Areas of the mossy fiber varicosity not directly associated with the postsynaptic element appeared accessible to astrocyte-like profiles. The axoplasmic matrix of these mossy fiber terminals had undergone a further darkening and occasionally was found to contain whorled membranous bodies (Fig. 51c). By 80 days following pontine ablation, the number of degenerating pontocerebellar fibers and varicosities was markedly reduced (Fig. 52a, c). The few remaining degenerative varicosities occurred as small islands of necrotic debris (Fig. 52c). Most of the organelles (specifically the vesicular component and the mitochondrial profiles) were barely distinguishable from the electron-dense axoplasmic matrix. These degenerative varicosities were highly shrunken in appearance. Along the periphery of

degenerating pontocerebellar varicosities, only those granule cell dendrites in synaptic contact with the mossy fiber axons remained to form the inner layer of dendritic covering. It is suggested that as the pontocerebellar varicosity degenerates it shrinks in size and draws inward the postsynaptic elements in which a synaptic contact is present. Thus, during the final stages of pontocerebellar degeneration, the inner dendritic layer of the glomerulus is comprised solely of granule cell dendritic profiles in synaptic contact with the pontocerebellar varicosity.

The adherence of the pontocerebellar-granule cell synapse was demonstrated by the changed contour of the granule cell digitiform branches. In transverse sections of the normal pontocerebellar glomerulus, the granule cell digitiform branches have an ovoid shape and the synaptic plaque (pre- and postsynaptic densities) of the pontocerebellar-granule cell synapse accounts for approximately 50% of the total contact surface. With a progressive loss in the mossy fiber varicosity size, the synaptic plaque accounted for the entire contact surface of the pontocerebellar-granule cell synapse, forcing the dendritic digitiform branches to become pyramidal in shape (Fig. 52c).

In animals which had long-term pontine ablations (80 days), dendritic islands ensheathed by the profiles of Golgi cell axons were occasionally encountered which structurally resembled a pontocerebellar glomerulus devoid of its normal axonal core (Fig. 52d). These axon-free glomeruli, which otherwise appeared

normal, were common to areas which received a partial mossy fiber-deafferentation. It is suggested that these dendritic islands represent the final stage of long-term pontocerebellar degeneration.

b) The Granule Cell Dendrite

Transneuronal degeneration

\* Following long-term (34 - 40 days) pontine ablation, the granule cell digitiform branches showed marked signs of transneuronal degeneration. Most obvious was a swelling of the smooth endoplasmic reticulum (Fig. 49d, 50b, e). Normally, the lumen of the smooth endoplasmic reticulum is tubular in shape. Following long-term pontocerebellar ablation, the lumen of the smooth endoplasmic reticulum enlarged and became oval or semilunar in outline. While the mitochondria were not as severely affected, their overall appearance suggested an increased darkening of the intercrystal matrix and an enlargement of the intracrystal spaces. In many instances, the cristae appeared as blebs or vacuoles rather than as longitudinal folds. These changes were found in the digitiform branches ensheathing both the simple and the complex forms of mossy fiber varicosities.

By 57 days following pontine ablation, the profiles of the granule cell digitiform branches appeared markedly reduced in size. In these branches, the cisternal spaces of the smooth endoplasmic reticulum were frequently enlarged and filled much of the dendritic matrix (Fig. 51b). In addition, a concurrent loss of electron opacity of the granule cell dendritic matrix has given these profiles an electron-lucent appearance. In contrast, the intercrystal matrix has increased in electron density. While several of the

intercrystal spaces appeared enlarged, many others were collapsed and indistinguishable from the darkened mitochondrial matrix.

In several instances, filopodia-like projections from the granule cell digitiform branches were found surrounded by the degenerating pontocerebellar varicosity (Figs. 49d, 51a,c inset). At the same time, membrane bound vacuoles were found within the axoplasm of the pontocerebellar varicosity. These varicosities contained debris resembling the filopodia-like projections of the granule cell dendrite (Figs. 49c, 51c). These findings suggest that the degenerating pontocerebellar terminals are engaged in the engulfment of their postsynaptic elements, the granule cell digitiform dendrites.

By 57 days following pontine ablation, many of the pontocerebellar varicosities showed large areas along their surface which were denuded of a normal granule cell dendritic sheath. The persisting granule cell digitiform branches appeared vacuolated and electron-lucent. These findings suggest that many of the digitiform branches which ensheath the mossy fiber varicosities are possibly removed through the activity of the degenerating mossy fiber varicosity.

#### c) The Granule Cell Soma

##### Normal cytoarchitecture

The thin rim of cytoplasm which encases the granule cell nucleus is found to contain a small complement of mitochondria, free clusters of rosettes of ribosomes and an occasional profile of

smooth endoplasmic reticulum. The nucleus is eccentrically located and is enclosed by a typical double-membraned nuclear envelope with a narrow perinuclear space (Fig. 53a). The nuclear content of heterochromatin is localized mainly within pyramidal shaped bodies and is distributed along the periphery of the nucleus. The chromatin content within the central region of the nucleus is dispersed and forms the euchromatin portion.

#### Transneuronal degeneration

Following long-term pontocerebellar deafferentation, the somata of the granule cells showed marked degenerative changes. In many instances, the granule cells appeared to undergo an electron-lucent form of degeneration following pontocerebellar-deafferentation (Fig. 53c,d). The areas of heterochromatin appeared to have become more electron-dense while the adjacent regions of euchromatin appeared more loosely arranged or electron-lucent. In addition, the perinuclear space of these cells had become highly enlarged. Within the cytoplasmic matrix of the granule cell, the Golgi complex frequently appeared more highly vacuolated and distended. The rim of cytoplasmic matrix was more attenuated and electron-lucent than in the normal granule cell perikaryon.

In several locations, small dark pyknotic cells were found whose somata possessed a thin rim of cytoplasmic matrix which was both highly irregular in outline and thickness. The cytoplasmic matrix of these cells was electron opaque and contained a rich complement of polysomes. These somata resembled reactive glial cells



and are thought to represent oligodendroglial cells activated by the secondary degeneration of the pontocerebellar projection (Fig. 53b, c).

d) The Granule Cell Axon

Normal cytoarchitecture

The ascending axon of the granule cells has been shown to bifurcate within the molecular layer to form two parallel fibers which run in opposite directions along the longitudinal axis of the cerebellar folium (Palay and Chan-Palay, 1974). Their diameters range from 0.1 to 0.2  $\mu\text{m}$  and their axoplasmic content consists largely of a few microtubules and profiles of smooth endoplasmic reticulum. These profiles frequently form a solid mosaic which lacks an intervening covering of neuroglia and numerically represent the most important afferent input to the molecular layer. While their diameters show little variation in size, enlargements are found both at sites of mitochondrial localization and presynaptic varicosities (either terminal or en passant) (Fig. 54b). These presynaptic varicosities are associated directly with Purkinje cell dendritic spines. At the site of a presynaptic varicosity, the axonal profile becomes enlarged and contains a dispersed population of round synaptic vesicles which frequently shows some clustering in association with the presynaptic membrane. The synaptic junction of the parallel fiber-Purkinje spine synapse possesses a widened intercellular cleft which has marked asymmetrical post- and presynaptic densities. Sections through the longitudinal axis of the Purkinje cell dendritic

spine have revealed that the synaptic contact with the parallel fiber varicosity frequently occurs along the side of the head of the spine rather than at its apex (Palay and Chan-Palay, 1974).

#### Transneuronal degeneration

An examination of the cerebellar cortex following long-term pontine ablation (40 days) revealed a marked transneuronal degeneration within the molecular layer. In general, the electron-density of many of the cellular constituents within the molecular layer had increased. The highly compact and organized arrangement, which was typical of the normal molecular layer, became rather loose and disorganized following long-term pontine ablation (Fig. 55a,c). Of the neuronal elements which became electron-dense, the parallel fibers were the most conspicuous. Their normally electron-lucent axoplasmic matrix was markedly electron opaque (Fig. 55b,d,e). As a result, both the vesicular component and the smooth endoplasmic reticulum were barely discernible within the presynaptic varicosities of these fibers. Furthermore, the intercrystal matrix was increased in electron-density. Parallel fiber axons showed extreme variations in diameter following long-term pontine ablation. In sections parallel to the longitudinal axis of these degenerating fibers, they appeared as long, attenuated electron-dense strands with globular swellings corresponding to the sites of both mitochondria and presynaptic varicosities (Fig. 55e). Despite the transneuronal degeneration of the presynaptic component, the postsynaptic Purkinje cell spine appeared intact (Fig. 55d). These spines were readily

distinguished within the molecular layer because of their synaptic contact with the electron-dense parallel fiber varicosity. In addition, the appearance of the dendritic matrix, the smooth endoplasmic reticulum and the postsynaptic membrane density of these spines appeared normal.

#### e) The Purkinje Cell Dendritic Tree

##### Normal cytoarchitecture

The appearance of the Purkinje cell dendritic tree in the longitudinal plane of the folium has been described by Cajal and others as resembling an "espaliere fruit tree" (Palay and Chan-Palay, 1974). At the electron microscopic level it represents the most common dendritic element encountered within the molecular layer. These dendrites are easily distinguished by their well-developed subsurface hypolemmal cisternae and covering of Bergmann glia. Both these features, common to the Purkinje cell dendrites, are also distinguishing characteristics of the Purkinje cell thorns and spines (Fig. 54).

##### Transneuronal degeneration

Following long-term (40 days) pontine ablation, the dendritic content of the molecular layer underwent a marked reduction in comparison with the adult controls. In particular, the number of Purkinje cell dendritic profiles was found to be significantly reduced. The plasmalemma surface of many of the branches within the Purkinje cell dendritic tree was found to be more irregular and

contorted in outline (Fig. 55a,c). The adjacent neuropil of Purkinje cell arborizations was loosely organized and appeared to be withdrawn from the Bergmann glial covering of the dendritic tree (Fig. 55b). Within all branches of the Purkinje cell dendritic tree, elements of the smooth endoplasmic reticulum were markedly swollen and were frequently found associated with the hypolemmal cisternal system. As a result, discrete pyramidal-shaped stacks of swollen endoplasmic reticulum were localized immediately beneath the plasmalemma of these Purkinje cell dendrites (Fig. 55a,c). Along with the fragmentation of the mitochondrial cristae, the intercrystal matrix of the mitochondria increased dramatically in electron density. Concurrently, the microtubular component of these smooth branches, although present, became significantly less prominent. More importantly, the effects of long-term pontine albatton were most conspicuous within the smallest branches of the Purkinje cell dendritic tree, the terminal branchlets. The number of terminal branchlets was found to be severely reduced at all levels of the molecular layer. Careful inspection revealed small electron-dense profiles of degenerating dendrites throughout the thickness of the molecular layer. Although markedly electron opaque these profiles possessed a concentration of mitochondria and remnants of a hypolemmal cisternal system which resembled that of the terminal branchlets (Fig. 56b,d). While these degenerating dendrites were rarely cut so as to confirm their covering of spines, these profiles were undoubtedly the terminal branches of the Purkinje cell dendritic

tree. In a few instances, terminal branchlets were found which did not appear electron-dense, although they showed degenerative changes in their mitochondria and smooth endoplasmic reticulum which resembled those reported above within the smooth branches.

f) The Dendritic Arborization of the  
Cerebellar Interneuron

Transneuronal degeneration

Following long-term pontine ablation, electron-dense dendritic profiles were found which could be distinguished from those of Purkinje cells. These profiles lacked both a hypolemmal cisternal system and a covering of dendritic spines. In fact, the dendritic shafts of these profiles were marked by multiple axodendritic synapses (Fig. 57a - c). While Purkinje cells receive afferent inputs on both their somatic and dendritic surfaces (shaft and appendages), the main areas of postsynaptic contact have been shown to be restricted largely to the spines (parallel fiber input) and the thorns (climbing fiber input) along the dendritic arborization (Chan-Palay and Palay, 1970; Palay and Chan-Palay, 1974; Desclin, 1976). While axodendritic synapses are found along the main dendritic shafts and soma (basket, stellate and recurrent Purkinje cell collaterals), their numbers are comparatively few and their distribution is such that only rarely are there two or more axodendritic synapses in close proximity. Thus, it is suggested that an additional population of dendrites other than that which arises from Purkinje cells has undergone an electron-dense form of

degeneration following long-term pontine ablation. Because the identification of the various dendrites within the molecular layer relies solely on distinguishing features which are mainly visible in the longitudinal plane, these electron-dense dendrites could not be identified as belonging to a specific interneuron type (Golgi, basket or stellate).

The absence of a normal population of interneuron dendrites within the molecular layer following long-term pontine ablation suggests that this second group of dendrites represents a combined population of all interneuron dendrites (Golgi, basket and stellate).

#### 4.8 Lesion Site within the Adult or Weanling Lateral Cerebellar Hemisphere

At the end of the 3rd or the 12th postnatal week, the lateral cerebellar hemisphere of the weanling or adult rat respectively was transected perpendicular to the longitudinal axis of the cerebellar folia to remove the parallel fiber input to the spiny branchlets of adjacent Purkinje cells. Serial coronal sections of thionine-stained material were examined throughout the rostrocaudal extent of the cerebellum to determine the mediolateral location and the depth of the transection. Animals having lesions which were restricted mainly to the cortical layer of the ansiform lobule were subsequently used in investigations of the short- and

long-term effects of parallel fiber-deafferentation (Fig. 58).

#### 4.9 The Ansiform Lobule of the Cerebellum

##### A. Short-Term Changes Following Parallel Fiber-Deafferentation of the Adult or Weanling Rat

###### Electron microscopy

Ultrastructural preparations of the cerebellar granule cell layer subsequent to cortical transections revealed that many of the granule cell perikarya immediately adjacent to the lesion (within the first 2 mm) showed alterations which could be interpreted as early signs of retrograde degeneration (Fig. 59b). While many of the organelles were normal, the ribosomal content of these perikarya appeared reduced and the peripheral portion of the cytoplasmic matrix appeared devoid of cytoplasmic organelles, giving the cytoplasm of these cells a more electron-lucent appearance than in the control granule cells (Fig. 59a).

Following an examination of the molecular layer immediately adjacent to the lesion, many electron-dense profiles were found scattered throughout the neuropil between 3.5 - 4 days following the cortical transection (Fig. 60c,d).

Although in an advanced stage of degeneration, many of these degenerative fragments were found attached to profiles

which structurally resembled the dendritic spines of the Purkinje cell terminal branchlets (compare Fig. 60b with Fig. 60e). While profiles with less marked degenerative changes were difficult to find at this stage, there is little doubt that they represent the proximal stumps of parallel fibers transected following cortical lesions because of their exclusive input to the dendritic spines of the Purkinje cell terminal branchlet (Eccles et al., 1967). Although the numbers of degenerating parallel fiber-dendritic spine profiles within any particular field of molecular layer were relatively small, the actual percentage of parallel fibers which degenerate following cortical transections is thought to far exceed the numbers observed for the time periods sampled.

Bergmann glial profiles which normally ensheath the Purkinje cell dendritic spine but not its afferent input were found forming an ectopic covering around large portions of degenerating parallel fibers (Fig. 60d,e). In these instances, the Bergmann glial profiles appeared hypertrophied. In other situations, these glial elements were found in direct contact with the postsynaptic thickening of a Purkinje cell dendritic spine and occasionally were thought to be involved in phagocytizing portions of the Purkinje cell dendritic spine (Fig. 60f). Furthermore, electron-dense profiles were found separated by glia from adjacent Purkinje cell dendritic spines which displayed postsynaptic membrane thickenings. These spines were thought to have become denuded following cortical transections by Bergmann glial elements. These findings suggest



that Bergmann glial cells may play an active role in the phagocytic removal of both degenerating parallel fibers and their postsynaptic targets, the Purkinje cell dendritic spines. Cortical transections performed on the 21st postnatal day of weanling rats produced a similar pattern of electron-dense parallel fiber degeneration within the molecular layer neuropil (Fig. 60h).

Elsewhere within the granule cell layer, several of the digitiform branches of granule cell dendrites appeared electron opaque (Fig. 60g). While many of the dendritic profiles along the periphery of mossy fiber rosettes appeared normal (4 days following parallel fiber transection), others showed distinct signs of having undergone an increase in the electron-density of their dendritic matrix. Those digitiform branches which were affected, however, were found to maintain their synaptic contact with the presynaptic element.

#### B. Long-Term Changes Following Parallel Fiber-Deafferentation of the Adult Rat

Animals deafferentated of their parallel fiber input as adults were allowed to survive for a period of 57-120 days. Deafferentated cerebella were subsequently examined following Golgi impregnation or processing for electron microscopy.

##### 1. Golgi-Cox Material

###### a) The Purkinje Cell Dendritic Tree

Purkinje cells deafferentated of their parallel

fiber input in the adult were not found to be significantly different from the adult control Purkinje cells with regards to the mean length of their primary trunks, smooth branches and spiny branchlets (Fig. 32; Tables 1, 2, 4). Their dendritic arborizations, however, were characterized by a marked decrease in the number of smooth branches and spiny branchlets when compared with the adult control values (Figs. 32, 61f; 62A; Table 4). More specifically, the smooth branches and spiny branchlets were significantly decreased in number by 55% and 61% respectively following parallel fiber-deafferentation. The decrease in the number of smooth branches was responsible for a 49% decrease in the mean total smooth branch length, while the loss of spiny branchlets resulted in a 58% reduction in the mean total spiny branchlet length. These losses, furthermore, represented a 32% reduction in the number of smooth branches and a 41% loss in the number of spiny branchlets when compared to the values obtained for the weanling controls, and thus have been interpreted as transneuronal degeneration (Fig. 33; Tables 1, 2, 5).

#### b) Spine Morphology and Distribution

While in climbing fiber-deafferentated adult rats the loss of spiny branchlets appeared to account for the total loss of spines, parallel fiber-deafferentated adult Purkinje cells showed an additional loss in the number of spines along persisting spiny branchlets (compare Figs. 28b, 29C with Fig. 62B). Unlike the

deafferentated weanling rats (below), the parallel fiber-deafferentated adults were not found to have a gradient of spine loss among the Purkinje cell spiny branchlets. However, these adult deafferentated Purkinje cells were found to possess spines along the terminal branchlets which appeared markedly hypertrophied (elongated) (Figs. 61e, 62B).

### C. Long-Term Changes Following Parallel Fiber-Deafferentation of the Weanling Rat

Animals deafferentated of their parallel fiber input as weanlings were allowed to survive for a period of 57-122 days. Deafferentated cerebella were subsequently examined following Golgi impregnation or processing for electron microscopy.

#### 1. Golgi-Cox Material

##### a) The Purkinje Cell Dendritic Tree

Adult Purkinje cells which had been deafferentated of their parallel fiber input as weanlings were found to have primary trunks with a 67% increase in mean length and smooth branches with a 49% reduction in mean length when compared to the adult controls (Fig. 32; Table 4). The increase in mean primary trunk length occurred as a result of the lesion, while the reduction in the mean length of the smooth branches was due to an additive effect between the variables, lesion and time (Tables 1, 2; Appendix I, II). Furthermore, these Purkinje cells were found to have smooth branches and spiny branchlets which were decreased in number by 51% and 67% respectively, but due to the significant

interaction between the two variables (lesion and time) the main effects of either one could not be determined (Tables 1, 2; Appendix IV, V). Expressed in mean total branch length, parallel fiber-deafferentation of weanling rats caused a 74% increase in the primary trunks, a 66% decrease in the smooth branches and a 69% decrease in the spiny branchlets when compared to the adult controls (Fig. 32).

These findings suggest that the decrease in the mean length of the smooth branches following parallel fiber-deafferentation of weanling rats cannot be accounted for as merely a loss of postnatal growth (compare Figs. 32 and 33 and Tables 4 and 5). A substantial portion of this decrease appears to be the result of transneuronal degeneration. The loss in the number of smooth branches, on the other hand, does not appear to involve transneuronal degeneration, but rather is thought to be due to a loss of postnatal branching (compare Figs. 32 and 33). While their mean length was not affected, spiny branchlets in weanling rats are thought to undergo transneuronal degeneration following parallel fiber-deafferentation because their numbers were found to be significantly reduced in comparison to the weanling control values (Fig. 33; Table 5).

#### b) Spine Morphology and Distribution

In general, the number of spines found along the terminal branchlets was markedly reduced following long-term parallel fiber-deafferentation in weanling rats. While the branchlets showed

an overall loss of spines, several Purkinje cells demonstrated a gradient of spine loss among these branches. Among these cells, a severe reduction of spines was found primarily along terminal branchlets within superficial levels of the molecular layer (Figs 61b, 63c). Spiny branchlets which lay more deeply within the molecular layer appeared less severely affected (Figs. 61c, 63B). In several instances, peripheral portions of the Purkinje cell dendritic tree were found to be totally devoid of spines.

#### D. Long-Term Changes Following Parallel Fiber-Deafferentation of the Adult and Weanling Rat

##### 1. Electron microscopy

##### a) Transneuronal Degeneration

##### (1) The Granule Cell Layer

By 75 days following parallel fiber-deafferentation of either the adult or weanling rat, the granule cell layer immediately adjacent to the lesion was found to undergo marked degenerative changes (Fig. 59c). While the profiles of many of these granule cells were markedly increased in electron opacity (primarily as a result of chromatin condensation), others appeared depleted of their complement of cytoplasmic organelles and therefore were electron-lucent. Both conditions are thought to reflect advanced retrograde degenerative changes within perikarya of granule cells which have been axotomized. While an estimation of the percentage of degenerating granule cells was not undertaken within the area affected by the lesion, the involvement within many areas of the granule cell layer appeared total.

## (2) The Purkinje Cell Dendritic Tree

Following long-term parallel fiber-deafferentation of the adult rat, degenerative changes occurred within the smooth portion of the Purkinje cell dendritic tree. Under low magnification, large electron-lucent profiles were found within the molecular layer. In several areas, the predominance of these profiles gave the cortical layer a highly vacuolated appearance (Fig. 64a). A closer examination of these spaces revealed that many of these areas contained organelles characteristic of the dendritic cytoplasmic matrix (Fig. 64b). Allowing for their size, these profiles appeared to correspond to the largest segments of the smooth portion or possibly primary trunks of the Purkinje cell dendritic tree. Degenerative somata were not apparent, however, within the Purkinje cell layer. Not surprisingly, higher order smooth branches were found which appeared to have undergone degenerative changes following parallel fiber-deafferentation. These dendritic profiles frequently contained multilaminated bodies which occupied a substantial portion of the dendritic cytoplasm (Fig. 64c,d,e). In other areas of the molecular layer, long expansions of electron-lucent glial profiles were found which contained thin strands of an electron opaque material (Fig. 65b,c). Since few dendritic elements within the cerebellar molecular layer have a smooth contour and a flat parasagittal orientation (the dendrites of cerebellar interneurons are more frequently cut in the oblique plane and appear highly irregular in profile), this electron-dense debris is thought to represent the remains of small dendrites.

within the smooth portion of the Purkinje cell dendritic tree. These branches have undergone extensive degeneration and are in the final stages of electron-dense dissolution (Fig. 65b,c,d).

While the molecular layer normally contains a rich complement of small dendritic profiles, they were most conspicuous following long-term parallel fiber-deafferentation of either the adult or weanling rat because of a significant decrease in their numbers. Although several different dendritic elements were affected following parallel fiber-deafferentation of the adult rat, the Purkinje cell terminal branchlets were the most noticeably reduced in number and were the only dendritic element affected following parallel fiber-deafferentation of the weanling rat. Many of the Purkinje cell terminal branchlets were found to have undergone varying degrees of electron-dense degeneration (Fig. 66a,c,d). These dendritic profiles were unquestionably Purkinje cell terminal branchlets because of their hypolemmal, cisternal system and covering of dendritic spines.

Concurrent with the degenerative changes within the terminal branchlets, the neuropil associated with these small dendritic branches became less compact, and more loosely organized (Fig. 66a,d). This appeared to be a direct result of parallel fiber loss within the interdendritic field. Moreover, the Bergmann glial profiles associated with these terminal branchlets and within the interdendritic field appeared markedly hypertrophied (Fig. 66b,c,d). As a result, the spines which projected from these degenerative

branches in many instances were ensheathed by a thick layer of glia and were less frequently associated synaptically with parallel fiber varicosities (Fig. 66a,c,d).

### (3) The Stellate Cell

In addition to the alterations reported within the Purkinje cell (see above), degenerative changes were found within perikaryal and dendritic profiles which were clearly not of a Purkinje cell nature following parallel fiber-deafferentation of the adult rat. The degenerating somata were localized most often within superficial levels of the molecular layer (Fig. 67c). The nuclear envelope of these cells was simple in outline and their cytoplasmic matrix appeared electron opaque. Profiles of these somata rarely showed more than three axosomatic contacts with parallel fiber varicosities and did not appear to have a Bergmann glial covering. As a result, these profiles are thought to represent stellate cells which have undergone transneuronal degenerative changes following long-term parallel fiber-deafferentation. Microglia-like cells were also found within the molecular layer at this time, although confirmation of a possible phagocytic role was not obtained (Fig. 67d).

In support of the degenerative changes found within the stellate cell soma, smaller electron-dense profiles were found within the molecular layer neuropil (Fig. 67e,f). Many of these profiles displayed multiple synaptic contacts with parallel fiber varicosities and are thought to represent profiles of the stellate cell dendritic arborization. Under normal conditions, however, neuroglial cells are not associated with the surface of stellate



cells or their processes. Astrocyte-like profiles were found to be in direct contact with a substantial portion of the surface of those dendrites which appeared to have undergone electron opaque degeneration.

#### b) Spine Morphology and Distribution

In addition to the significant decrease in the number of parallel fiber profiles within the molecular layer, there appeared to be a loss of dendritic spines within a number of interdendritic fields (Fig. 66a,d). In areas where dendritic spines were found, the parallel fiber milieu appeared to be offset a considerable distance from these appendages due to the hypertrophied Bergmann glial profiles (Fig. 68b,d,e). More noticeable, however, was the increase in length of many of the spines which cover the terminal branchlets of the Purkinje cell dendritic tree following long-term parallel fiber-deafferentation of either the adult or weanling rat. The population of dendritic spines which project from the terminal branchlets of the control Purkinje cell dendritic tree was found to average 1.04  $\mu\text{m}$  in length (Fig. 68a, Table 13).

Morphologically, they were clavate in shape, i.e. had long slender stems which terminated as slightly-enlarged knobs (Fig. 68a inset). While the Bergmann glial covering along the shaft of the normal terminal branchlet is incomplete, it usually forms a complete layer around the dendritic spines (excluding areas of synaptic contact).

Parallel fiber-deafferentation of the Purkinje cell terminal branchlet was found to result in a significant increase in the

length of many of the dendritic spines (Tables 12, 13). Depending upon the time of deafferentation (21st or 150th postnatal day), the length of the dendritic spines was found to be significantly increased by 35% (Fig. 68b-d, Table 13) or 20% (Fig. 68e,f, Table 13) respectively. However, the difference in length between the time of deafferentation was not found to be statistically significant (Tables 12, 13). Therefore, the effect of the lesion alone would appear to be responsible for the increased dendritic spine length.

#### E. Comparisons Between Experimental Groups Following Long-Term Climbing, Mossy or Parallel Fiber-Deafferentation of the Adult and Weanling Rat

##### 1. The Purkinje Cell Dendritic Tree

###### a) Climbing Fiber Loss in the Adult Versus the Weanling

A comparison of the branching pattern of the adult and weanling climbing fiber-deafferentated Purkinje cells revealed that the mean length of both the smooth branches and the spiny branchlets of the deafferentated weanlings was significantly reduced by 20% and 13% respectively from those in the deafferentated adult (Fig. 69; Tables 1, 6). While deafferentation of the adult Purkinje cell did not significantly affect the length of these branches (Tables 2, 4), climbing fiber removal at the weanling stage of development did result in a significant reduction in length when compared to the adult control values (Fig. 32; Tables 1, 4; Appendix II, III). It was found that the reduction in the mean length of smooth branches and spiny branchlets was the result of a loss of postnatal growth between the 21st and 150th postnatal days (compare Figs. 32 and 33). On the other hand, adult Purkinje

cells which had been deafferentated of their climbing fiber input as weanlings showed a significantly smaller decrease in smooth branch (17%) and spiny branchlet (14%) numbers than their adult deafferentated counterparts (Fig. 69; Table 6). More specifically, climbing fiber-deafferentation at the weanling stage of development resulted in the loss of the postnatal branching which occurred within the smooth branch and spiny branchlet systems between the 21st and 150th postnatal days. In contrast however, climbing fiber removal in the adult resulted in a significant transneuronal degeneration of both smooth branch and spiny branchlet numbers. This loss resulted in mean values that were found to be significantly less than that recorded at even the weanling stage of development (Fig. 33).

b) Parallel Fiber Loss Versus Climbing  
Fiber Loss

Adult or weanling rats which had lost the efferent outflow of their granule cell system (transection of the parallel fibers) were found to have Purkinje cells whose primary trunk length averaged 172-185% of that obtained following climbing fiber-deafferentation of adult rats (Fig. 69; Table 4) and 196-200% of that obtained following climbing fiber-deafferentation of weanling rats (Fig. 70; Table 7). Since climbing fiber-deafferentation of the adult or weanling rat was not found to produce a significant change in the mean length of the primary trunks when compared to the adult control value, these findings were similar to those reported above following a comparison between the parallel fiber-deafferentated group and the adult control group. In each comparison, the lesion

main effect was significant while both the time variable and the interaction effect were non-significant (Table 1; Appendix 1). The present data, therefore, suggests a strong correlation between parallel fiber loss and an increased primary trunk length (Fig. 69; Tables 4, 7).

While the mean length of the smooth branches of the Purkinje cell dendritic tree was not significantly altered following climbing or parallel fiber-deafferentation of the adult rat (Fig. 32; Table 4), climbing or parallel fiber removal in the weanling rat caused a significant decrease in the mean smooth branch length when compared to the adult control or any of the experimental groups (Figs. 69-72; Tables 4, 6-9). As shown above, parallel fiber loss in either the weanling or adult rat resulted in a significant reduction in the number of smooth branches (51% - 55%) and spiny branchlets (61% - 67%) as compared to the adult control (Fig. 32; Table 4). A similar reduction in the number of smooth branches and spiny branchlets was found following climbing fiber-deafferentation in the adult rat (Fig. 69; Tables 4, 6). However, the removal of the olivocerebellar system in the weanling rat produced a significantly less detrimental effect on their numbers (Figs. 32, 69, 70; Tables 4, 7).

c) Parallel Fiber Removal Versus Mossy Fiber Removal

The present data strongly suggests that all three lesions affecting the granule cell system produce an increase in the mean primary trunk length, when compared to the adult control value, which is due to the effect of the lesion (Fig. 32; Tables 1, 3, 4, 8;

Appendix I). While parallel fiber-deafferentation in the weanling rat caused a significant decrease in the mean length of the smooth branches when compared to the adult control value, neither the functional loss of the granule cell system nor the surgical removal of the parallel fiber input in the adult rat caused a significant change in the length of these branches or the spiny branchlets (Fig. 32). However, all three lesions produced significant decreases in their numbers, although due to a significant interaction between variables A and B, a separation of the effects could not be determined (Fig. 71; Tables 1, 4; Appendix V, VI). The results from Table 8 and Fig. 71 indicate that identical changes occur in the Purkinje cell dendritic tree following either parallel fiber-deafferentation or a loss of granule cell function in the adult. However, parallel fiber-deafferentation of weanling rats produced a significant decrease in the mean smooth branch length when compared to either the parallel or mossy fiber-deafferentated adult rats (Figs. 70, 71; Tables 8, 9).

d) Parallel Fiber Deafferentation in the Adult Versus the Weanling

Although similar to the Purkinje cell dendritic tree of the parallel fiber-deafferentated adult rat, two notable differences were found in the Purkinje cell dendritic tree of the parallel fiber-deafferentated weanling rat. Firstly, the mean length of the smooth branches was decreased significantly by 45%, and secondly, a greater loss (15%) was found in the number of spiny branchlets following parallel fiber-deafferentation at the weanling stage of development, and accounted for a 24% decrease in the mean total spiny branchlet length (Figs. 71, 72; Tables 1, 8).

## CHAPTER 5

### DISCUSSION

#### 5.1 The Topography of the Afferents to the Lateral Cerebellar Hemisphere

Before beginning the experiments designed to provide information concerning the synaptic reorganization of the cerebellar cortex following deafferentation, it was necessary to select an area of the cortex which would be suited to surgical deafferentation. This required rather specific knowledge about the localization of afferents to the cortex; information which was not readily available for the rat. Preliminary experiments were therefore undertaken to determine the afferent projections to restricted areas of the rat cerebellar cortex.

The cerebellar cortex of the rat receives the characteristic extrinsic afferents of this structure, mossy and climbing fibers (Palay and Chan-Palay, 1974). These fibers are readily distinguished both anatomically (Scheibel and Scheibel, 1954; Desclin, 1974) and physiologically (Eccles, Llinas and Sasaki, 1964) and project characteristically to the granule cell layer and the molecular layer of the cortex respectively. Since a number of centers in the cat have been found which give rise to mossy (Miskolczy, 1931; Snider, 1936; Brodal, 1954; Grant, 1962; Szentagothai, 1962) and possibly climbing fiber varicosities (Carrea, et al., 1947; Szentagothai and Rajkovits, 1959)

within the cerebellar cortex, the source of cerebellar afferents in the rat, which had not yet been done, was examined following retrograde labeling with horseradish peroxidase (HRP). It was undertaken to localize an area of the cerebellar cortex which received as pure an afferent input as possible to facilitate surgical deafferentation of the granule cell layer (mossy fibers). Based on the anatomical (Grant, 1962; Kunzle, 1975; Rinvik and Walberg, 1975; Matsushita and Ikeda, 1976; Korti and Mugnaini, 1979; Brodal, 1980; Somana, et al., 1980) and physiological (Oscarsson, 1965; Cook, et al., 1971) data available on the cat and monkey, it appeared that the purest mossy fiber input might terminate in the lateral cerebellar hemisphere. Although it was not essential that all mossy or climbing fibers to the selected region of cortex be removed, the likelihood of inducing heterotypical reinnervation would be greater if as many fibers as possible were eliminated. In the event that some mossy fibers did persist, the interpretation of the results could not be confused because double lesion experiments were employed to demonstrate the origin of the new source of the synaptic input. This interpretation was facilitated by the fact that the region of the cerebellar cortex that was studied received its mossy and climbing fiber input from the least number of sources. With regards to the origin of climbing fibers, little doubt exists that the inferior olivary complex is the sole source of this projection (Desclin, 1974; Desclin and Escubi, 1976; present study). To gain such information, horseradish peroxidase was injected into select regions of the cerebellar cortex of the rat and the presence of labeled cell bodies in the pre-cerebellar relay nuclei was mapped.

HRP injections in the lateral cerebellar hemisphere of the rat have revealed that the ansiform lobule receives a massive mossy

fiber input from the basilar pontine gray. Labeled cells were found bilaterally within two longitudinal cell columns located ventromedial and ventrolateral to the cortical peduncle. Because the HRP labeling of the pontocerebellar projection to the ansiform lobule consistently indicated a significant ipsilateral component, electrolytic ablations of the basilar pontine gray were made as often on the ipsilateral as on the contralateral side in an attempt to procure a complete pontocerebellar deafferentation. The pontocerebellar fibers from the contralateral side course through the substance of the ipsilateral pontine gray before forming the middle cerebellar peduncle (Mihailoff, McArdle and Adams, 1981). Lesions restricted to the ipsilateral side would thus involve not only cells originating on this side but also those having a contralateral origin. Although a few small foci of labeled cells have been described from other centers (for details see 4.1,A,3-9), they represent a rather minor portion of the afferents to this area. It would appear from this information that a near total ablation of either the mossy or climbing fibers is possible by lesioning a single nuclear complex; either the basilar pontine gray or the inferior olivary complex. This has in fact been found to be the case following short- and long-term investigations in the present study.

#### 5.2 3-Acetylpyridine: a Neurotoxin Specific for the Climbing Fiber Projection

A light and electron microscopic investigation of the effects of 3-acetylpyridine (3AP) intoxication on the inferior olivary complex of the rat was undertaken to investigate the possibility that this neurotoxin could be used for the purpose of chemically lesioning this complex and causing the subsequent degeneration of the climbing fiber



projection to the cerebellum. Olivary degeneration was suggested by early functional disorders characterized by laboured breathing, impaired swallowing, motofacient tremor and a disorderly gait which was consistently restricted to the hindlimbs (cerebellar ataxia). These symptoms may occur as a direct consequence of olivocerebellar atrophy (Denk et al., 1968; Desclin and Escubi, 1974; Butterworth, Hamel and Barbeau, 1978).

In earlier studies on the effects of 3AP, Koikegami and Fuse (1961) were unable to detect any sign of pathological change in the inferior olive following 3AP treatment, while Denk et al. (1968) found only a partial involvement of this center. Desclin and Escubi (1974), on the other hand, employed both silver and Nissl methods to demonstrate a bilateral destruction of the inferior olivary complex and found a marked absence of any regional sparing. The data of the present study, based on both light and electron microscopic observations, provide unequivocal evidence to support their findings, and also suggest a morphological basis for them. Desclin and Escubi (1974) reported argyrophilic perikarya within the inferior olivary complex as early as 7 hours following 3AP treatment, while cell fragmentation, followed by a loss of argyrophilia, was suggested within the first week. The present electron microscopic observations provide direct morphological evidence to support these findings and further reveal a rapid form of neuronal degeneration following 3AP intoxication. Within 12 hours of treatment an extensive condensation of the nuclear chromatin resulted in the formation of irregular masses of heterochromatin throughout the nucleus. At the same time, a dispersal and disruption of the Nissl substance occurred, resembling a chromatolytic reaction. Similar pathological changes have been reported by Coyle,

Molliver and Kuhar (1978) following stereotaxic injections of kainic acid into the rat striatum. The neuronal shrinkage and loss of cytoplasmic Nissl substance which occurred in the olive also showed a marked resemblance to the transneuronal cellular degeneration that results following deafferentation in other centers (Matthews, et al., 1960; Coyle, et al., 1978). Desclin and Escubi (1974) were unable to detect any significant change in Nissl body staining until ten days after 3AP administration. In the present study, however, preparations of the interior olive were completely refractory to Nissl stains as early as 24 hours post-treatment, and the electron microscope has substantiated this early cellular involvement.

Following their investigations employing light microscopic methods Denk et al. (1968) and Desclin and Escubi (1974) have suggested that 3AP-induced neuronal degeneration is not accompanied by any apparent glial reaction. At variance with these results, however, the present electron microscopic observations clearly indicated an hypertrophy of perineuronal glial elements. As a result, extensive regions of the somatic surface which were normally adjacent to axonal and dendritic profiles of the neuropil came into direct contact with hypertrophied astrocytic sheaths within 12 hours of 3AP treatment. Between 12 and 72 hours, a progressive infiltration and fragmentation of the neuronal cytoplasm by glial processes occurred as a result of an increased proliferation and hypertrophy of the perineuronal astrocytic elements. At 72 hours, the neuronal cytoplasm showed marked signs of fragmentation and disruption, with hypertrophied astrocytic processes completely surrounding the pyknotic nuclei.

That perineuronal glial cells proliferate during neuronal

response to injury has been well documented. As early as 1939, Brodal observed hyperplasia and hypertrophy in astrocytes of the inferior olivary complex following surgical lesions in the cerebellum. Kirkpatrick (1968) has suggested that such a marked glial hypertrophy might reflect an increase in the functional cooperation between the neurons and glia in an attempt to overcome neuronal death. Sjostrand (1965 and 1966) has found that axonal lesions such as nerve crush, that permit complete neuronal recovery, are characterized by an extensive proliferation of both microglia and astrocytes. As a result, it has been postulated that glial cells may have an important function in transporting metabolites from the blood to injured neurons during nerve cell regeneration (Kirkpatrick, 1968).

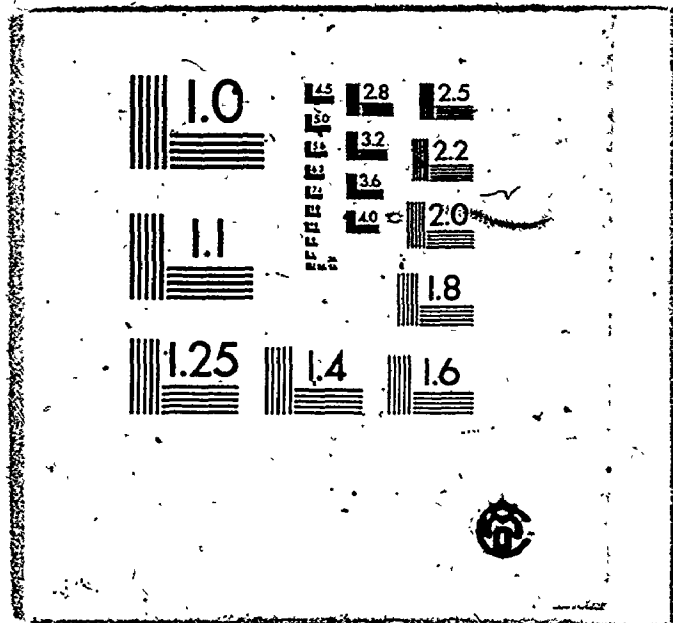
The phagocytic potential of astrocytes has also been well documented (Vaughn, 1965; Lampert and Cressman, 1966; Kirkpatrick, 1968; Lemkey-Johnston, Butler and Reynolds, 1976; Coyle et al., 1978) particularly in relation to synaptic boutons and preterminal axons (Herndon, 1968; Vaughn and Pease, 1970; Fernando, 1973; Desclin, 1974; Nathaniel and Nathaniel, 1977). Kruger et al. (1970) have reported extensive astrocytic involvement following alpha particle irradiation of the cerebral cortex. In areas of degenerating dendrites reactive astrocytes showed marked signs of phagocytosis and engulfment, resulting in the removal of extensive portions of the dendritic field.

Kirkpatrick (1968) was one of the first to observe an actual infiltration of degenerative neurons by glial processes following axotomy. In accordance with this observation he suggested that the glial profiles were actively engaged in the phagocytic removal of somal debris. Lemkey-Johnston et al. (1976) found enlarged astrocytic processes

throughout the arcuate nucleus within twenty minutes of the administration of monosodium glutamate. These authors maintained that astrocytic involvement was essential in the phagocytic removal of neuronal perikarya, preterminal fragments and synaptic terminals, and found complete cellular loss to occur within the first week. Coyle et al. (1978) have described the pathological changes that occur in the rat striatum following kainic acid injection. They found an initial phase of rapid cell degeneration within the first 48 hours and a second phase characterized by intense astrocytic proliferation with marked signs of phagocytosis and subsequent glial scar formation. Cerebellar granular necrosis resulting from subcutaneous injections of thiophen has also involved marked astrocytic alterations (Herndon, 1968). The potential for phagocytosis of axons and terminals by these cells was prominent in the molecular layer whereas astrocytic processes in the granular layer were less active in somal phagocytosis. Herndon (1968) postulated that somal phagocytosis was largely carried out by vascular adventitial cells (pericytes) and hematogenous macrophages instead. In the present investigation, direct evidence for active phagocytosis by astrocytic processes was seldom observed. As a result, their function was considered to be mainly to promote fragmentation and segregation of the degenerating olivary neuron, and to subsequently cause glial scar formation following neuronal disintegration.

At 60 hours following 3AP treatment, a glial element, morphologically distinct from the astrocytic profiles, appeared at the periphery of the degenerating neuronal mass and was actively engaged in the phagocytic removal of neuronal debris. Sufficient documentation

# 3



exists to justify speculation that phagocytic cells originate from several different sources depending mainly on the type of brain injury. Heavy doses of alpha particle irradiation to the cerebral cortex (resulting in marked vascular damage) have induced a phagocytic response from the pericytes in the vascular adventitia (Maxwell and Kruger, 1965a,b). Other reports have documented an hematogenous origin (agranular leucocytes) for brain macrophages following injuries resulting in hemorrhage (Bunge, Bunge and Ris, 1961; Konigsmark and Sidman, 1963; Gonatas, Levine and Shoulson, 1965; and Bignami and Dahl, 1975). Cook and Wisniewski (1973) maintained that the oligodendroglia were the only glial cells actively engaged in phagocytosis following Wallerian degeneration in the optic nerve. Hason and Glees (1972) reported similar findings in chronically deafferentated monkey lateral geniculate nucleus. Observations of marked hypertrophy, hyperplasia and phagocytosis by microglial cells have also been reported. Sjostrand (1971) and Fernando (1973) found neuronal perikarya ensheathed by hypertrophied microglial processes actively engaged in phagocytosis during the 2nd and 3rd week following hypoglossal nerve transection. Torvik and Skjorten (1971) have reported similar findings following facial nerve transection in adult mice. Prior to the ultimate phagocytosis of the somal and dendritic debris by microglia, slender processes from these phagocytic cells were often found extending along the surface of the neuronal soma and dendrite, thereby segregating boutons from their synaptic contacts. Within 6 hours of monosodium glutamate treatment, Lemkey-Johnston et al. (1976) found an active phagocytosis of arcuate neurons by microglia with the subsequent removal of degenerative material by the 3rd or 4th day. With the advent of recent morphological techniques, the silver carbonate labeling of

microglial cells has provided a definitive characterization for these cells at the electron microscopic level (Mori and LeBlond, 1969). They can be easily distinguished from astrocytic processes by an absence of glial fibrils and an overall darker electron density (Fernando, 1973) and from oligodendrocytes by their lack of microtubules and organized stacks of granular endoplasmic reticulum (Cook and Wisniewski, 1973). The phagocytic glial elements reported here are thus thought to be microglial in nature.

In summary, the inferior olive was found to undergo a rapid form of electron-dense degeneration following 3AP administration. This effect was so rapid that all olivary neurons observed appeared functionally dead as early as 12 hours. Because of the nonselective nature of electrolytic lesions in involving passing fibers and adjacent nuclei, it was concluded that the chemical induction of inferior olivary lesions, using the neurotoxin 3AP, would prove valuable as a complementary method to conventional electrolytic procedures.

#### A Possible Mode of Action

Because earlier studies found that the response to 3AP mimicks the symptoms induced by nicotinic acid deficiency (Woolley, Strong, Madden and Elvehjem, 1938; Woolley and White, 1943; Woolley, 1945) and that 3AP possesses many of the biochemical properties of nicotinamide (Kaplan and Ciotti, 1956), it was suggested that the central nervous system lesions observed following 3AP treatment represent an accelerated picture of nicotinamide deficiency (Hicks, 1955). This was supported by the fact that the effects could be abolished by the subsequent injection of nicotinamide (Llinàs, Walton and Hillman, 1975; Simantov, et al., 1976). As a result of its antagonistic action with

nicotinamide, abnormal 3-acetylpyridine-adenine dinucleotides (3APAD) rather than nicotinamide adenine dinucleotide ( $\text{NAD}^+$ ) may be produced following 3AP treatment (Perry, MacLean, Perry and Hansen, 1976). NAD is an important cofactor for the activity of several important enzymes (cysteine oxidase and glucose 6-phosphate dehydrogenase) and pathways in rat brain (Lehninger, 1970; Misra and Olney, 1975; Himwich, 1976).

Others have suggested that because of the structural similarities of 3-acetylpyridine and pyrimidine-based nucleotides that the primary toxic effect of 3AP might be the production of abnormal nucleotides (Desclin and Escubi, 1974; Llinas et al., 1975). Hicks (1955), on the other hand, suggested that the selectivity of its action might reflect differences in metabolism between specific areas of the neuraxis. The metabolism of brain glucose is considered to involve two main pathways: the Embden-Meyerhof pathway (glycolysis) and the Warburg-Dickens shunt (hexosemonophosphate shunt) (Himwich, 1976). Evidence exists that the hexosemonophosphate pathway in young animals is important in generating both NADPH for amino acid synthesis and units of ribose for the synthesis of nucleic and amino acids (Lehninger, 1970).

### 5.3 The Origin of Climbing Fiber Afferents

While the histological studies of Szentagothai and Rajkovits (1959) and Grant (1970) along with a number of electrophysiological investigations (Eccles et al., 1964, 1966; Eccles et al., 1967; Oscarsson, 1969) support the finding that cerebellar climbing fibers originate from the inferior olive, the lack of adequate silver impregnation techniques for labeling degenerating climbing fibers has led to a rash of inconsistent findings regarding their terminal field of projection. Szentagothai and Rajkovits (1959) were the first to give



morphological evidence in support of the inferior olive as the possible origin of climbing fibers. However, the degenerating axons could not be traced beyond the infraganglionic plexus which precluded their identification as climbing fibers. Experimental results have hitherto provided conflicting evidence. Several authors have reported massive mossy fiber degeneration following electrolytic ablations of the inferior olivary complex (Miskolczy, 1931; Carrea et al., 1947; Fink and Heimer, 1967; O'Leary et al., 1970) while others have suggested that the olivocerebellar tract termination is of the climbing fiber type (Szentagothai and Rajkovits, 1959; Hamori and Szentagothai, 1964; Grant, 1970). Based on Nissl preparations initially, the only consistent finding following 3AP treatment was the complete destruction of the inferior olivary complex (Denk et al., 1968). Its later use in combination with newly developed suppressive silver methods confirmed the total bilateral destruction of the inferior olivary complex and a secondary degeneration of a massive fiber projection to the molecular layer of the cerebellar cortex (Desclin, 1974). The synaptic localization of the climbing fiber terminal arborization was investigated at the electron microscopic level and was confirmed to be climbing fiber in nature (Desclin, 1976). Whether or not other afferent systems terminate as climbing fibers has been an area of speculation since Cajal first reported in 1911 that the basilar pontine gray and vestibular complex give rise to a climbing fiber projection. Carrea et al. (1947) reported a secondary degeneration of climbing fibers within the molecular layer following lesions in the deep cerebellar nuclei. Szentagothai and Rajkovits (1959) commented on degeneration in the contralateral flocculus which resembled that of climbing fibers after lesioning the brachium conjunctivum. Furthermore, mention has been made

of a climbing fiber projection as a consequence of lesions and autoradiographic injections of tritiated leucine within both the basilar pontine gray (Murphy et al., 1973) and the nucleus reticularis tegmenti pontis (Szentagothai and Rajkovits, 1959). The electron microscopic observations of this study provide additional support for the suggestion of Desclin that the inferior olive is the sole source of climbing fibers. The present study has examined the molecular layer of the ansiform lobule following 3AP treatment and has confirmed a total loss of the climbing fiber innervation to this area. An absence of normal appearing climbing fibers was found 24 hours following treatment and only a few small electron-dense fragments were evident as remnants of their existence by 7 days. More importantly however, the cerebellar cortex remained devoid of a climbing fiber input as late as 86 days following 3AP treatment. Furthermore, electron microscopic findings in the present study have failed to confirm an extra-olivary source of climbing fibers from either the basilar pontine gray or the nucleus reticularis tegmenti pontis following short-term pontine ablations. At present, therefore, the only known source for the climbing fiber projection to the ansiform lobule, and probably the sole origin, is the inferior olivary complex.

#### 5.4 Do Climbing Fiber Glomerular Collaterals Exist?

While the first attempts at silver impregnation of degenerating climbing fibers revealed an unbranched course within the granule cell layer (Szentagothai and Rajkovits, 1959), Golgi preparations have revealed a number of collateral branches from these axons which terminate in nodule-like expansions both at the level of the infraganglionic plexus (Scheibel and Scheibel, 1954) and along their ascent through

the granule cell layer (Pensa, 1931; Fox, Andrade and Schwyn, 1969). In fact, Fox et al. (1969) have postulated that these collaterals eventually make synaptic contact with both the granule and Golgi cells. More recently however, the occurrence of these collaterals was not confirmed following 3AP treatment in spite of the use of a highly sensitive modification of the Fink and Heimer method (DeOlmos-Ingram technique) (Desclin, 1974). Following mercuric chloride impregnation, Chan-Palay and Palay (1971) believed that they had identified two distinct types of climbing fiber collaterals which originate from within the granule cell layer. The basis for their electron microscopic identification, however, relied primarily on morphological similarities to the climbing fiber tendril varicosities within the molecular layer (Palay and Chan-Palay, 1974). Recent evidence of radioactivity in mossy fiber rosettes in rats receiving an inferior olivary injection of tritiated  $^{35}\text{S}$ -methionine (Chan-Palay et al., 1977) or  $^3\text{H}$ -leucine (Murphy et al., 1973) supports the Golgi findings that these mossy fibers are olivary in origin. While the findings of the latter studies appeared convincing, Groenewegen and Voogd (1977) have since had little success in reproducing mossy fiber rosette labeling following olivary injections. While the autoradiographic method avoids the problem of excessive damage to fibers of passage and adjacent nuclei, difficulties are encountered in restricting the spread of radioactive solution to the nucleus of interest. It is generally agreed that the neuronal perikaryon is the primary site of uptake of injected tritiated amino acids which are subsequently incorporated into protein and transported in the anterograde direction, labeling the course of the axon and its terminal field (Cowan et al., 1972).

The use of electrolytic lesions and degeneration methods

as a means of investigating the possibility of olivary mossy fiber projections is seriously limited. Lesions of the olive unavoidably involve other tracts and nuclei which may give rise to the mossy fiber degeneration within the cerebellar cortex. The use of 3AP in inducing olivary lesions avoids this problem, since no other pre-cerebellar centers undergo degeneration following its administration. The absence of degenerating glomerular or tendril collaterals within the granule cell layer following 3AP administration implies that the existence of these collaterals is questionable. Using a similar approach, Desclin and Colin (1980) have also found no evidence to support the existence of a mossy fiber projection from the inferior olive.

Although previous studies with 3AP have failed to demonstrate climbing fiber collaterals, in the present study a small number of degenerating terminals were found within the granule cell layer of the ansiform lobule following long-term survival. These electron-dense profiles make synaptic contact with the granule cell digitiform dendrite and appear to form rosette-like formations which might suggest the existence of climbing fiber glomerular collaterals (Scheibel and Scheibel, 1955; Palay and Chan-Palay, 1974; Chan-Palay et al., 1977). However, it is more likely that these terminals represent transneuronal degenerative changes within recurrent collaterals of Purkinje cell axons following long-term climbing fiber-deafferentation rather than climbing fiber glomerular collaterals. The present study has demonstrated transneuronal degeneration of the Purkinje cell dendritic arborization following climbing fiber-deafferentation. Because of this, degenerative changes within its axon, and particularly its finer collateral branches, is a distinct possibility. More recently, recurrent Purkinje cell axons

have been found to synapse with the digitiform dendrites of the granule cell and to form pseudo-glomerular structures within the normal cerebellum (Chan-Palay, 1971; Palay and Chan-Palay, 1974). Although the morphology of the synaptic component of these two terminals (glomerular collaterals and recurrent Purkinje cell axons) is markedly different (Palay and Chan-Palay, 1974), the differences were not distinguishable in this study because of the advanced state of electron-dense degeneration. Because the time course for the removal of this terminal debris was much longer than observed following mossy fiber rosette degeneration of the ponto-cerebellar projection (80 days) (present study), a system which gives rise to a similar form of axonal efflorescence within the granule cell layer as the climbing fiber glomerular collateral, it is thought that this degenerative debris may reflect transneuronal alterations within recurrent collaterals of Purkinje cell axons. A similar time course for transneuronal degeneration has been described in various regions of the central nervous system following deafferentation (LeVay, 1971; Berger, 1973; Desclin and Colin, 1980).

#### 5.5 Recurrent/Climbing Fiber Collaterals to the Inferior Olive

Several physiological studies have postulated that recurrent collaterals of olivocerebellar axons innervate the inferior olivary complex (Ochi, 1965; Armstrong and Harvey, 1966; Eccles et al., 1967; Llinas, Baker and Sotelo, 1974), however, no evidence has been provided by morphologists to confirm or disprove the existence of such a connection. The morphological observations of the present study provide evidence which conflicts with the physiological findings. This study has shown that degenerative changes occur within both the soma and the axon

of these cells shortly following 3AP treatment (12 hours). While the electron-dense debris of olivary somata are present for several weeks, the phagocytosis and clearing of their axons, the climbing fibers, within the cerebellar molecular layer proceeds at a much faster rate (2-7 days). At no time during the observed course of electron-dense degeneration of the olivary somata, nor at longer survival periods up to 86 days, were degenerative axon terminals observed within the neuropil of the inferior olivary complex. Unless the recurrent collaterals were phagocytized and cleared prior to the earliest observations of this study (12 hrs), the absence of axon terminal degeneration following total ablation of the inferior olivary complex casts considerable doubt on the existence of recurrent climbing fiber collaterals.

Ochi (1965) and Armstrong and Harvey (1966) found that electrical stimulation of the cerebellar white matter produced an excitation of olivary neurons which followed the initial antidromic response. This second response was believed to represent the activity of recurrent collaterals of the climbing fibers. Since the stimulating electrode presumably would also have activated mossy fibers, this system could represent an alternative source of collateral innervation to the inferior olivary complex. Since then, many centers (lateral reticular nucleus, dorsal column nuclei, spinal trigeminal nucleus and medial and descending vestibular nuclei) have been found which send afferents to both the cerebellar granule cell layer (Rinvik and Walberg, 1975; Matsushita and Ikeda, 1976; Kimota et al., 1978; Kotchabhakdi and Walberg, 1978) and the inferior olivary complex (Henkel, Linauts and Martin, 1975; Brown,

Chan-Palay and Palay, 1977; Swenson and Castro, 1980). Whether the projections to the inferior olivary complex from these centers represent a collateral branch of the mossy fiber projection is not known, but such an input could account for the excitation of olivary neurons following stimulation of the corpus medullaris.

Earlier conclusions reached from physiological studies were based on the premise that olivo-cerebellar projections existed but not the reverse. Recent investigations have described a direct cerebello-olivary projection in several species (Martin, Henkel and King, 1976; Tolbert, Massopust, Murphy and Young, 1976; Faull, 1977). In fact, a precise topographical localization has been mapped from the dentate and the interpositus anterior and posterior nuclei to the inferior olivary complex (Beitz, 1976). A cerebello-olivary projection from the fastigial nucleus has not been reported in degeneration studies of the cat, rat or monkey (Graybiel, Nauta, Lasek and Nauta, 1973; Brown et al., 1977; Tolbert et al., 1976), however, one has been described in the opossum (Dom, King and Martin, 1973) and the rat following horseradish peroxidase injections of the caudal pole of the medial accessory olive (Swenson and Castro, 1980). It seems plausible that these direct cerebello-olivary projections might represent the morphological equivalent of what electrophysiologists have interpreted as recurrent climbing fiber collaterals.

5.6 Regional Sparing Following 3-Acetylpyridine Intoxication

While the earlier studies reported few, if any degenerative changes in the inferior olivary complex following 3AP treatment (Hicks, 1955; Coggeshall and MacLean, 1958; Koikegami and Fuse, 1961;

Kierse, 1965), more recent investigations including the present study have reported a total loss of the olivary neurons and the climbing fiber input to the cerebellar cortex (Desclin, 1974; Sotelo et al., 1975; Desclin, 1976). Although a total, bilateral loss of the olivary perikarya was reported within the inferior olivary complex of the adult rat, regional differences in the onset of degenerative change were observed (as determined by the variation in time for the silver impregnation of different olivary somata) (Desclin and Escubi, 1974). The medial accessory olive and the rostral part of the main nucleus were the last portions of the inferior olivary complex to become impregnated with silver, and it was felt that this reflected regional differences in the sensitivity to 3AP. This suggestion has since been confirmed by Woodhams et al. (1978) and in the present study. These investigations suggest further that the susceptibility of the inferior olive to the toxic effects of 3AP is age related. Immature olivary neurons appear to be more resistant to the toxic effects of 3AP. Woodhams et al. (1978) found that injections of high concentrations of 3AP which produced an LD<sub>100</sub> in adults caused minimal damage within the inferior olivary complex of two day old rats. These authors were able to produce only a partial lesion of the weanling inferior olivary complex before the 16th postnatal day. Beyond the 16th postnatal day, however, they found that adult dosages of 3AP (65mg/kg) were adequate for the climbing fiber-deafferentation of the cerebellar cortex of weanling rats. The findings of the present study are not in agreement. Following the injection of weanling rats between the 21st and 23rd postnatal days, the inferior olivary nuclei revealed a consistent sparing of olivary neurons within the genu of the principal olive and the caudal portion of the medial accessory olive. This pattern



of sparing corresponded closely to the regions described by Desclin and Escubi (1974) as being more refractory to staining with the silver methods.

The present findings suggest, therefore, that the dosage used to achieve olivary ablations in the adult (65mg/kg) is inadequate for the total destruction of the inferior olivary complex in the weanling rat (21-23 days). However, it was possible in the present study to obtain a total ablation of the weanling inferior olivary complex by increasing the concentration of 3AP to 90 mg/kg, although this has not been found to have the same effect in neonates (Woodhams et al., 1978). The findings of both investigations indicate that the immature inferior olivary neuron is less sensitive to the toxic effect of 3AP, but becomes increasingly susceptible with maturation of the inferior olivary system. The majority of the cells which are spared at the earlier stages are located within the caudal portion of the medial accessory olive and are unique in several respects. Phylogenetically, they are the oldest cells of the inferior olive (Kappers, Huber and Crosby, 1936) and have been described by some authors as having perikarya with sparsely branched dendritic arbors as compared to the cells within the main nucleus and the rostral half of the accessory nuclei (Scheibel and Scheibel, 1955). Furthermore, this region of the inferior olive has been shown to receive the bulk of its afferents from the spinal cord (Gwyn, Nicholson and Flumerfelt, 1977) and to send climbing fibers to the posterior vermis of the cerebellar cortex (vermal visual area, lobules VI, VIIA, B, VIIIA, B, uvula and nodulus) (Armstrong et al., 1974; Brodal, 1976; Hoddevik et al., 1976; Batini, Buisseret-Delmas, Corvisier, Hardy and Jassik-Gerschenfeld, 1978; Kimoto et al., 1978) and the paramedian lobule (Brown, 1980). It

is likely that the metabolic characteristics of these cells also differ from the other olivary neurons in certain fundamental respects which may explain the differences in their response to 3AP.

#### 5.7 Climbing Fiber Suppression of Spine Growth

Although the importance of the afferent input for both the growth and maintenance of proper spine numbers has been described in many centers of the central nervous system (Colonnier, 1964; White and Westrum, 1964; Globus and Scheibel, 1966; Valverde and Esteban, 1968; Raisman and Field, 1973; Parnavelas, Lynch, Brecha, Cotman and Globus, 1974), evidence is provided in the present study which supports the view that climbing fibers suppress Purkinje cell spine development. The removal of the climbing fiber input to the cerebellum in the weanling rat produced an ectopic formation of spine-like appendages along the main stem Purkinje cell dendrites. Although Hamori (1973) reported a reduction in the number of Purkinje cell dendritic spines following climbing fiber-deafferentation, it is generally accepted that the climbing fiber does not exert a trophic influence on the development or maintenance of Purkinje cell dendritic spines. In fact, several authors have found in agreement with the present study that the removal of the olivocerebellar input in neonates and young adults results in the formation of ectopic spine-like processes along the smooth portion of the Purkinje cell dendritic tree (Bradley and Berry, 1975, 1976a, b; Sotelo et al., 1975; Sotelo and Arsenio-Nunes, 1976). This study supports the suggestion that the climbing fiber may suppress the inherent (autonomous) capacity of the Purkinje cell to produce dendritic spines (Sotelo et al., 1975; Bradley and Berry, 1976c). Developmental studies have found, similarly, that

although dendritic spines form along "smooth" portions of the Purkinje cell dendritic tree, they later become absorbed upon contact with a climbing fiber (Larramendi and Victor, 1967). In addition, the present study provides information which suggests that the autonomous potential for the growth of spines on the Purkinje cell may be dependent on age. It has been reported that the extent of ectopic spine formation along the smooth portion of the Purkinje cell dendritic tree differs sharply between climbing fiber-deafferentated young adults and neonatal rats (Bradley and Berry, 1976c). Ectopic spine distribution is most commonly restricted to the distal portion of the smooth branches of the Purkinje cell dendritic tree following deafferentation of young adults (Bradley and Berry, 1976a,c) whereas spines are occasionally found at the level of the soma if deafferentation occurs at birth (Bradley and Berry, 1976a,c; Sotelo and Arsenio-Nunes, 1976). In the present study, ectopic spine distribution was limited to tertiary and distal portions of secondary branches of the Purkinje cell dendritic tree following climbing fiber-deafferentation on the 21st postnatal day. In other words, ectopic spines were never found along the primary trunks, or the proximal portions of the secondary branches.

This region of spine distribution was reduced from that reported following deafferentation at birth but was more extensive than that described following deafferentation of adult rats at the 50th (Bradley and Berry, 1976c) and 84th postnatal days (present study). While several studies support an autonomous formation of Purkinje cell dendritic spines (Seil and Herndon, 1970; Privat, 1975; Bradley and Berry, 1976b), the findings reported in this study suggest that this ability to form spines may be age-dependent. The 12th week may represent

a stage of maturation at which the Purkinje cell is no longer capable of forming dendritic spines. It is possible that the gradual suppression of ectopic spine formation following climbing fiber-deafferentation between birth and the 12th postnatal week may reflect a loss of dendritic plasticity. An important consideration in the present study was the length of the postoperative survival time. Previous investigations were limited to observations taken between 30 and 60 days following deafferentation and may not allow for the possibility that ectopic spines might be transient formations. The observations of the present study were made between 121 and 130 days following deafferentation and may represent more closely the actual size and distribution of the ectopic spine population produced following climbing fiber-deafferentation of adult and weanling rats. In addition, the present study has shown that the presumptive ectopic spines not only resemble the dendritic spines cytologically but are not statistically different from them with respect to their length. Furthermore, it has been shown that these ectopic spines do not represent elongated dendritic thorns. The population of Purkinje cell dendritic thorns appeared normal morphologically and numerically and on several occasions were found to be heterotypically innervated by parallel fiber varicosities.

#### 5.8 Purkinje Cell Growth Beyond the 21st Postnatal Day

Measurements of deafferentated Purkinje cells were compared to both the adult and weanling control groups in the present study. Since in most instances, deafferentation resulted in a loss of dendritic branches or a reduction in their length, comparisons of these features between deafferentated adult animals and control groups (adult and

weanling) served as a measure of the extent of transneuronal degeneration. Comparisons were also made between weanling deafferentated animals and the control groups to distinguish between a simple loss of postnatal growth and transneuronal degeneration following deafferentation. A comparison with the weanling controls was deemed necessary because measurements of the Purkinje cell dendritic tree at the 21st and 150th postnatal day have indicated postnatal growth over this period. Altman (1972a) reported that Purkinje cell dendritic growth was complete by the 22nd postnatal day. Moreover, it has recently been suggested that a resorption of dendrites occurs both during and after Purkinje cell dendritic growth (Weiss and Pysch, 1978). In contrast, the results of this study have revealed a significant increase (65%) in the total dendritic length of the Purkinje cell between the 21st and 150th postnatal day. Previous studies have suggested a marked decrease in the branching density of the Purkinje cell dendritic tree, particularly beyond the 20th postnatal day (Berry and Bradley, 1976b; Weiss and Pysch, 1978). The dendritic field size of these cells, however, was found to increase dramatically over this same time period (Berry and Hollingworth, 1972; Berry and Bradley, 1976b; Weiss and Pysch, 1978). It was postulated by Weiss and Pysch (1978) that a loss of dendritic segments must occur to account for the significant decline in the total dendritic length. Although spontaneous degeneration has been suggested during the normal development of terminals, axons and dendrites, and in specific mature dendritic arborizations (Bodian, 1966; Jacobsen, 1970; Das and Hine, 1972; Aguayo, Terry and Bray, 1973; Desclin, 1974; Conradi and Ronnevi, 1975; Arees and Astrom, 1976), the observed increase in total dendritic length between the 21st and 150th postnatal days in the present study questions the existence of such a

process during the late maturation of the Purkinje cell.

The discrepancies between this study and the others are likely due to differences in the methodology of their quantitative procedures. Previous estimates of total dendritic length have been based on measurements of two indirect parameters; dendritic field area and branching density as determined by the line-intersection method (Berry and Bradley, 1976b; Weiss and Pysch, 1978). While this is a valid method for gaining an indication of total dendritic length, the Image Analysis System (the method of choice for the present study) is much more precise since it permits a direct measurement of length and enables quantification of a large sample of cells. In view of the growth of the Purkinje cell beyond the 21st day, decreases in the length or the number of dendritic branches revealed in comparisons of weanling deafferentated animals with the adult control group may reflect a loss of postnatal growth rather than transneuronal atrophy. It was therefore determined in the case of weanling deafferentated animals, that only those values which were significantly reduced from the weanling control group would represent sufficient evidence for transneuronal atrophy.

#### 5.9 Characterization of Pontocerebellar Rosettes

Palay and Chan-Palay (1974) have recently identified three variations of mossy fiber formations (simple, complex and filigree) following rapid Golgi impregnations of the granule cell layer in the rat. The differences between each type are based on the presence or absence and localization of filopodial-like processes on the rosette formation. These authors have also described a variation in the concentration of synaptic vesicles in each type of rosette and they were termed dispersed

or clustered accordingly (Chan-Palay and Palay, 1970). In the present study, the mossy fiber rosettes within the lower three-quarters of the granule cell layer of the ansiform lobule have been characterized according to the same morphological characteristics. According to the calculations for the ansiform lobule, the simple mossy fiber rosette represents 72% of the axon terminals within cerebellar glomeruli while 27% were distinguished as complex rosettes. The simple dispersed type of rosette was found to be the most common of the four types (60%). Since it has previously been reported that the simple and complex efflorescences within the vermis occur in approximately equal frequencies (Chan-Palay and Palay, 1974), the findings reported here reflect a difference between the vermis and the ansiform lobule. In accordance with the variety of centers which have been shown to contribute mossy fibers to the granule cell layer (Snider, 1936; Lundberg and Oscarsson, 1960, 1962; Szentagothai, 1961, 1962; Grant, 1962; Oscarsson, 1965), the various types of mossy fiber rosettes are thought to reflect a difference in mossy fiber origin. Brodal and Drablos (1963), in fact, have provided evidence that the vestibulocerebellar rosettes of the flocculonodular lobe are structurally different from those described in other areas of the cerebellum.

To investigate the pontocerebellar input to the ansiform lobule, mossy fiber degeneration was induced and subsequently examined at the electron microscopic level. Survival times between 3.5 and 4 days, following electrolytic ablation of the basilar pontine gray yielded altered terminals in which the degenerative processes did not obscure the morphological characteristics under observation. In support of the heavy labeling of the basilar pontine gray following horseradish peroxidase injections of the ansiform lobule which suggests a large pontocerebellar

projection, few normal rosettes were found in this area following long-term pontine ablation. It has been shown further that both simple (60%) and complex (25%) dispersed types of rosettes were affected following basilar pontine ablation. Moreover, these findings showed that a small population of simple rosettes (15%), characterized by a clustered population of synaptic vesicles, underwent electron-dense degeneration. Thus, the evidence from this study suggests that the pontocerebellar input is not represented by one particular rosette type, as recently suggested for the spinocerebellar input (Mugnaini, 1972; Chan-Palay, 1973), but rather consists of a mixture of rosette types of which the simple dispersed variety is by far in the majority. It should be noted that several categories of neurons have recently been described within the basilar pontine gray of the rat which may account for the diversity found in the form of the pontocerebellar rosettes (Mihailoff et al., 1981).

It was found that degeneration of the simple and complex dispersed types of mossy fiber rosettes underwent a similar time course which extended over a period of 80 days. An unexpected finding in the course of this study was the small population of rosettes which underwent a rapid form of electron-dense degeneration (within 4 days). These varicosities were simple in outline and were characterized by a clustered population of synaptic vesicles. It is likely that this population represents the simple clustered type of efflorescence. Moreover, the frequency of these degenerating terminals (15%) was found to correspond closely to the estimated value (12%) determined in this study for the simple clustered type of mossy fiber rosette in the ansiform lobule.

Since a normal population of simple clustered rosettes was not found within the ansiform lobule following pontine ablation, it



is likely that the total population of simple clustered rosettes to the ansiform lobule originates from the basilar pontine gray. However, since pontine lesions from the dorsal approach unavoidably involve not only the basilar pontine gray but also a portion of the nucleus reticularis tegmenti pontis, which is also a source of mossy fibers (Brown and Carman, 1978; Brodal, 1980), this center could not be excluded as the possible source of simple clustered rosettes.

#### 5.10 Deafferentation of the Cerebellum Following Parasagittal Cuts.

Until recently, the region of the molecular layer which is deafferentated of parallel fibers following a parasagittal cut of the cerebellar cortex was unknown. Parallel fibers in the rat were found to vary from 0.9mm (Smolyanivov, 1971) to 4.7mm in length (Mugnaini, 1976). Furthermore, it has been shown in the cat that a gradient exists in the length of parallel fibers between the Purkinje cell layer and the pia, which has a trapezoidal configuration (Brand et al., 1976). Autoradiographic labeling of this system has shown that the maximum branch length in the cat is 2.0mm (Courville and Kitahara, 1980). Although not a direct indication of parallel fiber length, Mouren-Mathieu and Colonnier (1969) have reported a loss of Purkinje cell dendritic spines for distances of up to 2mm from the lesion site. Autoradiographic labeling of parallel fiber axons in the rat has revealed a minimal branch length of 1mm and a maximal difference in length between the superficial and deep fibers of 1mm (Schild, 1980). An attempt was made in the present study to label these fine unmyelinated fibers using anterograde degeneration (DeOlmos-Ingram method), but they continue to resist all efforts of impregnation. In view of the electron microscopic findings reported by Mouren-Mathieu

and Colonnier (1969) and the autoradiographic study of Schild (1980), all samples of the molecular layer were taken from the first 1.5mm of the cerebellar lesion. It is estimated from the above findings that the first millimeter of molecular layer adjacent to the lesion is deafferented of approximately 50% of its parallel fiber input. This should constitute a sufficient stimulus to induce a cerebellar response to parallel fiber-deafferentation. Marked transneuronal alterations have also been reported in the inferior olivary complex and the basilar pontine gray of the cat following a similar loss in their number of afferents (Torvik, 1956).

#### 5.11 Transneuronal Degeneration of the Purkinje Cells and Granule Cells

##### A. Climbing Fiber Deafferentation

Image analysis of the climbing fiber-deafferentated adult and weanling Purkinje cells has suggested two distinct morphological reactions within the dendritic arbor. Following removal of the climbing fiber input on the 21st postnatal day, Purkinje cell growth was reduced. More specifically, there was no significant increase in the number of smooth branches and spiny branchlets following deafferentation. In contrast, removal of the climbing fiber input on the 150th postnatal day induced transneuronal degeneration of both the smooth branches and spiny branchlets. The ultrastructural examination of the climbing fiber-deafferentated cerebellar cortex has provided morphological evidence which supports these findings. The transneuronal degeneration was of an electron-lucent nature. Many of the terminal branchlets had a honeycombed appearance due to hypertrophy and swelling of the membrane-bound systems

of these dendrites. It has also been found in other centers that the spine population and the dendritic branching pattern are affected following deafferentation (Jones and Thomas, 1956, 1962; LeGrös Clark, 1957; Globus and Scheibel, 1966; Mouren-Mathieu and Colonnier, 1969; Pinching and Powell, 1971; Benes et al., 1977). In the present study, the structural changes within the terminal branchlets closely resembled the watery (electron-lucent) and tubulovesicular dendrites (profiles containing swollen mitochondria and endoplasmic reticulum) described in the lateral geniculate nucleus of the monkey following long-term deafferentation (LeVay, 1971; Ghetti et al., 1975). Multilaminated bodies and clumped neurotubular elements, which were prominent features of deafferentated Purkinje cell dendrites, have been described in dendrites from other centers following the long-term removal of their afferent input (Glees et al., 1967; Pinching and Powell, 1971; Berger, 1973). In this study, the multilaminated bodies resembled mitochondria in their orientation and configuration.

The two distinct morphological reactions (loss of postnatal growth or transneuronal degeneration) which occur following climbing fiber-deafferentation of the weanling and adult Purkinje cell respectively are thought to be directly related to the Purkinje cell's ability to form ectopic spines. In the present study, an ectopic formation of spine-like appendages was found along many of the smooth branches of Purkinje cells following climbing fiber-deafferentation on the 21st postnatal day. Ultrastructural examination revealed that many of these ectopic spine-like appendages were synaptically innervated by parallel fiber and basket axon varicosities. Furthermore, the population of dendritic thorns, which was deinnervated following climbing fiber-deafferentation, was found to be

heterotypically reinnervated by the parallel fiber system. It is therefore suggested that the formation of ectopic spines represents a plastic change in the dendrite of the Purkinje cell designed to obtain a sufficient afferent input for the continued maintenance of the cell following deafferentation. It may be that sufficient afferent contacts are made with these spines and the dendritic thorns following deafferentation in the weanling rat to avoid significant transneuronal changes. On the other hand, the inability of the adult Purkinje cell to form ectopic spines following climbing fiber-deafferentation, and to thereby acquire additional synaptic input, may account for the subsequent transneuronal degeneration of the smooth branches and spiny branchlets of these cells. Thus, while the dendrites of Purkinje cells in weanling rats are capable of plastic change, this ability appears to be lost by the 150th postnatal day.

#### B. Parallel Fiber Deafferentation

The most prominent finding from the image analysis of Purkinje cells from both parallel fiber-deafferentated adult and weanling rats was a marked reduction in the number of spiny branchlets. The measurements of these adult Purkinje cells, in fact, revealed decreases in the number of spiny branchlets which are significantly lower than those recorded on the 21st postnatal day, a finding which is interpreted as indicating a transneuronal degeneration of the terminal branchlet system. The electron microscopic observations made in this study confirm the findings derived from the image analysis of Golgi impregnated material. The molecular layer neuropil appeared loosely organized due to a decrease in the number of parallel fiber profiles, which were replaced by a

smaller number of hypertrophied Bergmann profiles. More importantly, however, the terminal branchlet system of the Purkinje cell dendritic tree was found to undergo electron-dense degeneration following parallel fiber deafferentation in either the adult or weanling. Many of these degenerating terminal branchlets were invested by an hypertrophied Bergmann glial sheath. These glial profiles were found to be active in phagocytizing both parallel fiber varicosities and dendritic spines following short-term cerebellar lesions. A similar loss of the parallel fiber input in the adult cat resulted in degeneration of both small caliber Purkinje cell dendrites and stellate cell dendrites (Mouren-Mathieu and Colonnier, 1969). In agreement with Mouren-Mathieu and Colonnier's finding, the long-term opacification of this portion of the Purkinje cell observed in the present study is thought to reflect a transneuronal degeneration of this system. The importance of the parallel fiber system for the maintenance of the terminal branchlets is therefore evident. The fact that the degenerative changes in this study were more evident within the small caliber dendrites of the Purkinje cell than within the soma or larger dendrites suggests that this represents a transneuronal response rather than a retrograde degenerative reaction (Grant and Westrum, 1968). This is particularly important in the present study because the cerebellar cut could possibly have damaged the efferent outflow of the Purkinje cell such that the soma and dendrites of these cells could be susceptible to retrograde degenerative changes. However, an examination of the region of the ansiform lobule medial to the cerebellar cut revealed no degenerating somata. The response of the Purkinje cell to axotomy was observed in tissue taken from the ansiform lobule lateral to the cerebellar cut. The entire Purkinje cell soma and

dendritic tree were readily visualized because of the marked increase in the electron opacity of the cytoplasmic matrix. These Purkinje cells had clearly undergone necrotic changes. The responses following axotomy and deafferentation were therefore readily distinguishable and were clearly a reflection of the two types of lesions. In the weanling-deafferentated cerebellum, electron-dense transneuronal degeneration was restricted to the system of terminal branchlets. The ultrastructural morphology of the smooth branches and primary trunks appeared unchanged. The loss of parallel fibers in the adult, however, produced a more significant degeneration of the Purkinje cell dendritic tree. Large vacuolated profiles were visualized within regions of the molecular layer and it is likely that they represent the remains of primary trunks or large caliber smooth dendritic branches.

The present study has shown a decrease in the number of spines covering the terminal branchlets following parallel fiber-deafferentation of both adult and weanling rats. These results agree favourably with the findings described previously in the cat following an identical method of deafferentation (Mouren-Mathieu and Colonnier, 1969). A number of studies on other regions of the central nervous system have also reported a loss of dendritic spines following deafferentation (Matthews and Powell, 1962; Valverde, 1971; Raisman and Field, 1973; Frotscher, Hamori and Wenzel, 1977). While the mechanism of spine loss was not readily discernible in this study, indications of phagocytic activity by Bergmann glial processes were found. A similar explanation has been suggested for spine loss in the cerebellum of the cat following parallel fiber loss and in the cerebral cortex following deafferentation (Colonnier, 1964; Gray, 1964; Mouren-Mathieu and

Colonnier, 1969; Ghetti and Wisniewski, 1972). It appears, therefore, that the maintenance of dendritic spines in these centers and on the Purkinje cells (present study) is dependent upon an intact afferent system. However, spine formation on Purkinje cells is independent of an afferent input (Hirano et al., 1972; Llinas et al., 1973; Altman and Anderson, 1973; Privat and Drian, 1975; Sotelo, 1975a). In fact, developmental studies have shown that resorption of perisomatic processes and dendritic spines occurs at the time of climbing and basket fiber synaptogenesis (Altman, 1972a; Bradley and Berry, 1976b). Although the Purkinje cell has an intrinsic growth potential for the development of dendritic appendages, the spines which form in the absence of the parallel fiber input develop on large caliber dendrites. Since the formation of the terminal branchlet system is under the trophic influence of the parallel fiber system (Altman and Anderson, 1973; Privat and Drian, 1975; Bradley and Berry, 1976b), it is not surprising that in the present study a loss of both terminal branchlets and spines was found following parallel fiber-deafferentation of both weanling and adult rats.

### C. Mossy Fiber Deafferentation

Following electrolytic ablation of the basilar pontine gray, there was a near total degeneration of the mossy fiber rosette population within the ansiform lobule. The present study, in addition, showed a transneuronal degeneration of the granule cell system following long-term pontocerebellar ablation. Transneuronal degenerative changes were most conspicuous within the axoplasm of the parallel fiber system. Beyond 40 days postoperative these alterations involved a major portion of the parallel fiber system of the molecular layer. The observed

reduction in the number of parallel fiber profiles within the molecular layer is thought to reflect the transneuronal loss of these fibers. The fact that many of the persisting fibers were reduced in size and had undergone a dramatic increase in their overall electron opacity supports this suggestion. Similar morphological changes in other systems have been interpreted as a coagulative form of degeneration (Gentshev and Sotelo, 1973). In support of these findings, cortical ablations in neonatal rats have resulted in a transneuronal cortico-ponto-cerebellar atrophy of the contralateral cerebellar hemisphere, with a subsequent loss of postsynaptic dendritic digits of the granule cells and a reduction in size of Purkinje cell dendritic spines (Hamori, 1969; Uzonova and Hambri, 1974).

#### A Possible Phagocytic Role For Pontocerebellar Terminals

The results of this investigation have provided morphological evidence to suggest that the degenerating pontocerebellar rosette plays an active role in the fragmentation and removal of the granule cell digitiform dendrite. Filopodial projections of degenerating pontocerebellar rosettes which appeared to pinch off and engulf portions of the granule cell dendrite were found. Profiles in the process of being engulfed ranged from small nibs of the postsynaptic dendrite to large fragments as much as one-fifth of the total cross-sectional area of the digitiform dendrite in size. The axoplasm of many of the pontocerebellar rosettes contained a number of membrane-bound vacuoles which possessed small fragments of debris. It is highly likely that these profiles represent the product of axonal engulfment.

It has been argued by many authors that terminal boutons



become detached from their postsynaptic contact during the process of anterograde degeneration, thus allowing phagocytosis by glial cells to take place without including the postsynaptic profile (Westrum, 1966; Pinching, 1969; Lund and Lund, 1971; Westrum and Black, 1971). On the other hand, it has been shown in the visual system that both the pre- and postsynaptic structures are phagocytized by glia simultaneously (Colonnier, 1964; Ghetti and Wisniewski, 1972; Ghetti et al., 1975). In summary therefore, this study suggests a possible phagocytic role for axons. Walberg (1963) was the first to suggest that dendrites are capable of phagocytizing portions of degenerating axons. Since then, phagocytosis by dendritic elements has been observed in various centers in the central nervous system and has been shown to involve both small and large fragments of the pre- and postsynaptic elements (Conradi, 1969; Larramendi, 1969; Ghetti and Wisniewski, 1972; Gentshev and Sotelo, 1973; Rustioni and Sotelo, 1974). However, others have qualified this phagocytic role for dendrites by suggesting that it occurs only when reactive astrocytes and microglia are unable to carry out this function (Wisniewski et al., 1972).

Reactive glial cells were not found in the granule cell layer following pontocerebellar ablations in the present study. Smith, Hudgens and O'Leary (1966) have also found limited glial activity following peduncular lesions in cat cerebellum. In the present study, the only exception to this was the presence of reactive astrocytic and microglial elements found in association with the simple clustered rosettes. This mossy fiber population underwent a rapid form of electron-dense degeneration, followed by its removal before the 5th postoperative day. Microglial elements, in particular, were observed in the process of

separating the pre- and postsynaptic elements and phagocytizing the simple clustered type of rosette. The reason for the greater susceptibility of the simple clustered mossy fiber rosette to the phagocytic action of reactive glial elements, and the factors which determine its rapid course of electron-dense degeneration remain to be elucidated.

#### Secondary transneuronal degeneration

While the loss of afferent fibers is frequently followed by the transneuronal degeneration of the postsynaptic structure, Frotscher et al. (1977) have suggested that this effect may not be entirely limited to the first postsynaptic neuron. Evidence to support secondary transneuronal degeneration is provided in this study. Image analysis of Purkinje cell dendritic trees following long-term pontine ablation revealed a significant decrease in the number of smooth branches and spiny branchlets. Ultrastructural examinations in this study have revealed degeneration secondary to that of the parallel fibers. Transneuronal degenerative changes were observed within the smooth branches and terminal branchlet system of the Purkinje cell (the postsynaptic target of the parallel fiber varicosity). Secondary transneuronal degeneration has been reported in several regions of the central nervous system following deafferentation (Powell and Erulkar, 1972; Frotscher et al., 1977). In fact, cortical ablations in neonatal rats have resulted in a transneuronal cortico-ponto-cerebellar atrophy of the contralateral cerebellar hemisphere with a subsequent reduction in size of the Purkinje cell dendritic spines (Hamori, 1969; Uzonova and Hamori, 1974).

#### 5.12 Hypertrophied Purkinje Cell Spines

A prominent feature of the Purkinje cell following either

parallel fiber-deafferentation or mossy fiber degeneration was the increase in the length of many of the dendritic spines on the terminal branchlets. The fact that no ectopic spines were formed following the cerebellar lesion (parallel fiber-deafferentation) suggests that the climbing fiber input to the cerebellar cortex had been spared in the region of the cerebellar cortex medial to the transection. However, dendritic spines which exceeded 3.6  $\mu\text{m}$  in length were found on the terminal branchlets following parallel fiber or mossy fiber-deafferentation. The length of several of these spines was three times greater than the average. Abnormally large dendritic spines have been identified on Purkinje cell dendritic trees which have developed in the absence of a parallel fiber input (Hamori, 1969; Llinas et al., 1973; Sotelo, 1975a; Berry and Bradley, 1976b). Heterologous mossy and climbing fiber contacts have been reported in agranular cerebella on the dendritic shafts of the various cell types and in association with large stout Purkinje cell dendritic spines (Hamori, 1969; Herndon et al., 1971b; Llinas et al., 1973; Sotelo, 1975a). It has been postulated that the climbing and mossy fibers provide the necessary stimulus for the increased growth of the spines (Hamori, 1969; Berry and Bradley, 1976c). Contrary to this, it would seem more appropriate, in view of the developmental studies of Privat and Drian (1975), that the elongation of the dendritic spines may be due to the intrinsic growth potential of the Purkinje cell. It is suggested that the Purkinje cell is capable of increasing the length of its dendritic spines following parallel fiber-deafferentation in order to reach appropriate contacts. Those spines which become reinnervated may represent the hypertrophied spines seen in Golgi preparations, while spines which are unable to acquire appropriate innervation may degenerate,

accounting for the reduction of dendritic spine numbers. Evidence in fact, was found in the present study and by Mouren-Mathieu and Colonnier (1969) to suggest a possible phagocytic removal of the dendritic spines following parallel fiber-deafferentation.

### 5.13 Transneuronal Degeneration of Molecular Layer Interneurons

#### A. Climbing Fiber Deafferentation

An unexpected finding following long-term climbing fiber-deafferentation was the transneuronal degenerative changes within the cerebellar interneurons of the molecular layer (basket and stellate cells). These alterations can be attributed to the loss of the olivocerebellar input, rather than to the direct effect of 3AP, because similar changes were also observed following electrolytic ablation of the inferior olive.

Although an enormous axonal milieu lies adjacent to the dendritic fields of both stellate and basket cells, morphological studies have suggested that a rather small proportion of the somatic surface of either basket (30%) or stellate cells (18%) is directly involved in receiving synaptic contacts (Lemkey-Johnston and Larramendi, 1968). While the postsynaptic target of the climbing fiber has long been considered to be the dendritic tree of the Purkinje cell, at least one Golgi study has suggested a climbing fiber input to the soma and dendrites of both basket and stellate cells (Scheibel and Scheibel, 1954). More recently, ultrastructural investigations have identified synaptic varicosities associated with the somata of both stellate and basket cells which are morphologically similar to the climbing fiber terminals. Such findings have led several authors to postulate a direct climbing fiber input to the cerebellar interneurons (Hamori and Szentagothai, 1966;

Palay and Chan-Palay, 1974). The experimental findings of this study support this view, although it does not provide quantitative or morphological evidence for such an input. The degeneration of both the soma and dendrites of these cells following removal of the climbing fibers suggests that the existence of the olivocerebellar input is essential for the maintenance of these cells. These findings are supported by several reports in the literature of a transneuronal degeneration of perikarya following deafferentation (Penman and Smith, 1950; Torvik, 1956; Goldby, 1957; Polyak, 1957).

#### B. Parallel Fiber Deafferentation

The present study has revealed a transneuronal degeneration of stellate cells following parallel fiber-deafferentation of the adult rat, whereas basket cells have remained unaffected. It has been determined that axosomatic parallel fiber varicosities in mice represent 74% of the synaptic input of the basket cell and 92% of the input to the stellate cell; whereas the input to the dendritic surface of these cells is entirely parallel fiber in nature (Lemkey-Johnston and Larramendi, 1968). Although, for reasons described above, the cerebellar lesion provides only a partial deafferentation of the cerebellar molecular layer, the parallel fiber loss is sufficient to cause transneuronal degeneration of the stellate cells.

Mouren-Mathieu and Colonnier (1969) interpreted the increase in opacity of stellate cell dendrites following parasagittal cerebellar lesions to be the result of retrograde dendritic degeneration. These authors assumed that their lesions within the cerebellar cortex had involved axons from the stellate cell population. Because of the detailed

morphology now available for the rat cerebellar cortex, Mœuren-Mathieu and Colonnier's explanation, which may be applicable for the cat, does not appear to be acceptable for the rat. The findings of Palay and Chan-Palay (1974) have shown that the axons of the superficial stellate cells are confined to the width of their own dendritic tree (40  $\mu\text{m}$ ). Although the axons of deep stellate cells are much longer (450  $\mu\text{m}$ ), they have an identical course to that of the basket cell axon, which runs in the parasagittal plane parallel to the cerebellar lesion. In view of this evidence, the findings of the present study strongly suggest that the degenerative changes within the stellate cells are transneuronal rather than retrograde in nature.

The afferent input to the basket cell soma is less homogeneous than that to the stellate cells (Lemkey-Johnston and Larramendi, 1968). The existence of the other afferents in the rat may provide a morphological basis for the maintenance of these cells following parallel fiber-deafferentation. Ultrastructural examination of the cerebellar cortex in the present study has revealed that the parallel fiber is the only neuronal element to undergo electron-dense degeneration following short-term cerebellar lesions. The climbing, basket, stellate and recurrent Purkinje cell axons showed no evidence of degeneration following the cerebellar lesion and may represent important elements for the maintenance of the population of basket cells, which receives synapses from all these sources.

A parasagittal lesion made on the 21st postnatal day did not produce transneuronal degenerative changes within either the stellate or the basket cell population. Although the formation of the internal granule cell layer of the rat has been described as complete by the 22nd

postnatal day (Altman, 1972a), it has recently been suggested that parallel fibers may continue to elongate beyond this period (Lauder, 1978).

The possibility therefore exists that those afferents to the cerebellar interneurons which degenerate following a cerebellar lesion could be at least partially replaced by undamaged parallel fibers, which continue to increase in length along the longitudinal axis of the cerebellar folium. Neurons deafferented following a cerebellar lesion may induce actively growing axons to increase in length and reinnervate a larger number of cells than normal. Such growth could be responsible for the maintenance of the stellate cell population in deafferented weanling rats.

#### 5.14 The Cerebellum: Its Potential to Remodel

The transneuronal degeneration which resulted following climbing, mossy or parallel fiber-deafferentation of the adult cerebellum is direct evidence that collateral reinnervation does not occur.

Although many fiber systems within the central nervous system of both adult and immature animals have the potential to produce collateral sprouts following injury to adjacent axons, the adult and weanling cerebella have shown little potential to form heterologous synapses following the removal of either the extrinsic or intrinsic afferents.

##### A. Climbing Fiber Deafferentation

In climbing fiber-deafferented weanling rats ectopic spines were routinely formed upon the smooth branches of the Purkinje cell dendritic arbor. In these animals, both the ectopic spines and the denervated dendritic thorns became innervated by the parallel fiber system. As a result, the weanling deafferented Purkinje cells showed only minor signs of transneuronal degeneration. In climbing fiber-deafferented

adult rats, however, the Purkinje cell loses the potential to form ectopic spines.

Although the primary trunks and smooth branches of the Purkinje cell are surrounded by an axonal milieu, it is likely that very little of this dendritic surface is accessible to these fibers following climbing fiber-deafferentation because of the Bergmann glial covering. As a result, the only area able to receive parallel fiber terminals following climbing fiber-deafferentation is associated with the dendritic thorns. Even if a total reinnervation of the dendritic thorns by parallel fibers occurs following climbing fiber-deafferentation of the adult, it is probably not sufficient to maintain the Purkinje cell because the parallel fiber input is weaker. It has recently been reported that the amount of transmitter substance released into the synaptic cleft is directly related to the size of the presynaptic terminal (Kuno, 1971). Thus, since the climbing fiber varicosity is several times larger than its parallel fiber counterpart (Palay and Chan-Palay, 1974), it is likely that it produces a greater depolarization of the postsynaptic Purkinje cell dendrite than the parallel fiber terminal. On this basis, a one-to-one replacement of the climbing fibers by parallel fibers on the dendritic thorns could not adequately replace the excitatory postsynaptic potential of the climbing fiber varicosity. The inability of the adult Purkinje cell to form ectopic spines following climbing fiber-deafferentation and thus acquire more parallel fiber input appears to be directly related to the Purkinje cell's subsequent transneuronal degeneration.

In the weanling rat, the formation of ectopic spines following climbing fiber-deafferentation may represent a means of overcoming the Bergmann glial barrier in order to acquire more synaptic



contacts with parallel fibers of the molecular layer neuropil. For example, in areas of the Purkinje cell dendritic tree where spines are prominent, that is the terminal branchlets, the spines are partially devoid of glial covering and are therefore accessible for direct contact. Following climbing fiber-deafferentation of the weanling rat, the loss of excitation from the climbing fiber input may be partially compensated for by an increased number of excitatory inputs from the parallel fiber system. In addition to the reinnervation of the dendritic thorn population by aberrant parallel fiber varicosities, an input from the parallel fiber system appears to be transmitted through the population of ectopic spines. The ectopic formation of dendritic spines and their subsequent innervation by the parallel fiber system may represent an attempt to compensate for the lost excitation by the climbing fiber. The fact that transneuronal degeneration is limited in extent following climbing fiber-deafferentation of the weanling rat suggests that sufficient reinnervation has taken place to maintain the cell.

#### B. Mossy Fiber Deafferentation

Although extensive degeneration of the mossy fiber rosette population occurred within the ansiform lobule of the cerebellum following basilar pontine lesions, no indication of remodeling from intact afferents was observed at any time. Moreover, a large number of postsynaptic elements of the pontocerebellar rosette were found to undergo degeneration. Large portions of mossy fiber rosette debris were found to persist up to 80 days following pontine ablation, which is undoubtedly an important factor in the lack of reinnervation. This finding contrasts sharply with the rapid course of degeneration described for the spinocerebellar system

(Palay and Chan-Palay, 1974). The persistence of the pontocerebellar debris could certainly represent a physical barrier to the reinnervation of the mossy fiber rosette. An equally important finding was the marked absence of reactive glial cells during the course of pontocerebellar degeneration, which may relate to the persistence of degenerating debris. It has been suggested that denuded postsynaptic specializations represent the stimulus for axonal sprouting (Sotelo, 1975a; Lynch et al., 1974). Because of the persistence of the degenerative debris, therefore, synaptic reinnervation of the granule cell may not be possible. The inability of the adult cerebellum to facilitate the phagocytic removal of the pontocerebellar debris likely excludes it from the possibility of reinnervation even if the potential for remodeling does exist in the adult. In the absence of sufficient compensation for the loss of the pontocerebellar input, the granule cell and its contacts (the Purkinje cell and molecular layer interneurons) undergo transneuronal degeneration.

### C. Parallel Fiber Deafferentation

Following parallel fiber-deafferentation of adult and weanling rats, a marked transneuronal degeneration of the Purkinje cell terminal branchlet system was observed. Although a substantial portion of the parallel fiber input was lost following the cerebellar lesion, heterologous contacts with dendritic spines were not found. It has been suggested from the preponderance of asynaptic spines in both weaver and reeler mutants that the terminal branchlets may be highly selective as to their afferent input (Rakic, 1975). The findings of the present study suggest that this may also be the case following surgical deafferentation of the terminal branchlet system. The climbing fibers, stellate and

basket cell axons, and the recurrent Purkinje cell axons, which are all normal synaptic components along the smooth portion of the Purkinje cell dendritic tree, were not found to innervate the dendritic spine population. The degeneration of the terminal branchlet system of the Purkinje cell dendritic tree, however, is direct evidence that extensive parallel fiber-deafferentation has occurred.

When no degenerative changes were apparent in the terminal branchlet system, hypertrophied dendritic spines were common and in each case were synaptically innervated by a parallel fiber varicosity. It is suggested that these dendritic spines elongated in response to parallel fiber-deafferentation and thereby became accessible for reinnervation from the intact parallel fiber milieu. Those branchlets which underwent electron-dense degeneration are thought to represent terminal branchlets, which had not acquired a sufficient parallel fiber input. Herndon et al. (1971b) have provided evidence to suggest that synaptic spines may be capable of inducing parallel fiber sprouting.

It would appear therefore, that the terminal branchlet of the Purkinje cell is highly selective as to its afferent input. In a similar manner, the commissural/association zone of the dentate gyrus is unreceptive to either septal or entorhinal fibers even though they are the closest source of afferents (Lynch et al., 1974). The parallel fibers may be the only axons which are genetically predetermined to form connections with the terminal branchlet system of the Purkinje cell dendritic tree. In the absence of a parallel fiber input, other systems would then be excluded from reinnervating the spines.

## CHAPTER 6

### PART I - SUMMARY

1. The origins of the afferents to the lateral cerebellar hemisphere were investigated using the horseradish peroxidase (HRP) retrograde tracing method. This technique revealed that the ansiform lobule of the cerebellum receives its mossy fiber input primarily from the basilar pontine gray. Labeled cells in the pons were found bilaterally within two longitudinal cell columns located ventromedial and ventrolateral to the cortical peduncle. Although a few small foci of labeled cells were also observed in other nuclei, they represent a rather minor proportion of the afferents to the ansiform lobule. In addition, the olivocerebellar input to the ansiform lobule was found to originate within both the dorsal and ventral lamellae of the principal olive throughout its rostrocaudal extent.
2. The inferior olive of the adult rat was found to undergo a rapid form of electron-dense neuronal degeneration

following 3-acetylpyridine (3AP) administration. This toxic effect resulted in a complete bilateral involvement. Astrocytic proliferation was evident at 12 hours and appeared to be essential for the fragmentation and disintegration of the neuronal soma. Microglial involvement in the later stages participated in the actual phagocytic removal of degenerating neuronal fragments. The removal of all cytoplasmic and nuclear debris was complete by the end of the second week.

3. It was revealed that the weanling rat possesses a much higher tolerance to 3AP than the adult. Injections containing at least 90 mg/kg body weight of 3AP were necessary to produce a total bilateral olivary ablation in the weanling rat.

4. Degenerative changes in the cerebellar cortex of the adult rat were evident from 12 hours onwards following 3AP treatment. Climbing fiber varicosities appeared degenerative by 24 hours and were largely phagocytized and cleared by 7 days. A total loss of the climbing fiber input to the ansiform lobule was found following 3AP treatment, a finding which supports the view that the inferior olive is the sole source of climbing fibers. A similar time course of climbing fiber degeneration was found following electrolytic ablation of the inferior olivary complex.

5. The absence of degenerating axon terminals within the inferior olivary complex following 3AP treatment indicates that recurrent collaterals of climbing fibers do not exist within the inferior olivary complex.
  
6. Following short-term treatment with 3AP, terminal degeneration was not found within the granule cell layer of the ansiform lobule. Ultrastructural examination confirmed that all cerebellar glomeruli were normal in appearance. These findings indicate that few, if any, glomerular collaterals arise from climbing fibers to terminate within the ansiform lobule.
  
7. An electron microscopic examination of the mossy fiber rosette population of the ansiform lobule revealed that most of the terminals are of either the simple dispersed (60%) or the complex dispersed (26%) variety. In addition, a small number of mossy fiber rosettes have been found which belong to either the simple clustered (12%) or the complex clustered (2%) type of terminal.
  
8. Electron microscopy has revealed that the degenerating mossy fiber rosettes which occur following pontine ablation represent two distinct populations with respect to their time course of degeneration. The majority of the mossy fiber rosettes (simple and complex dispersed

terminals) underwent a very slow course of electron-dense degeneration over an 80 day period. However, a small population of terminals (simple clustered variety) was observed which underwent a rapid course of electron-dense degeneration (by the 5th day). Since the electrolytic lesions of the basilar pontine gray included the nucleus reticularis tegmenti pontis, this center could not be excluded as the possible origin of these terminals. Morphological evidence is provided which suggests that the pontocerebellar varicosity may play a phagocytic role in the removal of the granule cell digitiform dendrite.

9. Electron microscopic examination confirmed that the only neuronal elements affected following cerebellar cuts (medial to the lesion) are the axons of the granule cells, the parallel fibers. These axons and their terminals underwent a rapid course of electron-dense degeneration. The debris was cleared by Bergmann glial cells by the 5th day. Evidence is provided to suggest that Bergmann glial cells play an active role in the phagocytic removal of both degenerating parallel fibers and their postsynaptic target, the Purkinje cell dendritic spines.

10. The possibility of synaptic remodeling in the cerebellar cortex was investigated following deafferentation of both the weanling and the adult rat. Although several

experimental methods were employed, including silver impregnation, autoradiography and electron microscopy, no evidence was found to suggest sprouting of either climbing or mossy fibers. The synaptic specificity of the cerebellar cortex appears to be maintained following extensive mossy or climbing fiber-deafferentation. Evidence is provided, however, which suggests that basket axons; and in particular the parallel fiber system possess some capabilities for sprouting following deafferentation.

11. Image analysis of Golgi impregnated cerebella at the 21st and 150th postnatal days revealed a significant growth in the Purkinje cell dendritic tree beyond the 21st postnatal day. The results indicate significant increases in both the length and number of smooth branches and spiny branchlets.
12. An ectopic formation of dendritic spines occurred following climbing fiber-deafferentation of the weanling rat, but not the adult. These spines were restricted largely to the distal portions of the smooth branches of the Purkinje cell dendritic tree. Ultrastructural examination revealed, furthermore, that these ectopic spines were synaptically innervated by either the parallel fiber system or basket axons.



13. Golgi-Gox preparations revealed that a loss of dendritic spines occurs along the terminal branchlets following mossy or parallel fiber-deafferentation. In addition, many of the existing spines underwent marked changes in form such that many of them were significantly longer than normal.

14. Image analysis of the Golgi impregnated Purkinje cell indicated significant losses in both smooth branch and spiny branchlet numbers following climbing fiber, mossy fiber or parallel fiber-deafferentation. The loss of smooth branches and spiny branchlets which occurred, however, following climbing fiber-deafferentation of weanling rats was due to a reduction in postnatal branching, rather than transneuronal degeneration. Ultrastructural evidence for transneuronal degeneration which supports the quantitative findings is provided.

15. Transneuronal degenerative changes occurred in the population of molecular layer interneurons following climbing fiber-deafferentation of both weanling and adult rats. These changes suggest a direct climbing fiber input to these cells. Degeneration of the molecular layer interneurons following mossy fiber-deafferentation, however, is secondary to the transneuronal loss of the granule cell system.

## PART II - CONCLUSIONS

This study suggests that the dendritic tree of the Purkinje cell has a potential for reorganization following deafferentation. An ectopic formation of dendritic spines which is restricted to the distal portion of the smooth branches of these cells occurs following climbing fiber-deafferentation of the weanling rat. In these animals both the ectopic spines and the denervated dendritic thorns become synaptically innervated by the parallel fiber and basket axon system. These Purkinje cells show no signs of transneuronal degeneration. Climbing fiber-deafferentated adult Purkinje cells undergo marked transneuronal degenerative changes and appear to lose the potential to form ectopic spines. The inability of the adult Purkinje cell to form ectopic spines in an attempt to replace the excitatory postsynaptic potential of the climbing fiber varicosity appears to be directly related to the Purkinje cell's subsequent transneuronal degeneration.

The present study suggests that the elongation of the Purkinje cell dendritic spine occurs in response to parallel fiber-deafferentation in an attempt to make the spine accessible for reinnervation by the reduced parallel fiber milieu of the molecular layer.

Although an extensive degeneration of the mossy fiber rosette population occurs following basilar pontine lesions; no indication of remodeling from intact afferents is observed. The inability of the mature cerebellum to facilitate the phagocytic removal of the degenerating pontocerebellar varicosity within a reasonable period of time appears to eliminate the possibility of collateral reinnervation of cerebellar glomeruli. The persistence of the pontocerebellar debris probably represents a physical barrier to reinnervation. As a result,

primary transneuronal degeneration of the granule cell system and subsequent secondary transneuronal degeneration of the Purkinje cell dendritic tree and molecular layer interneurons takes place.

The synaptic specificity of the mature cerebellar cortex is largely maintained following deafferentation of the climbing, mossy and parallel fiber input. Although the mature cerebellum has a limited potential to form heterologous synapses the transneuronal degeneration which results following deafferentation is direct evidence that reinnervation seldom occurs. The characteristic response of the mature cerebellum to deafferentation, therefore, is transneuronal degeneration.

## BIBLIOGRAPHY

- Addison, W.H. (1911). The development of the Purkinje cells and of the cortical layers in the cerebellum of the albino rat. *J. Comp. Neurol.* 21: 459-488.
- Aguayo, A.J., L.C. Terry and G.M. Bray (1973). Spontaneous loss of axons in sympathetic unmyelinated nerve fibers of the rat during development. *Brain Res.* 54: 360-364.
- Allison, A.C. (1953). The structure of the olfactory bulb and its relationship to the olfactory pathways in the rabbit and the rat. *J. Comp. Neurol.* 98: 309-350.
- Allison, A.C. (1954). The secondary olfactory areas in the human brain. *J. Anat. (Lond.)* 88: 481-488.
- Altman, J. (1966). Autoradiographic and histological studies of postnatal neurogenesis. II. A longitudinal investigation of the kinetics, migration and transformation of cells incorporating tritiated thymidine in infant rats, with special reference to postnatal neurogenesis in some brain regions. *J. Comp. Neurol.* 128: 431-474.
- Altman, J. (1969). Autoradiographic and histological studies of postnatal neurogenesis. III. Dating the time of production and onset of differentiation of cerebellar microneurons in rats. *J. Comp. Neurol.* 136: 269-294.
- Altman, J. (1972a). Postnatal development of the cerebellar cortex in the rat. I. The external germinal layer and the transitional molecular layer. *J. Comp. Neurol.* 145: 353-398.

- Altman, J. (1972b). Postnatal development of the cerebellar cortex in the rat. II. Phases in the maturation of Purkinje cells and the molecular layer. *J. Comp. Neurol.* 145: 399-464.
- Altman, J. (1972c). Postnatal development of the cerebellar cortex in the rat. III. Maturation of the components of the granular layer. *J. Comp. Neurol.* 145: 465-514.
- Altman, J. (1973). Experimental reorganization of the cerebellar cortex. III. Regeneration of the external germinal layer and granule cell ectopia. *J. Comp. Neurol.* 149: 153-180.
- Altman, J. (1976a). Experimental reorganization of the cerebellar cortex. V. Effects of early x-irradiation schedules that allow or prevent the acquisition of basket cells. *J. Comp. Neurol.* 165: 31-48.
- Altman, J. (1976b). Experimental reorganization of the cerebellar cortex. VI. Effects of x-irradiation schedules that allow or prevent cell acquisition after basket cells are formed. *J. Comp. Neurol.* 165: 49-64.
- Altman, J. (1976c). Experimental reorganization of the cerebellar cortex. VII. Effects of late x-irradiation schedules that interfere with cell acquisition after stellate cells are formed. *J. Comp. Neurol.* 165: 65-76.
- Altman, J. and W.J. Anderson (1971). Irradiation of the cerebellum in infant rats with low-level x-ray: histological and cytological effects during infancy and adulthood. *Exp. Neurol.* 30: 492-509.
- Altman, J. and W.J. Anderson (1972). Experimental reorganization of the cerebellar cortex. I. Morphological effects of elimination of all microneurons with prolonged x-irradiation started at birth. *J. Comp. Neurol.* 146: 355-406.

Altman, J. and W.J. Anderson (1973). Experimental reorganization of the cerebellar cortex. II. Effects of elimination of most microneurons with prolonged x-irradiation started at four days. *J. Comp. Neurol.* 149: 123-152.

Altman, J., W.J. Anderson and K.A. Wright (1968). Gross morphological consequences of irradiation of the cerebellum in infant rats with repeated doses of low-level x-ray. *Exp. Neurol.* 21: 69-91.

Altman, J. and G.D. Das (1966). Autoradiographic and histological studies of postnatal neurogenesis. I. A longitudinal investigation of the kinetics, migration and transformation of cells incorporating tritiated thymidine in neonatal rats, with special reference to postnatal neurogenesis in some brain regions. *J. Comp. Neurol.* 126: 337-390.

Ambrose, C.T. and A. Donner (1973). Application of the analysis of variance to hemagglutination titrations. *J. Immunological Methods* 3: 165-210.

Armstrong, D.M. and R.J. Harvey (1966). Responses in the inferior olive to stimulation of the cerebellar and cerebral cortices in the cat. *J. Physiol.* 187: 553-574.

Armstrong, D.M., R.J. Harvey and R.F. Schild (1974). Topographical localization in olivo-cerebellar projection: an electrophysiological study in the cat. *J. Comp. Neurol.* 154: 287-302.

Arees, E.A. and K.E. Astrom (1976). Transneuronal changes in the lateral geniculate nucleus and optic tectum following unilateral eye enucleation in the newborn rat. *J. Neuropath. Exp. Neurol.* 35: 305.

- Barnes, C.D. and N. Worrall (1968). Reinnervation of spinal cord by cholinergic neurons. *J. Neurophysiol.* 31: 689-694.
- Barron, D.H. (1933). Structural changes in anterior horn cells following central lesions. *Proc. Soc. Exp. Biol. (N.Y.)* 30: 1327-1329.
- Batini, C., C. Buisseret-Delmas, J. Corvisier, O. Hardy and D. Jassik-Gerschenfeld (1978). Brain stem nuclei giving fibers to lobules VI and VII of the cerebellar vermis. *Brain Res.* 153: 241-261.
- Batini, C., J. Corvisier, J. Destombes, H. Gioanni and J. Everett (1976). The climbing fibers of the cerebellar cortex, their origin and pathways in cat. *Exp. Brain Res.* 26: 407-422.
- Batini, C. and R. Pumain (1968). Activation of Purkinje neurons through climbing fibres after chronic lesions of the olivo-cerebellar pathway. *Experientia (Basel.)* 24: 914-916.
- Beech, J.N. and G. Raisman (1980). Extended projections induced by partial deafferentation of the medial mammillary nucleus. *Brain Res.* 188: 347-355.
- Beitz, A.J. (1976). The topographical organization of the olivo-dentate and dentato-olivary pathways in the cat. *Brain Res.* 115: 311-315.
- Bell, C.C. and R.S. Dow (1967). Cerebellar circuitry. *Neurophysiol.* 32: 1044-1055.
- Benes, F.M., T.N. Parks and E.W. Rubel (1977). Rapid dendritic atrophy following deafferentation: an EM morphometric analysis. *Brain Res.* 122: 1-13.
- Berger, B. (1973). Dégénérescence transsynaptique dans la pulve olfactif du lapin, après des afferentation périphérique. Observation ultrastructurale. *Acta Neuropath. (Berl.)* 24: 128-152.

- Berger, H. (1900). Experimentall-anatomische Studien über die durch den Mangel optischer Reize veranlassten Entwicklungshemmungen im Occipitallappen des Hundes und der Katze. Arch. Psychiat. Nervenkrankh 33: 521-567.
- Bernstein, J.J. (1967). The regenerative capacity of the telencephalon of the goldfish and rat. Exp. Neurol. 17: 44-56.
- Bernstein, J.J. and M.E. Bernstein (1973). Neuronal alteration and reinnervation following axonal regeneration and sprouting in the mammalian spinal cord. Brain Behav. Evol. 8: 135-161.
- Berry, M. and P.M. Bradley (1976a). The application of network analysis to the study of branching patterns of large dendritic fields. Brain Res. 109: 111-132.
- Berry, M. and P.M. Bradley (1976b). The growth of the dendritic trees of Purkinje cells in the cerebellum of the rat. Brain Res. 112: 1-35.
- Berry, M. and P.M. Bradley (1976c). The growth of the dendritic trees of Purkinje cells in irradiated agranular cerebellar cortex. Brain Res. 116: 361-387.
- Berry, M. and T. Hollingworth (1972). Growth of dendrites of the Purkinje cells in the rat cerebellum. J. Anat. (Lond.) 111: 491-492.
- Berry, M., P. McConnell and J. Sievers (1980). Dendritic growth and the control of neuronal form. In: Current Topics in Developmental Biology (R.K. Hunt, ed.), vol. 15. Academic Press, Toronto. pp.67-101.
- Bignami, A. and D. Dahl (1975). Astroglial protein in the developing spinal cord of the chick embryo. Dev. Biol. 44: 204-209.



- Bjerre, B., B. Bjorklund and U. Stenevi (1973). Stimulation of growth of new axonal sprouts from lesioned monoamine neurones in adult rat brain by nerve growth factor. *Brain Res.* 60: 161-176.
- Bjorklund, A., R. Katzman, U. Stenevi and K. West (1971). Development and growth of axonal sprouts from noradrenaline and 5-hydroxytryptamine neurones in the rat spinal cord. *Brain Res.* 31: 21-33.
- Bjorklund, A. and U. Stenevi (1971). Growth of central catecholamine neurones into smooth muscle grafts in the rat mesencephalon. *Brain Res.* 31: 1-20.
- Bloom, F.E., B.J. Hoffer and G.R. Siggins (1971). Studies on norepinephrine-containing afferents to Purkinje cells of rat cerebellum. I. Localization of the fibers and their synapses. *Brain Res.* 25: 501-521.
- Bodian, D. (1966). Spontaneous degeneration in the spinal cord of monkey fetuses. *Bull. Johns Hopk. Hosp.* 119: 16-45.
- Bowman, M.H. and J.S. King (1973). The conformation, cytology and synaptology of the opossum inferior olivary nucleus. *J. Comp. Neurol.* 148: 491-524.
- Brand, S., A. Dahl and E. Mugnaini (1976). The length of parallel fibers in the cat cerebellar cortex. An experimental light and electron microscopic study. *Exp. Brain Res.* 26: 39-58.
- Bradley, P. and M. Berry (1975). The effect of specific deprivation of either the climbing or the parallel fibre input on the development of the dendritic tree of Purkinje cells in the cerebellum of the rat. *J. Anat. (Lond.)* 120: 407-408.
- Bradley, P. and M. Berry (1976a). Climbing fibre deafferentation - its effects on Purkinje cell dendritic tree development and stability. *J. Anat. (Lond.)* 122: 707.

- Bradley, P. and M. Berry (1976b). The effects of reduced climbing and parallel fibre input on Purkinje cell dendritic growth. *Brain Res.* 109: 133-151.
- Bradley, P. and M. Berry (1976c). Quantitative effects of climbing fibre deafferentation on the adult Purkinje cell dendritic tree. *Brain Res.* 112: 133-140.
- Bradley, P. and M. Berry (1978). Quantitative effects of methylazoxymethanol acetate on Purkinje cell dendritic growth. *Brain Res.* 143: 499-511.
- Brattgard, S.O. (1952). The importance of adequate stimulation for the chemical composition of retinal ganglion cells during early post-natal development. *Acta radio. (Stockh.)*, Suppl. 96: 1-80.
- Brodal, A. (1939). Experimentelle Untersuchungen über retrograde Zellveränderungen in der unteren Olive nach Läsionen des Kleinhirns. *Ztschr. f. d. ges. Neur. u. Psychiat.* 166: 624.
- Brodal, A. (1940). Experimentelle Untersuchungen über die olivocerebellare Lokalisation. *Z. Ges. Neurol. Psychiat.* 169: 1-153.
- Brodal, A. (1941). Die Verbindungen des Nucleus cuneatus externus mit dem Kleinhirn beim Kaninchen und bei der Katze. Experimentelle Untersuchungen. *Z. ges. Neurol. Psychiat.* 171: 167-199.
- Brodal, A. (1943). The cerebellar connections of the nucleus reticularis lateralis (nucleus funiculi lateralis) in the rabbit and the cat. Experimental investigations. *Acta. Psychiat. (Kbh.)* 18: 171-233.
- Brodal, A. (1954). Afferent cerebellar connections. In: *Aspects of Cerebellar Anatomy*. (J. Jansen and A. Brodal, eds.), Johan Grundt Tanum Forlag, Oslo, 158: pp.82-188.

- Brodal, A. (1976). The olivocerebellar projection in the cat as studied with the method of retrograde axonal transport of horseradish peroxidase. II. The projection to the uvula. *J. Comp. Neurol.* 166: 417-426.
- Brodal, A. and P.A. Drablos (1963). Two types of mossy fiber terminals in the cerebellum and their regional distribution. *J. Comp. Neurol.* 121: 173-187.
- Brodal, A. and G. Grant (1962). Morphology and temporal course of degeneration in cerebellar mossy fibers following transection of the spinocerebellar tracts in the cat. An experimental study with silver methods. *Exp. Neurol.* 5: 67-87.
- Brodal, A. and B. Høivik (1964). Site and mode of termination of primary vestibulocerebellar fibres in the cat. An experimental study with silver impregnation methods. *Arch. Ital. Biol.* 102: 1-21.
- Brodal, A. and A. Torvik (1957). Über den Ursprung der sekundären vestibulocerebellaren Fasern bei der Katze. Eine experimentell-anatomische Studie. *Arch. Psychiat. Nervenkr.* 195: 550-567.
- Brodal, A. and F. Walberg (1977a). The olivocerebellar projection in the cat studied with the method of retrograde axonal transport of horseradish peroxidase. IV. The projection to the anterior lobe. *J. Comp. Neurol.* 172: 85-108.
- Brodal, A. and F. Walberg (1977b). The olivocerebellar projection in the cat studied with the method of retrograde axonal transport of horseradish peroxidase. VI. The projection onto longitudinal zones of the paramedian lobule. *J. Comp. Neurol.* 176: 281-294.

- Brodal, A., F. Walberg and G.H. Hoddevik (1975). The olivocerebellar projection in the cat studied with the method of retrograde axonal transport of horseradish peroxidase. J. Comp. Neurol. 164: 449-470.
- Brodal, P. (1975). Demonstration of a somatotopically organized projection onto the paramedian lobule and the anterior lobe from the lateral reticular nucleus: an experimental study with the horseradish peroxidase method. Brain Res. 95: 221-239.
- Brodal, P. (1979). The pontocerebellar projection in the rhesus monkey: an experimental study with retrograde axonal transport of horseradish peroxidase. Neurosci. 4: 193-208.
- Brodal, P. (1980). The projection from the nucleus reticularis tegmenti pontis to the cerebellum in the rhesus monkey. Exp. Brain Res. 38: 29-36.
- Brown, P.A. (1980). The inferior olivary connections to the cerebellum in the rat studied by retrograde axonal transport of horseradish peroxidase. Brain Res. Bull. 5: 267-275.
- Brown, P. and J. Carman (1978). Cerebellar decussation of fibres from the nucleus reticularis tegmenti pontis in the brain of the albino rat. Experientia 34: 1039-1041.
- Brown, J.T., V. Chan-Palay and S.L. Palay (1977). A study of the afferent input to the inferior olivary complex in the rat by retrograde axonal transport of horseradish peroxidase. J. Comp. Neurol. 176: 1-22.
- Bunge, R.P., M.B. Bunge and H. Ris (1960). Electron microscopic study of demyelination in an experimentally induced lesion in adult cat spinal cord. J. Biophys. Biochem. Cytol. 7: 685-696.

Burgen, A.S.V. and L.M. Chipman (1951). Cholinesterase and succinic dehydrogenase in the central nervous system of the dog. *J. Physiol. (Lond.)* 114: 296-305.

Burke, R., A. Lundberg and F. Weight (1971). Spinal border cell origin of the ventral spinocerebellar tract. *Exp. Brain Res.* 12: 283-294.

Burne, R.A., M.A. Eriksson, J.A. Saint-Cyr and D.J. Woodward (1978). The organization of the pontine projection to lateral cerebellar areas in the rat: dual zones in the pons. *Brain Res.* 139: 340-347.

Butterworth, R.F., E. Hamel, F. Londerville and A. Barbeau (1978). Cerebellar ataxia produced by 3-acetyl pyridine in rat. *Can. J. Neurol. Sci.* 5: 131-134.

Cajal, S. Ramon y (1909). *Histologie du Systeme Nerveux de l'Homme et des Vertebres*. Tome J., A. Maloine, Paris. pp.398-402.

Calvet, M.C., M.J. Drian and A. Privat (1974). Spontaneous electrical patterns in cultured Purkinje cells grown with an antimetabolic agent. *Brain Res.* 79: 285-290.

Carpenter, M.B. and G.R. Hanna (1961). Fiber projections from the spinal trigeminal nucleus in the cat. *J. Comp. Neurol.* 117: 117-131.

Carrea, R.M.E., M. Reissing and F.A. Mettler (1947). The climbing fibres of the simian and feline cerebellum. *J. Comp. Neurol.* 87: 321-365.

Chan-Palay, V. (1971). The recurrent collaterals of Purkinje cell axons: a correlated study of the rat's cerebellar cortex with electron microscopy and the Golgi method. *Z. Anat. Entwickl.-Gesch.* 134: 200-234.

Chan-Palay, V. (1973). Neuronal plasticity in the cerebellar cortex and lateral nucleus. *Z. Anat. Entwickl.-Gesch.* 142: 23-35.

Chan-Palay, V. (1977). Cerebellar Dentate Nucleus. Organization, Cytology and Transmitters. Springer-Verlag, Berlin.

Chan-Palay, V. and S.L. Palay (1970). Interrelations of basket cell axons and climbing fibres in the cerebellar cortex of the rat. *Z. Anat. Entwickl.-Gesch.* 132: 191-227.

Chan-Palay, V. and S.L. Palay (1971). The synapse en marron between Golgi II neurons and mossy fibers in the rat's cerebellar cortex. *Z. Anat. Entwickl.-Gesch.* 133: 274-287.

Chan-Palay, V., S.L. Palay, J.T. Brown, and C. Van Itallie (1977). Sagittal organization of olivo-cerebellar and reticulocerebellar projections: autoradiographic studies with <sup>35</sup>S-methionine. *Exp. Brain Res.* 30: 561-576.

Chow, K.L. (1955). Failure to demonstrate changes in the visual system of monkeys kept in darkness or in colored lights. *J. Comp. Neurol.* 102: 597-606.

Chow, K.L., A.H. Riesen and F.W. Newell (1957). Degeneration of retinal ganglion cells in infant chimpanzees reared in darkness. *J. Comp. Neurol.* 107: 27-42.

Clemente, C.D. (1964). Regeneration in the vertebrate central nervous system. *Int. Rev. Neurobiol.* 6: 257-301.

Clendenin, M., G. Ekerot, O. Oscarsson and I. Rosen (1974a). Distribution in cerebellar cortex of mossy fibre afferents from the lateral reticular nucleus in the cat. *Brain Res.* 69: 136-139.

Clendenin, M., G. Ekerot, O. Oscarsson and I. Rosen (1974b). The lateral reticular nucleus in the cat. I. Mossy fibre distribution in cerebellar cortex. *Exp. Brain Res.* 21: 473-486.

Coggeshall, R.E. and P.D. MacLean (1958). Hippocampal lesions following administration of 3-acetylpyridine. Proc. Soc. Exp. Biol. 98: 687-688.

Coleman, P.D. and A.H. Riesen (1968). Environmental effects on cortical dendritic fields. I. Rearing in the dark. J. Anat. (Lond.) 102: 363-374.

Colonnier, M. (1964). Experimental degeneration in the cerebral cortex. J. Anat. (Lond.) 98: 47-53.

Conradi, S. (1969). Ultrastructure and distribution of neuronal and glial elements on the surface of the proximal part of a motoneuron dendrite, as analyzed by serial sections. Acta Physiol. Scand. Suppl. 332: 49-64.

Conradi, S. and L. Ronnevi (1975). Spontaneous elimination of synapses on cat spinal motoneurons after birth: do half of the synapses on the cell bodies disappear? Brain Res. 92: 505-510.

Cooke, J.D., B. Larson, O. Oscarsson and B. Sjolund (1971). Origin and termination of cuneocerebellar tract. Exp. Brain Res. 13: 339-358.

Cook, W.H., J.H. Walker and M.L. Barr (1951). A cytological study of transneuronal atrophy in the cat and rabbit. J. Comp. Neurol. 94: 267-292.

Cook, R.D. and H.M. Wisniewski (1973). The role of oligodendroglia and astroglia in Wallerian degeneration of the optic nerve. Brain Res. 61: 191-206.

Cooper, S. and C.S. Sherrington (1940). Gower's tract and spinal border cells. Brain 63: 123-134.

- Cotman, C.W., D.A. Matthews, D. Taylor and G. Lynch (1973). Synaptic rearrangement in the dentate gyrus: histochemical evidence of adjustments after lesions in immature and adult rats. *Proc. Nat. Acad. Sci. (Wash.)* 70: 3473-3477.
- Courville, J. (1975). Distribution of olivocerebellar fibers demonstrated by a radioautographic tracing method. *Brain Res.* 95: 253-263.
- Courville, J. and F. Faraco-Cantin (1978). On the origin of the climbing fibers of the cerebellum. An experimental study in the cat with an autoradiographic tracing method. *J. Neurosci.* 3: 797-809.
- Courville, J., F. Faraco-Cantin and N. Diakiv (1974). A functionally important feature of the distribution of the olivo-cerebellar climbing fibers. *Can. J. Physiol. Pharmacol.* 52: 1212-1217.
- Courville, J. and H. Kitahara (1980). Length of parallel fibers in various lobules of the cerebellar cortex of the cat. An autoradiographic study. *Neurosci. Abstracts* 6: 471.
- Cowan, W.M. (1970). Anterograde and retrograde transneuronal degeneration in the central and peripheral nervous system. In: *Contemporary Research Methods in Neuroanatomy* (W.J.H. Nauta and S.O.E. Ebbesson, eds.), Springer-Verlag, Berlin, pp. 217-249.
- Cowan, W.M., D.I. Gottlieb, A.E. Hendrickson, J.L. Price and T.A. Woolsey (1972). The autoradiographic demonstration of axonal connections in the central nervous system. *Brain Res.* 37: 21-51.
- Coyle, J.J., M.E. Molliver and M.J. Kuhar (1978). In situ injection of kainic acid: a new method for selectively lesioning neuronal cell bodies while sparing axons of passage. *J. Comp. Neurol.* 180: 301-323.



- Culling, C.F.A. (1963). Handbook of Histopathological Techniques.  
Butterworths, London, p.131.
- Das, G.D. and I.I. Hine (1972). Nature and significance of spontaneous degeneration of axons in the pyramidal tract. Z. Anat. Entwickl.-Gesch. 136: 98-114.
- Davenport, H.A. (1960). Histological and Histochemical Technics.  
W.B. Saunders Company, Philadelphia-London, pp.223-224.
- deGroot, J. (1959). The rat forebrain in stereotaxic coordinates. Trans. Royal Neth. Acad. Sci. 52: 1-40.
- DeLong, G.R. and R.L. Sidman (1962). Effects of eye removal at birth on histogenesis of the mouse superior colliculus: an autoradiographic analysis with tritiated thymidine. J. Comp. Neurol. 118: 205-224.
- Denk, H., M. Haider, W. Kovak und G. Studynka (1968). Verhaltensänderung und Neurophatologie bei der 3-acetylpyridinvergiftung der ratte. Acta Neuropath. 10: 34-44.
- Desclin, J.C. (1974). Histological evidence supporting the inferior olive as the major source of cerebellar climbing fibers in the rat. Brain Res. 72: 365-384.
- Desclin, J.C. (1976). Early terminal degeneration of cerebellar climbing fibers after destruction of the inferior olive in the rat. Synaptic relationships in the molecular layer. Anat. Embryol. 149: 87-112.
- Desclin, J.C. and F. Colin (1980). The oliyocerebellar system. II. Some ultrastructural correlates of inferior olive destruction in the rat. Brain Res. 187: 29-46.

- Desclin, J.C. and J. Escubi (1974). Effects of 3-acetylpyridine on the central nervous system of the rat, as demonstrated by silver methods. *Brain Res.* 77: 349-364.
- Desclin, J.C. and J. Escubi (1975). An additional silver impregnation method for demonstration of degenerating nerve cells and processes in the central nervous system. *Brain Res.* 93: 25-39.
- Devor, M. (1975). Neuroplasticity in the sparing or deterioration of function after early olfactory tract lesions. *Science* 190: 998-1000.
- Devor, M. (1976). Neuroplasticity in the rearrangement of olfactory tract fibres after neonatal transection in hamsters. *J. Comp. Neurol.* 166: 49-72.
- Dom, R., J.S. King and G.F. Martin (1973). Evidence for two direct cerebello-olivary connections. *Brain Res.* 57: 498-501.
- Dow, R.S. (1936). The fiber connections of the posterior parts of the cerebellum in the cat and rat. *J. Comp. Neurol.* 63: 527-548.
- Drury, R.A.B. and E.A. Wallington (1967). *Carleton's Histological Technique*. Oxford University Press, New York, Toronto, p. 128.
- Eccles, J.C., M. Ito and J. Szentagothai (1967). *The Cerebellum as a Neuronal Machine*. Springer-Verlag: New York.
- Eccles, J.C., R. Llinas and K. Sasaki (1964). Excitation of cerebellar Purkinje cells by the climbing fibers. *Nature (Lond.)* 203: 245-246.
- Eccles, J., R. Llinas and K. Sasaki (1966). The action of antidromic impulses on the cerebellar Purkinje cells. *J. Physiol. (Lond.)* 182: 316-345.

- Eisenman, L.M. and C.R. Noback (1980). The ponto-cerebellar projection in the rat: differential projections to sublobules of the uvula. *Exp. Brain Res.* 38: 11-17.
- Eller, T. and V. Chan-Palay (1976). Afferents to the cerebellar lateral nucleus: Evidence from retrograde transport of horseradish peroxidase after pressure injections through micropipettes. *J. Comp. Neurol.* 166: 285-301.
- Faull, R.L.M. (1977). A comparative study of the cells of origin of cerebellar afferents in the rat, cat, and monkey studied with the horseradish peroxidase technique: I. The non-vestibular brainstem afferents. *Anat. Rec.* 187: 577.
- Feringa, E.R., L.M. Shuer, H.L. Vahlsing and S.M. Davis (1977). Regeneration of corticospinal axons in the rat. *Ann. Neurol.* 2: 315-321.
- Fernando, D.A. (1973). Electron-microscopic study of neuroglial reaction in Wallerian degeneration of corticospinal tract. *Acta. Anatom.* 86: 459-473.
- Fink, R.P. and L. Heimer (1967). Two methods for selective silver impregnation of degenerating axons and synaptic endings in the central nervous system. *Brain Res.* 4: 369-374.
- Foerster, O. and O. Gagel (1932). Die Vorderseilensbrangdurchschneidung beim Menschen. Eine klinisch-patho-physiologisch-anatomische studie. *Z. ges. Neurol. Psychiat.* 138: 1-92.

- Foerster, O., O. Gagel and D. Sheehan (1933). Veränderungen an den Endosen im Rückenmark des Affen Nach Hinterwurzelwischschneidung Zeitschr. f. d. ges. Anat. 101: 553-565.
- Forstronen, R.F. (1963). The origin and morphogenetic significance of the external granular layer of the cerebellum, as determined experimentally in chick embryo. Acta. Neurol. Scand. Suppl. 39, 4: 314-316.
- Fox, C.A., A. Andrade, R.C. Schwyn (1969). Climbing fiber branching in the granular layer. In: Neurobiology of Cerebellar Evolution and development. (R. Llinas, ed.), Chicago:AMA-ERF Institute of Biomedical Research, pp.603-611.
- Frotscher, M., J. Hamori and J. Wenzel (1977). Transneuronal effects of entorhinal lesions in the early postnatal period on synaptogenesis in the hippocampus of the rat. Exp. Brain Res. 30: 549-560.
- Gall, C. and G. Lynch (1978). Rapid axon sprouting in the neonatal rat hippocampus. Brain Res. 153: 357-362.
- Gall, C., R. McWilliams and G. Lynch (1979). The effect of collateral sprouting on the density of innervation of normal target sites: implications for theories on the regulation of the size of developing synaptic domains. Brain Res. 175: 37-47.
- Gentschev, T. and C. Sotelo (1973). Degenerative patterns in the ventral cochlear nucleus of the rat after primary deafferentation. An ultrastructural study. Brain Res. 62: 37-60.

- Ghetti, B., D.S. Horoupian and H.M. Wisniewski (1975). Acute and long term transneuronal response of dendrites of lateral geniculate neurons following transection of the primary visual afferent pathways. In: *Physiology and Pathology of Dendrites*. (G.W. Kreutzberg, ed.), Raven Press, New York, pp.401-424.
- Ghetti, B. and H.M. Wisniewski (1972). Fate of synaptic membranes during degeneration of optic nerve terminals in the lateral geniculate nucleus. *J. Cell Biol.* 55: 84a.
- Glees, P. (1961). Terminal degeneration and transynaptic atrophy in the lateral geniculate body of the monkey. In: *The Visual System Neurophysiology and Psychophysics*. (R. Jung and H. Kornmuller, eds.), Springer, Berlin, pp.104-110.
- Glees, P., M. Hasan and K. Tischner (1967). Ultrastructural features of transneuronal atrophy in monkey geniculate neurones. *Acta Neuropath.* 7: 361-366.
- Glees, P. and W.E. LeGros-Clark (1941). The termination of optic fibres in the lateral geniculate body of the monkey. *J. Anat. (Lond.)* 75: 295-308.
- Globus, A. and A.B. Scheibel (1966). Loss of dendrite spines as an index of pre-synaptic terminal patterns. *Nature* 212: 463-465.
- Globus, A. and A.B. Scheibel (1967). Synaptic loci on visual cortical neurons of the rabbit: the specific afferent radiation. *Exp. Neurol.* 18: 116-131.
- Goldby, F. (1957). A note on transneuronal atrophy in the human lateral geniculate body. *J. Neurol. Neurosurg. Psychiat.* 20: 202-207.

- Gonatas, N.K., S. Levine and R. Shoulson (1965). Electron microscopic investigation of phagocytosis of myelin in an experimental leukoencephalopathy. *Ann. N.Y. Acad. Sci.* 122: 6-14.
- Goodman, L. (1932). Effect of total absence of function on the optic system of rabbits. *Amer. J. Physiol.* 100: 46-63.
- Goodman, D.C. and J.A. Horel (1966). Sprouting of optic tract projections in the brain stem of the rat. *J. Comp. Neurol.* 127: 71-88.
- Gottlieb, D.I. and W.M. Cowan (1972). Evidence for a temporal factor in the occupation of available synaptic sites during the development of the dentate gyrus. *Brain Res.* 41: 452-456.
- Grant, G. (1962). Projection of the external cuneate nucleus onto the cerebellum in the cat: an experimental study using silver methods. *Exp. Neurol.* 5: 179-195.
- Grant, G. (1970). Demonstration of degenerating climbing fibres in the molecular layer of the cerebellum. *Brain Res.* 22: 236-242.
- Grant, G. and J. Westrum (1968). Degenerative changes in dendrites central to axonal transection. Electron microscopical observations. *Experientia (Basel)* 24: 169-170.
- Gray, E.G. (1961). The granule cells, mossy synapses and Purkinje spine synapses of the cerebellum. Light and electron microscope observations. *J. Anat. (Lond.)* 95: 345-356.
- Gray, E.G. (1964). The fine structure of normal and degenerating synapses of the central nervous system. *Arch. Biol. (Liège)* 75: 285-299.
- Gray, E.G. and L.H. Hamlyn (1962). Electron microscopy of experimental degeneration in the avian optic tectum. *J. Anat. (Lond.)* 96: 309-316.

- Graybiel, A.M., H.J.W. Nauta, R.L. Lasek and W.J.H. Nauta (1973). A cerebello-olivary pathway in the cat. An experimental study using autoradiographic tracing techniques. *Brain Res.* 58: 205-211.
- Groenewegen, H.J. and J. Voogd (1976). The longitudinal zonal arrangement of the olivocerebellar, climbing fiber projection in the cat. An autoradiographic and degeneration study. *Exp. Brain Res. Suppl.* 1: 65-71.
- Groenewegen, H.J. and J. Voogd (1977). The parasagittal zonation within the olivocerebellar projection. I. Climbing fiber distribution in the vermis of cat cerebellum. *J. Comp. Neurol.* 174: 417-488.
- Guth, L. and J.J. Bernstein (1961). Selectivity in the reestablishment of synapses in the superior cervical sympathetic ganglion of a cat. *Exp. Neurol.* 4: 59-69.
- Gutmann, E. and J.Z. Young (1944). The re-innervation of muscle after various periods of atrophy. *J. Anat. (Lond.)* 78: 15-43.
- Gwyn, D.G., G.P. Nicholson and B.A. Flumerfelt (1977). The inferior olivary nucleus of the rat: a light and electron microscope study. *J. Comp. Neurol.* 174: 489-520.
- Ha, H. and C. Liu (1968). Cell origin of the ventral spinocerebellar tract. *J. Comp. Neurol.* 133: 185-206.
- Hamlyn, L.H. (1954). The effect of preganglionic section on the neurons of the superior cervical ganglion in rabbits. *J. Anat. (Lond.)* 88: 184-191.
- Hamori, J. (1969). Development of synaptic organization in the partially agranular and in the transneuronally atrophied cerebellar cortex. In: *Neurobiology of Cerebellar Evolution and Development.* (R. Llinas, ed.), Amer. Med. Assoc. Chicago, Ill., pp.845-858.

Hamori, J. (1973). The inductive role of presynaptic axons in the development of postsynaptic spines. *Brain Res.* 62: 337-344.

Hamori, J. and J. Szentagothai (1964). The crossing-over synapse: an electron microscope study of the molecular layer in the cerebellar cortex. *Acta. Biol. Acad. Sci.* 15: 95-117.

Hamori, J. and J. Szentagothai (1966). Identification under the electron microscope of climbing fibres and their synaptic contacts. *Exp. Brain Res.* 1: 65-81.

Hasan, M. and P. Glees (1972). Genesis and possible dissolution of neuronal lipofuscin. *Gerontologia.* 18: 217-236.

Hechst, B. (1933). Uber das Verhalten der ausseren Kniehocker und der Sehrinde ber. *J. Anat. (Lond.)* 94: 145-169.

Henkel, C.K., M. Linauts and G.F. Martin (1975). The origin of the annulo-olivary tract with notes on other mesencephalo-olivary pathways. A study by the horseradish peroxidase method. *Brain Res.* 100: 145-150.

Herndon, R.M. (1968). Thiophen induced\*granule cell necrosis in the rat cerebellum. An electron microscopic study. *Exp. Brain Res.* 6: 49-68.

Herndon, R.M., G. Morgolis and L. Kilham (1969). Virus induced cerebellar malformation. *J. Neuropathol. Exp. Neurol.* 28: 164.

Herndon, R.M., G. Margolis and L. Kilham (1971a). The synaptic organization of the malformed cerebellum induced by perinatal infection with the feline panleukopenia virus (PLV). I. Elements forming the cerebellar glomeruli. *J. Neuropath. Exp. Neurol.* 30: 196-205.



- Herndon, R.M., G. Margolis and L. Kilham (1971b). The synaptic organization of the malformed cerebellum induced by perinatal infection with the feline panleukopenia virus (PLV). II. The Purkinje cell and its afferents. *J. Neuropath. Exp. Neurol.* 30: 557-570.
- Herndon, R.M. and M.L. Oster-Granite (1975). Effect of granule cell destruction on development and maintenance of the Purkinje cell dendrite. *Adv. Neurol.* 12: 361-371.
- Hess, A. (1957). Optic centers and pathways after eye removal in fetal guinea pigs. *J. Comp. Neurol.* 109: 91-116.
- Hicks, S.P. (1955). Pathologic effects of antimetabolites. Acute lesions in the hypothalamus, peripheral ganglia, and adrenal medulla caused by 3-acetyl pyridine and prevented by nicotinamide. *Amer. J. Path.* 31: 189-197.
- Hicks, S.P. and C.J. D'Amato (1970). Motor-sensory and visual behavior after hemispherectomy in newborn and mature rats. *Exp. Neurol.* 29: 416-438.
- Himwich, H.E. (1976). *Brain Metabolism and Cerebral Disorders*. Spectrum Publications, Inc. New York.
- Hinds, J.W. and J. Hinds (1972). Reconstruction of dendritic growth cones in neonatal mouse olfactory bulb. *J. Neurocytol.* 1: 168-187.
- Hirano, A. and H.M. Dembitzer (1973). Cerebellar alternations in Weaver mutant mice. *J. Cell Biol.* 56: 478-487.
- Hirano, A. and H.M. Dembitzer (1974). Observations on the development of the Weaver-mouse cerebellum. *J. Neuropath. Exp. Neurol.* 33: 354-364.

Hirano, A. and H.M. Dembitzer (1975). Aberrant development of the Purkinje cell dendritic spine. In: Physiology and Pathology of Dendrites, Advances in Neurology (G.W. Kreutzberg, ed.), Vol. 12, Raven Press, New York, pp.353-360.

Hirano, A., H.M. Dembitzer and M. Jones (1972). An electron microscopic study of cycasin-induced cerebellar alterations. J. Neuropathol. Exp. Neurol. 31: 113-125.

Hirano, A. and M. Jones (1972). Fine structure of cycasin-induced cerebellar alterations. Fed. Proc. 31: 1517-1518.

Hoddevik, G.H. (1975). The pontocerebellar projection onto the paramedian lobule in the cat: an experimental study with the use of horseradish peroxidase as a tracer. Brain Res. 95: 291-307.

Hoddevik, G.H. and A. Brodal (1977). The olivo-cerebellar projection studied with the method of retrograde axonal transport of horseradish peroxidase. V. The projections to the flocculonodular lobe and the paraflocculus in the rabbit. J. Comp. Neurol. 176: 269-280.

Hoddevik, G.H., A. Brodal, K. Kawamura and T. Hashikawa (1977). The pontine projection to the cerebellar vermal visual area studied by means of the retrograde axonal transport of horseradish peroxidase. Brain Res. 123: 209-227.

Hoddevik, G.H., A. Brodal and F. Walberg (1976). The olivocerebellar projection in the cat studied with the method of retrograde axonal transport of horseradish peroxidase. III. The projection to the vermal visual area. J. Comp. Neurol. 169: 155-170.

Holmqvist, B., O. Oscarsson and I. Rosen (1963). Functional organization of the cuneocerebellar tract in the cat. Acta Physiol. Scand. 58: 216-235.

Ikeda, M. (1979). Projections from the spinal and the principal sensory nuclei of the trigeminal nerve to the cerebellar cortex in the cat, as studied by retrograde transport of horseradish peroxidase. *J. Comp. Neurol.* 184: 567-586.

Ikeda, M. and M. Matsushita (1977). The location of cerebellar projection neurons in the spinal trigeminal nucleus of the cat. A study with the horseradish peroxidase technique. *Acta. Anat. (Nippon)* 52: 41-42.

Ikeda, M. and M. Matsushita (1978). Projections from the spinal nucleus of the trigeminal nerve to the cerebellar cortex in the cat, as studied by retrograde transport of horseradish peroxidase. *Acta. Anat. (Nippon)* 53: 39.

Jacobsen, M. (1970). *Developmental Neurobiology*. Holt Rinehart and Winston, New York.

Jansen, J. and A. Brodal (1958). *Das Kleinhirn*. In: Mollendorff's *Handbuch der Mikroskopischen Anatomie des Menschen IV/8*. Springer-Verlag, Berlin.

Jones, W.H. and D.B. Thomas (1956). Transsynaptic atrophy in the cerebral cortex. *Nature* 178: 47-48.

Jones, W.H. and D.B. Thomas (1962). Changes in the dendritic organization of neurons in the cerebral cortex following deafferentation. *J. Anat. (Lond.)* 96: 375-381.

Kaplan, N.O. and M.M. Ciotti (1956). Chemistry and properties of the 3-acetylpyridine analogue of diphosphopyridine nucleotide. *J. Biol. Chem.* 221: 823-832.

- Kappers, C.U.A., G.C. Huber and E.C. Crosby (1936). The comparative anatomy of the nervous system of vertebrates, including man. The Macmillan Co., New York. Vol. 1, 663-695.
- Katzman, R., A. Björklund, C.H. Owman, U. Stenevi and K.A. West (1971). Evidence for regenerative axon sprouting of central catecholamine neurons in the rat mesencephalon following electrolytic lesions. Brain Res. 25: 579-596.
- Kawaguchi, S., T. Yamamoto, N. Mizuno and N. Iwahori (1975). The role of climbing fibers in the development of Purkinje cell dendrites. Neurosci. Letters 1: 301-304.
- Kerr, F.W.L. (1971). Electronmicroscopic observations on primary deafferentation of the subnucleus caudalis of the trigeminal nerve. In: Oral-Facial Sensory and Motor Mechanisms. (R. Dubner and Y. Kawamura, eds.), Appleton-Century-Crofts, New York, pp.159-181.
- Kilham, L. and G. Margolis (1964). Cerebellar ataxia in hamsters inoculated with rat virus. Science 143: 1047-1048.
- Kilham, L. and G. Margolis (1965). Cerebellar disease in cats induced by inoculation of rat virus. Science 148: 244-246.
- Kilham, L. and G. Margolis (1966a). Viral etiology of spontaneous ataxia of cats. Amer. J. Pathol. 48: 991-1011.
- Kilham, L. and G. Margolis (1966b). Spontaneous hepatitis and cerebellar "hypoplasia" in suckling rats due to congenital infections with rat virus. Amer. J. Pathol. 49: 457-485.

- Kimoto, Y., K. Satoh, T. Sakumoto, M. Tohyama and N. Shimizu (1978).  
Afferent fiber connections from the lower brain stem to the rat  
cerebellum by the horseradish peroxidase method combined with MAO  
staining with special reference to noradrenergic neurons. *J.*  
*Hirnforsch* 19: 85-100.
- Kirk, R.E. (1968). *Experimental Design: Procedures for the Behavioral*  
*Sciences*. Brooks/Cole Pub. Co. Belmont, California.
- Kirkpatrick, J.B. (1968). Chromatolysis in the hypoglossal nucleus of  
the rat: an electron microscopic analysis. *J. Comp. Neurol.* 132:  
189-212.
- Kirsche, W., H. David, E. Winklemann and J. Marx (1964). Elektron  
mikroskopische Untersuchungen und synaptischen Formationen in cortex  
cerebelli von Rattis Norvegicus Berkenhooft. *Z. mikro-anat. Forsch.*  
72: 49-80.
- Koelle, G.B. (1963). Cytological distributions and physiological  
functions of cholinesterase. In: *Handbook Experimental Pharmacology*  
(G.B. Koelle, ed.), Springer-Verlag, Berlin, pp.180-299.
- Koigsmark, B.W. and R.L. Sidman (1963). Origin of brain macrophages in  
the mouse. *J. Neuropathol. Exp. Neurol.* 22: 643-676.
- Koikegami, H. and S. Fuse (1961). Degeneration of hippocampus and other  
brain structures by administration of 3-acetylpyridine. *Acta Anat.*  
(Nippon) 36: 330-331.
- Konig, J.F.R. and R. Klippel (1963). *The Rat Brain. A Stereotaxic Atlas*  
of the Forebrain and Lower Parts of the Brain Stem. The Williams  
and Wilkins Company, Baltimore.

- Kornuth, S.E. and G. Scott (1972). The role of climbing fibers in the formation of Purkinje cell dendrites. *J. Comp. Neurol.* 146: 61-82.
- Korte, G.E. and E. Mugnaini (1979). The cerebellar projection of the vestibular nerve in the cat. *J. Comp. Neurol.* 184: 265-278.
- Kotchabhakdi, N. and F. Walberg (1978). Cerebellar afferent projections from the vestibular nuclei in the cat: an experimental study with the method of retrograde axonal transport of horseradish peroxidase. *Exp. Brain Res.* 31: 591-604.
- Kotchabhakdi, N., F. Walberg and A. Brodal (1978). The olivocerebellar projection in the cat studied with the method of retrograde axonal transport of horseradish peroxidase. VII. The projection to lobulus simplex, crus I and crus II. *J. Comp. Neurol.* 182: 293-314.
- Kristensson, K. and Y. Olsson (1976). Retrograde transport of horseradish peroxidase in transected axons. 3. Entry into injured axons and subsequent localization in perikaryon. *Brain Res.* 115: 201-213.
- Kruger, L., J. Hamori, R. Miller, S. Varon and D.S. Maxwell (1970). Electron microscopic studies of dissociated cells from chick embryos cerebrum in single layer cultures. *Anat. Rec.* 166: 333.
- Kuno, M. (1971). Quantum aspects of central and ganglionic synaptic transmission in vertebrates. *Physiol. Rev.* 51: 647-678.
- Kunzle, H. (1975). Autoradiographic tracing of the cerebellar projections from the lateral reticular nucleus in the cat. *Exp. Brain Res.* 22: 255-266.
- Kupfer, C. (1965). The distribution of cell size in the lateral geniculate nucleus of man following transneuronal cell atrophy. *J. Neuropath. Exp. Neurol.* 24: 653-661.

- Kupfer, C. and J.L. Downer (1967). Ribonucleic acid content and metabolic activity of lateral geniculate nucleus in monkey following afferent denervation. *J. Neurochem.* 14: 257-263.
- Kupfer, C. and P. Palmer (1964). Lateral geniculate nucleus: histological and cytochemical changes following afferent denervation and visual deprivation. *Exp. Neurol.* 9: 400-409.
- Lampert, D. and M. Cressman (1966). Fine structural changes of myelin sheaths after axonal degeneration in the spinal cord of rats. *Am. J. Pathol.* 49: 1139-1155.
- Landis, D.M.D. and T.S. Reese (1977). Structure of Purkinje-cell membrane in staggerer and weaver mutant mice. *J. Comp. Neurol.* 171: 247-260.
- Langman, J., M. Shimada and P. Rodier (1972). Floxuridine and its influence on postnatal cerebellar development. *Pediatr. Res.* 6: 758-764.
- Larramendi, L.M.H. (1965). Purkinje axo-somatic synapses at seven and fourteen post-natal days in the mouse: an electronmicroscopic study. *Anat. Rec.* 151: 460.
- Larramendi, L.M.H. (1969). Analysis of synaptogenesis in the cerebellum of the mouse. In: *Neurobiology of Cerebellar Evolution and Development.* (R. Llinas, ed.), Amer. Med. Ass., Chicago, pp.803-844.
- Larramendi, L.M.H. and E. Victor (1966). Soma-dendritic gradient of spine resorption in the Purkinje cell of the cerebellum of the mouse during post-natal development: an electron microscopic study. *Anat. Rec.* 154: 373-385.

- Larramendi, L.M.H. and T. Victor (1967). Synapses on the Purkinje cell spines in the mouse: an electronmicroscopic study. *Brain Res.* 5: 15-30.
- Lauder, J.M. (1978). Effects of early hypothyroidism and hyperthyroidism on development of rat cerebellar cortex. 4. Parallel fibers. *Brain Res.* 142: 25-39.
- LaVail, J.H. (1975). The retrograde transport method. *Fed. Proc.* 34: 1618-1624.
- LaVail, J.H. and M.M. LaVail (1972). Retrograde axonal transport in the central nervous system. *Science* 176: 1416-1417.
- Lee, K.S., E.J. Stanford, C.W. Cotman and G.S. Lynch (1977). Ultrastructural evidence for bouton proliferation in the partially deafferented dentate gyrus of the adult rat. *Exp. Brain Res.* 29: 475-485.
- LeGros Clark, W.E. (1932). A morphological study of the lateral geniculate body. *Brit. J. Ophthal.* 16: 264-284.
- LeGros Clark, W.E. (1957). Inquiries into the anatomical basis of olfactory discrimination. *Proc. Roy. Soc. B.* 146: 299-319.
- LeGros Clark, W.E. and G.G. Penman (1934). The projection of the retina in the lateral geniculate body. *Proc. Roy. Soc. B. (Lond.)* 114: 291-313.
- Lehninger, A.L. (1970). *Biochemistry. The Molecular Basis of Cell Structure and Function.* Worth Publishers Inc., New York.
- Lemkey-Johnston, N., V. Butler and A. Reynolds (1976). Glial changes in the progress of a chemical lesion. An electron microscopic study. *J. Comp. Neurol.* 167: 481-502.



- Leong, S.K. and R.D. Lund (1973). Anomalous bilateral corticofugal pathways in albino rats after neonatal lesions. *Brain Res.* 62: 218-221.
- LeVay, S. (1971). On the neurons and synapses of the lateral geniculate nucleus of the monkey, and the effects of eye enucleation. *Z. Zellforsch. Mikrosk. Anat.* 113: 396-419.
- Lierse, W. (1965). Ultrastrukturelle hirnerkrankungen der ratte nach gaben von 3-acetylpyridin. *Zeitschrift fur Zellforschung*, 67: 86-95.
- Lim, K.H. and S.K. Leong (1975). Aberrant bilateral projections from the dentate and interposed nuclei in albino rats after neonatal lesions. *Brain Res.* 96: 306-309.
- Liu, C. and W.W. Chambers (1958). Intrasprouting of dorsal root axons. *Arch. Neurol. Psychiat.* 79: 46-61.
- Liu, C.N. and C.Y. Liu (1971). Role of afferents in maintenance of dendritic morphology. *Anat. Rec.* 169: 369.
- Llinas, R., R. Baker and C. Sotelo (1974). Electrotonic coupling between neurons in the cat inferior olive. *J. Neurophysiol.* 37: 560-571.
- Llinas, R., D.E. Hillman and W. Precht (1973). Neuronal circuit reorganization in mammalian agranular cerebellar cortex. *J. Neurobiol.* 4: 69-94.
- Llinas, R., K. Walton and D.E. Hillman (1975). Inferior olive: its role in motor learning. *Science* 190: 1230-1231.
- Lund, R.D. (1972). Synaptic patterns in the superficial layers of the superior colliculus of the monkey, macaca mulatta. *Exp. Brain Res.* 15: 194-211.

Lund, R.D., T.J. Cunningham and J.S. Lund (1973). Modified optic projections after unilateral eye removal in young rats. *Brain Behav. Evol.* 8: 51-72.

Lund, R.D. and J.S. Lund (1970). Synaptic adjustments after deafferentation of the superior colliculus of the rat. *Science* 171: 804-807.

Lund, R.D. and J.S. Lund (1971). Modifications of synaptic pattern in the superior colliculus of the rat during development and following deafferentation. *Vision Res.* 3: 281-298.

Lundberg, A. and O. Oscarsson (1960). Functional organization of the dorsal spino-cerebellar tract in the cat. VII. Identification of units by antidromic activation from the cerebellar cortex with recognition of five functional subdivisions. *Acta Physiol Scand.* 50: 356-374.

Lundberg, A. and O. Oscarsson (1962). Functional organization of the ventral spino-cerebellar tract in the cat. IV. Identification of units by antidromic activation from the cerebellar cortex. *Acta Physiol. Scand.* 54: 252-269.

Lynch, G., N. Brecha, C.W. Cotman and A. Globus (1974). Spine loss and regrowth in hippocampus following deafferentation. *Nature (Lond.)* 248: 71-73.

Lynch, G., S. Deadwyler and C. Cotman (1973). Postlesion axonal growth produces permanent functional connections. *Science* 180: 1364-1366.

Lynch, G., G. Gall and C. Cotman (1977). Temporal parameters of axonal "sprouting" in the brain of the adult rat. *Exp. Neurol.* 54: 179-183.

- Lynch, G., C. Gall, G. Rose and C. Cotman (1976). Changes in the distribution of the dentate gyrus associational system following unilateral or bilateral entorhinal lesions in the adult rat. *Brain Res.* 110: 57-71.
- Lynch, G., D.A. Matthews, S. Mosko, T. Parks and C. Cotman (1972). Induced acetylcholinesterase-rich layer in rat dentate gyrus following entorhinal lesions. *Brain Res.* 42: 311-318.
- Lynch, G., S. Mosko, T. Parks and C. Cotman (1973). Relocation and hyperdevelopment of the dentate gyrus commissural system after entorhinal lesions in immature rats. *Brain Res.* 50: 174-178.
- Lynch, G., B. Stanfield and C. Cotman (1973). Developmental differences in post-lesion axonal growth in the hippocampus. *Brain Res.* 59: 155-168.
- Lynch, G., B. Stanfield, T. Parks and C. Cotman (1974). Evidence for selective post-lesion axonal growth in the dentate gyrus of the rat. *Brain Res.* 69: 1-11.
- Mariani, F., F. Crepel, K. Mikoshiba, J.P. Changeux and C. Sotelo (1977). Anatomical, physiological and biochemical studies of the cerebellum from reeler mutant mouse. *Philos. Trans. Roy. Soc. (Lond.)* 281: 1-28.
- Martin, G.F., C.K. Henkel and J.S. King (1976). Cerebello-olivary fibers; their origin, course and distribution in the North American opossum. *Exp. Brain Res.* 24: 219-236.
- Matsushita, M., Y. Hosoya and M. Ikeda (1979). Anatomical organization of the spinocerebellar system in the cat, as studied by retrograde transport of horseradish peroxidase. *J. Comp. Neurol.* 184: 81-106.

- Matsushita, M. and M. Ikeda (1970). Olivary projections to the cerebellar nuclei in the cat. *Exp. Brain Res.* 10: 488-500.
- Matsushita, M. and M. Ikeda (1976). Projections from the lateral reticular nucleus to the cerebellar cortex and nuclei in the cat. *Exp. Brain Res.* 24: 403-421.
- Matthews, M. (1964). Further observations on transneuronal degeneration in the lateral geniculate nucleus of the macaque monkey. *J. Anat.* (1964) 98: 255-263.
- Matthews, D.A., C. Cotman and G. Lynch (1976). An electron microscopic study of lesion-induced synaptogenesis in the dentate gyrus of the adult rat. I. Magnitude and time course of degeneration. *Brain Res.* 115: 1-21.
- Matthews, M.R., W.M. Cowan and T.P.S. Powell (1960). Transneuronal cell degeneration in the lateral geniculate nucleus of the macaque monkey. *J. Anat. (Lond.)* 94: 145-169.
- Matthews, M.R. and T.P.S. Powell (1962). Some observations on transneuronal cell degeneration in the olfactory bulb of the rabbit. *J. Anat. (Lond.)* 96: 89-102.
- Maxwell, D.S. and L. Kruger (1965a). Small blood vessels and the origin of phagocytes in the rat cerebral cortex following heavy particle irradiation. *Exp. Neurol.* 12: 33-54.
- Maxwell, D.S. and L. Kruger (1965b). The fine structure of astrocytes in the cerebral cortex and their response to focal injury produced by heavy ionizing particles. *J. Cell Biol.* 25: 141-157.
- McCouch, G.P., G.M. Austin, C.N. Liu and C.Y. Liu (1958). Sprouting as a cause of spasticity. *J. Neurophysiol.* 21: 205-216.

- McCrea, R.A., G.A. Bishop and S.T. Kitai (1977). Electrophysiological and horseradish peroxidase studies of precerebellar afferents to the nucleus interpositus anterior. II. Mossy fiber system. Brain Res. 122: 215-228.
- McMahan, U.J. (1967). Fine structure of synapses in the dorsal nucleus of the lateral geniculate body of normal and blinded rats. Zeitschrift fur Zellforschung 76: 116-146.
- McWilliams, R. and G. Lynch (1978). Terminal proliferation and synaptogenesis following partial deafferentation: the reinnervation of the inner molecular layer of the dentate gyrus following removal of its commissural afferents. J. Comp. Neurol. 180: 581-616.
- Mejia, H. (1976). Rate of climbing fiber degeneration in rabbit cerebellum following para-floccular stalk and medullopontine lesions. J. Comp. Neurol. 165: 433-455.
- Meller, K. and P. Glees (1969). The development of the mouse cerebellum: a Golgi and electron microscopic study. In: Neurobiology of Cerebellar Evolution and Development. (R. Llinas, ed.), A.M.A. Chicago, pp.783-801.
- Mesulam, M. (1976). The blue reaction product in horseradish peroxidase neurohistochemistry: incubation parameters and visibility. J. Histochem. Cytochem. 24: 1273-1280.
- Mihalloff, G.A., C.B. McArdle and C.E. Adams (1981). The cytoarchitecture, cytology and synaptic organization of the basilar pontine nuclei in the Rat. I. Nissl and Golgi studies. J. Comp. Neurol. 195: 181-201.
- Minkowski, M. (1920). Über den Verlauf, die Endigung und Zentrale Repräsentation von gekreuzten und ungekreuzten Sehnervenfasern bei einigen Säugetieren und beim Menschen. Schweiz. Arch. Neurol. Psychiat. 6: 201-252.

- Miskolczy, D. (1931). Ueber die Endigungsweise der spinocerebellaren Bahnen. *Z. Anat. Entwickl.-Gesch.* 96: 537-542.
- Misra, C.H. and J.W. Olney (1975). Cysteine oxidase in brain. *Brain Res.* 97: 117-126.
- Moore, R.Y., A. Bjorklund and U. Stenevi (1971). Plastic changes in the adrenergic innervation of the rat septal area in response to denervation. *Brain Res.* 33: 13-35.
- Morest, D.K. (1968). The growth of synaptic endings in the mammalian brain: a study of the calyces of the trapezoid body. *Z. Anat. Entwickl.-Gesch.* 127: 201-220.
- Morest, D.K. (1969a). The growth of dendrites in the mammalian brain. *Z. Anat. Entwickl.-Gesch.* 128: 290.
- Morest, D.K. (1969b). The differentiation of cerebral dendrites: a study of the postmigratory neuroblast in the medial nucleus of the trapezoid body. *Z. Anat. Entwickl.-Gesch.* 128: 271.
- Mori, S. and C.P. LeBlond (1970). Electron microscopic identification of three classes of oligodendrocytes and a preliminary study of their proliferative activity in the corpus callosum of young rats. *J. Comp. Neurol.* 139: 1-30.
- Mouren-Mathieu, A. and M. Colonnier (1969). The molecular layer of the adult cat cerebellar cortex after lesion of the parallel fibers: an optic and electron microscope study. *Brain Res.* 16: 307-323.
- Mugnaini, E. (1969). Ultrastructural studies on the cerebellar histogenesis. II. Maturation of nerve cell populations and establishment of synaptic connections in the cerebellar cortex of the chick. In: *Neurobiology of Cerebellar Evolution and Development* (R. Llinas, ed.), AMA-ERF Institute of Biomedical Research, Chicago, pp. 749-782.

- Mugnaini, E. (1972). The histology and cytology of the cerebellar cortex. In: The Comparative Anatomy and Histology of the Cerebellum: The Human Cerebellum, Cerebellar Connections and Cerebellar Cortex (O. Larsell and J. Jansen, eds.), University of Minnesota Press, Minneapolis, pp.201-265.
- Mugnaini, E. (1976). Organization of cerebellar cortex. *Exp. Brain Res.* Suppl. 1: 8-19.
- Murphy, M.G., J.L. O'Leary and D. Cornblath (1973). Axoplasmic flow in cerebellar mossy and climbing fibers. *Arch. Neurol.* 28: 118-123.
- Murray, M. and M.E. Goldberger (1974). Restitution of function and collateral sprouting in the cat spinal cord. The partially hemisected animal. *J. Comp. Neurol.* 158: 19-36.
- Murray, J.G. and J.W. Thompson (1957). The occurrence and function of collateral sprouting in the sympathetic nervous system of the cat. *J. Physiol.* 135: 133-162.
- Nadler, J.V., C.W. Cotman and G.S. Lynch (1973). Altered distribution of choline acetyltransferase and acetylcholinesterase activities in the developing rat dentate gyrus following entorhinal lesion. *Brain Res.* 63: 215-230.
- Nah, S.H. and S.K. Leong (1976a). Bilateral corticofugal projection to the red nucleus after neonatal lesions in the albino rat. *Brain Res.* 107: 433-436.
- Nah, S.H. and S.K. Leong (1976b). An ultrastructural study of the anomalous corticorubral projection following neonatal lesions in the albino rat. *Brain Res.* 111: 162-166.

- Nakamura, Y., N. Mizuno, A. Konishi and M. Sato (1974). Synaptic reorganization of the red nucleus after chronic deafferentation from cerebellorubral fibers: an electron microscope study in the cat. *Brain Res.* 82: 298-301.
- Nathaniel, E.J. and D.R. Nathaniel (1977). Astroglial response to degeneration of dorsal root fibers in adult rat spinal cord. *Exp. Neurol.* 54: 60-76.
- Nathanson, N., G.E. Cole and H. Van der Loss (1969). Heterotopic cerebellar granule cells following administration of cyclophosphamide to suckling rats. *Brain Res.* 15: 532-536.
- Ochi, R. (1965). Occurrence of postsynaptic potentials in the inferior olive neurones associated with their antidromic excitation. *XXIII Int. Congr. Physiol. Sci. Abstract* 944, p.401.
- Ochs, S. and C. Barnes (1969). Regeneration of ventral root fibers into dorsal roots shown by axoplasmic flow. *Brain Res.* 15: 600-604.
- O'Leary, J.L., S.B. Dunsker, J.M. Smith, J. Inukai and M. O'Leary (1970). Termination of olivocerebellar system in the cat. *Arch. Neurol. (Chic.)* 22: 193-206.
- O'Leary, J.L., J. Inukai and J.M. Smith (1971). Histogenesis of the cerebellar climbing fiber in the rat. *J. Comp. Neurol.* 142: 377-392.
- Olson, L. and K. Fuxe (1971). On the projections from the locus coeruleus noradrenaline neurons: The cerebellar innervation. *Brain Res.* 28: 165-171.
- Oscarsson, O. (1965). Functional organization of spino- and cuneo-cerebellar tracts. *Physiol. Rev.* 45: 495-522.



- Oscarsson, O. (1969). Termination and functional organization of the dorsal spino-olivo-cerebellar path. *J. Physiol. (Lond.)* 200: 129-149.
- Oscarsson, O. (1973). Functional organization of spinocerebellar paths. In: *Handbook of Sensory Physiology. Vol. II. Somatosensory Systems.* (A. Iggo, ed.), Springer-Verlag, New York, pp.339-380.
- Palay, S.L. and V. Chan-Palay (1974). *Cerebellar Cortex. Cytology and Organization*, Springer, Berlin.
- Palkovits, M., P. Mayar and J. Szentagothai (1971). Quantitative histological analysis of the cerebellar cortex in the cat. II. Cell numbers and densities in the granular layer. *Brain Res.* 32: 15-30.
- Parnavelas, J.G., G. Lynch, N. Brecha, C.W. Cotman and A. Globus (1974). Spine loss and regrowth in hippocampus following deafferentation. *Nature (Lond.)* 248: 71-73.
- Pellegrino, L.J. and A.J. Cushman (1967). *A Stereotaxic Atlas of the Rat Brain.* Appleton-Century-Crofts, New York.
- Penman, J. and M.C. Smith (1950). Degeneration of the primary and secondary sensory neurones after trigeminal injection. *J. Neurol. Neurosurg. Psychiat.* 13: 36-46.
- Pensa, A. (1931). Osservazioni e considerazioni sulla struttura della corteccia cerebellare dei mammiferi. *Reale Accad. Nazionale dei Lincei.* 5: 25.
- Perry, T.L., J. MacLean, T.L. Perry, Jr. and S. Hansen (1976). Effects of 3-acetylpyridine on putative neurotransmitter amino acids in rat cerebellum. *Brain Res.* 109: 632-635.

- Pickel, V.M., H. Krebs and F.E. Bloom (1973). Proliferation of norepinephrine-containing axons in rat cerebellar cortex after peduncle lesions. *Brain Res.* 59: 169-179.
- Pinching, A.J. (1969). Persistence of postsynaptic membrane thickenings after degeneration of olfactory nerves. *Brain Res.* 16: 277-281.
- Pinching, A.J. and T.P.S. Powell (1971). Ultrastructural features of transneuronal cell degeneration in the olfactory system. *J. Cell Sci.* 8: 253-287.
- Polysak, S. (1957). *The Vertebrate Visual System*. University of Chicago Press, Chicago.
- Powell, T.P.S. (1967). Transneuronal cell degeneration in the olfactory bulb shown by the Golgi method. *Nature (Lond.)* 215: 425-426.
- Powell, T.P.S. and S.D. Erulkar (1962). Transneuronal cell degeneration in the auditory relay nuclei of the cat. *J. Anat. (Lond.)* 96: 249-268.
- Precht, W., R. Volkind and R.H.I. Blanks (1977). Functional organization of vestibular input to anterior and posterior vermis of cat. *Exp. Brain Res.* 27: 143-160.
- Privat, A. (1975). Dendritic growth in vitro. In: *Physiology and Pathology of Dendrites, Advances in Neurology*. (G.W. Kreutzberg, ed.); Vol. 12, Raven Press, New York, pp.201-216.
- Privat, A. and M.J. Drian (1974). Première analyse ultrastructurale de la plasticité des circuits cérébelleux in vitro. *C.R. Acad. Sci. (Paris)* 278: 659-662.
- Privat, A. and M.J. Drian (1976). Postnatal maturation of rat Purkinje cells cultivated in the absence of two afferent systems: an ultrastructural study. *J. Comp. Neurol.* 166: 201-244.

Raisman, G. (1969). Neuronal plasticity in the septal nuclei of the adult rat. *Brain Res.* 14: 25-48.

Raisman, G., W.M. Cowan and T.P.S. Powell (1966). An experimental analysis of the efferent projection of the hippocampus. *Brain* 89: 83-108.

Raisman, G. and P.M. Field (1973). A quantitative investigation of the development of collateral reinnervation after partial deafferentation of the septal nuclei. *Brain Res.* 50: 241-264.

Rakic, P. (1971). Neuron-glia relationship during granule cell migration in developing cerebellar cortex. A Golgi and electronmicroscopic study in *Macacus rhesus*. *J. Comp. Neurol.* 141: 283-312.

Rakic, P. (1974). Intrinsic and extrinsic factors influencing the shape of neurons and their assembly into neuronal circuits. In: *Frontiers in Neurology and Neuroscience Research* (P. Seeman and G.M. Brown, eds.), University of Toronto Press, Toronto, pp.112-132.

Rakic, P. (1975). Synaptic specificity in the cerebellar cortex: study of anomalous circuits induced by single gene mutations in mice. *Cold Spring Harbor Symp. Quant. Biol.* 40: 333-346.

Rakic, P. and R.L. Sidman (1973a). Weaver mutant mouse cerebellum: defective neuronal migration secondary to abnormality of Bergmann glia. *Proc. Nat. Acad. Sci.* 70: 240-244.

Rakic, P. and R.L. Sidman (1973b). Sequence of developmental abnormalities leading to granule cell deficit in cerebellar cortex of Weaver mutant mice. *J. Comp. Neurol.* 152: 103-132.

Rakic, P. and R.L. Sidman (1973c). Organization of cerebellar cortex secondary to deficit of granule cells in Weaver mutant mice. *J. Comp. Neurol.* 152: 133-162.

- Ralston, H.J.III and K.L. Chow (1973). Synaptic reorganization in the degenerating lateral geniculate nucleus of the rabbit. *J. Comp. Neurol.* 147: 321-350.
- Rezai, Z. and C.H. Yoon (1972). Abnormal rate of granule cell migration in the cerebellum of "weaver" mutant mice. *Develop. Biol.* 29: 17-26.
- Riesen, A.H. (1960). Brain and behavior: 4. Effects of stimulus deprivation on the development and atrophy of the visual sensory system. *Amer. J. Orthopsychiat.* 30: 23-36.
- Riesen, A.H. (1962). Influences of afferent neurons on efferent neurons. II. Some specific effects of deafferentation on central and efferent neurons. *Progr. Neurobiol.* 5: 211-221.
- Rinvik, E. and F. Walberg (1975). Studies on the cerebellar projections from the main and external cuneate nuclei in the cat by means of retrograde axonal transport of horseradish peroxidase. *Brain Res.* 95: 371-381.
- Rivera-Dominguez, M., F.A. Mettler and C.R. Noback (1974). Origin of cerebellar climbing fibers in the rhesus monkey. *J. Comp. Neurol.* 155: 331-342.
- Ruggiero, D., R.R. Batton and A. Jayarama (1977). Afferents to fastigial nucleus in cat demonstrated by transport of horseradish peroxidase. *J. Comp. Neurol.* 172: 189-209.
- Rustioni, A. and C. Setelo (1974). Some effects of chronic deafferentation on the ultrastructure of the nucleus gracilis of the cat. *Brain Res.* 73: 527-533.
- Scheibel, M.E. and A.B. Scheibel (1954). Observations on the intracortical relations of the climbing fibers of the cerebellum. *J. Comp. Neurol.* 101: 733-760.

- Scheibel, M.E. and A.B. Scheibel (1955). The inferior olive: a Golgi study. *J. Comp. Neurol.* 102: 77-132.
- Scheibel, M.E. and A.B. Scheibel (1971). Selected structural-functional correlates in postnatal brain. In: *Brain Development and Behavior.* (M.B. Stein, D.J. McGinty and A.M. Adinolfi, eds.), Academic Press, New York, pp.1-21.
- Schild, R.F. (1980). Length of the parallel fibers in rat cerebellar cortex. *J. Physiol. (Lond.)* 303: 25.
- Schmidt, R. (1962). Die postnatale Genese der Kleinhirndefekte rontgenbestrahlter Housmause. *J. Hirnforsch.* 5: 163-209.
- Seil, F.J. and R.M. Herndon (1970). Cerebellar granule cells in vitro. A light and electron microscope study. *J. Cell Biol.* 45: 212-220.
- Shute, C.C.D. and P.R. Lewis (1961). The use of cholinesterase techniques combined with operative procedures, to follow nervous pathways in the brain. *Bibl. Anat. (Basel)* 2: 34-49.
- Sidman, R.L. (1968). Development of interneuronal connections in brains of mutant mice. In: *Physiological and Biochemical Aspects of Nervous Integration.* (F.D.C. Carlsson, ed.), Prentice-Hall, Englewood Cliffs, New Jersey, pp.163-193.
- Simantov, R., S.H. Snyder and M. Oster-Granite (1976). Harmaline-induced tremor in the rat: abolition by 3-acetylpyridine destruction of cerebellar climbing fibers. *Brain Res.* 114: 144-151.
- Sjostrand, J. (1965). Proliferative changes in glial cells during nerve regeneration. *Z. Zellforsch. Mikroskop. Anat.* 68: 481-493.
- Sjostrand, J. (1966). Glial cells in the hypoglossal nucleus of the rabbit during nerve regeneration. *Acta Physiol. Scan. Suppl.* 270, 67: 1-43.

- Sjostrand, J. (1971). Neuroglial proliferation in the hypoglossal nucleus after nerve injury. *Exp. Neurol.* 30: 178-189.
- Skoff, R.P. and V. Hamburger (1974). Fine structure of dendritic axonal growth cones in embryonic chick spinal cord. *J. Comp. Neurol.* 153: 107-147.
- Smith, K.R., R.W. Hudgens and J.L. O'Leary (1966). An electron microscopic study of degenerative changes in the cat cerebellum after intrinsic and extrinsic lesions. *J. Comp. Neurol.* 126: 15-36.
- Smolyaninov, V.V. (1974). Some special features of organization of the cerebellar cortex. In: *Models of the Structural-Functional Organization of Certain Biological Systems.* (I.M. Gelfand, V.S. Furfinkel, S.V. Fomin and M.L. Testlin, eds.), MIT Press, Cambridge, pp.250-423.
- Snell, R.S. (1961). The histochemical localization of cholinesterase in the central nervous system. *Bibl. Anat. (Basel).* 2: 50-58.
- Snider, R.S. (1936). Alterations which occur in mossy terminals of the cerebellum following transection of the brachium pontis. *J. Comp. Neurol.* 64: 417-431.
- Snyder, R.L. (1977). A comparative study of the neurons of origin of cerebellar afferents in the rat, cat, and squirrel monkey based on the horseradish peroxidase (HRP) retrograde tracer technique: The spinal afferents. *Anat. Rec.* 187: 719.
- Somana, R., N. Kotchabhakdi and F. Walberg (1980). Cerebellar afferents from the trigeminal sensory nuclei in the cat. *Exp. Brain Res.* 38: 57-64.
- Sotelo, C. (1968). Permanence of postsynaptic specialization in the frog sympathetic ganglion cells after denervation. *Exp. Brain Res.* 6: 294-305.

- Sotelo, C. (1973). Permanence and fate of paramembranous synaptic specializations in 'mutants' and experimental animals. *Brain Res.* 62: 345-351.
- Sotelo, C. (1975a). Dendritic abnormalities of Purkinje cells in the cerebellum of neurologic mutant mice (weaver and staggerer). *Adv. Neurol.* 12: 335-351.
- Sotelo, C. (1975b). Anatomical, physiological and biochemical studies of the cerebellum from mutant mice. II. Morphological study of cerebellar cortical neurons and circuits in the weaver mouse. *Brain Res.* 94: 19-44.
- Sotelo, C. (1977). Formation of presynaptic dendrites in the rat cerebellum following neonatal x-irradiation. *Neurosci.* 2: 275-283.
- Sotelo, C. and M. Arsenio-Nunes (1976). Development of Purkinje cells in absence of climbing fibers. *Brain Res.* 111: 389-395.
- Sotelo, C. and J. Changeux (1974). Transsynaptic degeneration 'en cascade' in the cerebellar cortex of staggerer mutant mice. *Brain Res.* 67: 519-526.
- Sotelo, C., D.E. Hillman, A.J. Zamora and R. Llinas (1975). Climbing fiber deafferentation: its action on Purkinje cell dendritic spines. *Brain Res.* 98: 574-581.
- Sotelo, C. and A. Privat (1978). Synaptic remodeling of the cerebellar circuitry in mutant mice and experimental cerebellar malformations. *Acta Neuropathol. (Berl.)* 43: 19-34.
- Stanfield, B. and W.M. Cowan (1976). Evidence for a change in the retino-hypothalamic projection in the rat following early removal of one eye. *Brain Res.* 104: 129-136.
- Stelzner, D.J., R.H. Baisden and D.C. Goodman (1976). Ventral lateral geniculate-nucleus, pars lateralis of rat-synaptic organization and conditions for axonal sprouting. *Cell Tissue Res.* 170: 435-455.

Stenevi, U., A. Bjorklund and R.Y. Moore (1973). Morphological plasticity of central adrenergic neurons. *Brain Behav. Evol.* 8: 110-134.

Steward, O., C.W. Cotman and G.S. Lynch (1973). Reestablishment of electrophysiologically functional entorhinal cortical input to the dentate gyrus deafferented by ipsilateral entorhinal lesions. Innervation by the contralateral entorhinal cortex. *Exp. Brain Res.* 18: 390-414.

Steward, O., C.W. Cotman and G.S. Lynch (1974). Growth of a new fiber projection in the brain of adult rats: re-innervation of the dentate gyrus by the contralateral entorhinal cortex following ipsilateral entorhinal lesions. *Exp. Brain Res.* 20: 45-66.

Steward, O. and S.L. Vinsant (1978). Identification of the cells of origin of a central pathway which sprouts following lesions in mature rats. *Brain Res.* 147: 223-243.

Steward, O., W.F. White, C.W. Cotman and G. Lynch (1976). Potentiation of excitatory synaptic transmission in the normal and in the reinnervated dentate gyrus of the rat. *Brain Res.* 26: 423-441.

Storm-Mathisen, J. (1974). Choline acetyltransferase and acetylcholinesterase in fascia dentata following lesion of the entorhinal afferents. *Brain Res.* 80: 181-197.

Svendgaard, N., A. Bjorklund and U. Stenevi (1976). Regeneration of central cholinergic neurones in the adult rat brain. *Brain Res.* 102: 1-22.

Swenson, R. and A.J. Castro (1980). An HRP study of brain-stem and cerebellar projections to the inferior olivary nucleus in the rat. *Anat. Rec.* 196: 186A.



Szentagothai, J. (1961). Somato-topic arrangement of synapses of primary sensory neurones in Clark's column. *Acta Morph. Acad. Sci (Hung.)* 10: 307-311.

Szentagothai, J. (1962). Anatomical aspects of junctional transformation. In: *Information Processing in the Nervous System*. (R.W. Gerard and J.W. Duff, eds.), Vol. 3, Proceedings of the International Union of Physiological Sciences. *Internat. Congr. Sr.* 49. pp.119-136.

Szentagothai, J. and U. Rajkovits (1959). Über den Ursprung der Kletterfasern des Kleinhirns. *Z. Anat. Entwickl.-Gesch.* 121: 130-141.

Terry, R.J., A.L. Roland and J. Race (1962). Effect of eye enucleation and eyelid closure upon the brain and associated visual structures in the mouse. I. A report of degenerative changes. *J. Exp. Zool.* 150: 165-183.

Tolbert, D.L., L.C. Massopust, M.G. Murphy and P.A. Young (1976). The anatomical organization of the cerebello-olivary projection in the cat. *J. Comp. Neurol.* 170: 525-544.

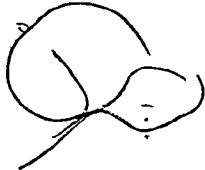
Torvik, A. (1956). Transneuronal changes in the inferior olive and pontine nuclei in kittens. *J. Neuropath. Exp. Neurol.* 15: 119-145.

Torvik, A. and Skjorten, F. (1971). Electron microscopic observations on nerve cell regeneration and degeneration after axonal lesion. II. Changes in the glial cells. *Acta Neuropathol. (Berl.)* 17: 265-282.

Tsang, Y. (1937). Visual centers in blinded rats. *J. Comp. Neurol.* 66: 211-261.

Tsukahara, N., H. Hultborn, F. Murakami and A. Fujito (1974). Sprouting of corticorubral synapses in red nucleus neurones after destruction of the nucleus interpositus of the cerebellum. *Experientia (Basel)* 30: 57-58.

- Tukey, J.W. (1977). Exploratory data analysis. Addison-Wesley Pub. Co., Reading, Massachusetts.
- Uzunova, R. and J. Hamori (1974). Quantitative electron microscopy of the cerebellar molecular layer in cortico-ponto-cerebellar atrophy. Acta. Biol. Acad. Sci. (Hung.) 25: 117-122.
- Valverde, F. (1967). Apical dendritic spines of the visual cortex and light deprivation in the mouse. Exp. Brain Res. 3: 337-352.
- Valverde, F. (1971). Rate and extent of recovery from dark rearing in the visual cortex of the mouse. Brain Res. 33: 1-11.
- Valverde, F. and M.E. Esteban (1968). Peristriate cortex of mouse: location and the effects of enucleation on the number of dendritic spines. Brain Res. 9: 145-148.
- VanGilder, J.C. and J.L. O'Leary (1970). Topical projection of the olivoarebellar system in the cat: an electrophysiological study. J. Comp. Neurol. 140: 69-80.
- Vaughn, J.E. (1965). Electron microscopic study of the vascular response to axonal degeneration in rat optic nerve. Anat. Rec. 151: 428.
- Vaughn, J.E., C.K. Henrikson and J.A. Grieshaber (1974). A quantitative study of synapses on motor neuron dendritic growth cones in developing mouse spinal cord. J. Cell Biol. 60: 664-672.
- Vaughn, J.E. and D.C. Pease (1970). Electron microscopic studies of Wallerian degeneration in rat optic nerves. II. Astrocytes, oligodendrocytes and adventitial cells. J. Comp. Neurol. 140: 207-226.

- 
- Voogd, J. (1964). The cerebellum of the cat. Van Gorcum and Co. Netherlands.
- Walberg, F. (1963). Role of normal dendrites in the removal of degenerating terminal boutons. *Exp. Neurol.* 8: 112-124.
- Wall, P.D. and M.D. Egger (1971). Formation of new connections in adult rat brains after partial deafferentation. *Nature (Lond.)* 232: 542-545.
- Weiss, G.M. and J.J. Pysh (1978). Evidence for loss of Purkinje cell dendrites during late development: a morphometric Golgi analysis in the mouse. *Brain Res.* 154: 219-230.
- Westrum, L.E. (1966). Electron microscopy of degeneration in the prepyriform cortex. *J. Anat. (Lond.)* 100: 683-685.
- Westrum, L.E. and R.G. Black (1971). Fine structural aspects of the synaptic organization of the spinal trigeminal nucleus (pars interpolaris) of the cat. *Brain Res.* 25: 365-387.
- White, L.E. and L.E. Westrum (1964). Dendritic spine changes in prepyriform cortex following olfactory bulb lesions - rat, Golgi method. *Anat. Rec.* 148: 410-411.
- Wiesel, T.N. and D.H. Hubel (1963). Effects of visual deprivation on morphology and physiology of cells in the cat's lateral geniculate body. *J. Neurophysiol.* 26: 978-993.
- Wiesel, T.N. and D.H. Hubel (1965). Extent of recovery from the effects of visual deprivation in kittens. *J. Neurophysiol.* 28: 1060-1072.

- Winkler, C.A. (1918). The olfactory tract in the rabbit. In: Opera Omnia, Vol. 5, F. Bpni, Haalem. pp.397-413.
- Wisniewski, H.M., B. Ghetti and D.S. Horoupian (1972). The fate of synaptic membranes of degenerating optic nerve terminals, and their role in the mechanism of trans-synaptic changes. J. Neurocytol. 1: 297-310.
- Woodhams, P., R. Rodd and R. Balazs (1978). Age dependent susceptibility of inferior olive neurones to 3-acetylpyridine in the rat. Brain Res. 153: 194-198.
- Woolley, D.W. (1945). Production of nicotinic acid deficiency with 3-acetylpyridine; the ketone analogue of nicotinic acid. J. Biol. Chem. 157: 455-459.
- Woolley, D.W., F.M. Strong, R.J. Madden and C.A. Elvehjenr (1938). Anti-black tongue activity of various pyridine derivatives. J. Biol. Chem. 124: 175.
- Woolley, D.W. and A.G.C. White (1943). Attempts to produce vitamin deficiency diseases by feeding compounds related structurally to vitamins. Proc. Soc. Exp. Biol. and Med. 52: 106.
- Zimmer, J. (1973). Extended commissural and ipsilateral projections in postnatally de-entorhinated hippocampus and fascia dentata demonstrated in rats by silver impregnation. Brain Res. 64: 293-311.

VITA

NAME: William Athen Anderson

PLACE OF BIRTH: New Glasgow, Nova Scotia

YEAR OF BIRTH: 1953

POST-SECONDARY  
EDUCATION AND  
DEGREES: Acadia University  
Wolfville, Nova Scotia  
1971-1974 B.Sc.  
1974-1976 M.Sc.

University of Western Ontario  
London, Ontario  
1976-1981 Ph.D.

HONOURS AND  
AWARDS: National Research Council Studentship  
1976-1977

Medical Research Council Studentship  
1977-1980

Medical Research Council Fellowship  
1982

RELATED WORK  
EXPERIENCE: Laboratory Demonstrator  
Acadia University  
Histology  
1974-1976

Laboratory Demonstrator  
University of Western Ontario  
Histology  
1976-1978

Laboratory Demonstrator and Lecturer  
University of Western Ontario  
Gross Anatomy  
1977-1979

## PUBLICATIONS:

Articles:

Boutillier, R.G., M.A. Gibson, D.P. Towes and W.A. Anderson (1977). Gas exchange and acid-base regulation in the blood and extra-embryonic fluids of the developing chicken embryo. *Respiration Physiology* 31: 81-89.

Anderson, W.A. and B.A. Flumerfelt (1980). A light and electron microscopic study of the effects of 3-acetylpyridine intoxication on the inferior olivary complex and cerebellar cortex in the adult rat. *J. Comp. Neurol.* 190: 157-174.

Anderson, W.A. and M.A. Gibson (1981). Some effects of glucagon on chick embryo development. *J. Embryol. Exp. Morphol.* 62: 95-107.

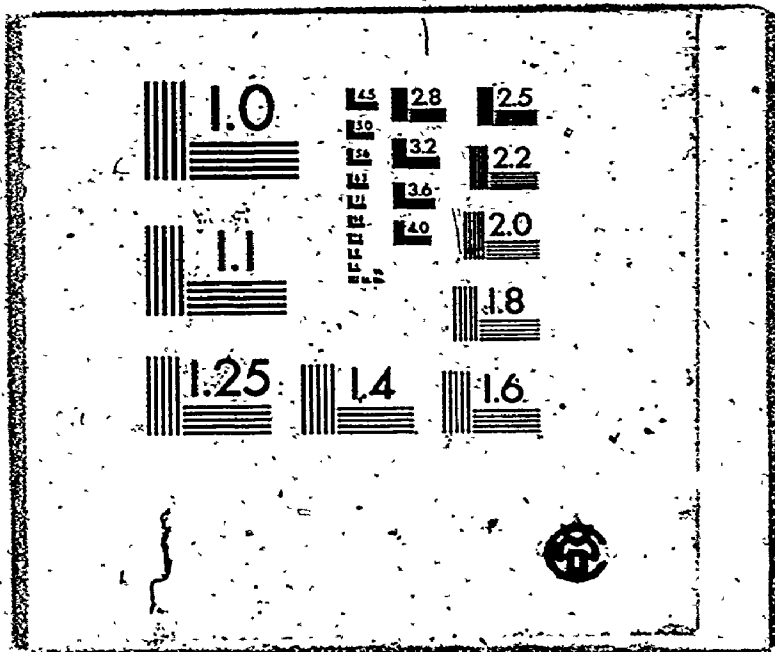
Hrycyshyn, A.W., Anderson, W.A. and B.A. Flumerfelt (1981). The topography of the lateral reticulo-cerebellar projection in the rat. A horseradish peroxidase study. *J. Comp. Neurol.* (Submitted).

Abstracts:

Anderson, W.A. and B.A. Flumerfelt (1978). An ultrastructural study of the inferior olivary nucleus and cerebellar cortex of the rat following 3-acetylpyridine administration. *Canadian Federation of Biological Societies* 21: 153.

Hrycyshyn, A.W., Anderson, W.A. and B.A. Flumerfelt (1981). The lateral reticulo-cerebellar projections in the rat: A horseradish peroxidase study. *Anatomical Record.* 199: 120A.

# 4



THE EFFECTS OF DEAFFERENTATION OF  
THE CEREBELLAR CORTEX IN THE RAT

APPENDICES

VOLUME II

by  
William Athen Anderson

Department of Anatomy

Submitted in partial fulfillment  
of the requirements for the degree of  
Doctor of Philosophy

Faculty of Graduate Studies  
The University of Western Ontario  
London, Ontario  
December, 1981

© William Athen Anderson 1981.



TABLE OF CONTENTS

	Page
TABLE OF CONTENTS . . . . .	xxviii
FIGURES . . . . .	264
TABLES . . . . .	412
APPENDICES . . . . .	428

FIGURES

## ABBREVIATIONS

APF	ansoparamedian fissure
CT	central tegmental nucleus
CUL	lateral cuneate nucleus
DAO	dorsal accessory olive
DCT	decussation of the trapezoid body
FLM	medial longitudinal fasciculus
FP	pontine fibers
GR	gracilis nucleus
ICS	intercrural sulcus
IPN	interpeduncular nucleus
LC	locus ceruleus
LL <sub>v</sub>	ventral nucleus of the lateral lemniscus
LM	medial lemniscus
LRN	lateral reticular nucleus
LRNst	subtrigeminal portion of the lateral reticular nucleus
MAO	medial accessory olive
NCD	dorsal cochlear nucleus
NCS	superior central nucleus
ND	dentate nucleus
NF	fastigial nucleus
NI	interpositus nucleus
NIA	anterior part of the interpositus nucleus
NIP	posterior part of the interpositus nucleus
NMT	nucleus of the mesencephalic tract of the trigeminal nerve
NPD	dorsal parabranchial nucleus
NPH	prepositus nucleus
NRTP	reticulo-tegmental pontine nucleus
NST	sensory nucleus of the trigeminal nerve
NTD	dorsal tegmental nucleus
NIM	motor nucleus of the trigeminal nerve
NTST	nucleus of the spinal tract of the trigeminal nerve
NTSTd	dorsal part of the nucleus of the spinal tract of the trigeminal nerve

NTST(i) interpolaris part of the nucleus of the spinal tract of the trigeminal nerve

NTST(o) oralis part of the nucleus of the spinal tract of the trigeminal nerve

NTST<sub>v</sub> ventral part of the nucleus of the spinal tract of the trigeminal nerve

NTZ nucleus of the trapezoid body

NVL lateral vestibular nucleus

NVM medial vestibular nucleus

NVS superior vestibular nucleus

NVSP spinal vestibular nucleus

NV trigeminal nerve

NVII facial nerve

nAMB ambiguous nucleus

nIII nucleus of the oculomotor nerve

nIV nucleus of the trochlear nerve

nVII nucleus of the facial nerve

nX nucleus of the vagus nerve

nXII nucleus of the hypoglossal nerve

P pons

PC cerebral peduncle

PCI inferior cerebellar peduncle

PCM middle cerebellar peduncle

PCS superior cerebellar peduncle

PO principal olive

PSF posterior superior fissure

RFL reticular formation

RGI lateral gigantocellular nucleus

RPC caudal pontine nucleus

SOC superior olivary complex

SOL solitary nucleus

TCS corticospinal tract

TST spinal tract of the trigeminal nerve

FIGURE 1

Photomicrographs of an HRP injection within the lateral cerebellar hemisphere and retrogradely labeled fibers within the corpus medullaris.

- a. A typical HRP injection site within the ansiform lobule of the cerebellum. Benzidine dihydrochloride. (CM - corpus medullaris). X 19.
- b. A low power view of retrogradely labeled axons within the corpus medullaris (CM) of the cerebellum following an HRP injection into the ansiform lobule. 48 h post operative (p.o.). Benzidine dihydrochloride. Dark field illumination. X 54.
- c. A high power view of the retrogradely labeled axons shown in Fig. 1-b. Note the large number of retrogradely labeled fibers found within the corpus medullaris within 48 h of the HRP injection. Benzidine dihydrochloride. Dark field illumination. X 112.

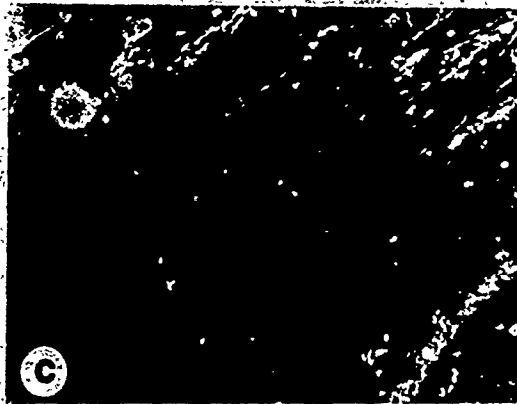
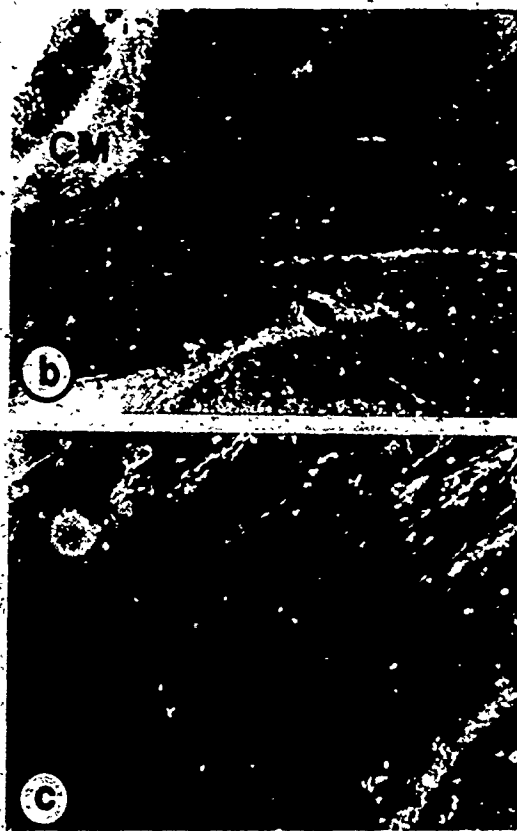
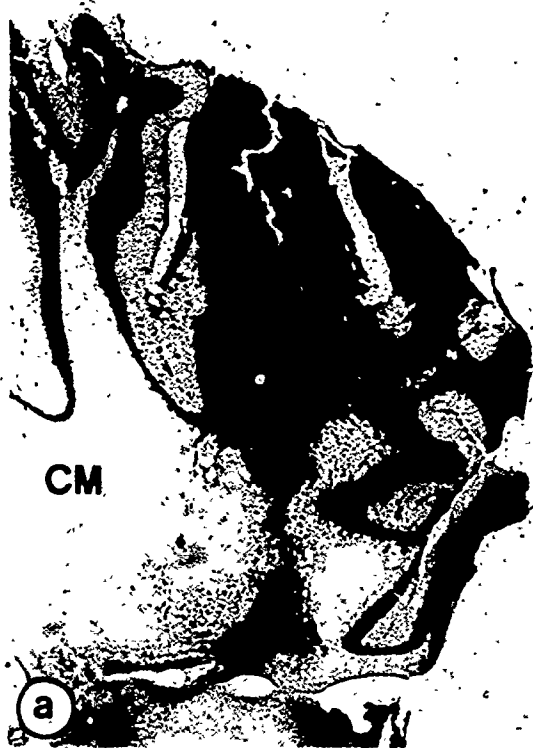


FIGURE 2

A diagrammatic representation (top) of the maximum extent of HRP diffusion (hatched area) following an injection of the ansiform lobule (C8AR). On the left, the surface view (dorsal) of the cerebellar cortex shows the rostrocaudal and mediolateral boundaries of the HRP injection site while on the right a diagram of a parasagittal section reveals its dorsoventral extent. The vertical dashed line on the left indicates the approximate level of the cerebellar diagram on the right.

The lower portion of this figure shows the resulting distribution of retrogradely labeled somata within the rostralmost portion of the hindbrain (sections through the pons). HRP-labeled cells are indicated with dots on a series of standardized transverse sections. While each dot represents more than a single retrogradely labeled soma, the appropriate proportions of labeled cells were carefully maintained during mapping. (See text for details). (A-F indicate levels through the pons):

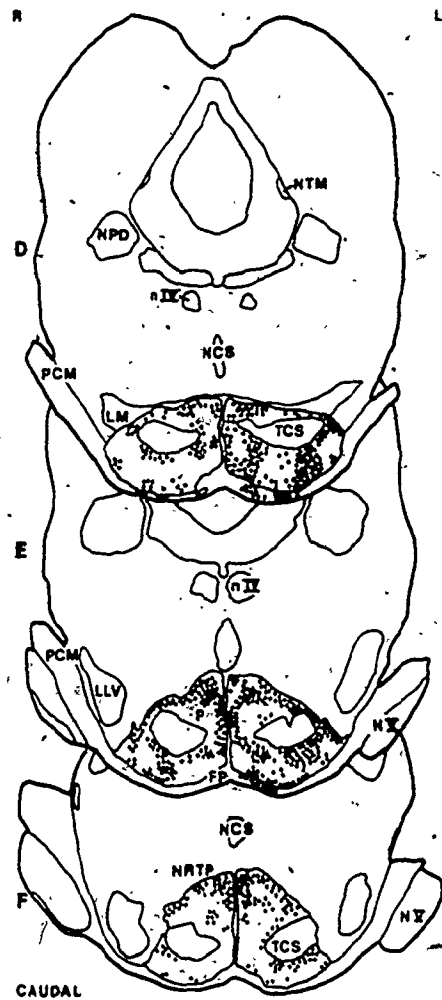
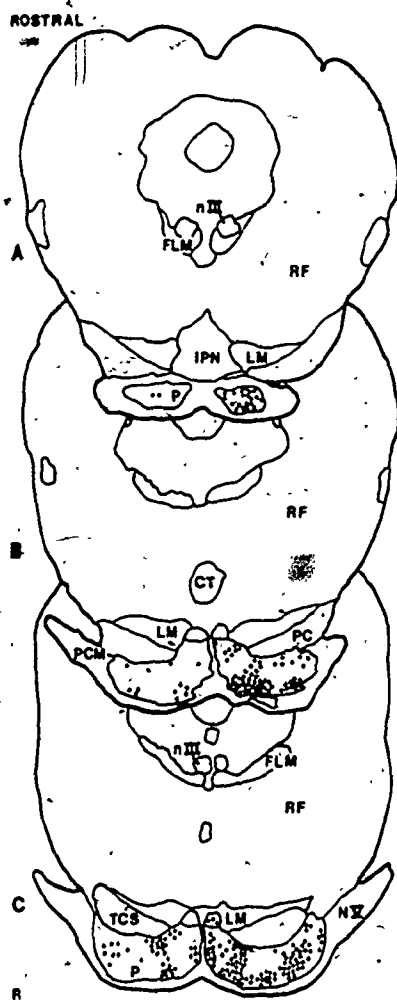
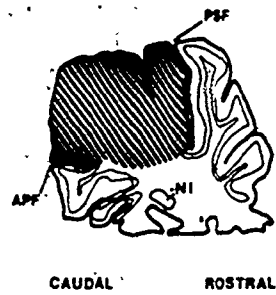
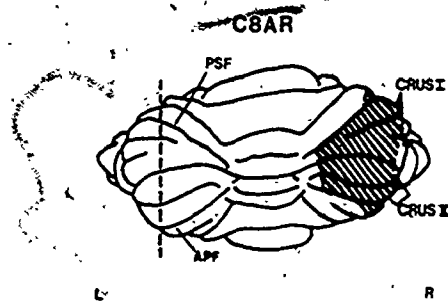




FIGURE 3

Typical HRP-labeled cells in the basilar pontine gray, the inferior olivary complex and the lateral reticular nucleus following cerebellar injections.

- a,d,g. Low power views of heavily labeled neurons within (a) the contralateral basilar pontine gray (BPG) and the nucleus reticularis tegmenti pontis (NRTP); (d) the contralateral inferior olivary complex (IOC) and (g) the ipsilateral lateral reticular nucleus (LRN). Benzidine dihydrochloride. X 45.
- b. High magnification of the area indicated at A in 3 a. Note that both large and small cells are retrogradely labeled. Benzidine dihydrochloride. X 160.
- c. High magnification of the area indicated at B in 3 a. Notice that the dendrites of many of these pontine neurons are retrogradely filled with HRP. Diaminobenzidine. Dark field illumination. X 67.
- e,f. High magnifications of HRP labeled cells within the ventral lamella of the principal olive (PO<sub>v</sub>) and the ventrolateral aspect of the medial accessory olive (MAO) respectively. Benzidine dihydrochloride. Light field (e) and dark field (f) illumination. X 160.
- h,i. High magnifications of HRP labeled cells within the dorsolateral aspect of the subtrigeminal portion of the ipsilateral lateral reticular nucleus (LRNst). Benzidine dihydrochloride (h) and diaminobenzidine (i). Light field (h) and dark field (i) illumination. X 56.

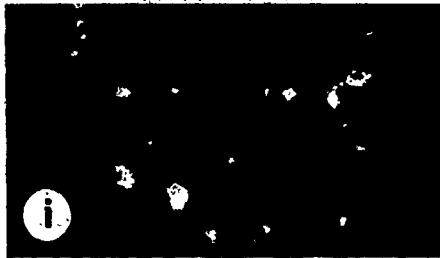
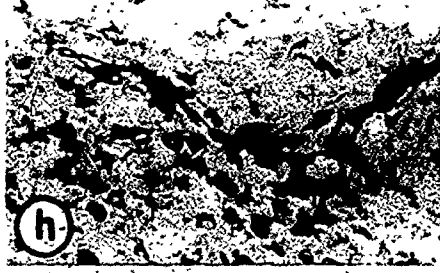
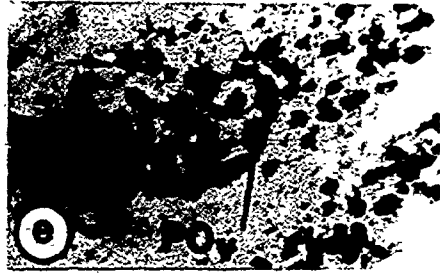
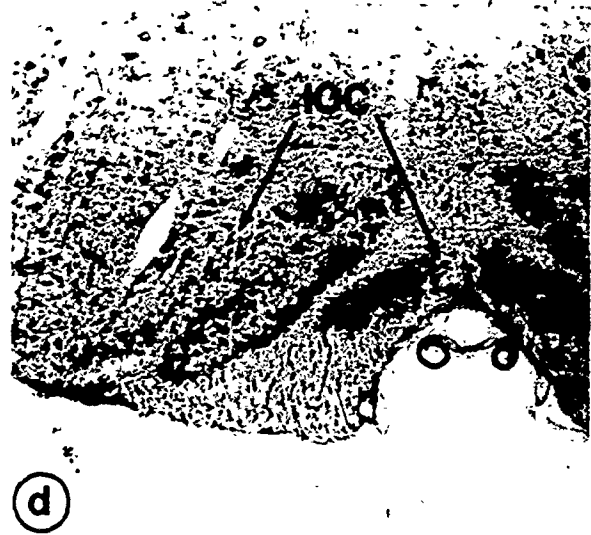
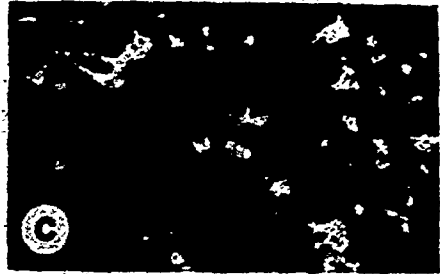
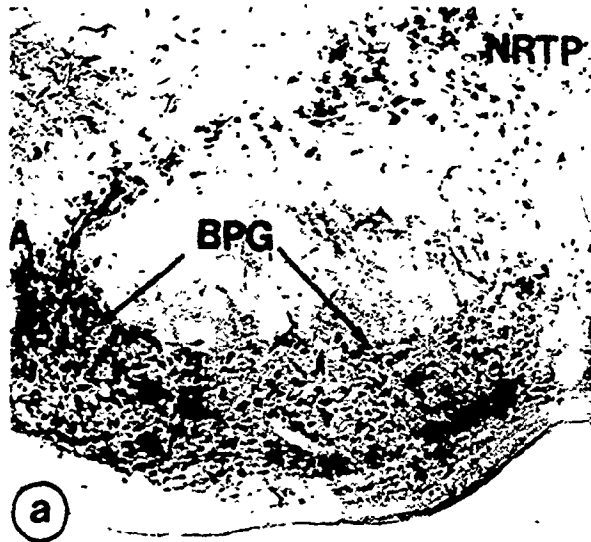


FIGURE 4

A diagrammatic representation (top) of the maximum extent of HRP diffusion (hatched area) following an injection of lobulus simplex (C6AR). On the left, the surface view (dorsal) of the cerebellar cortex shows the rostrocaudal and mediolateral boundaries of the HRP injection site while on the right a diagram of a parasagittal section reveals its dorsoventral extent. The vertical dashed line on the left indicates the approximate level of the cerebellar diagram on the right.

The lower portion of this figure shows the distribution of retrogradely labeled somata within the rostralmost portion of the hindbrain (sections through the pons). HRP-labeled cells are indicated with dots on a series of standardized transverse sections. (See text for details.) (A-F indicate levels through the pons.)

C6AR

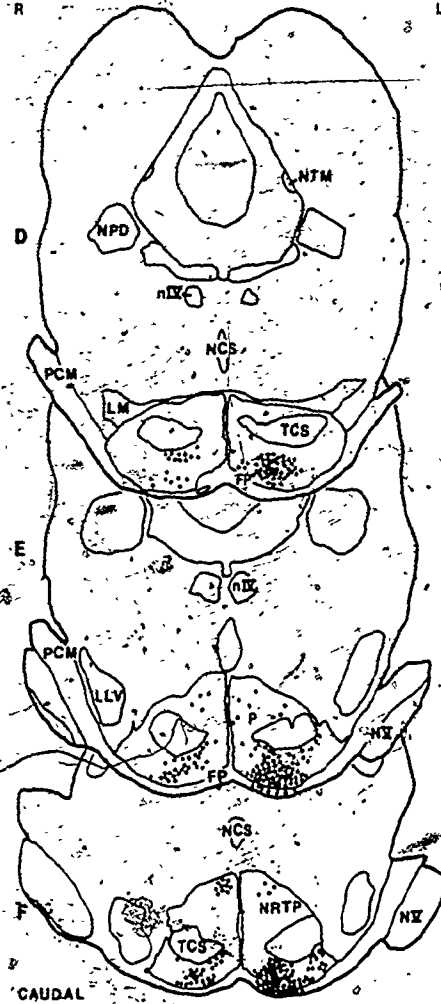
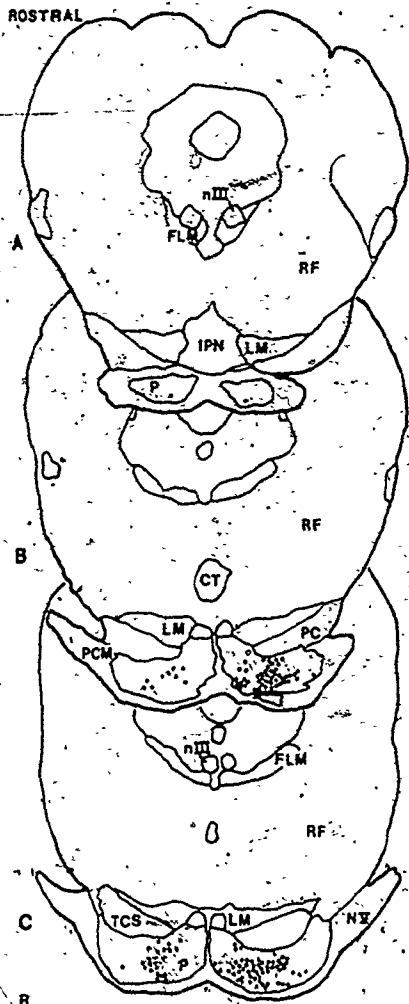
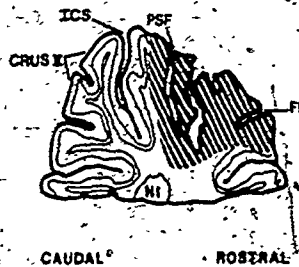
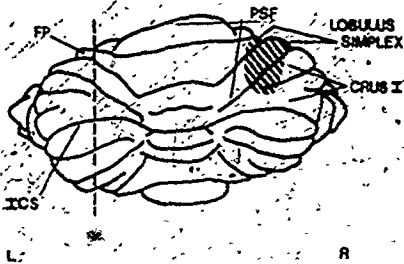


FIGURE 5.

A diagrammatic representation (top) of the maximum extent of HRP diffusion (hatched area) following an injection of Crus I and the medial portion of Crus II (C2AR). On the left, the surface view (dorsal) of the cerebellar cortex shows the rostrocaudal and mediolateral limit of the HRP injection site while on the right a diagram of a coronal section reveals its dorsoventral extent. The central black area represents the region of intense HRP staining while the stippling corresponds to the less intensely stained peripheral portion. The horizontal dashed line on the left indicates the approximate level of the cerebellar diagram on the right.

The lower portion of this figure shows the subsequent distribution of retrogradely labeled somata within the rostralmost portion of the hindbrain (sections through the pons). HRP-labeled cells are indicated with dots on a series of standardized transverse sections. (See text for details.) (A-F indicate levels through the pons.)

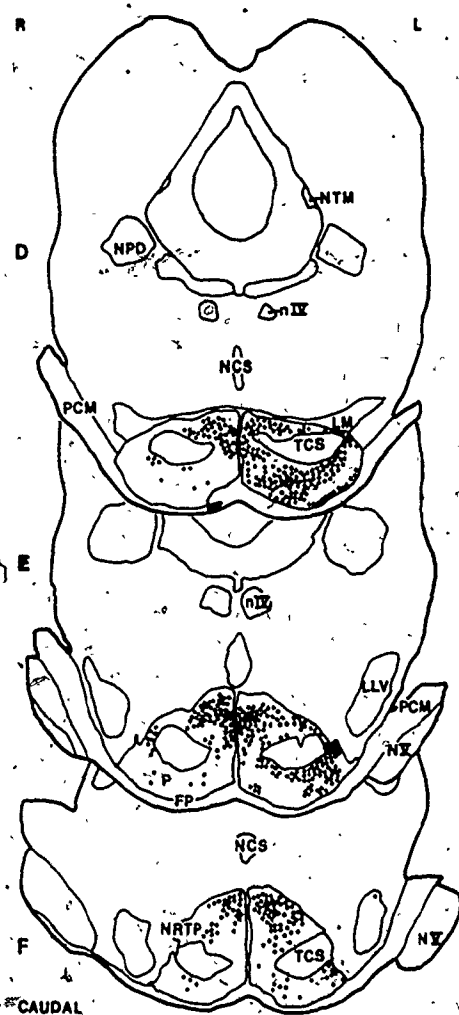
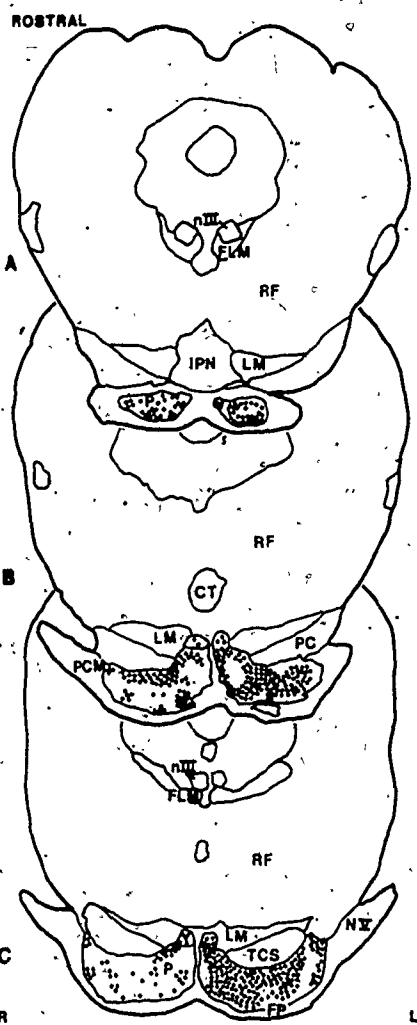
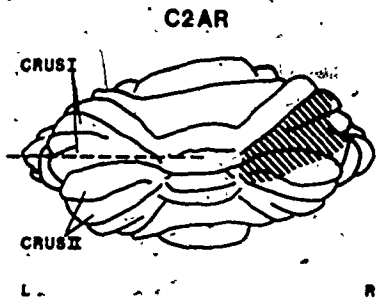


FIGURE 6

A diagrammatic representation (top) of the maximum extent of HRP diffusion (hatched area) following an injection of Crus I and the lateral portion of Crus II (C9AR). On the left, the surface view (dorsal) of the cerebellar cortex shows the rostrocaudal and mediolateral boundaries of the HRP injection site while on the right a diagram of a parasagittal section reveals its dorsoventral extent. The vertical dashed line on the left indicates the approximate level of the cerebellar diagram on the right.

The lower portion of this figure shows the resulting distribution of retrogradely labeled somata within the rostralmost portion of the hindbrain (sections through the pons). HRP-labeled cells are indicated with dots on a series of standardized transverse sections. (See text for details.) (A-F indicate levels through the pons.)

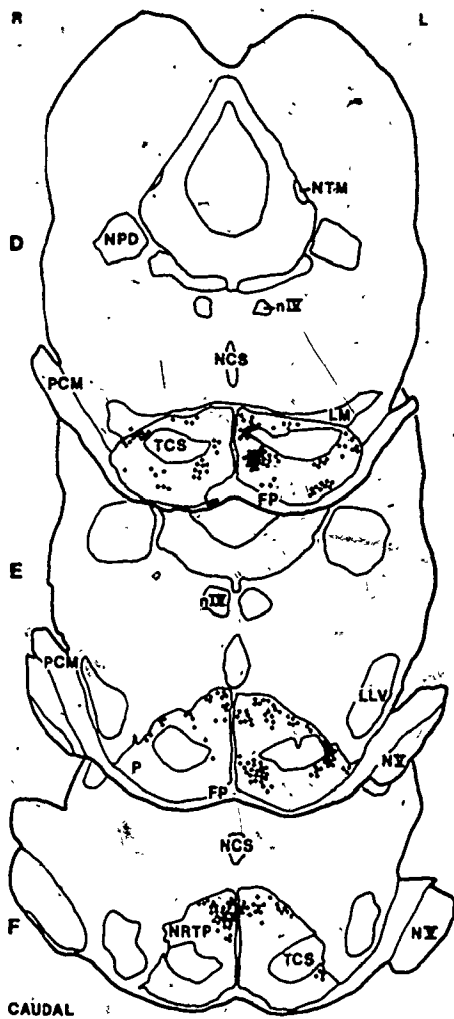
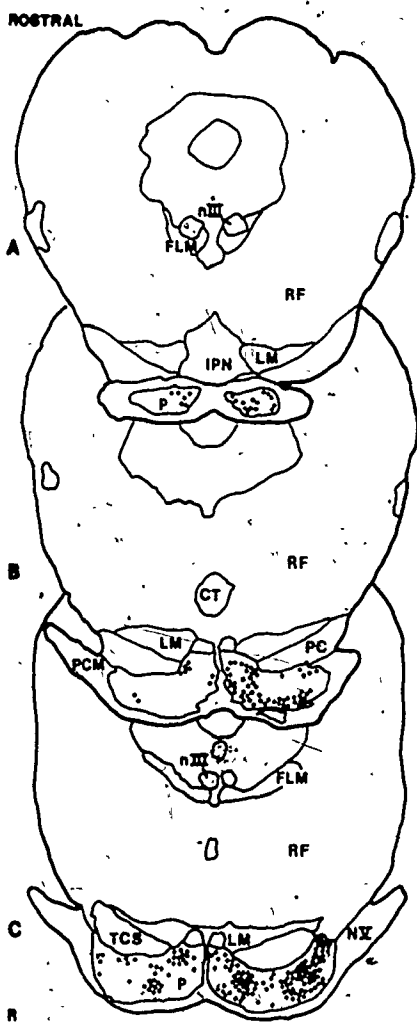
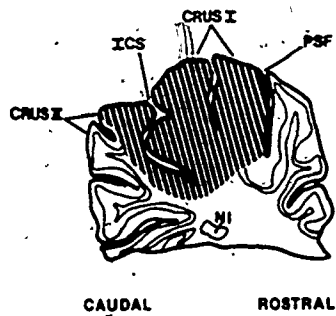
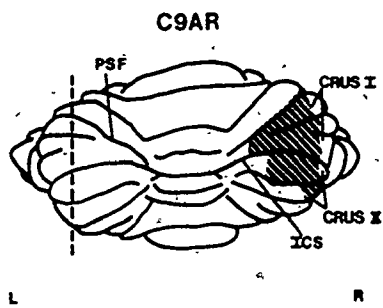




FIGURE 7

A diagrammatic representation of the distribution of retrogradely labeled somata within the caudal portion of the medulla oblongata following an HRP injection of the ansiform lobule (C8AR). HRP-labeled cells are indicated with dots on a series of standardized transverse sections. (See text for details.) (A-H indicate levels through the inferior olivary complex.)

C8AR

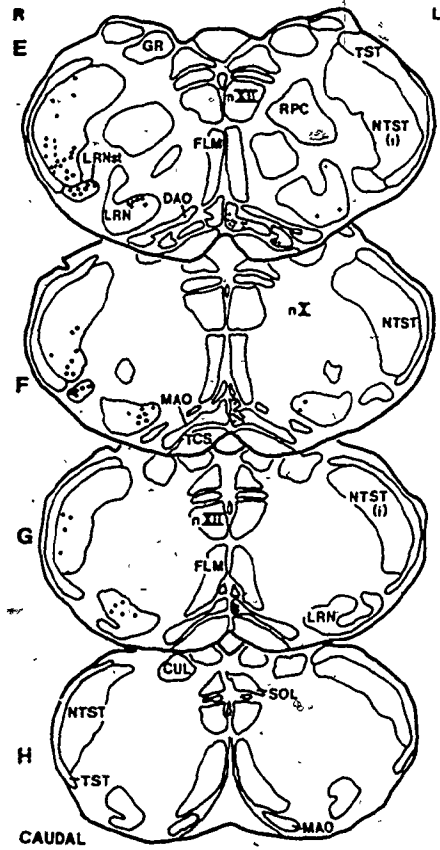
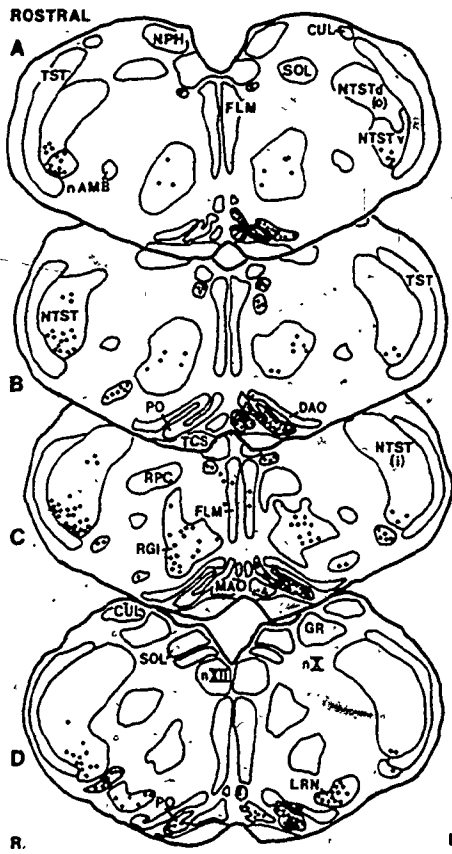


FIGURE 8

A diagrammatic representation of the distribution of retrogradely labeled somata within the caudal portion of the medulla oblongata following an HRP injection of lobulus simplex (C6AR). HRP-labeled cells are indicated with dots on a series of standardized transverse sections. (See text for details.) (A-I indicate levels through the inferior olivary complex.)

C6AR

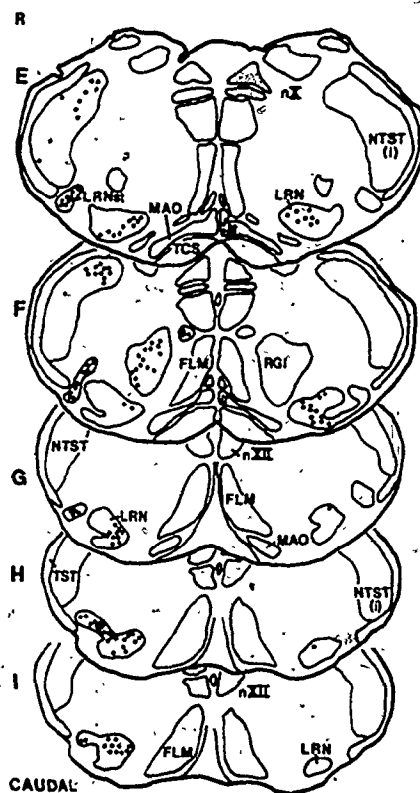
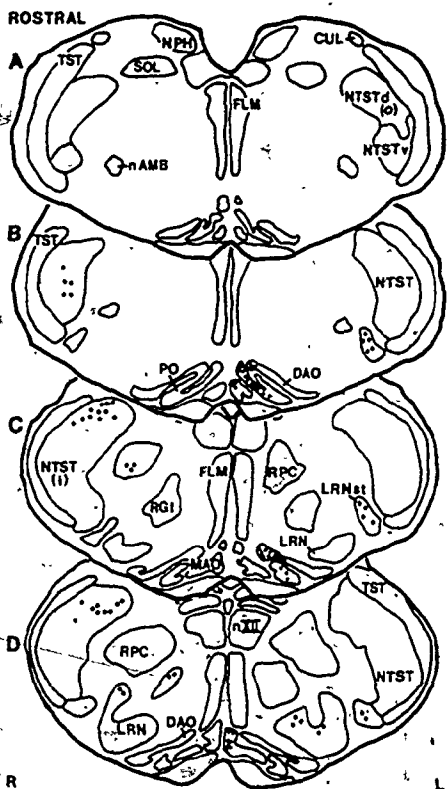


FIGURE 9

A diagrammatic representation of the distribution of retrogradely labeled somata within the caudal portion of the medulla oblongata following an HRP injection of Crus I and the medial portion of Crus II (G2AR). HRP-labeled cells are indicated with dots on a series of standardized transverse sections. (See text for details.) (A-I indicate levels through the inferior olivary complex.)

C2AR

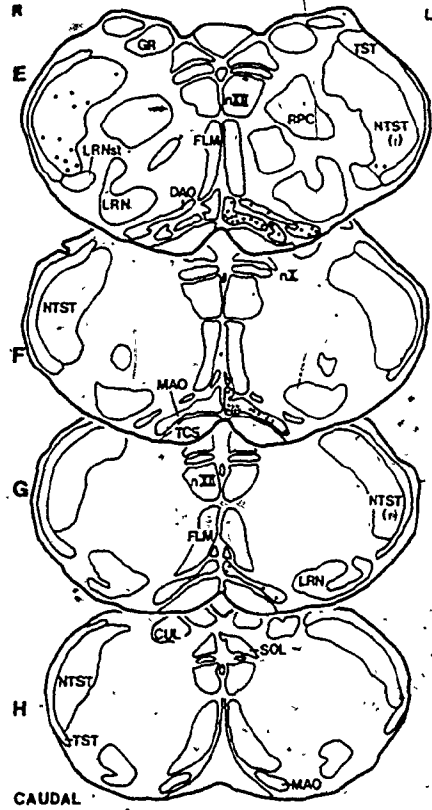
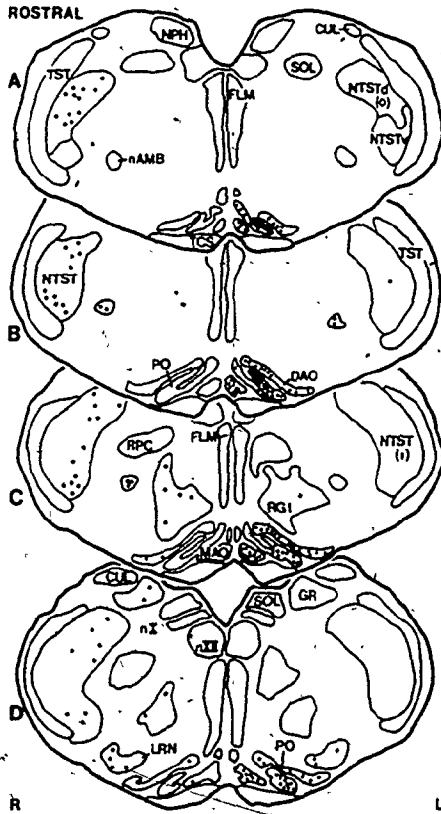
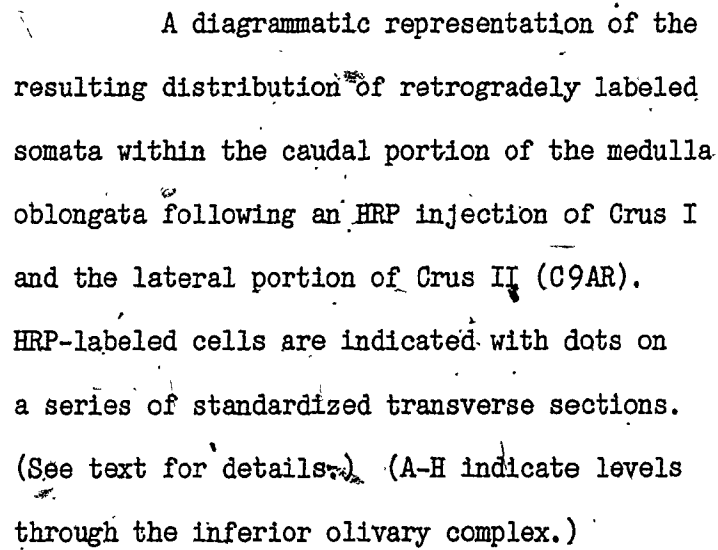


FIGURE 10

A diagrammatic representation of the resulting distribution of retrogradely labeled somata within the caudal portion of the medulla oblongata following an HRP injection of Crus I and the lateral portion of Crus II (C9AR). HRP-labeled cells are indicated with dots on a series of standardized transverse sections. (See text for details.) (A-H indicate levels through the inferior olivary complex.)



C9AR

ROSTRAL

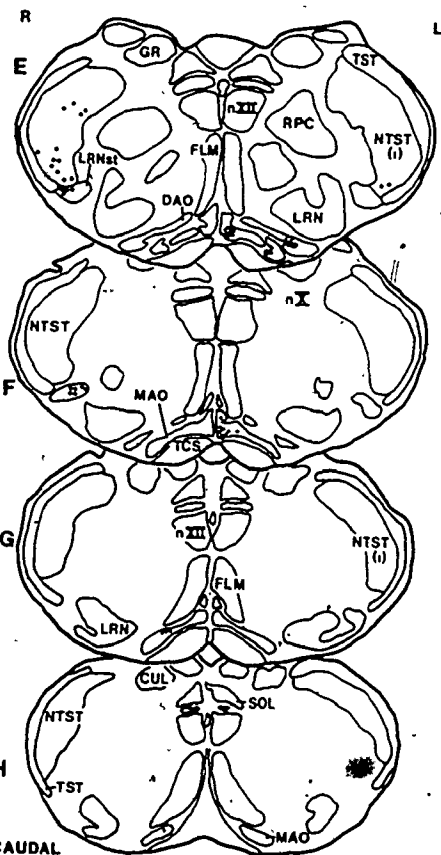
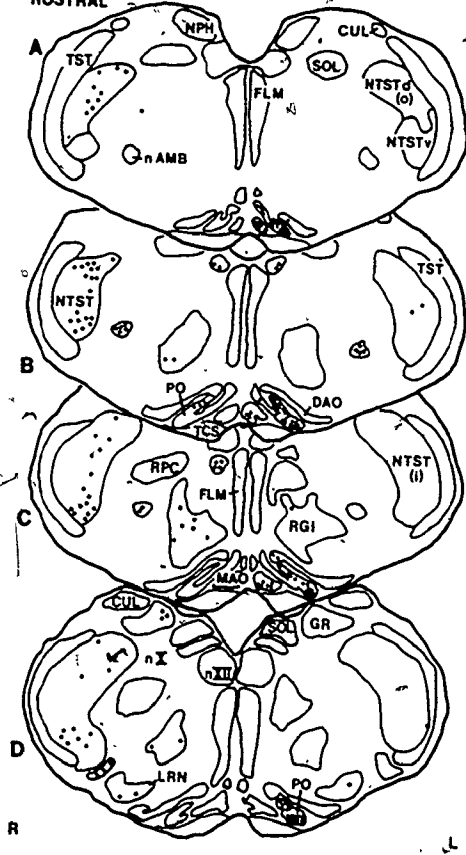




FIGURE 11

A diagrammatic representation of the distribution of retrogradely labeled somata within the rostral portion of the medulla oblongata following an HRP injection of Crus I and the lateral portion of Crus II (C9AR). HRP-labeled cells are indicated with dots on a series of standardized transverse sections. (See text for details.) (A-F indicate levels through the rostral portion of the medulla oblongata.)

C9AR

ROSTRAL

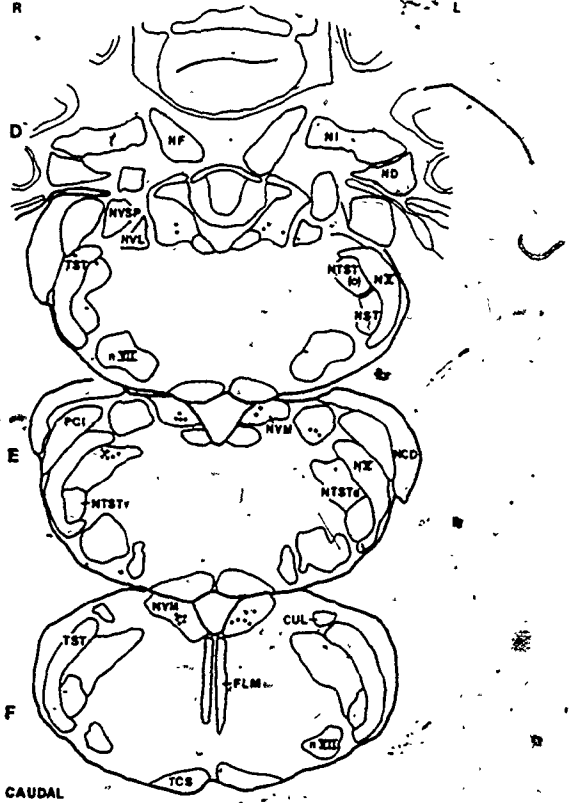
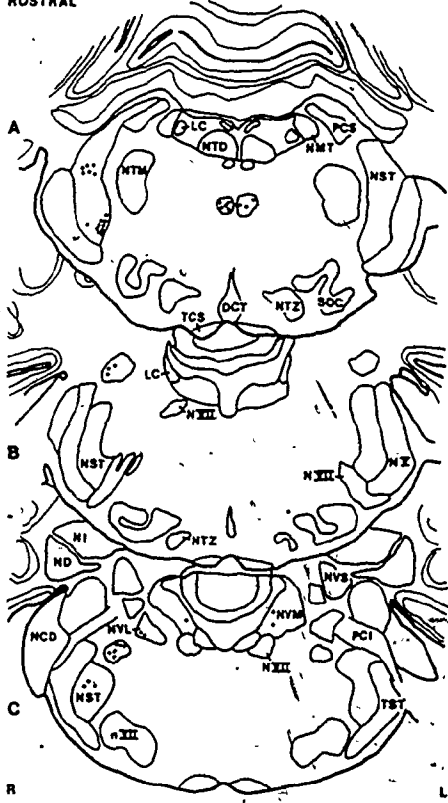


FIGURE 12

Typical HRP-labeled cells in the spinal nucleus of the trigeminal nerve, the medial vestibular nucleus, the nucleus reticularis gigantocellularis and the locus ceruleus following cerebellar injections.

- a, d, g, j. Low power views of heavily labeled cells within (a) the ipsilateral spinal nucleus of the trigeminal nerve (NTST); (b) the medial vestibular nuclei (MVN); (c) the ipsilateral nucleus reticularis gigantocellularis lateralis (RGI) and (d) the contralateral locus ceruleus (LC). Benzidine dihydrochloride.  
a: X 45, d: X 64, g: X 35, j: X 240.
- b, c. High magnifications of HRP-labeled cells within the ventrolateral aspect of the spinal nucleus of the trigeminal nerve. Benzidine dihydrochloride (b) and diaminobenzidine (c). Light field (b) and dark field (c) illumination. X 51.
- e, f. High magnification of HRP-labeled cells within the ipsilateral medial vestibular nucleus. Benzidine dihydrochloride (e) and diaminobenzidine (f). Light field (e) and dark field (f) illumination. X 167.
- h, i. High magnifications of HRP-labeled cells within the ipsilateral nucleus reticularis gigantocellularis lateralis. Benzidine dihydrochloride (h) and diaminobenzidine (i). Light field (h) and dark field (i) illumination. h: X 131, i: X 170.
- k, l. High magnifications of HRP-labeled cells within the contralateral nucleus locus ceruleus. Benzidine dihydrochloride and diaminobenzidine (l). Light field (k) and dark field (l) illumination. k: X 400, l: X 176.

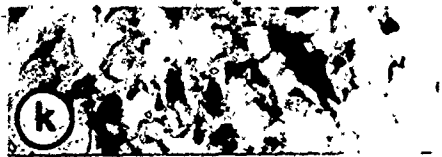
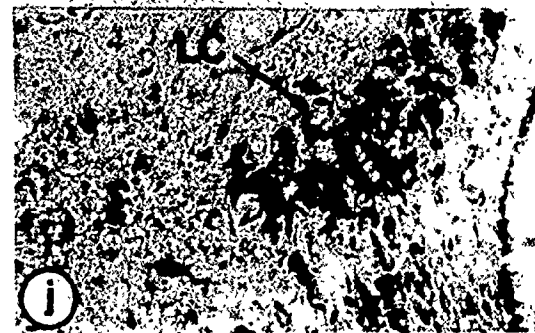
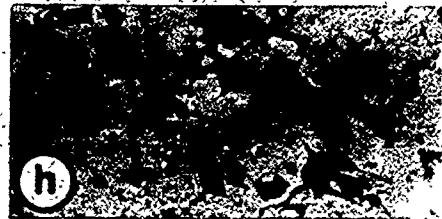
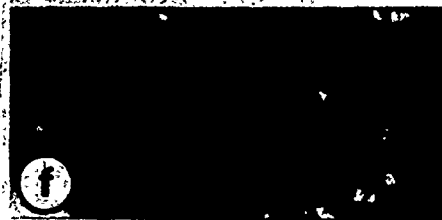
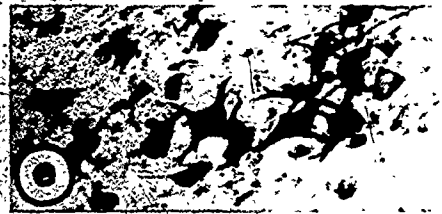
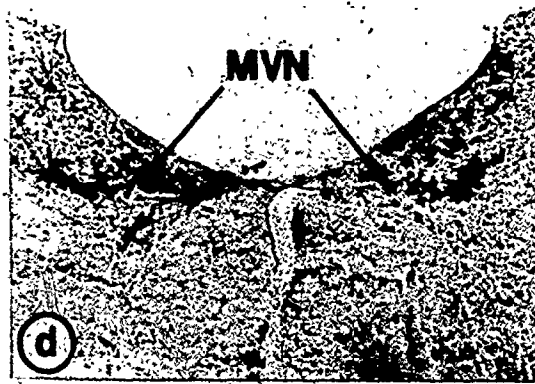
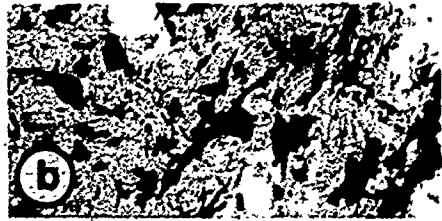


FIGURE 13

A diagrammatic representation of the distribution of retrogradely labeled somata within the rostral portion of the medulla oblongata following an HRP injection of the ansiform lobule (Q8AR). HRP-labeled cells are indicated with dots on a series of standardized transverse sections. (See text for details.) (A-F indicate levels through the rostral portion of the medulla oblongata.)

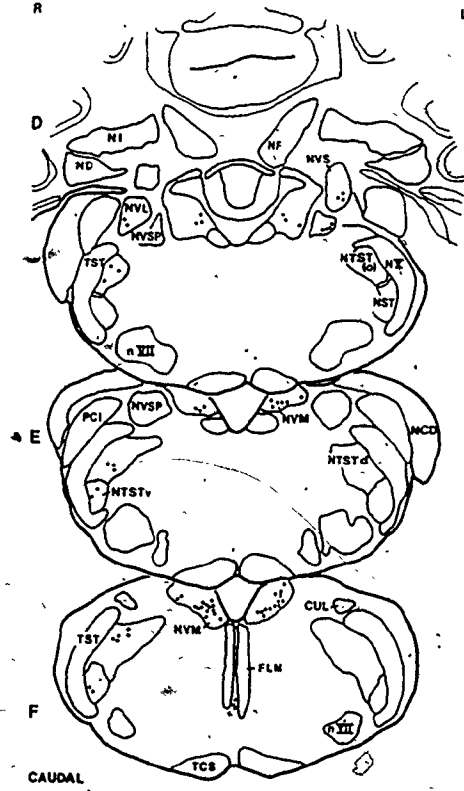
C8AR

ROSTRAL



R

L



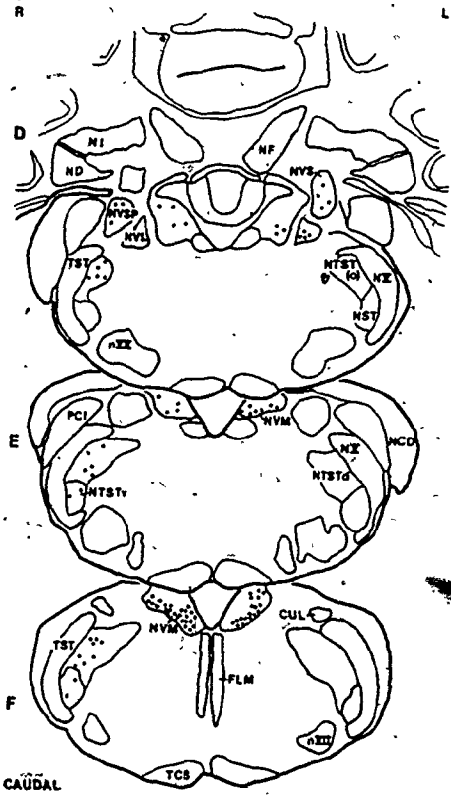
CAUDAL

FIGURE 14

A diagrammatic representation of the distribution of retrogradely labeled somata within the rostral portion of the medulla oblongata following an HRP injection of Crus I and the medial portion of Crus II (C2AR). HRP-labeled cells are indicated with dots on a series of standardized transverse sections. (See text for details.) (A-F indicate levels through the rostral portion of the medulla oblongata.)

C2AR

ROSTRAL



CAUDAL



FIGURE 15

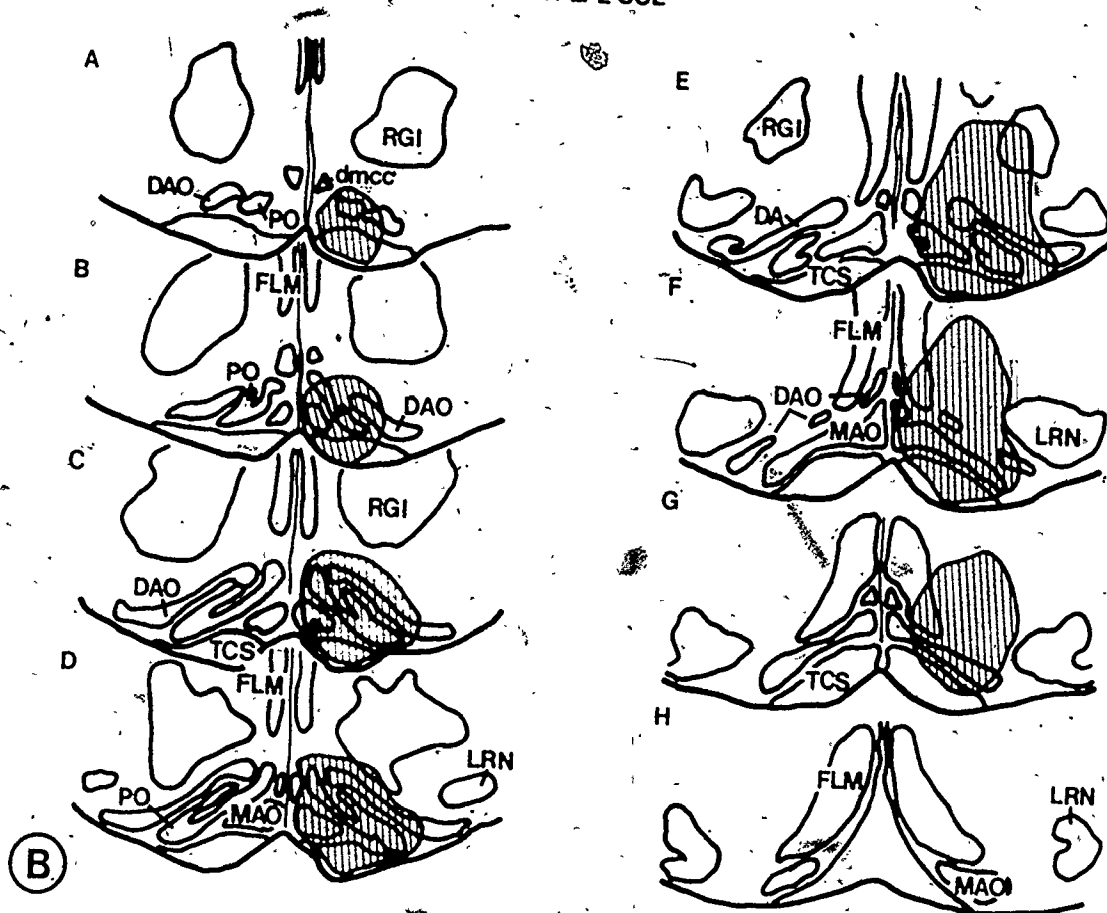
A photomicrograph (A) and a series of line drawings (B) representing transverse sections through the rostrocaudal extent of a lesion within the inferior olivary nucleus of an adult rat. (DAO - dorsal accessory olive; dmcc - dorsomedial cell column; FIM - medial longitudinal fasciculus; LRN - lateral reticular nucleus; MAO - medial accessory olive; PO - principal olive; RGI - nucleus reticularis gigantocellularis lateralis; TCS - corticospinal tract).



(A)

LEVEL D

C2AR LPL SOL



(B)

FIGURE 16

Light micrographs of the inferior olivary complex from control and short-term 3AP treated rats following Nissl body staining.

- a. A light micrograph of a paraffin section through the inferior olive of a control rat. The caudal portion of the medial accessory nucleus is shown with its typically small neurons characterized by an intensely basophilic cytoplasm.
- b. A light micrograph of the inferior olive 24 hours following 3AP treatment. Note the complete absence of Nissl staining in the olivary neurons, whereas staining in the glial cells (gl) remains normal.
- c. The inferior olive 7 days following 3AP intoxication. The absence of Nissl staining in the olivary complex suggests a total involvement of all the olivary neurons.
- d. The inferior olive 14 days following 3AP treatment. Note the continued absence of Nissl staining in the cell bodies.

a - d, Thionine; X 74.

a

b

c

d

gl

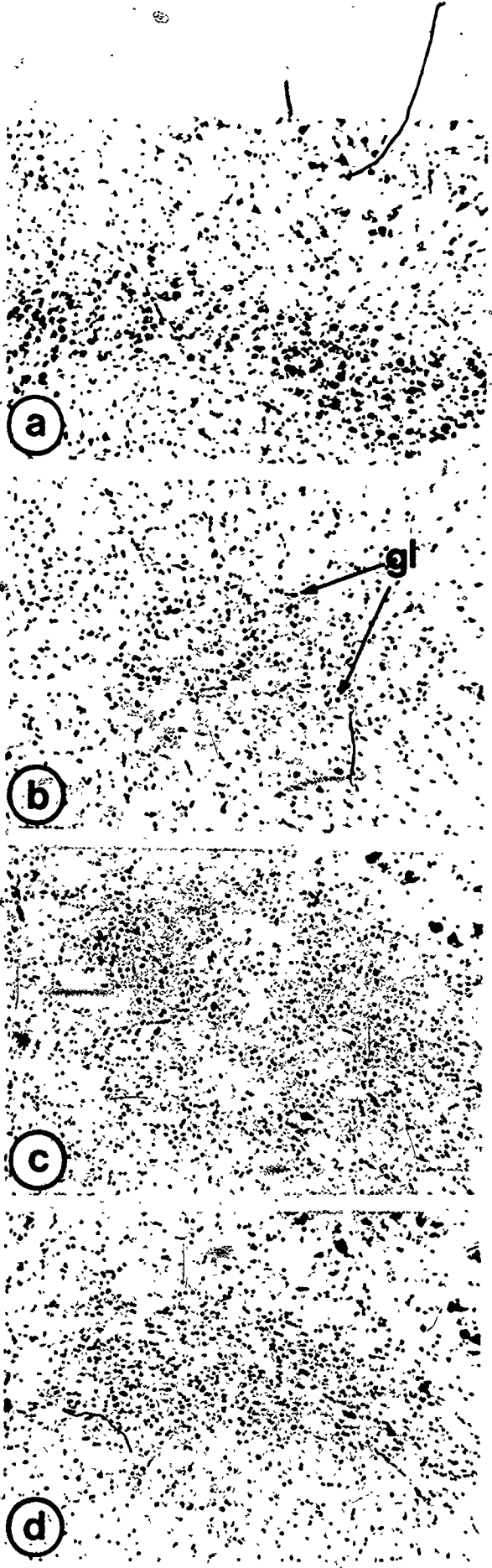




FIGURE 17

Light micrographs of the inferior olivary complex from control and short-term 3AP treated rats following hematoxylin and eosin or silver staining.

- a. A light micrograph of paraffin embedded medulla oblongata taken from a control rat. The caudal portion of the medial accessory nucleus of the inferior olive is shown.
- b. A light micrograph of the inferior olive 24 hours following 3AP treatment. Note the complete loss of basophilia in the nuclei and eosinophilia in the neuronal cytoplasm.
- c. The inferior olive 7 days following 3AP treatment. Note the absence of all neurons in the inferior olivary complex.
- d. The inferior olive taken from an animal perfused 14 days following 3AP treatment. No signs of a return in basophilia or eosinophilia are apparent.

a - d, Hematoxylin and Eosin; X 74.

- e. A light micrograph of a silver-stained paraffin section through the medial accessory nucleus of a control rat. With this method, normal neurons appear lightly stained.
- f. A light micrograph of the inferior olive taken from an animal perfused 24 hours following 3AP treatment. Note that all of the olivary neurons appear markedly argyrophilic (arrows).
- g. The inferior olive 7 days following 3AP treatment. The number of degenerating neuronal fragments is greatly reduced and those that do remain appear less argyrophilic.
- h. The inferior olive 14 days following 3AP treatment. All signs of degenerating neuronal fragments have disappeared, suggesting that they have been phagocytized and cleared by glial activity.

e - h, Modification of the DeOlmos Ingram technique: X 74.

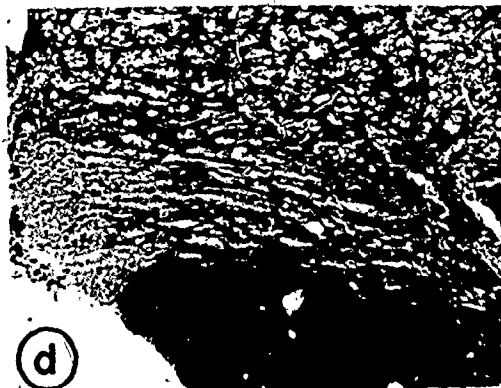
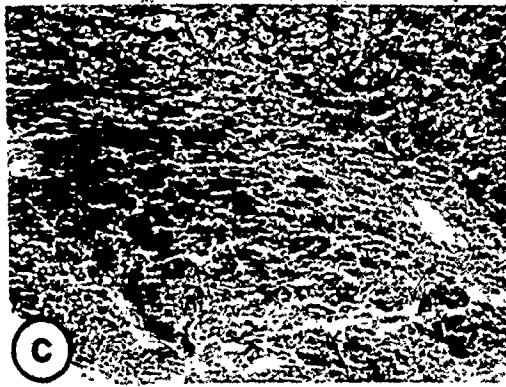


FIGURE 18

Electronmicrographs of a normal and a 3AP treated inferior olivary neuron.

a. An electronmicrograph of a normal inferior olivary neuron. Note the prominent nucleus with its randomly dispersed chromatin and nucleolus. The cytoplasm is marked by numerous Golgi complexes (open block arrows) and aggregations of rough endoplasmic reticulum which form well demarcated Nissl bodies (solid block arrows). X 7,350.

b. An inferior olivary neuron 12 hours following 3AP treatment. Note the presence of numerous astrocytic profiles which surround and infiltrate the degenerating neuron (black arrows). Several glial processes can be found directly adjacent to the fragmenting nuclear membrane. In the adjacent neuropil, several degenerating dendritic profiles can be seen which still show synaptic contacts (open black arrows). X 12,250.

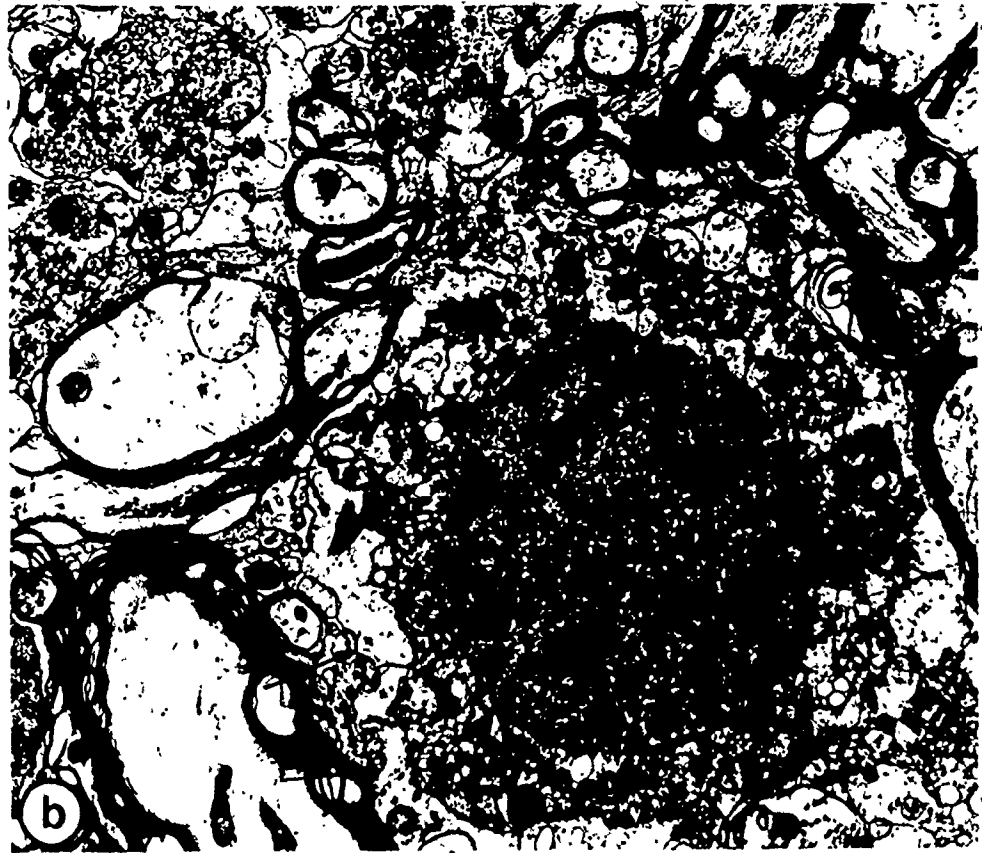
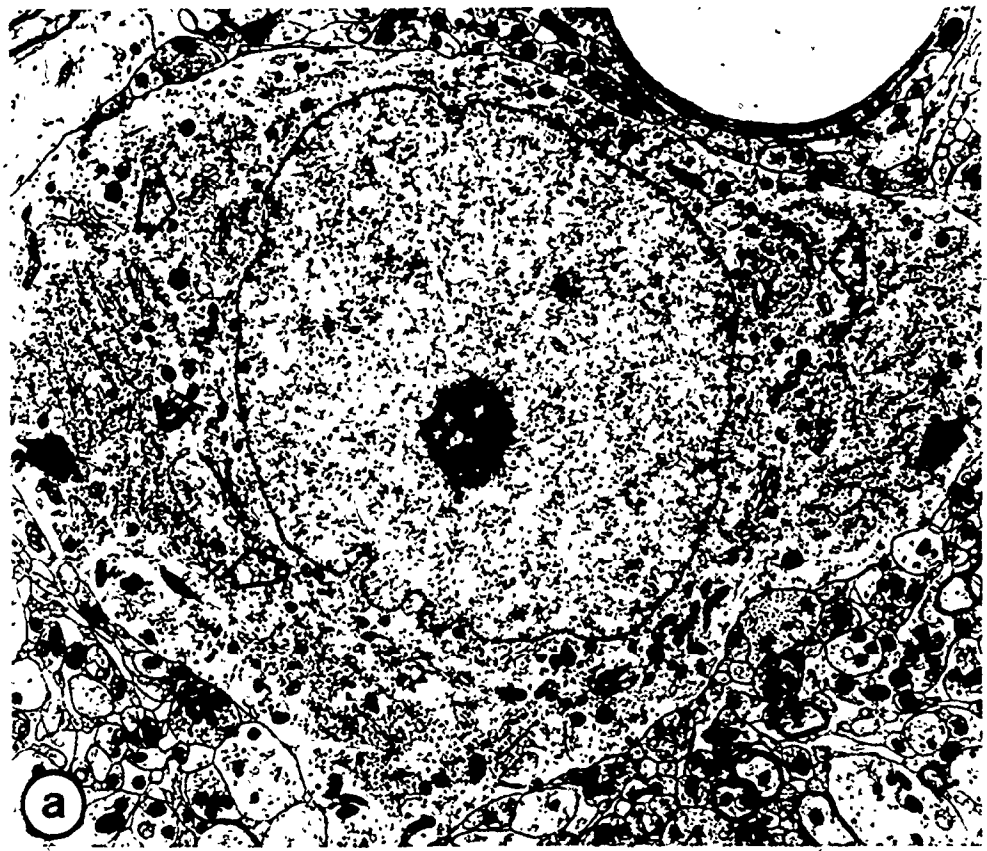




FIGURE 19

Electronmicrographs of the inferior olivary complex at 24 and 60 hours following 3AP treatment.

a. An inferior olivary neuron 24 hours following 3AP treatment. Note the marked shrinkage of both the cytoplasmic and nuclear size. Concurrently, chromatin condensation has produced an irregular pattern of heterochromatin (white arrows). An increase in cytoplasmic fragmentation has resulted from continued astrocytic proliferation (open block arrows).

X 12,250.

b. At 60 hours following 3AP treatment, the cytoplasmic mass of this degenerating neuron is largely fragmented and in most areas is reduced to a thin necrotic rim. Note the large astrocytic profile (As) which contains its characteristic bundle of filaments. At the periphery of the degenerating neuronal mass, microglia-like profiles (Mp) can be found actively engulfing cellular debris (black arrows).

X 12,250.

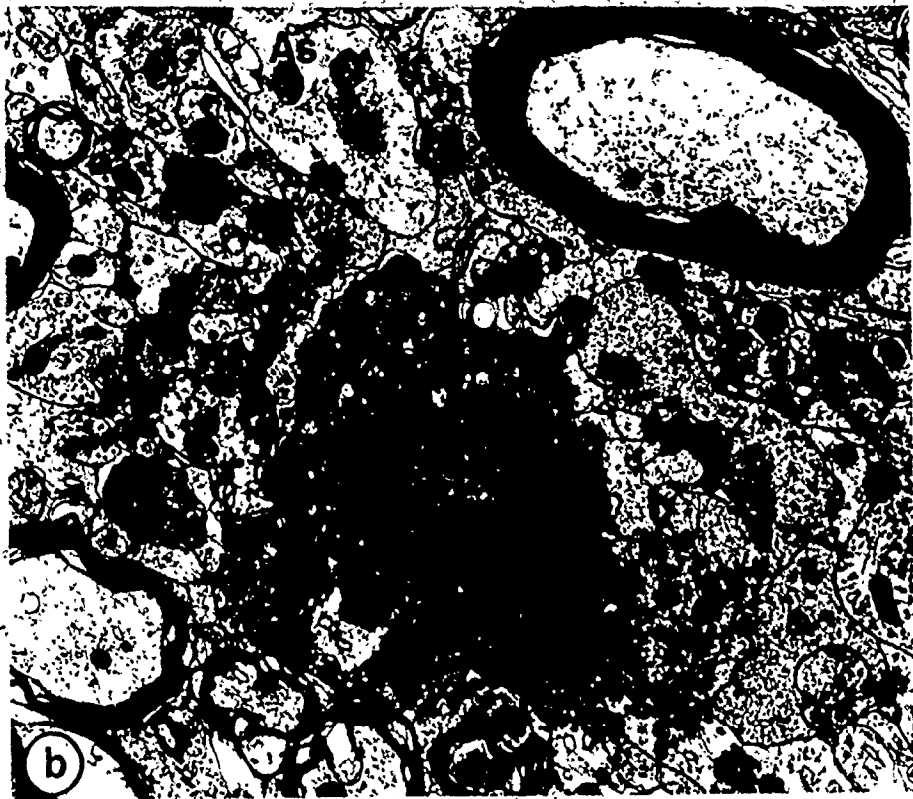
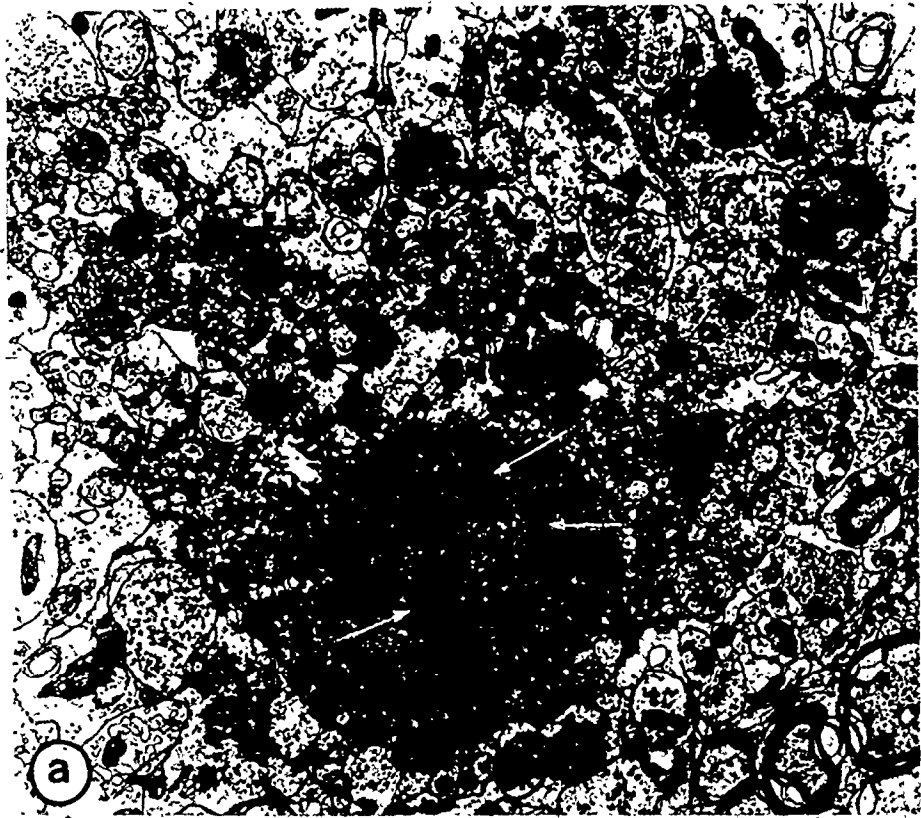


FIGURE 20

An electronmicrograph of a microglia-like cell.

At 60 hours post 3AP treatment, a microglia-like cell (MC) can be found encroaching on a degenerating olivary neuron (ON). Note its long pseudopodial-like process which has insinuated among the degenerative fragments of an olivary neuron (arrows). X 18,750.



U

FIGURE 21

Electronmicrographs of a reactive microglia-like cell and an inferior olivary neuron.

- a. An electronmicrograph of a reactive glial cell which resembles microglia. Note the dense osmiophilic bodies (open block arrows) located throughout its cytoplasm. These lysosomal bodies probably represent the remains of degenerating olivary neurons. In several regions around the periphery of the cell, long pseudopodia (solid block arrows) can be found, suggestive of active phagocytosis. X 12,250.
- b. An inferior olivary neuron 72 hours following 3AP treatment. The pyknotic nucleus is completely surrounded by a thick hypertrophic astrocytic sheet (AS). Note the presence of an adjacent microglia-like cell (MC). X 12,250.

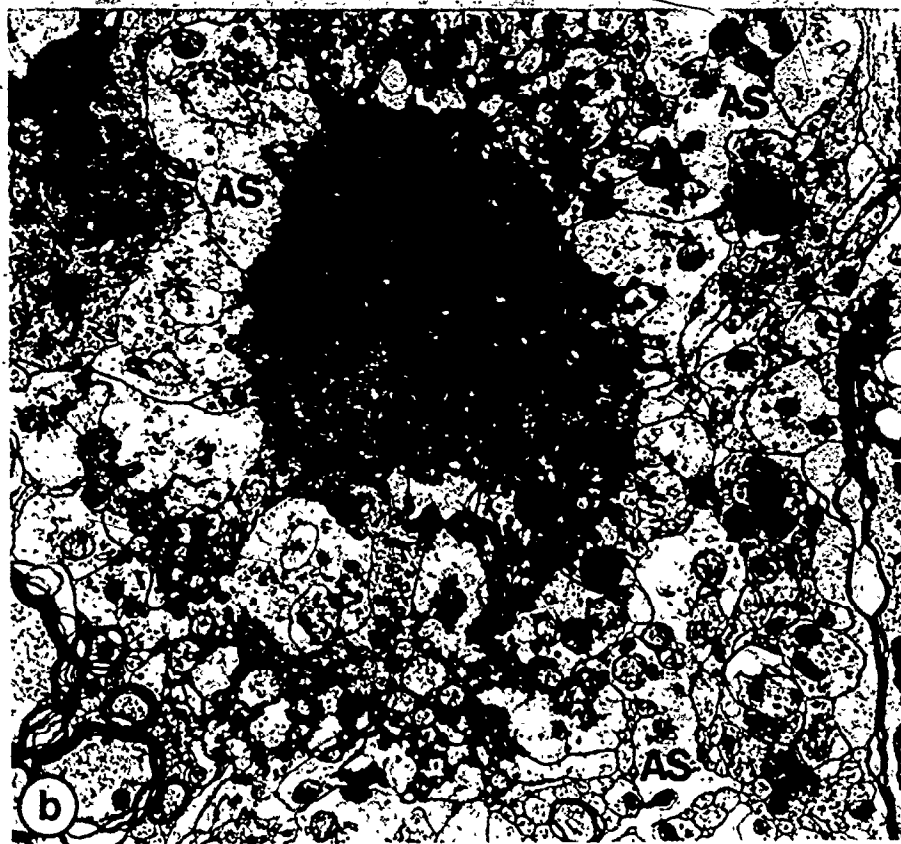
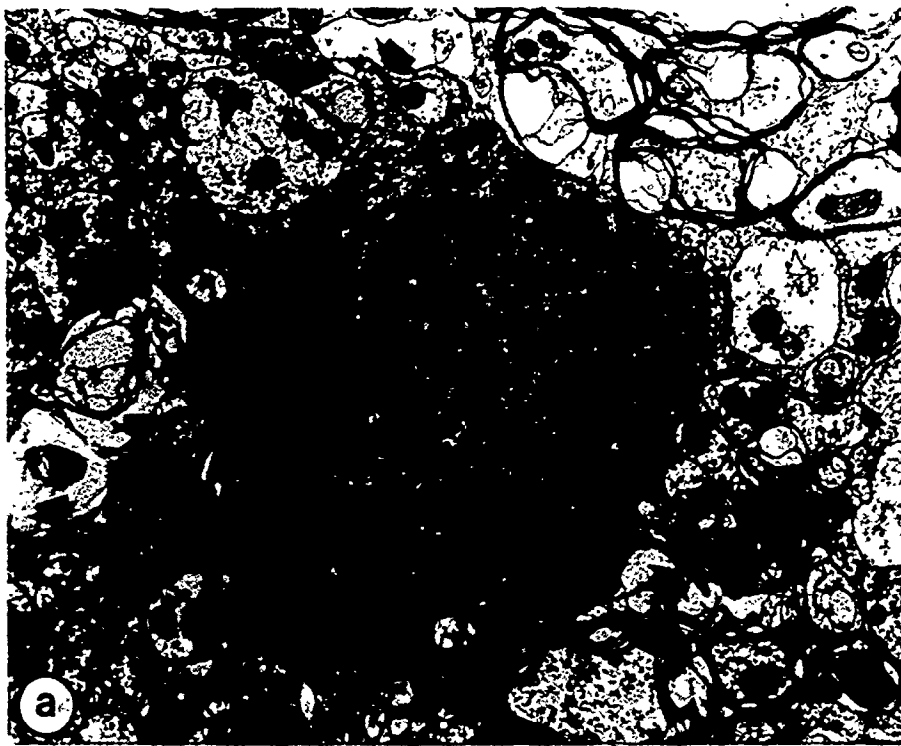


FIGURE 22

Electronmicrographs of inferior olivary neurons.

a,b. Inferior olivary neurons 7 days following 3AP treatment. Note that with the eventual clearing of all cytoplasmic debris the degenerating nuclei are characteristically surrounded by two distinct glial layers. These pyknotic nuclei (Pn) are engulfed by an inner layer of astrocytic processes (As), which in turn are surrounded by a zone of microglial activity (Mp). X 12,250.

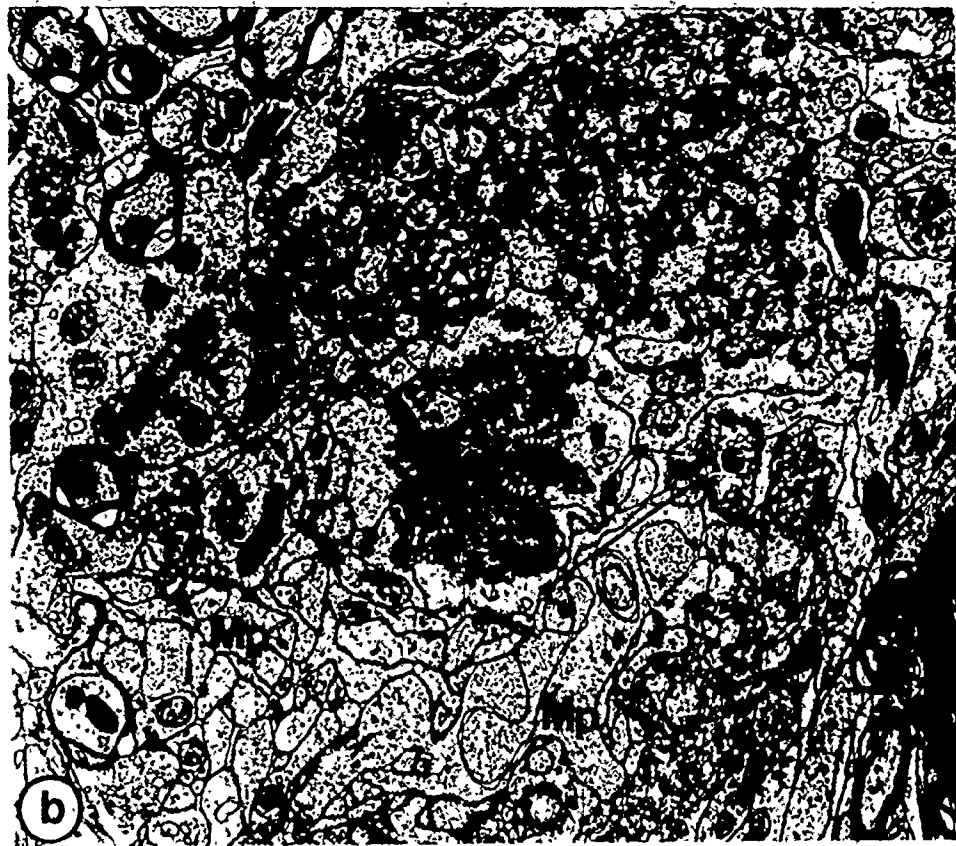
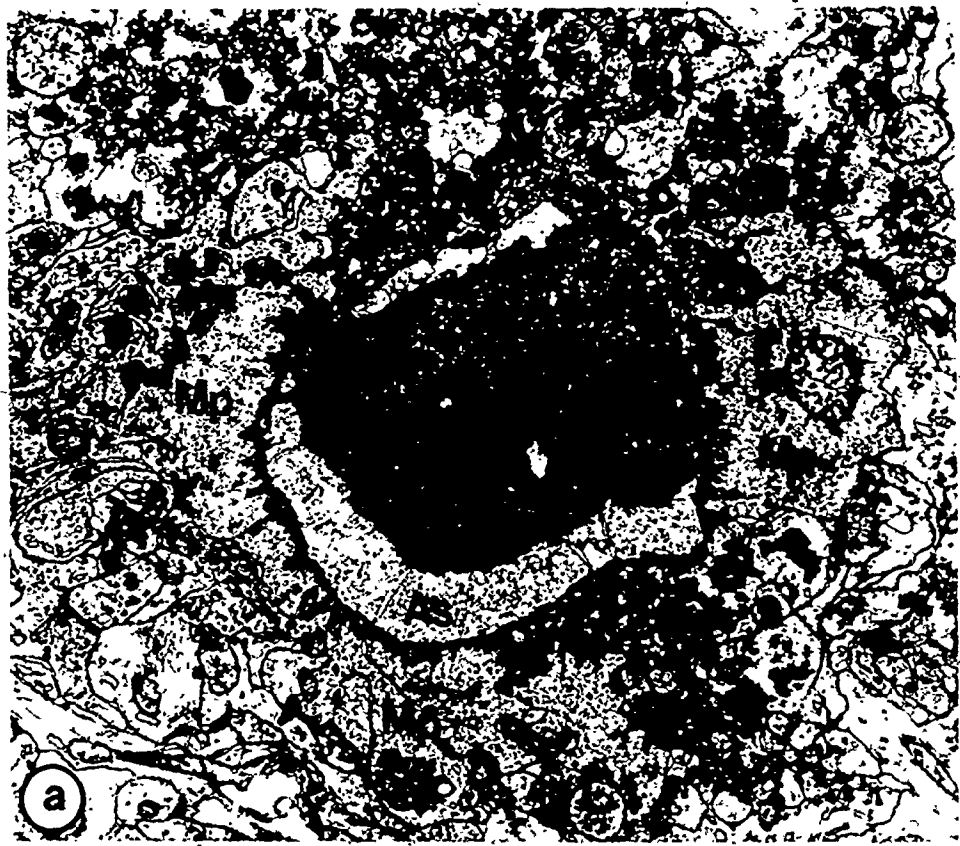
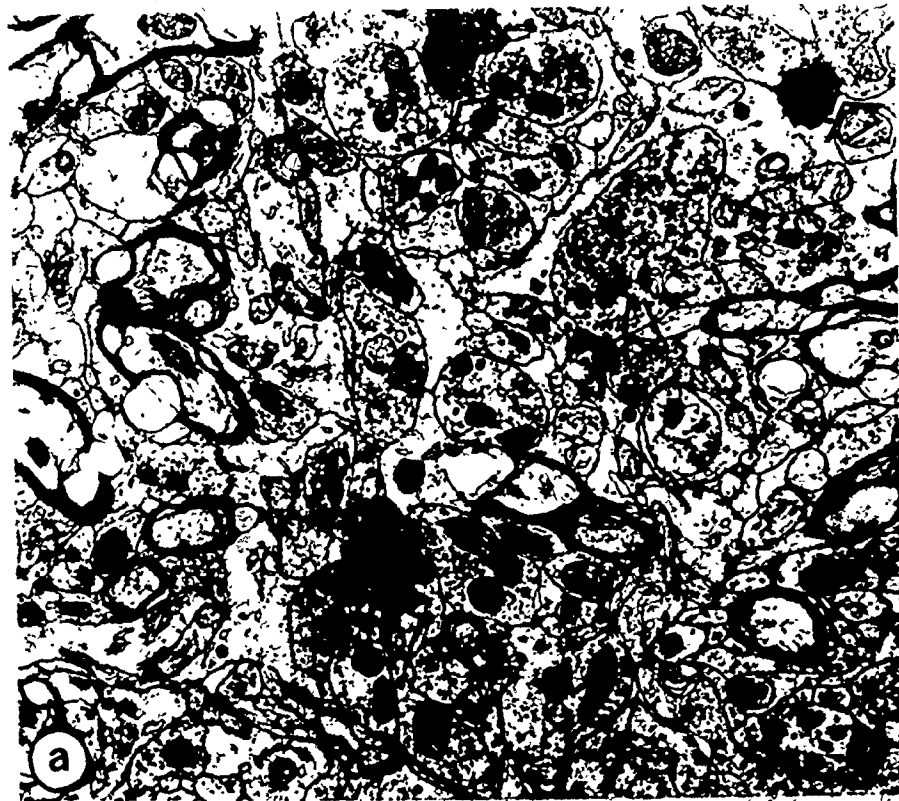




FIGURE 23

Electronmicrographs of degenerative olivary dendrites and a normal climbing fiber.

- a. Note that only a few degenerative fragments remain by the end of the second week following 3AP treatment. Because of the synaptic contacts in relation to these profiles (open block arrows), they are probably dendritic in nature. X 12,250.
- b. A control micrograph of rat cerebellar cortex. Note the longitudinally orientated climbing fiber (cf) adjacent to a Purkinje cell dendrite (Pcd). The climbing fiber gives rise to two varicosities (cfv) which make synaptic contact with six dendritic spines (ds). X 20,400.



## ABBREVIATIONS

- A CONT untreated adult rat 150 days old
- W CONT untreated weanling rat 21 days old
- W 3AP a weanling rat which has been treated with 3-acetylpyridine (3AP) on the 21st day and permitted to survive until reaching the approximate age of the A CONT
- p. 3AP following 3-acetylpyridine treatment

FIGURE 24

Photomicrographs of the medulla oblongata from control and 3AP treated rats showing the cellular configuration of the inferior olivary complex.

- a. A CONT. The caudal pole of the inferior olivary complex. Note the intense basophilic staining of the olivary neurons within the medial accessory olive (MAO) and the beta nucleus ( $\beta$ ).
- b. A CONT. Within the mid-portion of the inferior olivary complex two other nuclei are distinguishable: a thin dorsal lamella which forms the dorsal accessory olive (DAO) and a U-shaped band of cells between the dorsal accessory olive and the circular profile of the medial accessory olive (MAO) which represents the principal olivary nucleus (PO). Note that along the medial extremity of the principal olivary nucleus there is a discrete cell group which forms immediately adjacent to the ventral lamella of the principal olive and is distinguished as the dorsomedial cell column (dmcc).
- c,d. W CONT. The cellular configuration of the inferior olivary complex of a weanling rat at levels corresponding to a and b. Note that it appears identical to that found in the adult rat following Nissl staining.
- e. W 3AP. A light micrograph of the caudal portion of the medial accessory olive from a weanling rat following 3AP intoxication at the same dosage level used with the adults. Note the normal appearance of the Nissl stained olivary neurons along the medial aspect of the medial accessory olive of both sides (open block arrow). In addition, discrete areas of neuronal sparing are present along the main lamina of the medial accessory olive (open circles) and the beta nucleus (open square). 120d post (p.) 3AP. 65 mg/kg.
- f. W 3AP. The mid-portion of an adult inferior olivary complex following 3AP administration. Note the Nissl spared neurons within the genu of the principal olive (open circles). 120d p. 3AP. 65 mg/kg.
- g. W 3AP. The caudal portion of the medial accessory olive following 3AP treatment. Note the persistence of a few isolated islands of Nissl stained neurons along the main lamina of the medial accessory olive (open circles). 120d p. 3AP. 90 mg/kg.
- h. W 3AP. The mid-portion of an adult inferior olivary complex following 3AP administration. Note the absence of Nissl stained cell bodies. 120d p. 3AP. 90 mg/kg.

a-h, thionine; X 30.

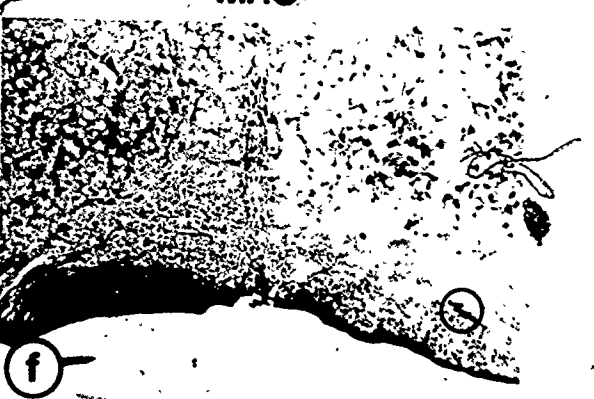
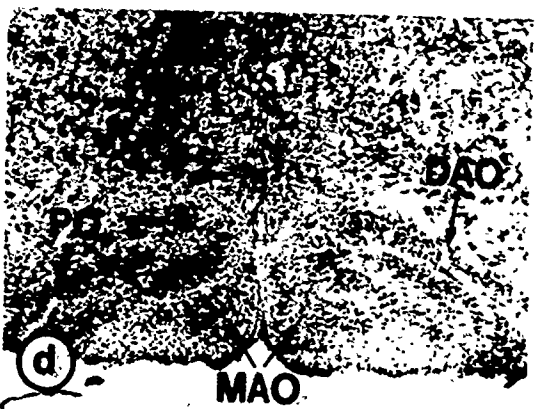
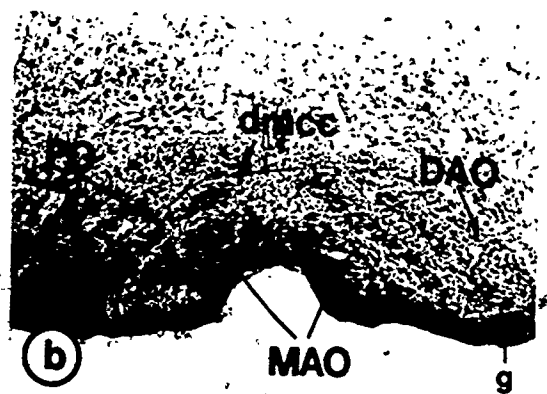


FIGURE 25

Electronmicrographs of the medial accessory olive following long-term 3AP treatment of the weanling rat.

- a. A normal inferior olivary neuron (ION) located within the medial aspect of the caudal portion of the medial accessory nucleus. Note that this cell contains a prominent nucleus and a normal complement of cytoplasmic organelles (Golgi complex - open block arrows; Nissl bodies - solid block arrows): 120d p, 3AP 65 mg/kg. X 6,000
- b. A field of neuropil within the medial aspect of the caudal portion of the medial accessory olive. This portion of the inferior olivary complex appears to be spared following 3AP treatment. 120d p, 3AP. 65 mg/kg. X 12,000.

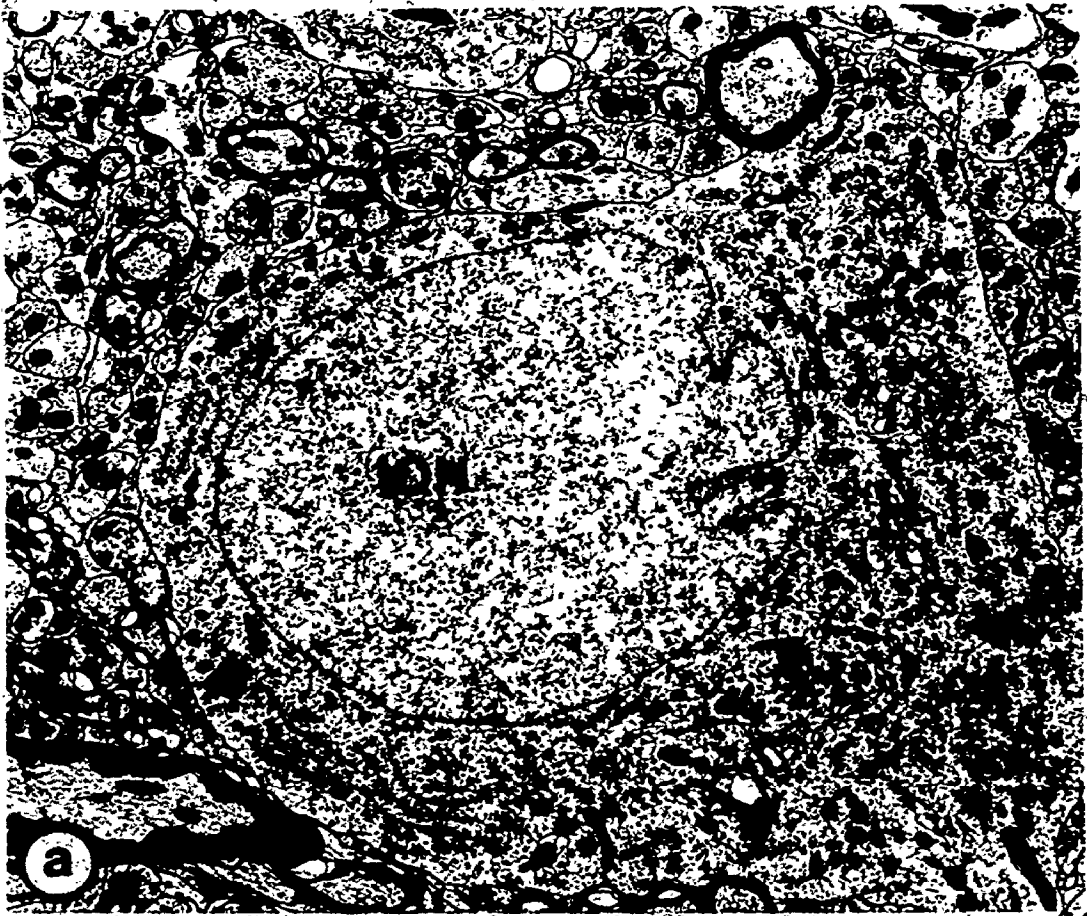


FIGURE 26

Electronmicrographs of the normal Purkinje cell dendritic tree and climbing fiber varicosity.

- a. A normal Purkinje cell soma (PC) lying at the junction of the molecular and granule cell layers. The nucleus of this Purkinje cell contains a prominent nucleolus and a nucleolus-associated chromatin mass (large black arrow). The remaining nuclear chromatin is homogeneously distributed throughout most of the nucleus. Note that the cytoplasm contains a number of Golgi complexes, aggregates of rough endoplasmic reticulum and a highly developed agranular endoplasmic reticulum which forms a specialized cisternal system immediately below the plasmalemma of the cell (the hypolemmal cisternae) (small black arrows).  
X 3,000
- b. A varicosity of a climbing fiber tendril branch (CFv) which is running adjacent to the outer surface of a primary trunk of a Purkinje cell (Pcd<sub>1</sub>).  
X 21,667.
- c. A transverse section through the primary dendrite of a Purkinje cell showing the profile of a dendritic thorn (dt). The thorn bears a short neck, a clavate head and contains a few tubules of smooth endoplasmic reticulum. This profile represents the postsynaptic site of the climbing fiber varicosity.  
X 11,250.
- d. The connecting stem of a climbing fiber tendril branch (open block arrow). Note that it possesses a microtubular core and that it gives rise to two climbing fiber varicosities (CFv). These varicosities possess a dense population of round synaptic vesicles and make synaptic contact with several dendritic thorns (asterisks) which project from the smooth portion of the Purkinje cell dendritic tree.  
X 15,000
- e. A tendril branch of a climbing fiber (CFt) which extends along the surface of a smooth branch of a Purkinje cell dendritic tree.  
X 11,110.
- f. Two dendritic spines projecting from the surface of a Purkinje cell terminal branchlet. Note that these spines have a smaller head region and a longer neck portion as compared to the dendritic thorn in Fig. 26g.  
X 20,000.
- g. A higher power view of the dendritic thorn shown in Fig. 26c. Note the large size of the head region as compared to the narrow neck portion.  
X 20,000.
- h. A Purkinje cell spiny branchlet. This branchlet is partially covered by a layer of Bergmann glia and displays five dendritic spines projecting from its surface.  
X 16,071.





FIGURE 27

Electronmicrographs of degenerating climbing fiber varicosities.

- a. A climbing fiber varicosity 12 hours after 3AP treatment. Note a Bergmann glial process (Bg) which appears to be actively engaged in phagocytizing a degenerating climbing fiber varicosity (open block arrow). X 15,300.
- b. Note that by 60 hours following 3AP treatment the climbing fiber varicosity is at a late stage of degeneration as evidenced here by a marked increase in the electron density of both the axoplasmic matrix and the mitochondrial profiles. Note that the synaptic contacts (open block arrows) are still intact. X 20,400.
- c. A degenerating climbing fiber varicosity 72 hours following 3AP administration. Note that a dendritic spine (ds) with its postsynaptic membrane thickening (open block arrow) is denuded of its synaptic contact with the climbing fiber varicosity. X 30,600.
- d. An electron micrograph of a degenerating climbing fiber profile surrounded by Bergmann glia processes (Bg) 7 days following 3AP treatment. X 20,400.



FIGURE 28

Photomicrographs of Golgi-Cox preparations of control Purkinje cells.

- a. A low power view of an adult Purkinje cell (150 days). The dendritic arborization of this cell fans out within the parasagittal plane of the cerebellar cortex. Note that a large proportion of the dendritic tree consists of small, spine-covered, terminal branchlets. X 320.
- b, e. High power views of adult Purkinje cell terminal branchlet fields. The spines projecting from these branches appear stubby and possess slightly narrowed neck portions (open block arrows). X 1,120.
- c. Large caliber dendrites from a control Purkinje cell dendritic tree. Note the absence of spines along both the primary trunk and secondary branches. X 704.
- d. A low power view of a weanling Purkinje cell (21 days). Like the adult Purkinje cell, the dendritic arborization of this cell is planar and fans out within the parasagittal plane of the cerebellum. X 330.
- f. A high power view of a weanling Purkinje cell terminal branchlet field. The number and shape of these spines closely resembles the dendritic appendages which project from the adult Purkinje cell terminal branchlet. X 1,120.
- g. A montage of the surface of a large caliber dendrite of the weanling Purkinje cell shown in Fig. 28d. Note the smooth appearance of these large branches which contrasts sharply with the dense covering of spines along the terminal branchlets. X 810.

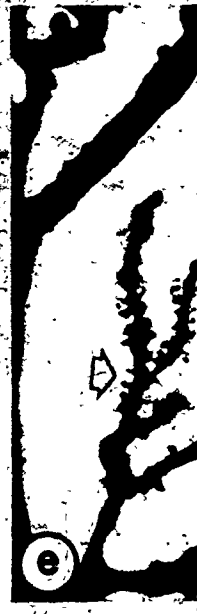
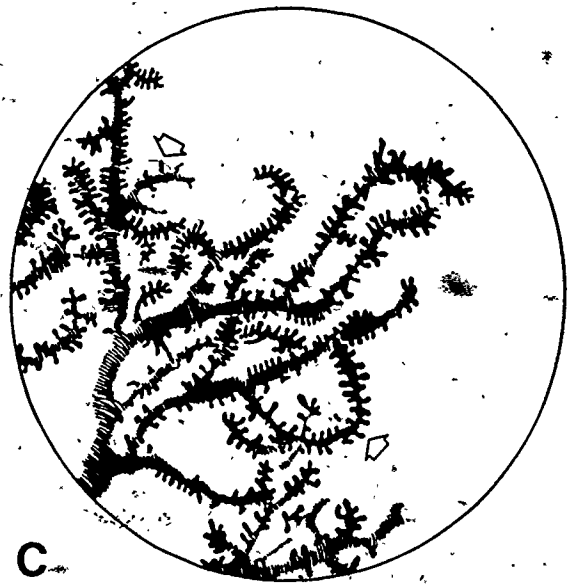
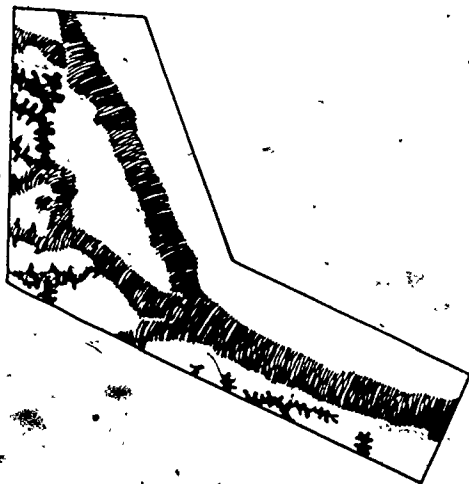
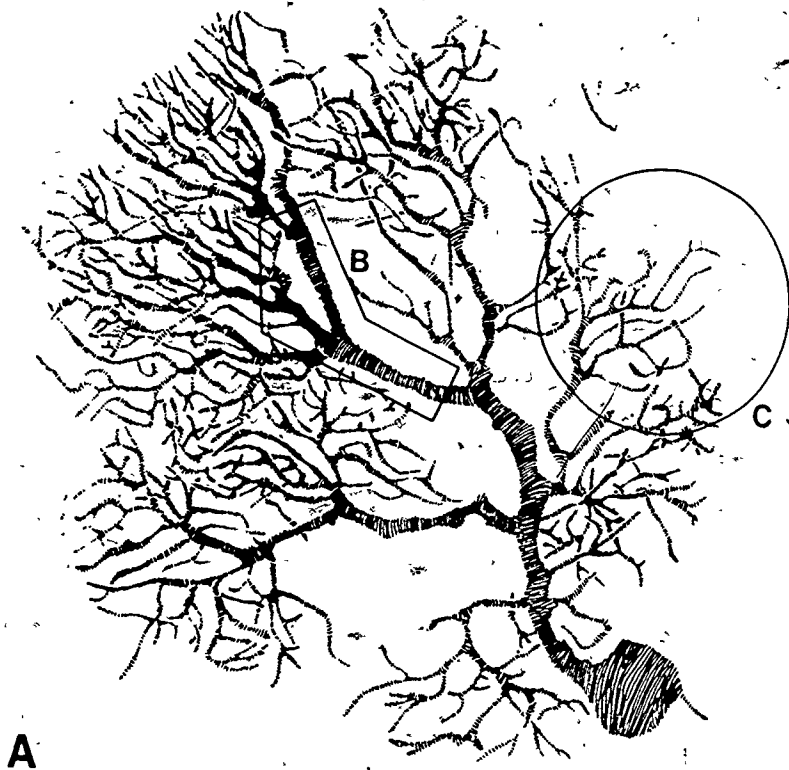


FIGURE 29

A camera lucida drawing of a Golgi-Cox preparation of an adult control Purkinje cell.

- A. A drawing of the Purkinje cell in Fig. 28 a. Note the number of small caliber branches (terminal branchlets) within the dendritic arborization of this Purkinje cell.
- B. An enlargement of the area within the pentagon (B) includes portions of a secondary and several tertiary branches from the smooth portion of an adult Purkinje cell. Note the absence of spines along these large caliber dendrites.
- C. An enlargement of the terminal branchlet field (C) which shows more accurately the density and morphology of the spines that project from these branches.



B

C

\* FIGURE 30

Photomicrographs of Golgi-Cox preparations of Purkinje cells following long-term climbing fiber-deafferentation of the adult rat.

a,c,e. The dendritic arborizations of three deafferentated Purkinje cells. Note that the dendritic arborizations of these cells are markedly reduced in size from either the adult control (Fig. 28 a) or the climbing fiber-deafferentated weanling rat (Fig. 36-a, d). There is also an obvious loss in the number of both smooth branches and terminal branchlets. 140d p.o. a: X 320, b: X 267, c: X 320.

b,f. The large dendritic branches of these Purkinje cells are smooth. Note that spines do not project from the surface of these branches. 140d p.o. b: X 1,171, f: X 1,216.

d,h. Despite the prominent loss of terminal branchlet numbers, the density of spines along the persisting branches does not appear to be altered (open block arrows). 134d p.o. X 1,171.

g. Small stubby appendages (open block arrows) along the smooth portion of the Purkinje cell dendritic tree following climbing fiber-deafferentation. This dendritic appendage probably corresponds to the dendritic thorn which projects from the "smooth portion" of the control Purkinje cell dendritic tree. X 640.



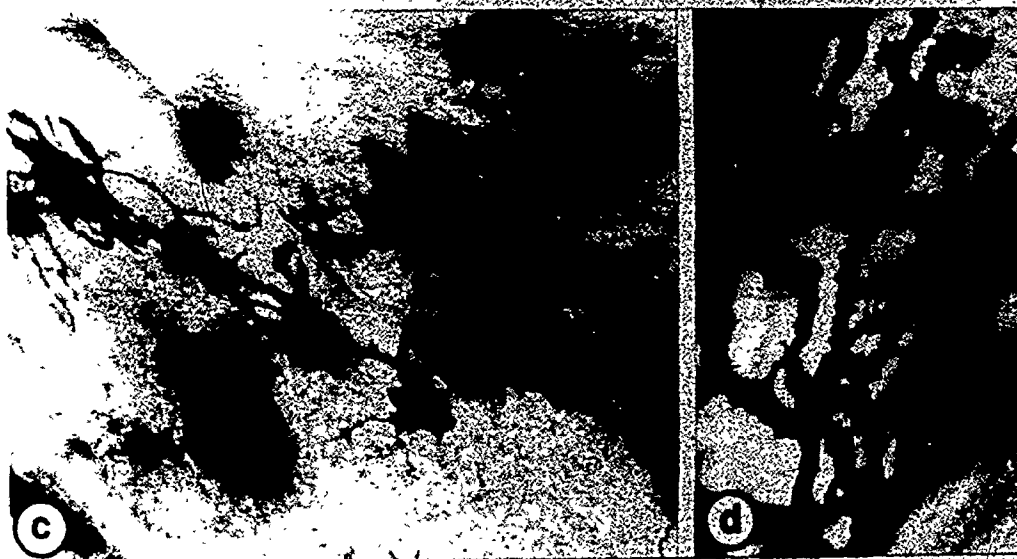


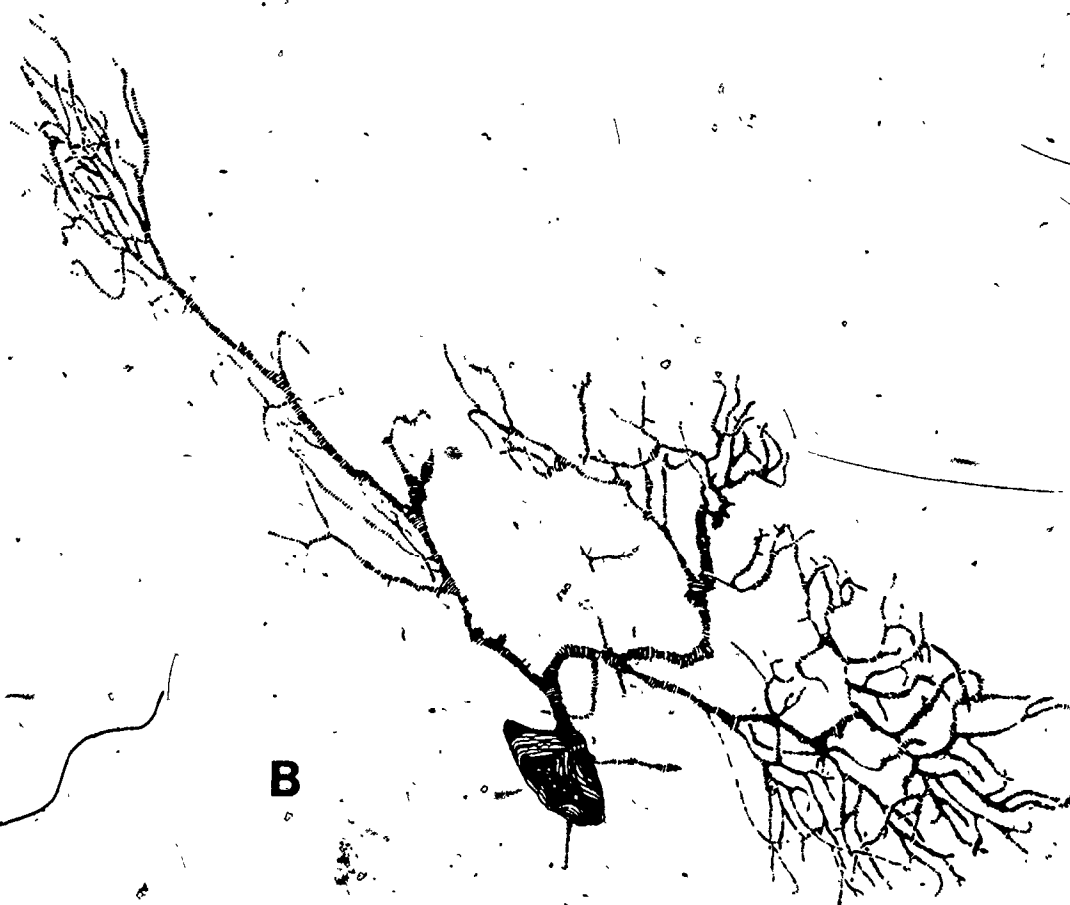
FIGURE 31

Camera lucida drawings of Golgi-Cox preparations of Purkinje cells following long-term climbing fiber-deafferentation of the adult rat.

A, B. Drawings of the dendritic arborizations of the two deafferentated Purkinje cells in Fig. 30 a and c. Note the marked decrease in the size of the dendritic arborizations of these cells as compared to the adult control (Fig. 29A). This decrease appears to involve a significant loss of both smooth branches and terminal branchlets. 140d p.o.



**A**



**B**

## ABBREVIATIONS AND SYMBOLS

A CONT	untreated adult rat 150 days old
W CONT	untreated weanling rat 21 days old
A 3AP	an adult rat which has been treated with 3-acetylpyridine (3AP) on the 57th day and allowed to survive until reaching the approximate age of the A CONT
W 3AP	a weanling rat which has been treated with 3AP on the 21st day and permitted to survive until reaching the approximate age of the A CONT
A CERB L	an adult rat which has received a unilateral cerebellar lesion (parasagittal transection of the lateral cerebellar cortex) on the 57th day and allowed to survive until reaching the approximate age of the A CONT
W CERB L	a weanling rat which has received a unilateral cerebellar lesion on the 21st day and permitted to survive until reaching the approximate age of the A CONT
A PONT L	an adult rat which has received a contralateral pontine ablation on the 57th day and allowed to survive until reaching the approximate age of the A CONT
S.E.M.	standard error of the mean
ANOVA	analysis of variance
A	the independent variable, lesion
B	the independent variable, time
df	degrees of freedom
MS	mean squared error

F represents the ratio obtained by dividing the mean squared error among groups by the residual (one way analysis of variance)

represents the ratios obtained by dividing the mean square's for variable A, B and for the interaction (A X B) by the residual (two way analysis of variance)

Residual mean squared error within groups (MS wg)

open bar, histogram non-significant

solid bar histogram p = .01

lined bar histogram p = .05

dotted bar histogram p = .10

CNM comparison not made

FIGURE 32

A histogram of the length and number of Purkinje cell dendritic segments in the experimental groups or W CONT expressed as a percentage of the A CONT,

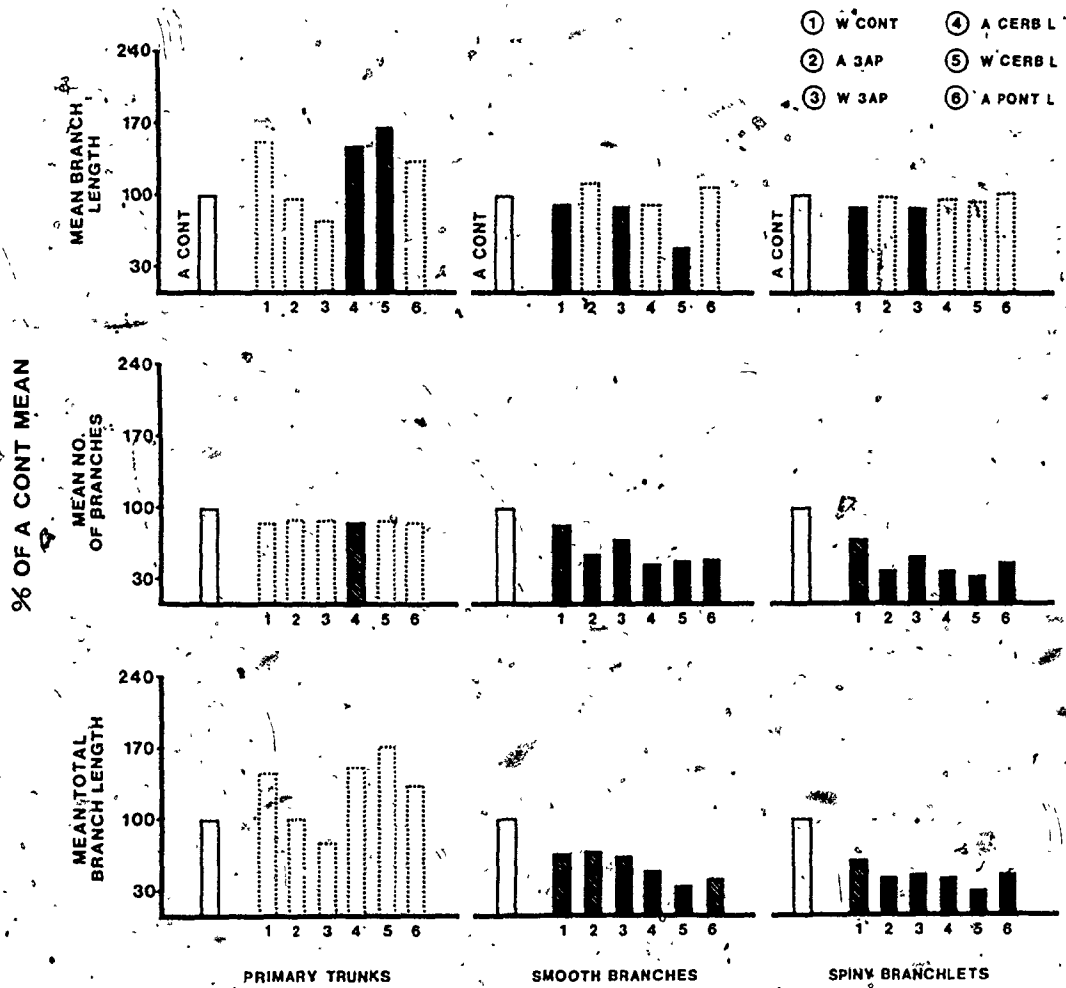


FIGURE 33

A histogram of the length and number of Purkinje cell dendritic segments in the experimental group expressed as a percentage of the W CONT.





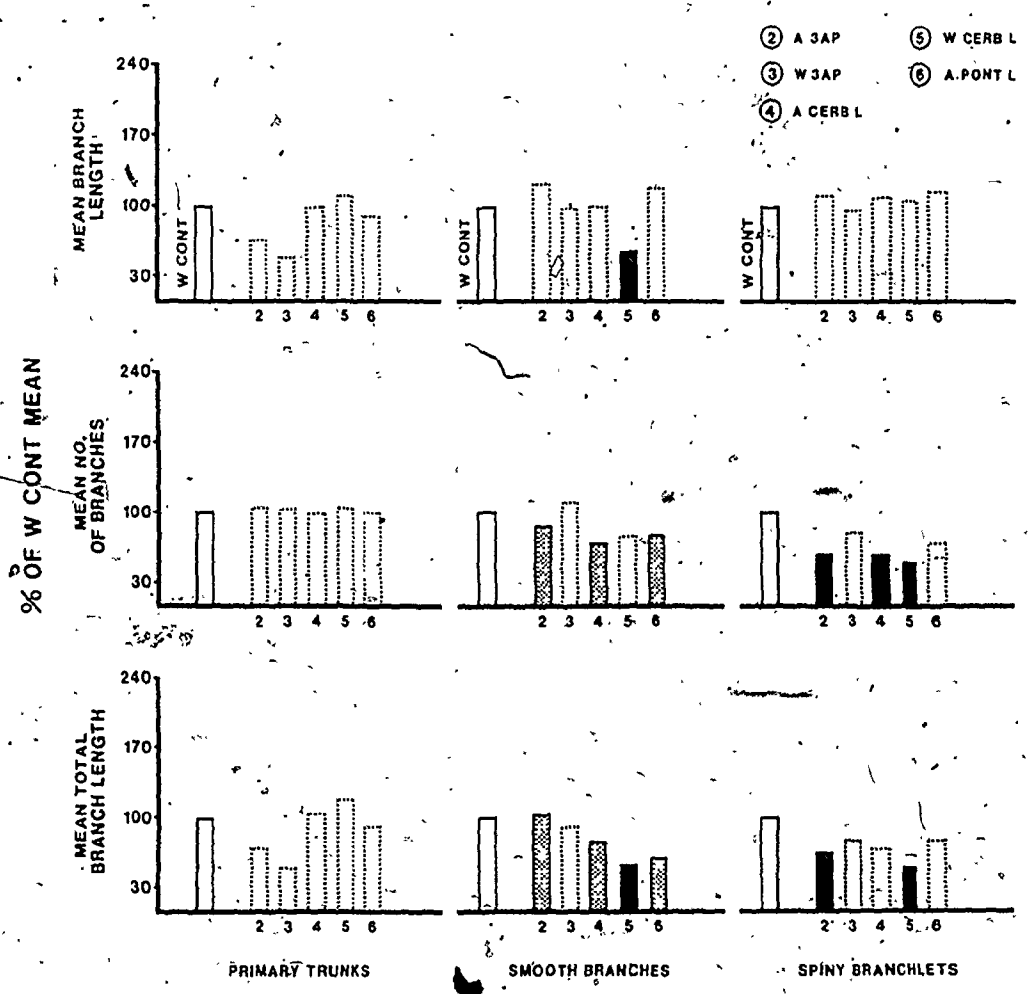


FIGURE 34

Electronmicrographs of the smooth portion of the Purkinje cell dendritic tree following long-term climbing fiber-deafferentation of the adult rat.

- a. An oblique section through a smooth branch of a Purkinje cell dendritic tree (sPcd). The degenerative changes within it are minor, consisting largely of swelling of the agranular endoplasmic reticulum, particularly the hypolemmal cisternal system (solid block arrows): 123d p. 3AP. X 21,428.
- b. A smooth branch from a Purkinje cell dendritic tree (possibly a tertiary branch) (Pcd<sub>3</sub>). Note the presence of several swollen multivesicular-like bodies (mvb) and the absence of most dendritic organelles with the exception of its mitochondrial component. This dendrite bifurcates within the center of this field giving rise to a spiny branchlet (SpB) which possesses a dendritic spine (ds) near its origin. 136d p. 3AP. X 16,363.
- c. A smooth branch from a Purkinje cell dendritic tree. Note the two prominent whorled membrane bodies (large black arrows) and the swollen hypolemmal cisterna (small arrows) within this branch. 136d p. 3AP. X 13,269.

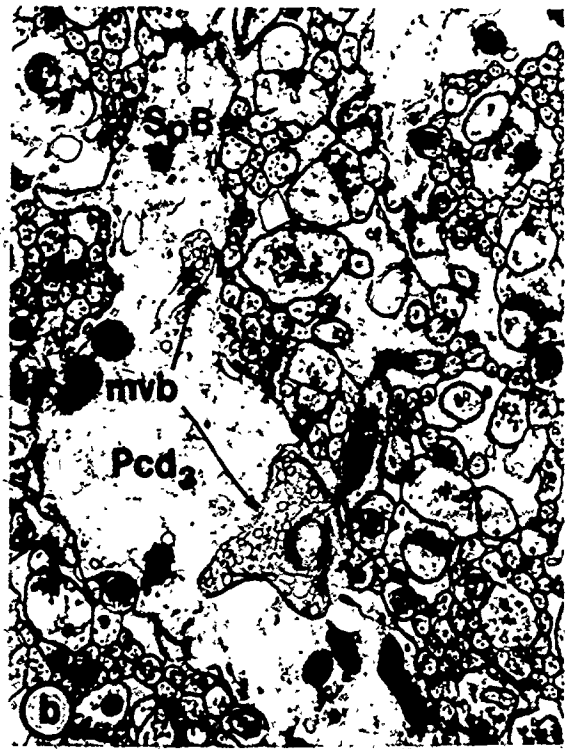


FIGURE 35

Electronmicrographs of terminal branchlets of the Purkinje cell dendritic tree following long-term climbing fiber-deafferentation.

- a. A 3AP. A degenerating terminal branchlet. The matrix of this branchlet is extensively vacuolated making the outline of this profile barely visible. Note the dendritic spines (ds) projecting from this terminal branchlet and the synaptic terminal in contact with one of them (black arrow). 136d p.o. X 16,875.
- b. W 3AP. A degenerating terminal branchlet from a Purkinje cell dendritic tree. 136d p.o. X 17,500.
- c. A 3AP. The electron dense debris of a climbing fiber rosette (CFg). Note that synaptic contacts still persist between the digitiform branches of granule cell dendrites and the electron-dense fragment of the climbing fiber rosette (black arrows). 136d p.o. X 22,500.
- d. A 3AP. A degenerating terminal branchlet from a Purkinje cell dendritic tree. The core of this dendritic profile is largely replaced by glia (gl), leaving only a thin lamina of subplasmalemmal dendritic matrix and the dendritic spines (ds) (arrows) which are characteristic features of a Purkinje cell terminal branchlet. 296d p.o. X 15,750.
- e, f. e: A 3AP, f: W 3AP. Note that in many areas of the molecular layer neuropil, the terminal branchlets are completely replaced by glial profiles leaving only a thin attenuated strand of electron-dense material as a remnant of the dendritic profile (black arrows). 296d p.o. 3: X 17,500; - f: X 16,071.

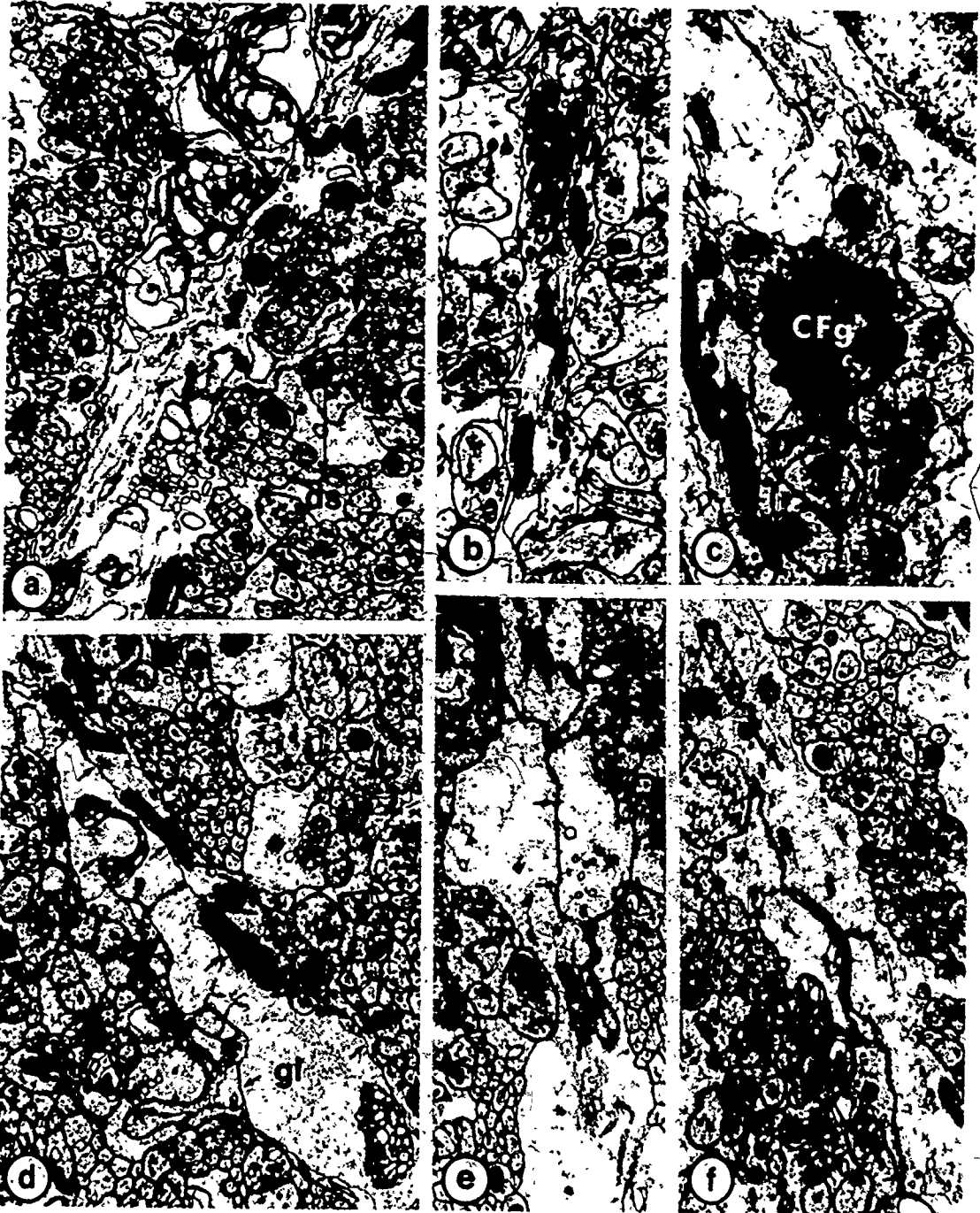


FIGURE 36

Photomicrographs of Golgi-Cox preparations of Purkinje cells following long-term climbing fiber-deafferentation of the weanling rat.

a, d. Two low power views of climbing fiber-deafferentated Purkinje cells. Note the reduction in overall complexity (branching) of the dendritic arborizations of these cells as compared to the adult control. 131d p.o. X 362.

b, c, e. At higher magnifications, these large caliber Purkinje cell dendrites are found to possess an ectopic covering of dendritic appendages (open block arrows). 131d p.o. b: X 1,066, c: X 1,280, e: X 1,066.



FIGURE 37

Camera lucida drawings of Golgi-Cox preparations of Purkinje cells following long-term climbing fiber-deafferentation of weanling rats.

- A, B. Drawings of the dendritic arborizations of the two deafferentated Purkinje cells in Fig. 36 a and d. The dendritic arborizations of both these cells are reduced from that of the adult control (Fig. 29 A). Note, in particular, the marked reduction in small caliber dendritic branches (terminal branchlets). Dendritic appendages are not shown (see below). A: 123d p.o., B: 131d p.o.
- C, D. Enlargements of secondary dendrites within the smooth portion of the Purkinje cell dendritic trees shown in A and B (see rectangles). Note that ectopic dendritic appendages are present along this portion of the dendritic tree of both cells (open block arrows).



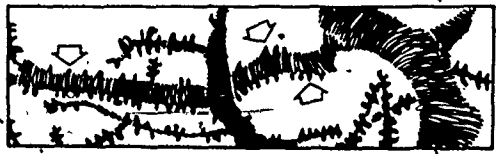
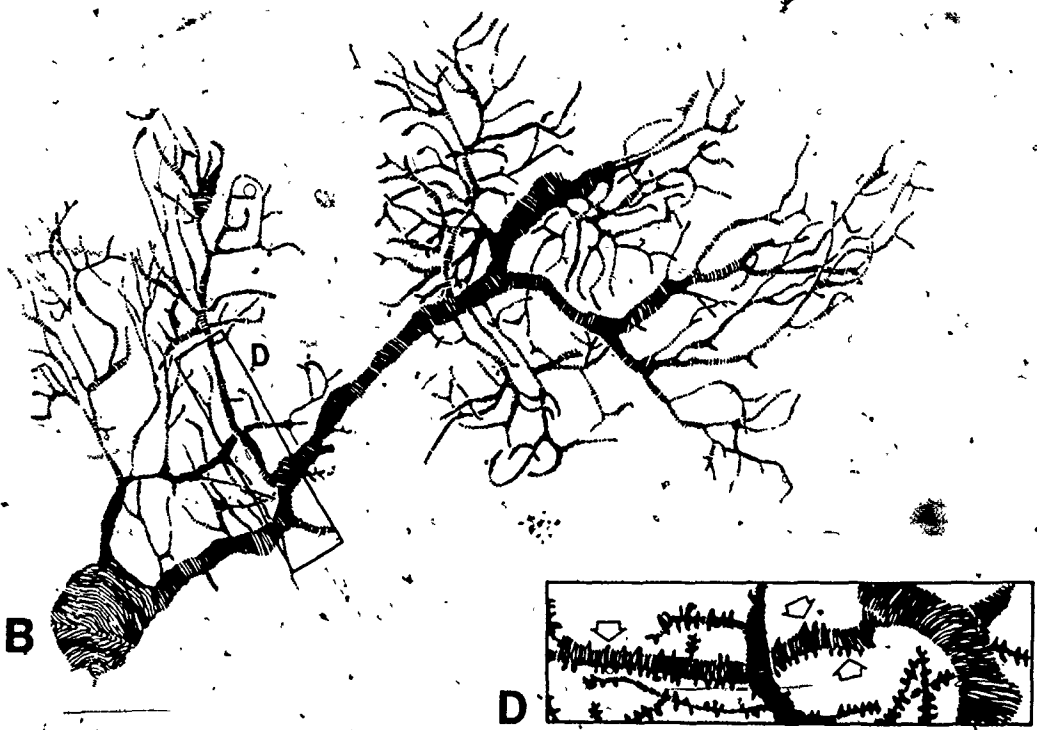
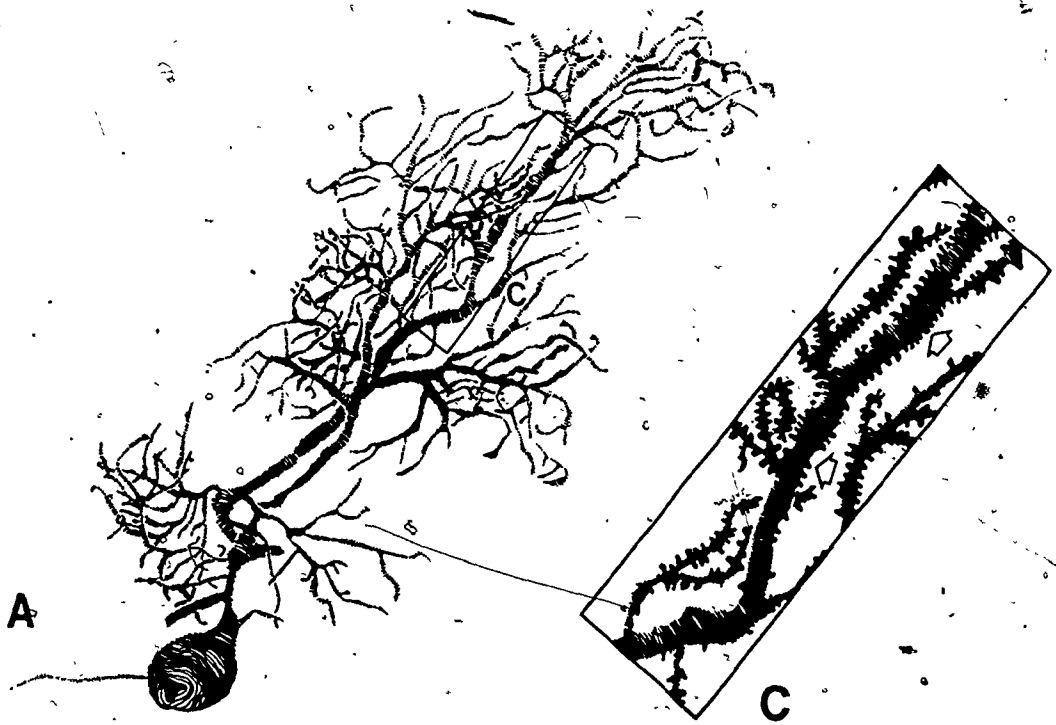


FIGURE 38

Electronmicrographs of dendritic appendages along the smooth portion of the Purkinje cell dendritic tree following long-term climbing fiber-deafferentation of the weanling rat.

- a. A section through the long axis of a smooth branch of a Purkinje cell dendritic tree (sPcd) which shows a profile of a dendritic thorn (dt). Note the aberrant contact formed as a result of the parallel fiber-dendritic thorn synapse (large black arrow). 131d p. 3AP. X 22,500.
- Insert - High power view of the aberrant parallel fiber-dendritic thorn synapse. Note that this dendritic thorn lacks a neck region and is represented merely by an elevation of the dendritic plasmalemma. X 34,500.
- b. A Golgi-Cox impregnation of a smooth branch from a Purkinje cell dendritic tree. Note the small stubby appendages along this large caliber dendrite. These profiles are thought to be equivalent to the dendritic thorns visualized with the electron microscope (open block arrow). 135d p. 3AP. X 1,120.
- c. This section passes through a portion of a smooth branch of a Purkinje cell dendritic tree (lower left corner). Note the dendritic thorn profile (dt) which has a short neck region and an enlarged knob, the head portion. Notice that this profile makes an aberrant synaptic contact with a parallel fiber varicosity (PFv). 180d p. 3AP. X 22,500.
- d. This electronmicrograph passes through a profile of a spine-like appendage (ds) which projects from the surface of a primary dendrite. This dendritic spine forms an aberrant synaptic contact with an ascending basket axon collateral (Bx) which also innervates the smooth surface of the primary dendrite (black arrows). 180d p. 3AP. X 22,500.
- e, g. Electronmicrographs of smooth branches from Purkinje cell dendritic trees. Note that within each field, two spine-like appendages (ds) project from the dendritic plasmalemma. One spine in each micrograph is seen to form a synaptic contact with a parallel fiber varicosity (asterisks). 180d p. 3AP. e: X 22,500 g: X 21,110
- f. A Golgi-Cox impregnation of a smooth branch of a Purkinje cell dendritic tree. Note the spine-like appendages which project from the surface of this large caliber dendrite (open block arrow). 140d p. 3AP. X 1,066.
- h. A high power view of a spine-like appendage along the primary trunk of a Purkinje cell dendritic tree. Note that this parallel fiber varicosity (PFv) is associated with both the neck region of a spine and the plasmalemma of a primary trunk but forms its synaptic contact exclusively with the head region of the spine. 180d p. 3AP. X 22,500.

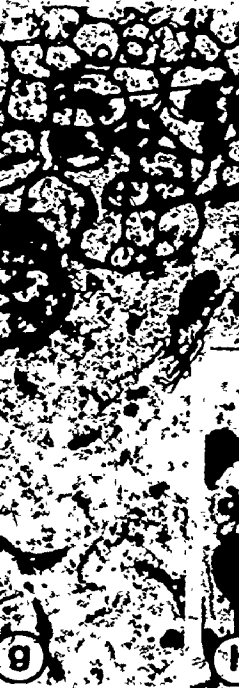


FIGURE 39.

Electronmicrographs of cerebellar interneurons within the molecular layer following long-term climbing fiber-deafferentation in the adult rat.

- a. A degenerating soma of a cerebellar interneuron (basket cell). Note the highly lobulated nature of the nucleus of this cell, its localization deep within the molecular layer (because of the adjacent myelinated recurrent Purkinje cell axon) (PCrx) and the number of axosomatic contacts. 296d p. 3AP. X 8,610.
- b. A degenerating soma of a cerebellar interneuron. Notice that this soma has a slightly lobulated nucleus, a less voluminous cytoplasmic content and only one axosomatic contact (black arrow) as compared to the basket cell shown in Fig. 39a. These features are all characteristics of a superficial stellate cell. 123d p. 3AP. X 9,000.
- c. A high power view of a portion of the somatic surface (rectangle) from the basket cell shown in Fig. 39a. This portion of the soma bears six synaptic contacts with parallel fiber varicosities (asterisks). 296d p. 3AP. X 33,333.
- d. A high power view of a portion of the somatic surface (rectangle) from the superficial stellate cell shown in Fig. 39b. Note the thin layer of cytoplasm associated with this cell and the paucity of axosomatic contacts. 123d p. 3AP. X 16,667.

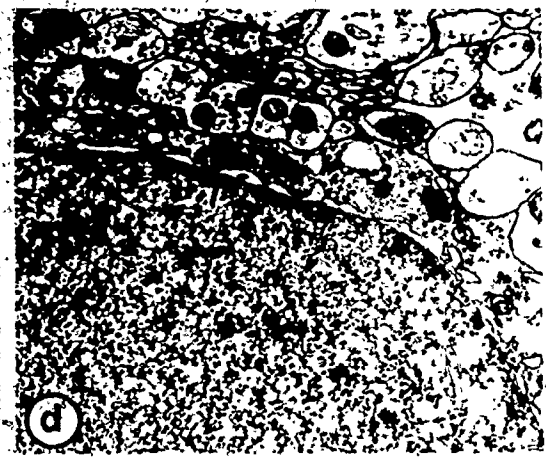
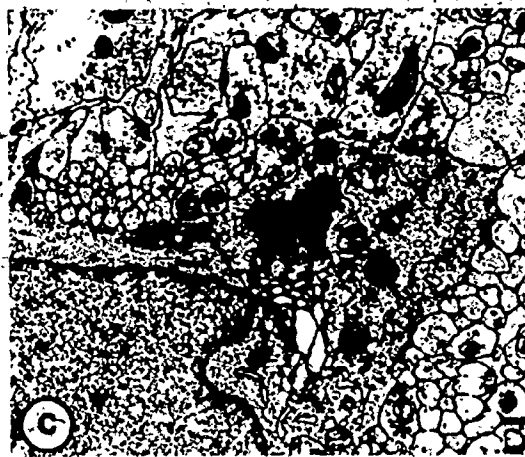


FIGURE 40

Electronmicrographs of dendrites of cerebellar interneurons following long-term climbing fiber-deafferentation.

a,c. A 3AP. Two degenerating dendrites of cerebellar interneurons. Note the increased irregularity of their outline and the dramatic increase in the electron opacity of their dendritic matrix. The parallel fiber varicosities which synapse with these dendritic profiles appear normal (asterisks). 296d p.o. a: X 11,206, c: X 10,454.

b. A 3AP. A profile of a degenerating dendrite from a cerebellar interneuron which is cut transversely. Note the large number of parallel fiber varicosities which synapse with this dendrite. A glial profile (gl) also makes contact with this dendrite and appears to be actively engaged in its phagocytic removal (black arrows). 296d p.o. X 16,500.

d. W 3AP. Note the degenerative debris which is thought to be dendritic fragments from cerebellar interneurons. These profiles are completely ensheathed by glia (gl) and appear to be in an advanced stage of electron-dense degeneration. 296d p.o. X 12,560.

e. W 3AP. A degenerating dendrite from a cerebellar interneuron cut parallel to its long axis. At this advanced stage of degeneration, the dendritic remains consist of a thin attenuated strand of electron-dense material (black arrows). The presynaptic parallel fiber varicosities appear normal and maintain synaptic contact with the electron-dense debris (asterisks). X 16,667.

f. W 3AP. A small caliber degenerating dendrite from a cerebellar interneuron. 180d p.o. X 17,500.

g. A 3AP. A small caliber degenerating dendrite from a cerebellar interneuron. 296d p.o. X 16,875.

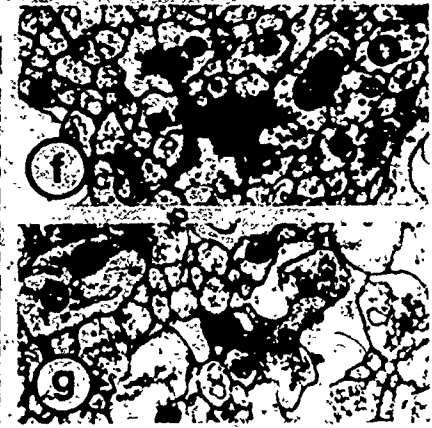
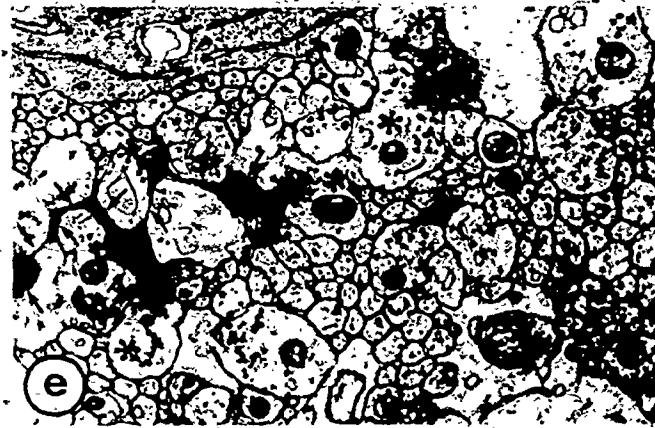
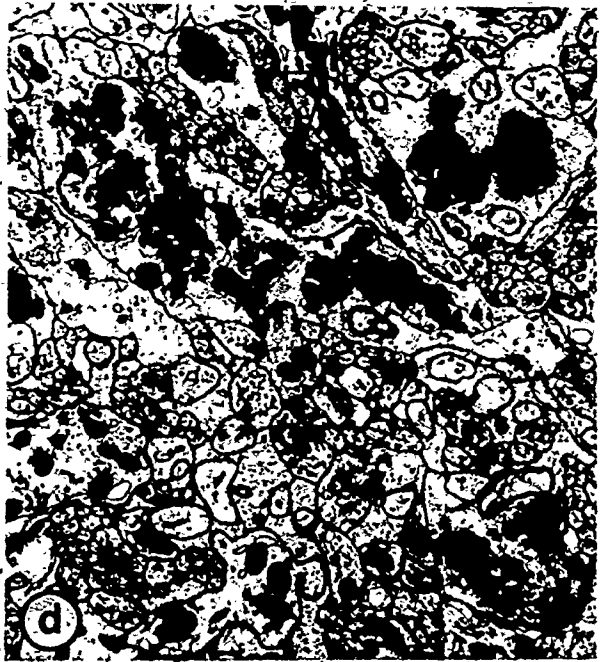
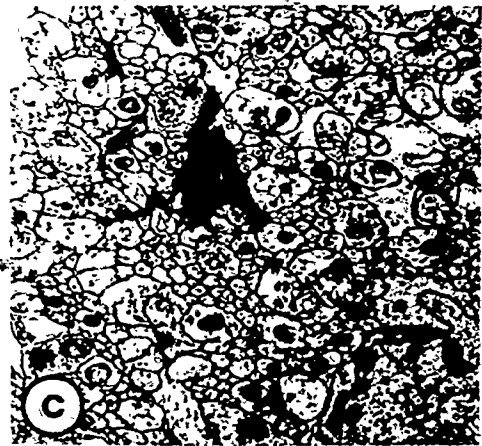
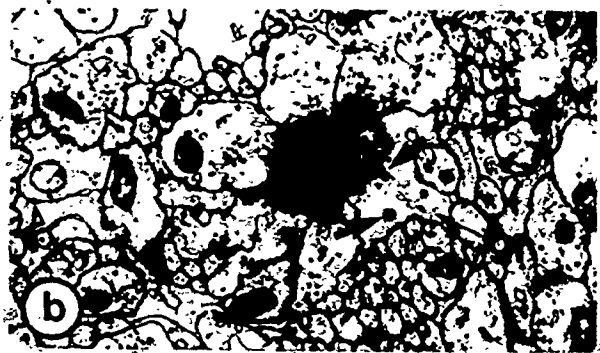
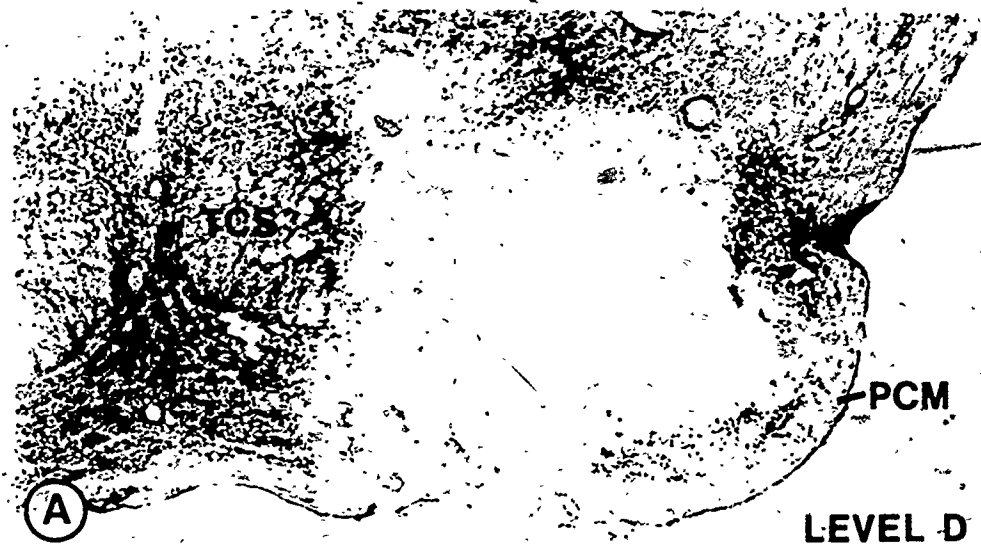


FIGURE 41

A photomicrograph (A) and a series of line drawings (B) representing transverse sections through the rostrocaudal extent of a lesion within the ventral pontine gray of an adult rat (CT - central tegmental nucleus; FLM - medial longitudinal fasciculus; IPN - interpeduncular nucleus; LL - lateral lemniscus; LL<sub>v</sub> - ventral nucleus of the lateral lemniscus; LM - medial lemniscus; nIII - nucleus of the oculomotor nerve; nIV - nucleus of the trochlear nerve; NV - the trigeminal nerve; NCS - superior central nucleus; NRTP - nucleus reticularis tegmenti pontis; NST - sensory nucleus of the trigeminal nerve; NTM - motor nucleus of the trigeminal nerve; NEX - nucleus of the trapezoid body; P - pons; PC - cerebral peduncle; PCM - middle cerebellar peduncle; RF - reticular formation; SN - substantia nigra; SOC - superior olivary complex; TCS - corticospinal tract).





C1L3AP SPLR

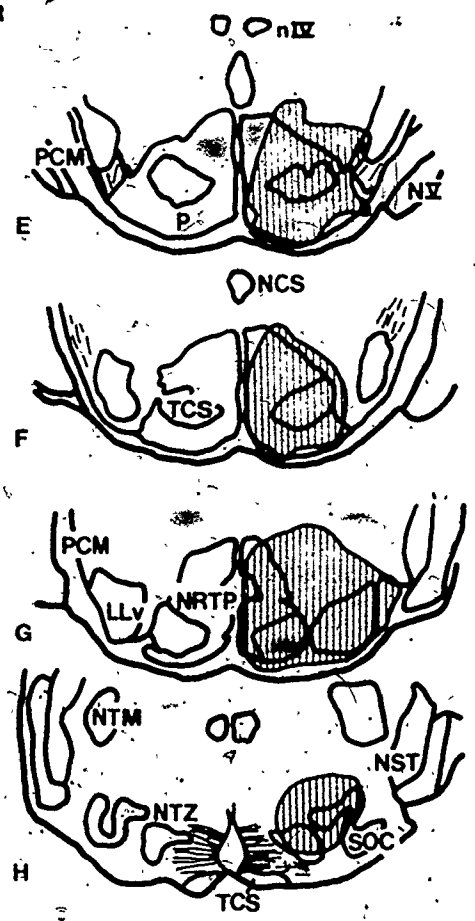
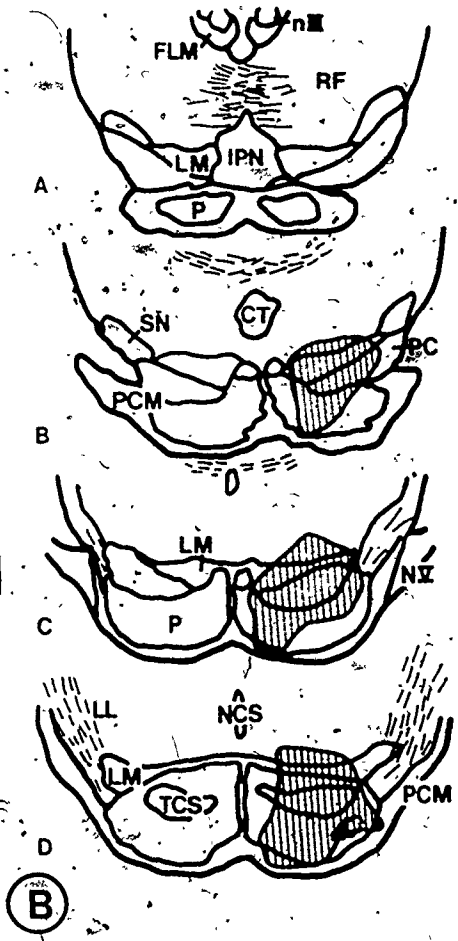


FIGURE 42

Electronmicrographs of the cytoarchitecture of the simple mossy fiber rosette of the adult cerebellar cortex.

- a. A simple mossy fiber rosette containing a population of dispersed synaptic vesicles (SMFd). This rosette is cut longitudinally and is surrounded by the digitiform branches of granule cell dendrites (Gcd). The central core of this enlargement contains a bundle of microtubules. X 15,000.
- b. A transverse section through a simple mossy fiber rosette. This section passes through the long axis of a digitiform dendrite from a granule cell (Gcd) and shows that an extensive area of apposition exists between the dendrite and its postsynaptic target, the mossy fiber rosette (open block arrows). X 17,045.
- c. A simple mossy fiber rosette. Note that the cortical zone of this rosette contains a dispersed population of spherical synaptic vesicles ranging from 300 - 560 Å in diameter (double headed arrow). This section passes transversely through the profiles of several granule cell dendrites (Gcd) and shows that they generally contain a single mitochondrial profile and an associated tubule of smooth endoplasmic reticulum. X 20,000.
- d. Note that the synaptic junction (Gray's type I) between the granule cell dendrite and the mossy fiber rosette is characterized by a widened interstitial cleft which contains filamentous material (open block arrow). A thick plaque of dense material is associated with the cytoplasmic side of the dendritic membrane while smaller tufts of opaque material project into the mossy fiber rosette from the axolemma. X 42,857.
- e. A simple mossy fiber rosette that contains a concentrated population of synaptic vesicles (SMFc). Note that in addition to the granule cell dendrites, the mossy fiber rosette is surrounded by several profiles of Golgi cell axons (Gox). X 20,000.
- f. A Golgi cell axon in synaptic contact with the outer surface of a granule cell digitiform dendrite (open block arrow). X 38,000.

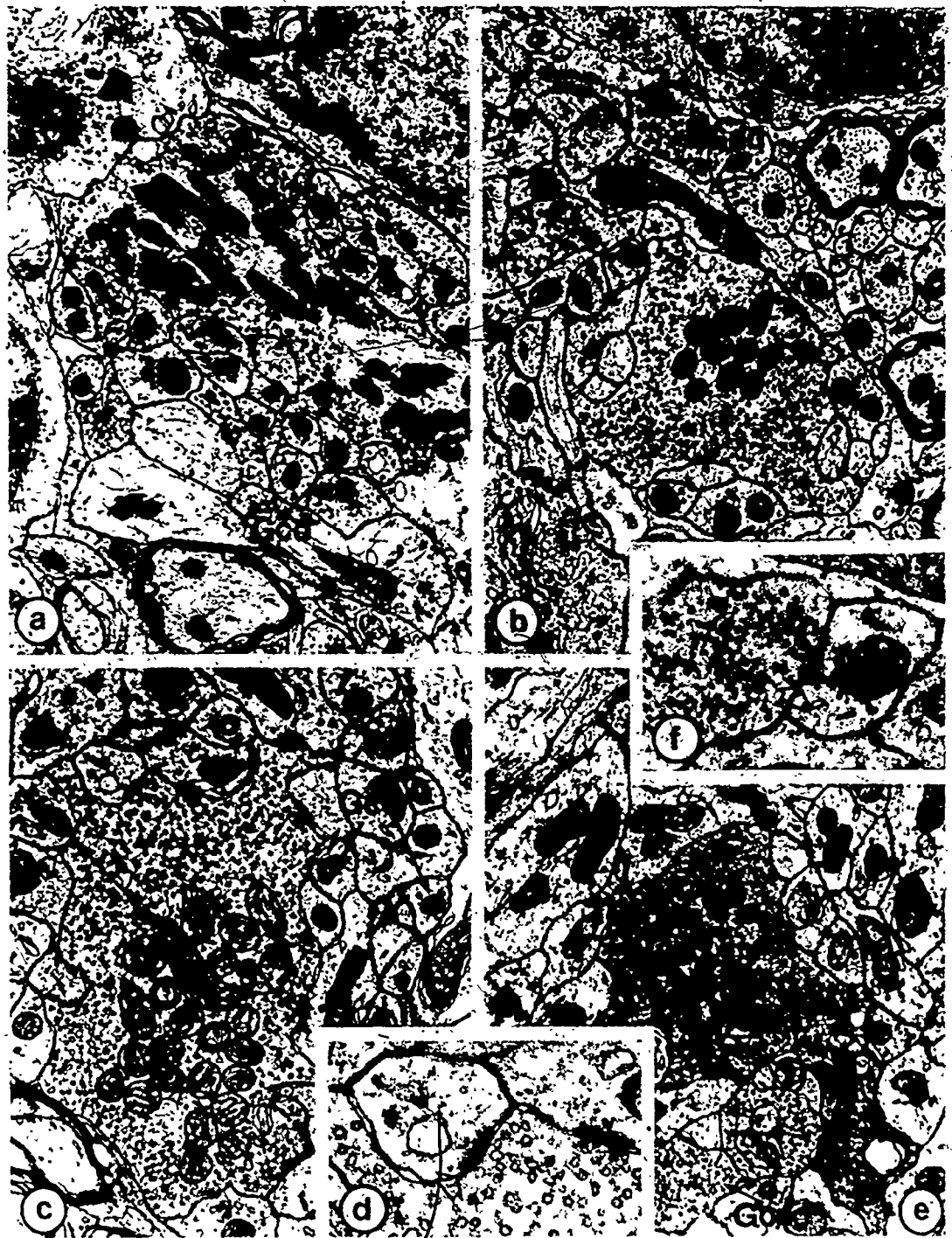


FIGURE 43

Electronmicrographs of the complex mossy fiber rosette of the adult cerebellar cortex.

- a. A complex mossy fiber rosette (cMFd) with a large central axonal enlargement, filiform appendages (open block arrows) and a dispersed population of synaptic vesicles. X 22,000.
- b. An oblique section of a complex mossy fiber rosette. The outline of this mossy fiber formation is not as smooth as that of the simple type. Filopodial extensions are found to project from the axonal enlargement giving it a more irregular profile (open block arrows). X 14,062.
- c. A filopodial extension from the complex mossy fiber rosette shown in Fig. 43a. Note that the vesicular and mitochondrial components extend into the axoplasm of these profiles. X 36,000.
- d. A filopodial extension from the complex mossy fiber rosette shown in Fig. 43b. This projection appears to form a synaptic contact with a granule cell dendrite (open block arrow). X 35,625.
- e. A highly irregular profile of a complex dispersed type of mossy fiber rosette (cMFd). Two filopodial appendages are shown projecting from this mossy fiber rosette (open block arrows). X 16,500.



FIGURE 44

Electronmicrographs of mossy fibers following short-term pontine ablation.

- a. A longitudinal section through the myelinated portion of a degenerating pontocerebellar fiber within the granule cell layer. 3d p.o. X 16,974.
- b. A transverse section through the myelinated portion of a degenerating pontocerebellar fiber. 4d p.o. X 15,000.
- c. A simple dispersed type of mossy fiber rosette (SMFd). Note the presence of several clear centered double membrane bound bodies. This mossy fiber rosette appears to be undergoing initial changes of degeneration. 3d p.o. X 15,000.
- d. A synaptic junction between a granule cell dendrite and the mossy fiber rosette shown in Fig. 44c. Note that the postsynaptic element, the granule cell dendrite, appears normal. X 37,500.
- e. A simple dispersed type of mossy fiber rosette. This rosette appears to be undergoing an electron-lucent form of degeneration. Note the formation of several clear centered double membrane bound bodies (dmb) and the clumping of the vesicular component (solid block arrows). 4d p.o. X 22,500.

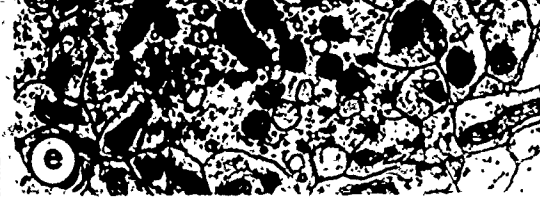
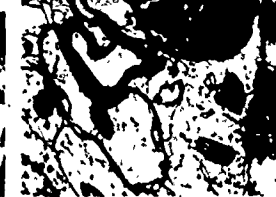
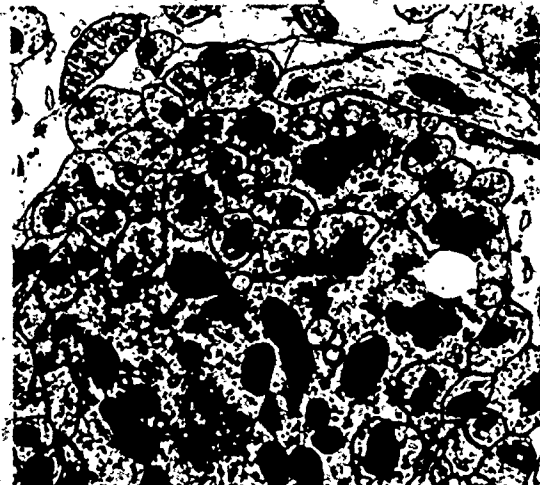
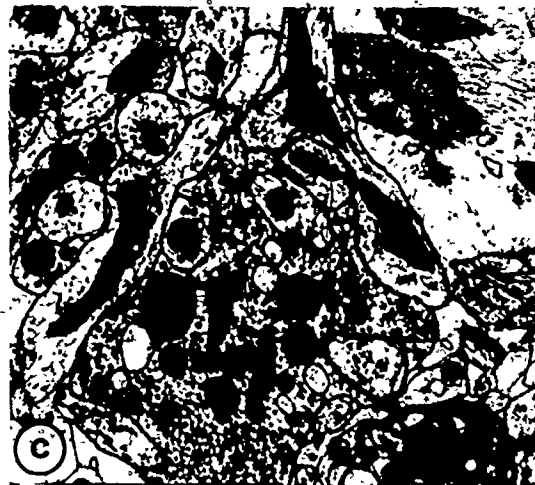


FIGURE 45

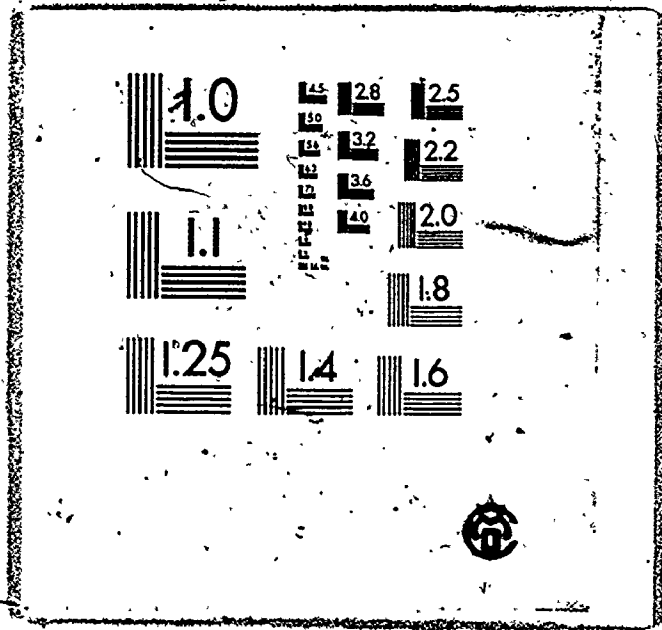
Electronmicrographs of cerebellar glomeruli following short-term pontine ablation.

- a, b. Two mossy fiber rosettes of the complex dispersed variety (cmFd) which appear to be undergoing an electron-lucent form of degeneration. Note that the vesicular component of both these mossy fiber rosettes is clustered forming small islands (solid block arrows). a: 3.5d p.o., b: 4d p.o. X 15,000.
- c. A synaptic junction between a digitiform dendrite of a granule cell and the mossy fiber rosette of the degenerating pontocerebellar fiber shown in Fig. 45a. Note that the postsynaptic element, the granule cell dendrite, appears normal. X 35,000.
- d. A simple mossy fiber rosette which is undergoing an electron dense form of degeneration. Both the axoplasmic matrix and the mitochondrial profiles within this rosette have become electron dense. 3.5d p.o. X 17,143.
- e. An extensive area along the periphery of this degenerating simple pontocerebellar rosette is denuded of its normal postsynaptic contact, the granule cell dendrite (solid block arrows). 4d p.o. X 19,500.



# 55

OF / DE



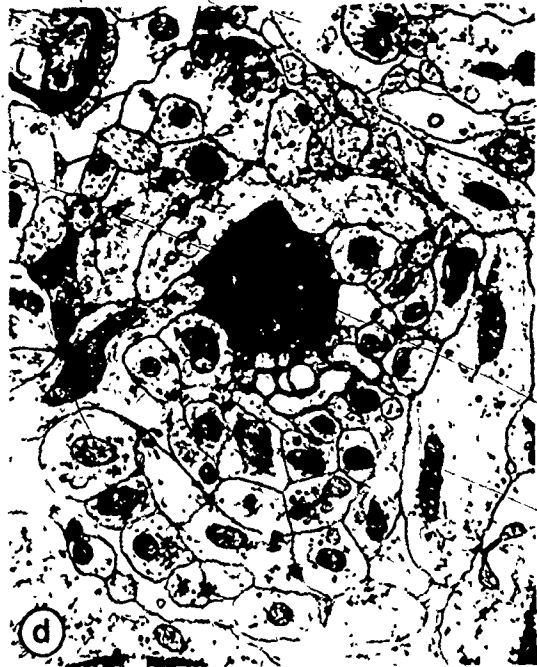


FIGURE 46

Electronmicrographs of cerebellar glomeruli following short-term pontine ablation.

- a. A pontocerebellar rosette which is in an advanced state of electron-dense degeneration. Note that this fragment of mossy debris maintains synaptic contact with several granule cell dendrites (open block arrows). 5d p.o. X 16,250.
- b,c. The preterminal portions of both these mossy fibers are totally engulfed by astrocytic-like glial profiles (gl) which may be active in the phagocytic removal of these degenerating fibers. 5d p.o.  
b: X 15,682, c: X 15,000.
- d. The cytoplasmic process of this phagocytic cell contains dense osmiophilic bodies (open block arrows) which are thought to represent the remains of electron dense pontocerebellar fibers. Note that in certain locations, the plasmalemma of this cell is directly adjacent to a degenerating mossy fiber rosette (solid block arrows); 5d p.o. X 15,682.

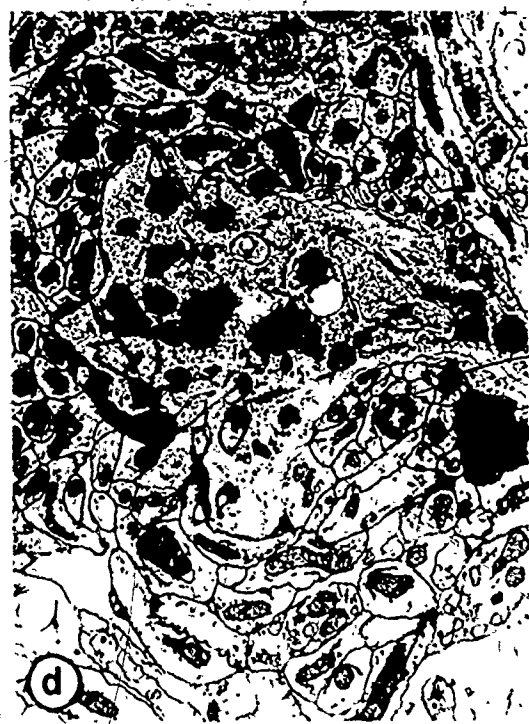
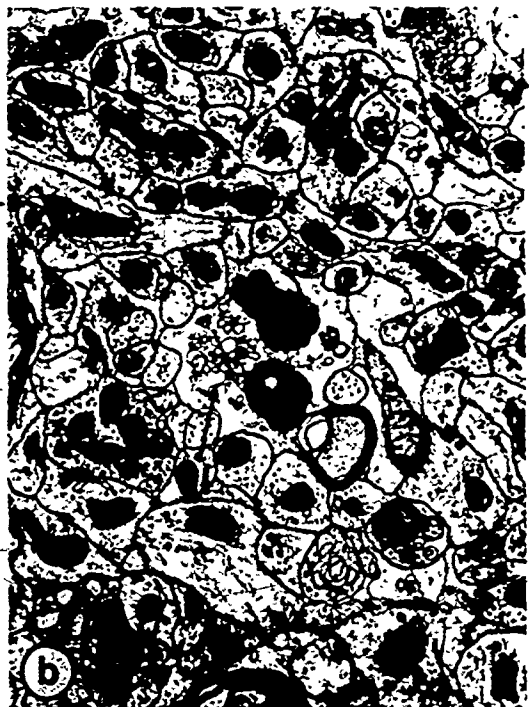


FIGURE 47

Photomicrographs of a Golgi-Cox preparation of a Purkinje cell following long-term mossy fiber ablation of the adult.

- A. A lower power view showing an entire Purkinje cell. Note that the reduction in size of the dendritic arborization of this cell, as compared to the adult control (Fig. 28a), appears to result primarily from a loss of terminal branchlets. 125d p.o. X 310.
- B. A higher power view showing that although the spines are not severely reduced in number, many of the spines which project from the terminal branchlets are hypertrophied (open block arrows). Several of these spines appear to have elongated to more than twice their original length. X 1,350.

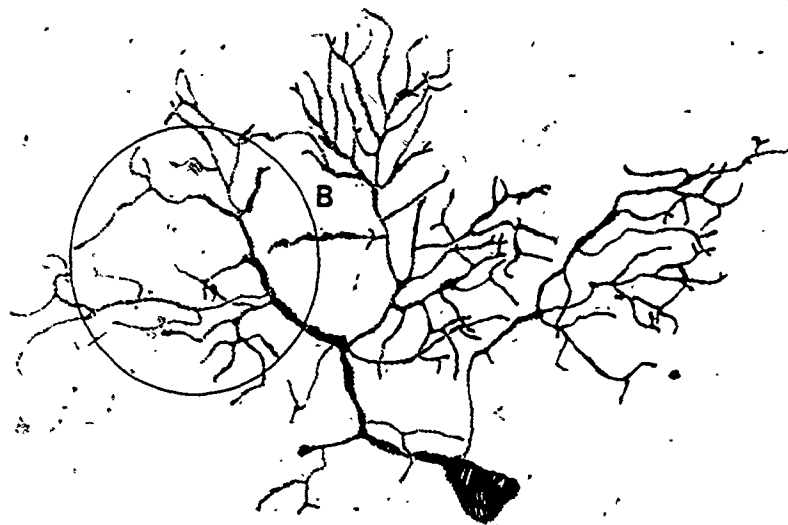


FIGURE 48

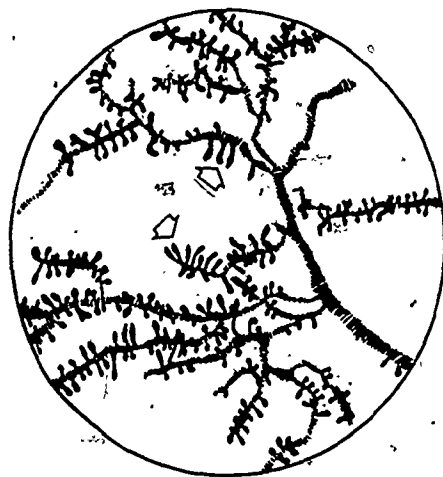
Camera lucida drawings of a Golgi-Cox preparation of a Purkinje cell following long-term mossy fiber ablation of the adult.

A. A drawing of the Purkinje cell in Fig. 42a. Note the marked decrease in the size of the dendritic tree of this cell as compared to the adult control (Fig. 29A). 125d p.o.

B. An enlargement of a terminal branchlet field (B). The number of dendritic spines does not appear to be altered but a large proportion of them are hypertrophied (open block arrows) in comparison with the adult control (Fig. 29C).



A



B



FIGURE 49

Electronmicrographs of cerebellar glomeruli following long-term pontine ablation.

a. A transverse section through a myelinated pontocerebellar fiber which is in an advanced stage of electron-dense degeneration. 40d p.o. X 16,250.

b. Degenerative debris within a preterminal portion of a pontocerebellar fiber. 35d p.o. X 15,682.

c. The electron-dense remains of a simple dispersed type of mossy fiber rosette (SMFd). Note that the increased electron opacity of the axoplasmic matrix and the pleomorphic shape of the vesicular population. 35d p.o. X 15,000.

d. A pseudopodial process (Pp) from a digitiform dendrite of a granule cell. This profile appears as if it is being engulfed by a pontocerebellar rosette which is in an advanced stage of electron-dense degeneration. X-34,687.

e. The electron-dense remains of a simple dispersed type of mossy fiber rosette (SMFd). Note the clear spaces within the center of this rosette and the persistence of synaptic contacts with the postsynaptic element, the granule cell dendrite. 40d p.o. X 15,804.

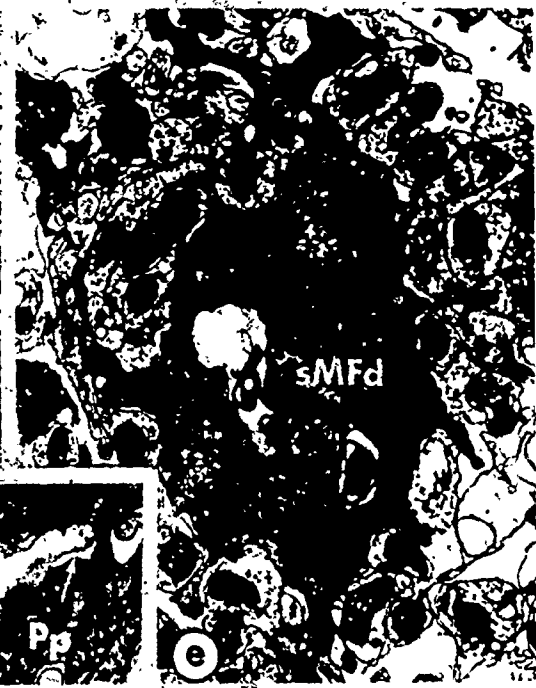
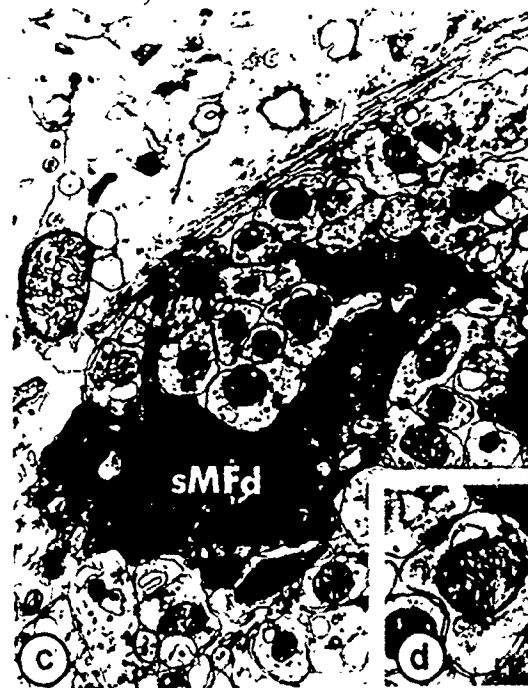
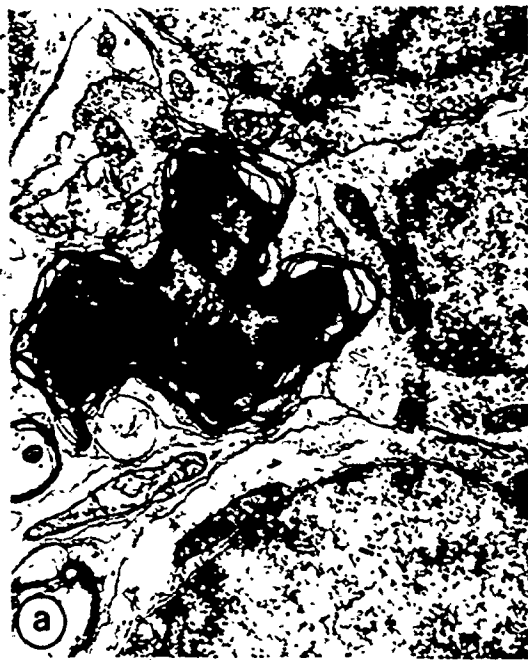


FIGURE 50

Electronmicrographs of cerebellar glomeruli following long-term pontine ablation.

- a. The electron-dense remains of a complex dispersed type of mossy fiber rosette (cMFd). Note the increased electron opacity of the axoplasmic matrix, the pleomorphic shape of the synaptic vesicle population and the absence of reactive glial profiles. 35d p.o. X 16,800.
- b. The degenerative debris of this mossy fiber rosette filopodial profile is highly irregular in shape. This profile is in synaptic association with an adjacent granule cell dendrite (Gcd) (open block arrow). 4d p.o. X 37,500.
- c. A normal appearing Golgi cell axon (Gox) which appears to synapse with the outer surface of several granule cell dendrites. 40d p.o. X 33,750.
- d. The electron-dense debris of several filopodial profiles of a complex dispersed type of mossy fiber rosette (cMFd). 40d p.o. X 16,875.
- e. Two postsynaptic granule cell dendrites (Gcd) adjacent to the electron-dense debris of a filopodial branch of a mossy fiber rosette. Note the highly swollen tubular profiles of smooth endoplasmic reticulum and the increased electron opacity of the mitochondrial profiles. 40d p.o. X 28,125.

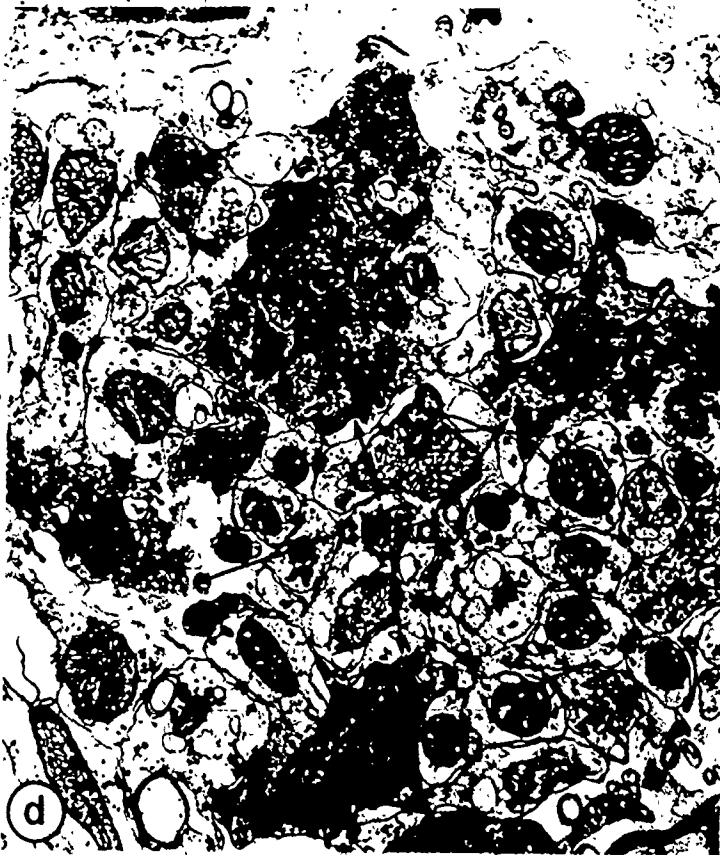
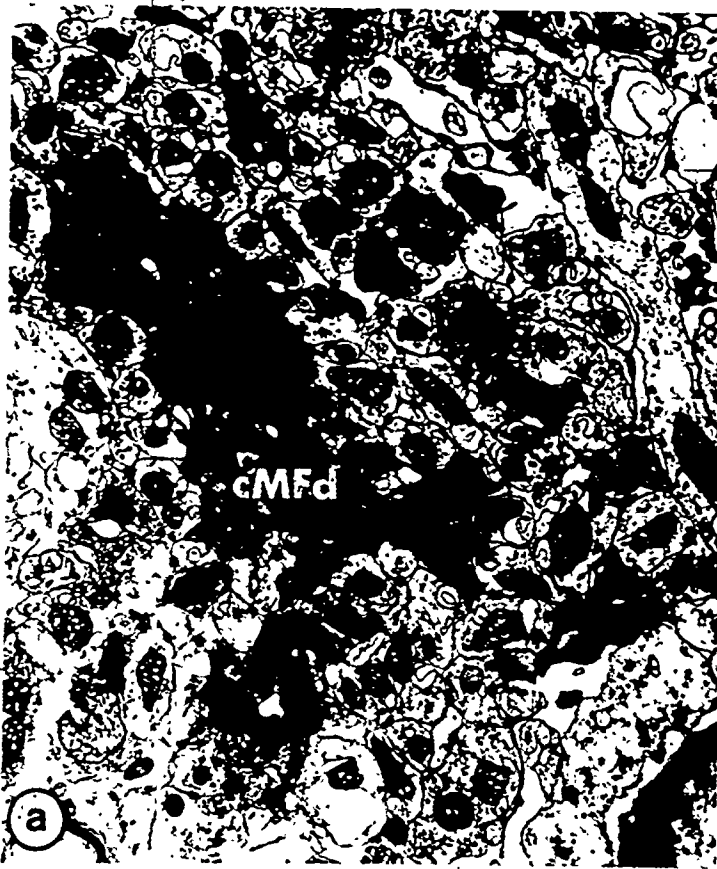


FIGURE 51

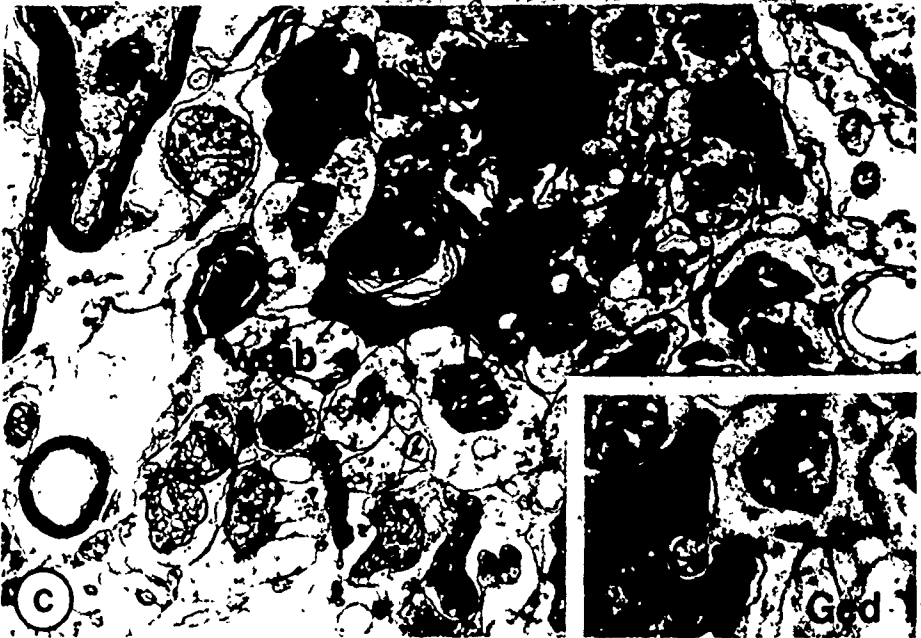
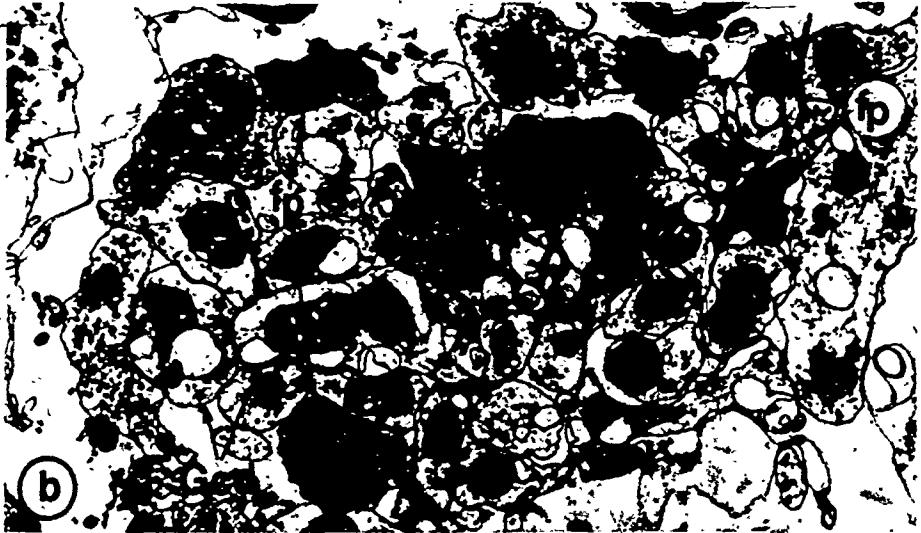
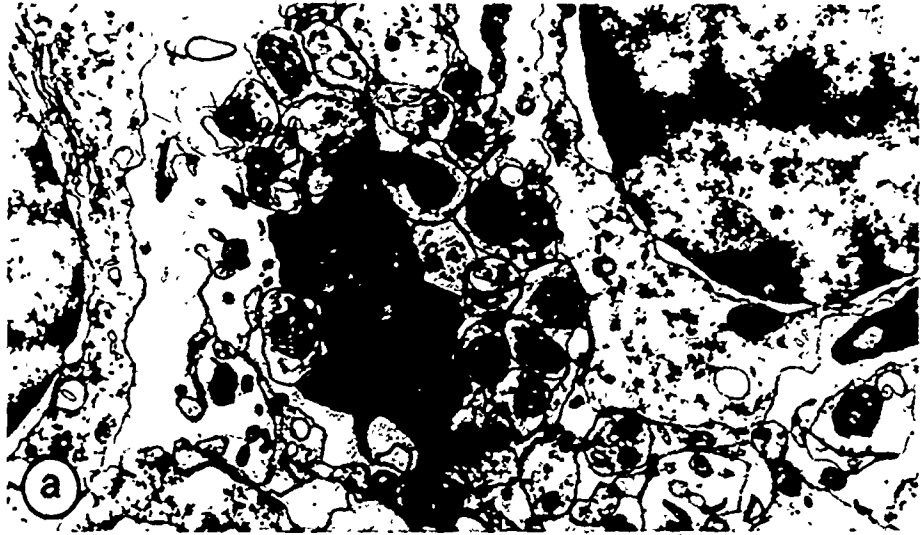
Electronmicrographs of cerebellar glomeruli following long-term pontine ablation.

a. Note that the size of this degenerating mossy fiber rosette appears markedly reduced and the axoplasm and its contents more electron opaque than the majority of the degenerating terminals found prior to this postoperative stage. The synaptic contacts between this simple mossy fiber rosette and the granule cell dendrite appear to be intact (solid block arrows). Note the pseudopodial-like process from this electron-dense pontocerebellar terminal which appears to be involved in pinching off a portion of the postsynaptic granule cell dendrite (open block arrow). 57d p.o. X 16,876.

b. Note that the filopodial profiles (Fp) of this complex mossy fiber rosette persist as small fragments of electron-dense debris. Transneuronal degenerative changes appear to have taken place within the postsynaptic elements of the pontocerebellar terminal, the granule cell dendrites (Gcd). Note the highly swollen tubular profiles of smooth endoplasmic reticulum and the electron-dense mitochondrial profiles. 57d p.o. X 16,184.

c. Along with an increase in electron opacity, this mossy fiber rosette contains whorled membranous bodies (wmb) and vacuolated regions which possess small electron opaque profiles (open block arrows). Note that these latter profiles closely resemble pseudopodial-like processes found projecting from the granule cell dendrite (solid black arrow and inset). 57d p.o. X 16,500.

Inset - A portion of a degenerating pontocerebellar terminal which appears to be involved in the removal of its postsynaptic element, the granule cell dendrite (Gcd). 57d p.o. X 30,000.



*[Handwritten notes and markings on the right margin, including a vertical line and illegible text.]*

FIGURE 52

Electronmicrographs of cerebellar glomeruli following long-term pontine ablation.

- a. A myelinated pontocerebellar fiber in an advanced stage of electron-dense degeneration within the granule cell layer. 80d p.o. X 19,412.
- b. A reactive glial cell that contains degenerative debris, fragments of the pontocerebellar system. 80d p.o. X 11,875.
- c. A remnant of a mossy fiber rosette that appears as a small island of necrotic debris during the final stage of resorption. 80d p.o.
- d. A dendritic island (DI) which is partially ensheathed by an outer layer of Golgi cell axons (Gox). This structure is thought to represent a glomerular profile which is deafferentated of its axonal core. 80 d p.o. X 15,750.

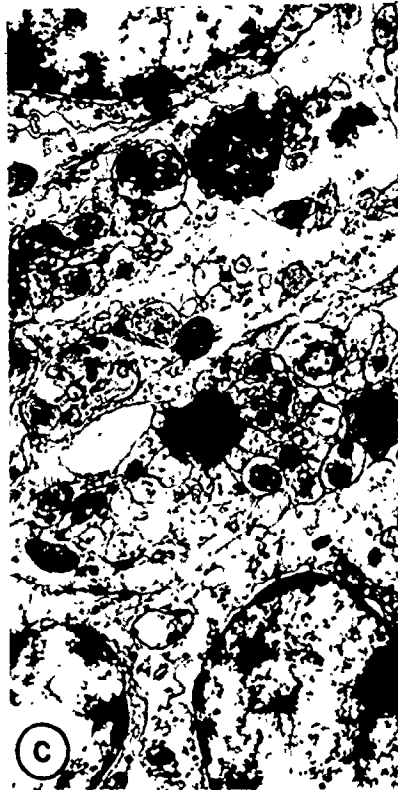
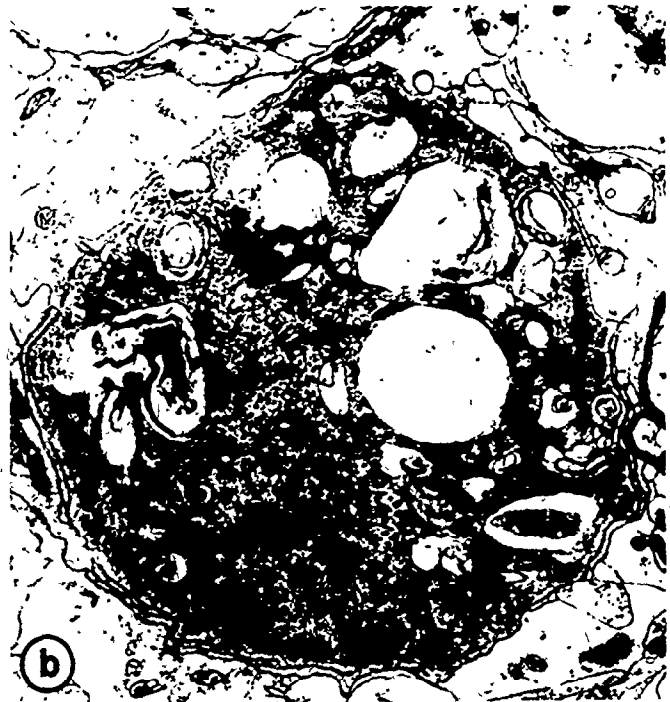




FIGURE 53

Electronmicrographs of cerebellar granule cells following long-term pontine ablation.

- a. A normal granule cell within the granule cell layer of the adult rat. Note the thin rim of cytoplasmic matrix which surrounds the nucleus of these cells. X 16,875.
- b. A reactive glial cell (RG) adjacent to a degenerating mossy fiber glomerulus. 57d p.o., X 10,714.
- c. A reactive glial cell (RG) and an adjacent degenerating soma of a granule cell (GC). This cell appears electron-lucent because of its highly swollen nuclear envelope and attenuated layer of cytoplasm. 57d p.o. X 10,714.
- d. A granule cell soma thought to be undergoing transneuronal degeneration because of its enlarged perinuclear space, attenuated cytoplasm and swollen Golgi complex. 57d p.o. X 10,625.



FIGURE 54

Electronmicrographs of a control Purkinje cell primary dendrite and spiny branchlet.

- a. A primary dendrite of a Purkinje cell (Pcd<sub>1</sub>). This primary trunk shows several features of a Purkinje cell, particularly the prominent microtubule element and the hypolemmal cisterna. X 5,000.
- b. A Purkinje cell spiny (terminal) branchlet. The hypolemmal cisterna, the concentration of mitochondrial profiles and the dendritic spines are all distinguishing features of the spiny branchlet. Note the thorn which emerges from this spiny branchlet to synapse with a parallel fiber varicosity (asterisks). X 13,600.



FIGURE 55

Electronmicrographs of the cerebellar molecular layer following long-term pontine ablation.

- a. A low power view of a large secondary Purkinje cell dendrite ( $Pcd_2$ ) and the adjacent neuropil. Notice the loose organization and the increased electron opacity of the adjacent neuropil. The outline of this dendrite is highly irregular, the hypolemmal cisternal system appears hypertrophied and the cisternal spaces enlarged (open block arrows). 40d p.o. X 10,000.
- b. Note that at a higher magnification, the increased electron density of the adjacent neuropil appears dependent upon the enhanced opacity of the parallel fiber profiles (pf). 40d p.o. X 26,667.
- c. Two degenerating electron opaque parallel fiber axons sectioned along their long axis (open block arrows). Notice also a transneuronally degenerating Purkinje cell dendrite (possibly a tertiary branch) with its highly irregular form and enlarged hypolemmal cisternal system (solid arrows). 57d p.o. X 11,364.
- d. Two varicosities of degenerating parallel fibers in (open block arrows) synaptic contact with their normal postsynaptic element, the Purkinje cell dendritic spine (ds). Note that the dendritic spines show no signs of degeneration. 57d p.o. X 25,000.
- e. A high power view of a parallel fiber (Pf) sectioned along its longitudinal axis. This axon appears to be undergoing an electron-dense form of transneuronal degeneration because of the increased electron opacity of the axoplasmic matrix. 57d p.o. X 25,000.

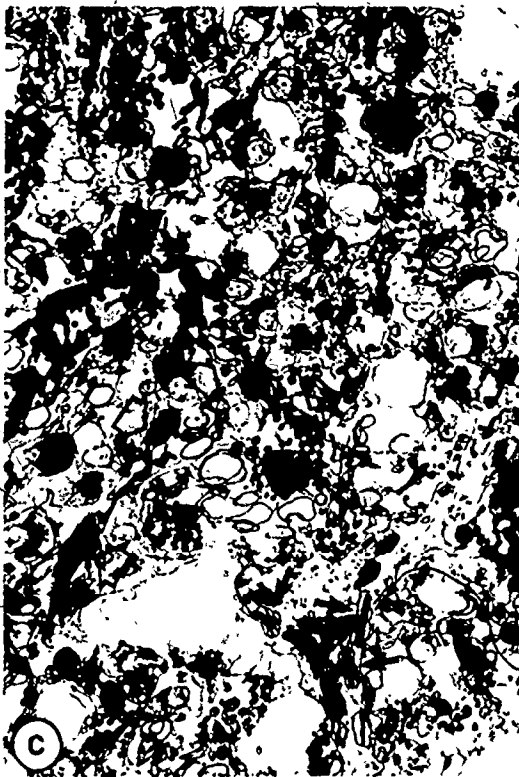
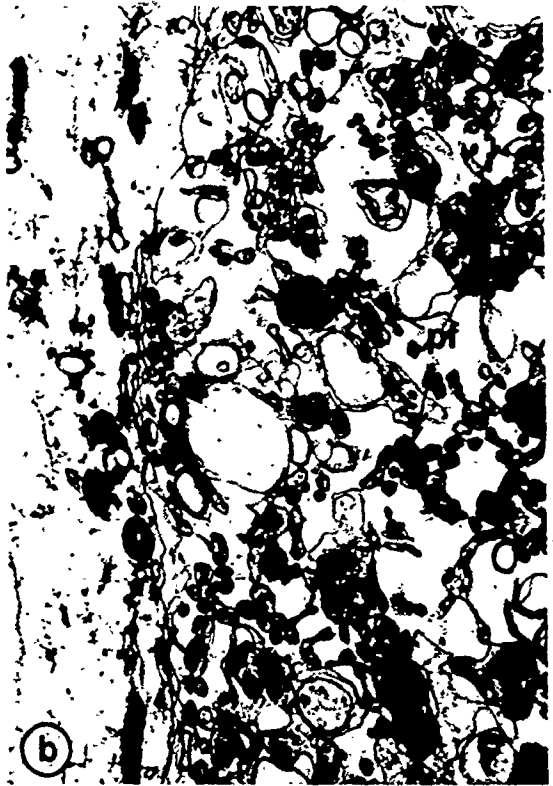
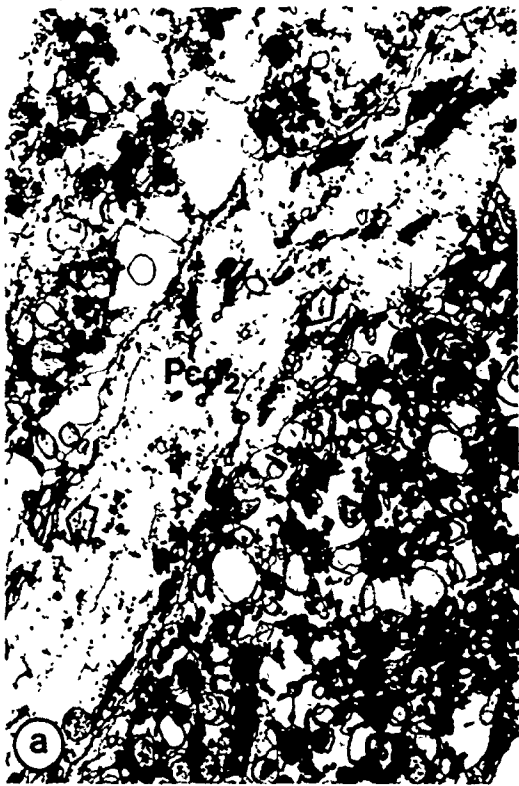


FIGURE 56

Electronmicrographs of the cerebellar molecular layer following long-term pontine ablation.

- a,c. Low power views of the neuropil in the molecular layer. Note that the transneuronal degeneration of various cerebellar dendritic elements has contributed to the overall electron opacity of the molecular layer (solid arrows). 57d p.o. a: X 10,909, b: X 11,667.
- b. A high power view of an electron-dense dendritic element within the molecular layer of Fig. 56a. Note the size of this dendritic profile and the presence of a hypolemmal cisternal system within this element. This dendritic profile is thought to be a terminal (spiny) branchlet (SpB) from a Purkinje cell dendritic tree. 57d p.o. X 24,545.
- d. A high magnification view of an electron opaque dendritic element within the molecular layer of Fig. 56c. Note the lack of spine processes but the presence of a hypolemmal cisternal system. This profile is thought to represent a smooth branch within a Purkinje cell dendritic tree (sPcd). 57d p.o. X 20,833.

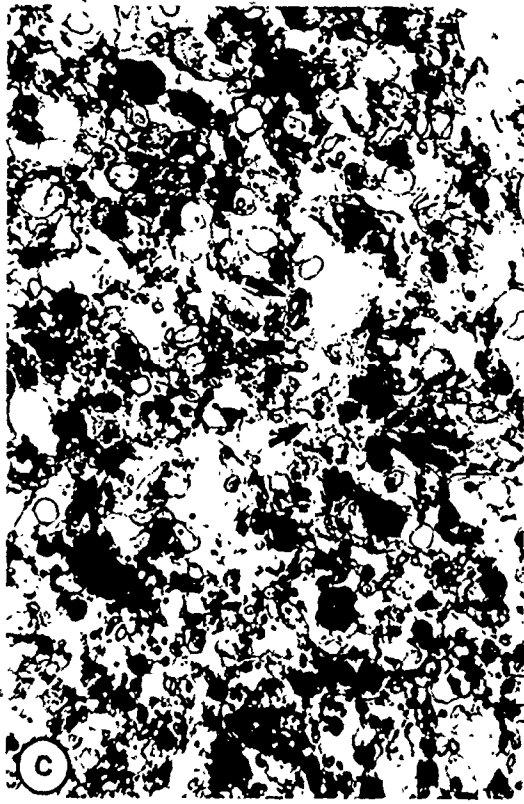
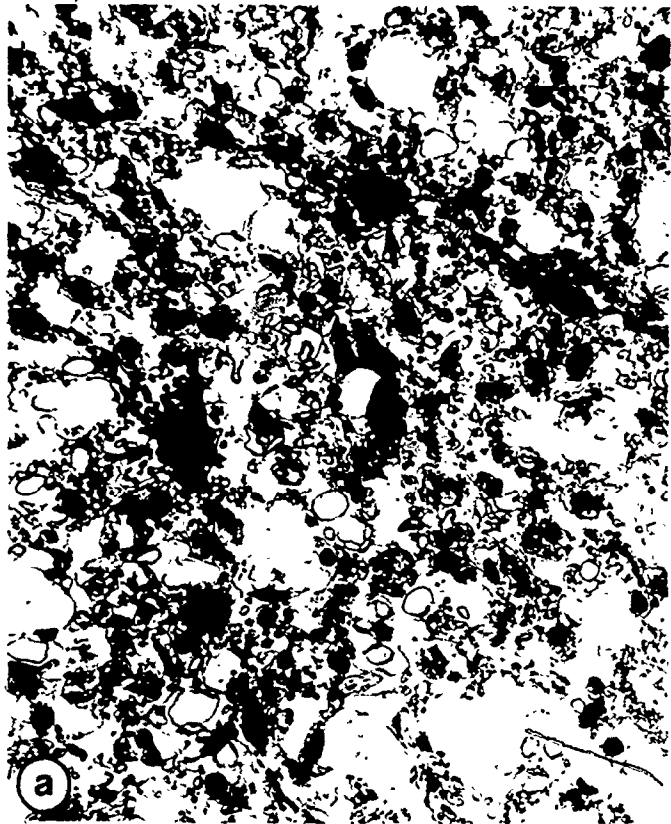




FIGURE 57

Electronmicrographs of the cerebellar molecular layer following long-term pontine ablation.

a,b,c. High power views of the molecular layer neuropil. Note that electron opaque dendritic profiles which do not originate from Purkinje cells are found within the molecular layer neuropil. The neuropil of all three electronmicrographs contains small degenerative fragments of dendrites which lack a complement of spines and a hypolemmal cisternal system. These dendritic profiles are characterized instead by multiple synaptic contacts along their dendritic shafts (open block arrows). These features are more characteristic of dendritic profiles which originate from the somata of cerebellar interneurons (basket and stellate cells). 80d p.o. a: X 33,182, b: X 32,500, c: X 25,000.

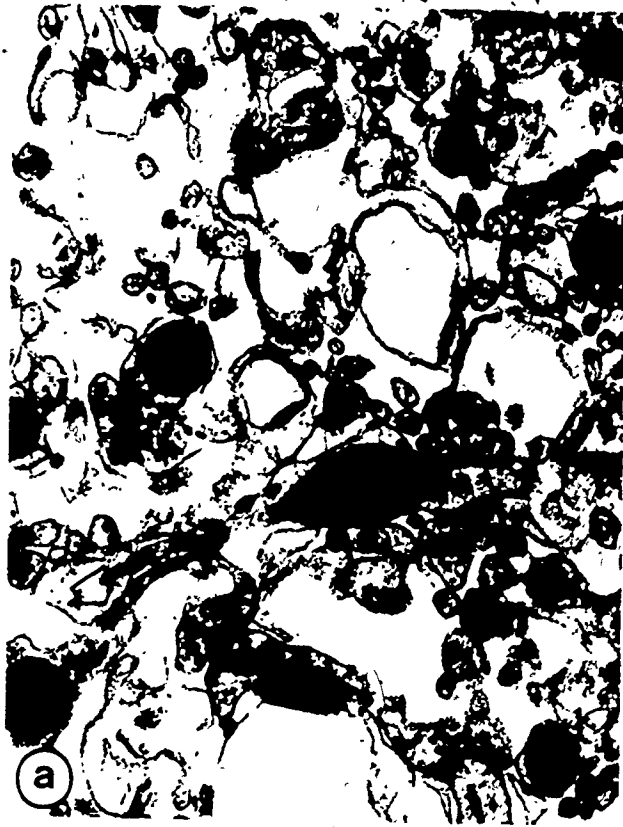


FIGURE 58

A photomicrograph (A) and a series of drawings (B) representing coronal sections through the rostrocaudal extent of a parasagittal lesion within the lateral cerebellar hemisphere (GL - granule cell layer; ML - molecular layer; ND - dentate nucleus; NF - fastigial nucleus; NI - interpositus nucleus; WM - white matter).



FIGURE 59

Electronmicrographs of the granule cell layer.

- a. A CONT. The Purkinje cell (PC) - granule cell (GC) junction within a normal cerebellar cortex. Note the close juxtaposition of the somata of these granule cells. Their nuclei are conspicuous because of their clumps of condensed chromatin. The thin layer of cytoplasm associated with these cells contains mitochondria, profiles of granular and smooth endoplasmic reticulum, free clusters and rosettes of ribosomes and Golgi complexes. X 2,969.
- b. A CERB L. The cytoplasmic matrix of these cells (GC) appears more electron-lucent than in the control granule cell because of a peripheral loss of cytoplasmic organelles within several of the somata. 4d p.o. X 1,857.
- c. A CERB L. Note the marked increase in electron density of several granule cells (solid block arrows) and the loss of cytoplasmic organelles in others (open block arrow) suggesting that extensive retrograde degeneration has occurred within this region of the granule cell layer following parallel fiber axotomy. 57d p.o. X 3,136.

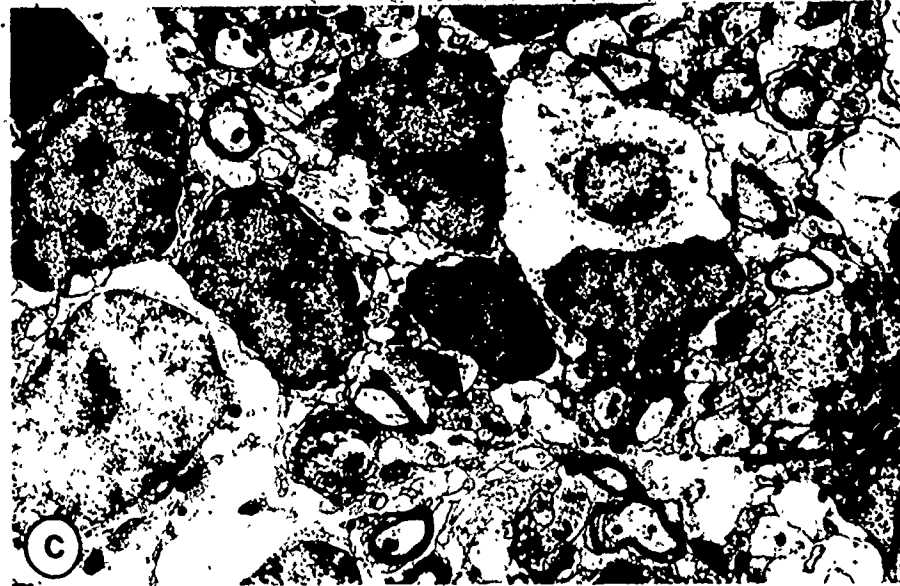
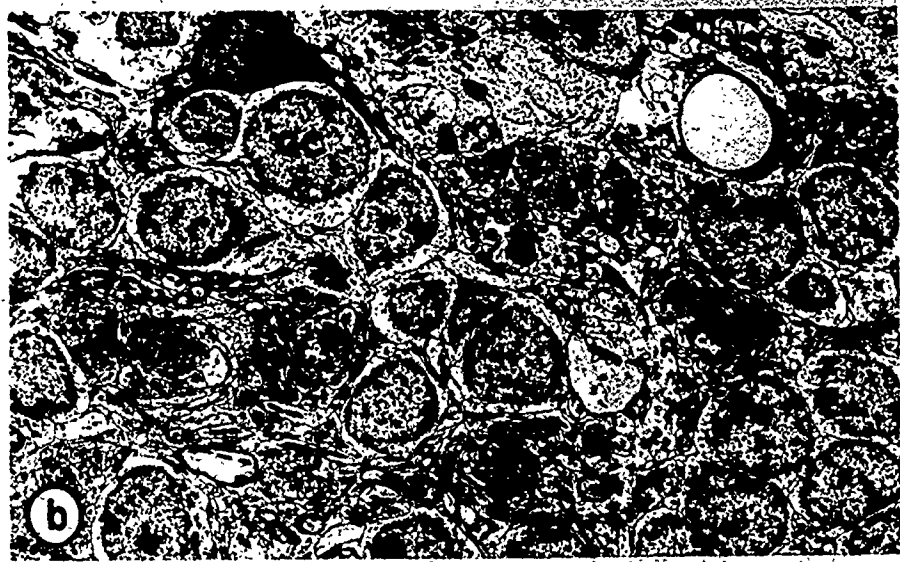


FIGURE 60

Electronmicrographs of the molecular layer of the cerebellar cortex following a parallel fiber transection.

- a. A CONT. A primary trunk of a Purkinje cell (Pcd<sub>1</sub>). Note that the adjoining neuropil consists primarily of parallel fibers (pf) which run perpendicular to this plane of section. X 15,000.
- b. A CONT. A high power view of a parallel fiber (pf) - dendritic spine (ds) synapse (open block arrow). Note the asymmetry of the pre- and postsynaptic densities, the widened interstitial cleft and the loose aggregate of synaptic vesicles associated with the axolemma. This Purkinje cell dendritic spine (ds) is cut transversely and contains a few profiles of smooth endoplasmic reticulum. X 30,000.
- c. A CERB L. A primary trunk of a Purkinje cell (Pcd<sub>1</sub>). Note that the adjoining neuropil contains several small electron-dense profiles of parallel fibers scattered throughout the molecular layer (black arrows). 4d p.o. X 11,250.
- d. A CERB L. These electron-dense profiles (black arrows) can be identified as parallel fiber varicosities because of their synaptic association with Purkinje cell dendritic spines (ds). 3.5d p.o. X 10,000.
- e. A CERB L. A high power view of an electron dense profile found in Fig. 60d. This profile closely resembles the control parallel fiber varicosity found in Fig. 60b. X 30,000.
- f. A CERB L. A high power view of the molecular layer. This dendritic spine (ds) possesses a probable postsynaptic density which appears to be denuded of its synaptic input. Note the electron-dense parallel fiber varicosity immediately adjacent to this dendritic spine (black arrow). 4d p.o. X 10,000.
- g. W CERB L. A mossy fiber glomerulus (cMFd) within the granule cell layer. Note the increased electron opacity of several of the digitiform dendrites along the circumference of this rosette (black arrows). 4d p.o. X 11,667.
- h. W CERB L. Note that a similar pattern of electron-dense degeneration results following parallel fiber transection of the weanling rat. 35d p.o. X 10,000.

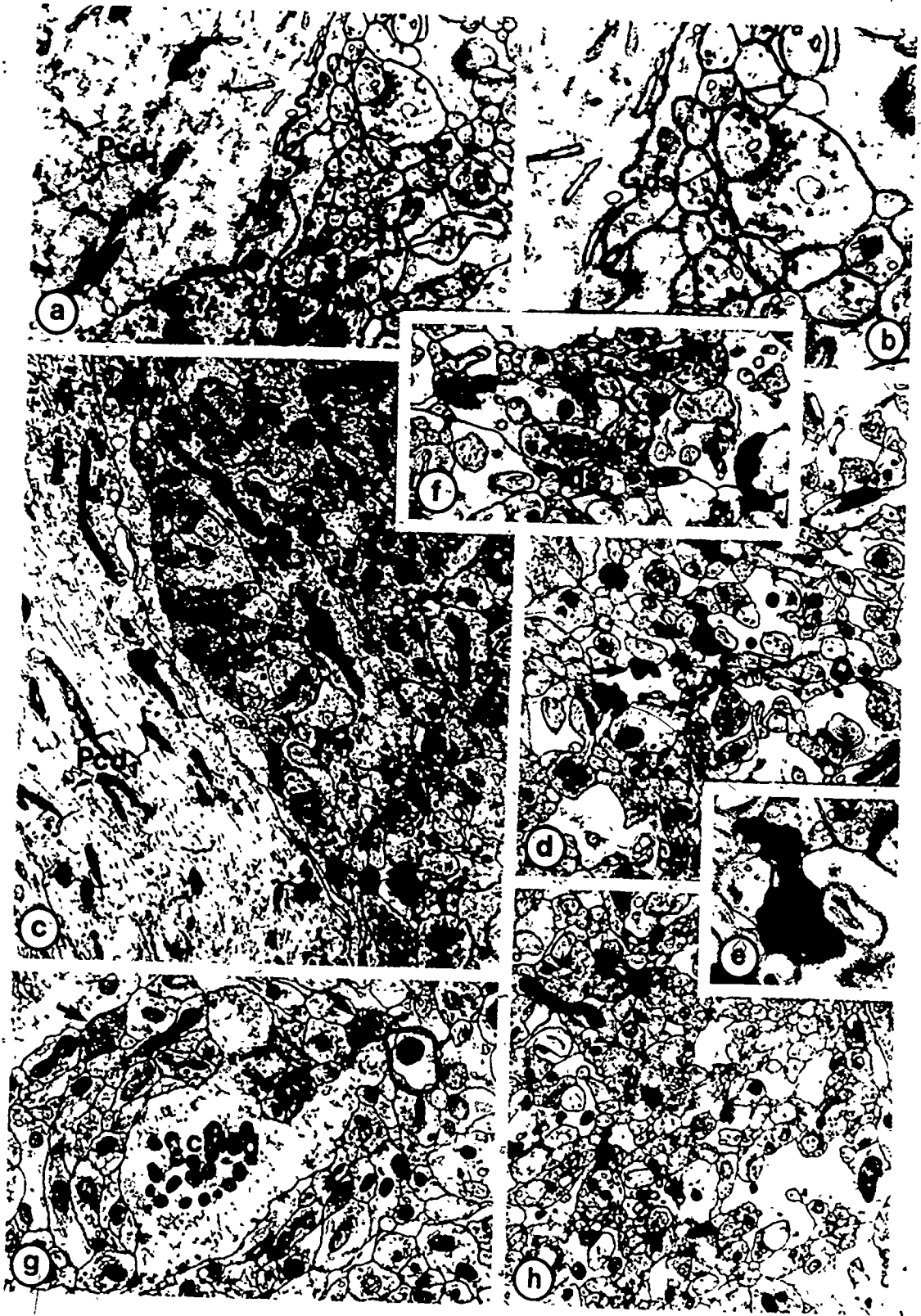




FIGURE 61

Photomicrographs of Golgi-Cox preparations of Purkinje cells following long-term parallel fiber-deafferentation.

- a. W CERB L. A low power view of a deafferentated Purkinje cell. Note the overall reduction in density of the dendritic arborization and in particular the decrease in the number of terminal branchlets. 120d p.o. X 282.
- b. W. CERB L. A high magnification view of a field of terminal branchlets taken from a peripheral region of the Purkinje cell dendritic tree shown in Fig. 61A. Note the near absence of dendritic spines that project from these terminal branchlets. 120d p.o. X 1,174.
- c. W CERB L. A high magnification view of a field of terminal branchlets\* taken from a deeper region of the Purkinje cell dendritic tree shown in Fig. 61A. While dendritic spines do persist along these branches, the density of these spines is considerably reduced (open block arrows). 120d p.o. X 1,216.
- d. W CERB L. Dendritic spines along the terminal branchlets. Note their reduced number and increased length (open block arrows). 122d p.o. X 1,120.\*\*
- e. A CERB L. Hypertrophied (elongated) dendritic spines, similar to that found in the W CERB L, projecting from terminal branchlets of deafferentated adult Purkinje cells (open block arrows). 120d p.o. X 1,200.
- f. A CERB L. A low power view of a deafferentated Purkinje cell. Note the sparsity of the dendritic arborization which consists largely of a primary trunk, two large secondary dendrites and a few isolated segments of terminal branchlets. 120d p.o. X 339.



FIGURE 62

Camera lucida drawings of a Golgi-Cox preparation of a Purkinje cell following long-term parallel fiber-deafferentation in an adult rat.

- A. A drawing of the Purkinje cell in Fig. 61f. Note the sparsity of the dendritic arborization of this deafferentated Purkinje cell. Its dendritic tree consists largely of a single primary trunk and two large secondary dendrites.  
120d p.o.
- B. An enlargement of the field of terminal branchlets indicated by the circle (B). While the loss of dendritic spines is substantial, persisting spines are markedly increased in size (open block arrows).



FIGURE 63

Camera lucida drawings of a Golgi-Cox preparation of a Purkinje cell following long-term parallel fiber-deafferentation of a weanling rat.

- A. A drawing of the dendritic arborization of the deafferentated Purkinje cell in Fig. 61a. Note the reduced number of terminal branchlets (smallest caliber dendrites) within the dendritic arborization of this cell. 120d p.o.
- B. An enlargement of the field of terminal branchlets (B). Note the reduction in the number of dendritic spines along these terminal branchlets as compared to the adult control (Fig. 29C).
- C. An enlargement of the peripheral field of terminal branchlets indicated by the circle (C). Note the lack of dendritic spines along terminal branchlets within this portion of the dendritic tree.

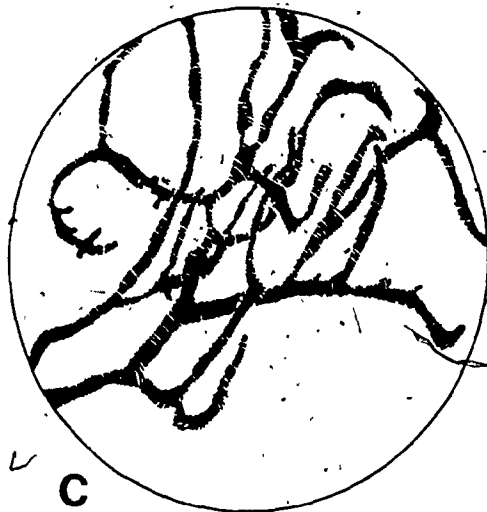
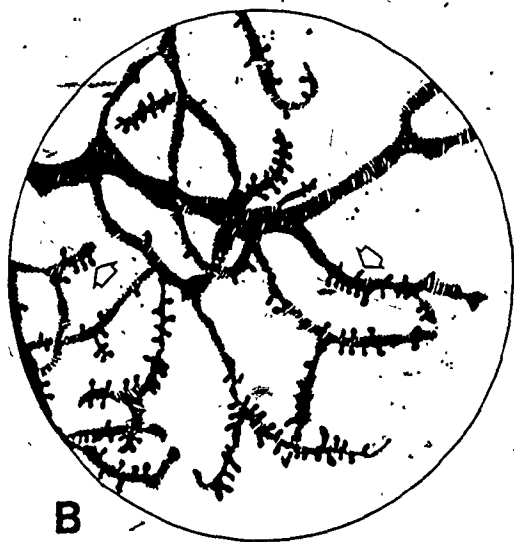
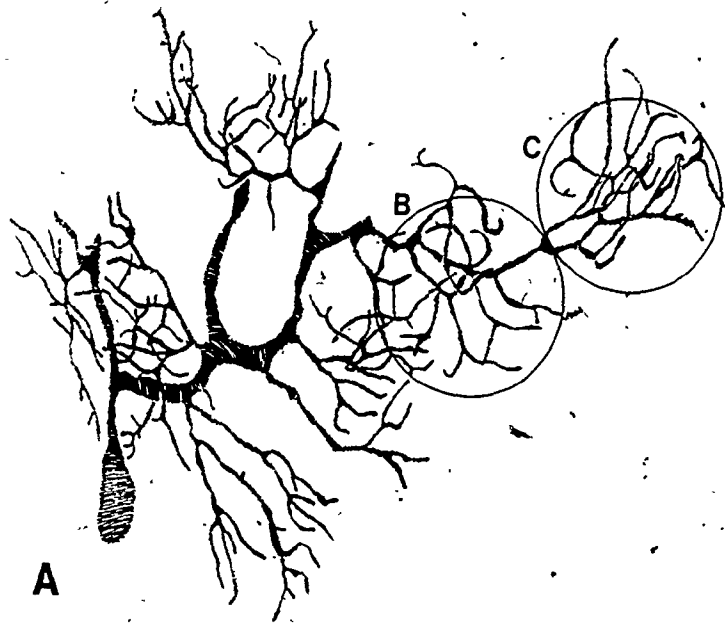


FIGURE 64

Electronmicrographs of the molecular layer of the cerebellar cortex following long-term parallel fiber-deafferentation of the adult rat.

- a. Under low power areas of the molecular layer are found to contain a number of large electron-lucent profiles. 57d p.o. X 4,071.
- b. A higher power view of 64a showing that these profiles contain remnants of organelles which are thought to represent the cytoplasmic remains of dendrites, probably primary trunks of Purkinje cells. X 7,500.
- c. An oblique section through a degenerating secondary dendrite within the smooth portion of the Purkinje cell dendritic tree (Pcd<sub>2</sub>). Note that this dendrite contains several whorled membranous bodies (hypolemmal cisternae - black arrows). 93d p.o. X 10,909.
- d. A high power view of the whorled membranous bodies (wmb) which occupy a major portion of the dendritic matrix of the secondary dendrite in Fig. 64b. Their localization immediately beneath the plasmalemma suggests that they may be a derivative of the hypolemmal cisternal system. X 20,938.
- e. An oblique section through a higher ordered smooth branch from a Purkinje cell dendritic tree (Pcd<sub>3</sub>). Note the whorled membranous bodies which are a prominent feature of this small caliber Purkinje cell smooth branch. 91d p.o. X 15,750.

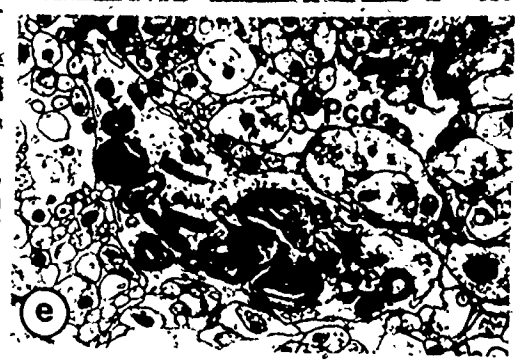




FIGURE 65

Electronmicrographs of the molecular layer of the cerebellar cortex following long-term parallel fiber-deafferentation of the adult rat.

- a. A transverse section through a degenerating profile of a terminal branchlet from a Purkinje cell dendritic tree (SpB). Note the hypertrophied spine (Hs) projecting from this terminal branchlet and the enlarged glial profiles (gl) which engulf a major portion of this dendritic profile and spine. 57d p.o. X 20,000.
- b,c. Two fields of molecular layer neuropil. Note the long attenuated strands of electron dense debris which traverse long expanses of molecular layer. These profiles are completely ensheathed by glia. Note the fine caliber and planar orientation of this electron dense debris which is thought to represent small caliber dendrites within the smooth portion of the Purkinje cell dendritic tree. 93d p.o. X 16,875.
- d. A transverse section of a small caliber Purkinje cell dendrite (possibly a terminal branchlet) in an advanced stage of electron-dense degeneration. 93d p.o. X 15,750.

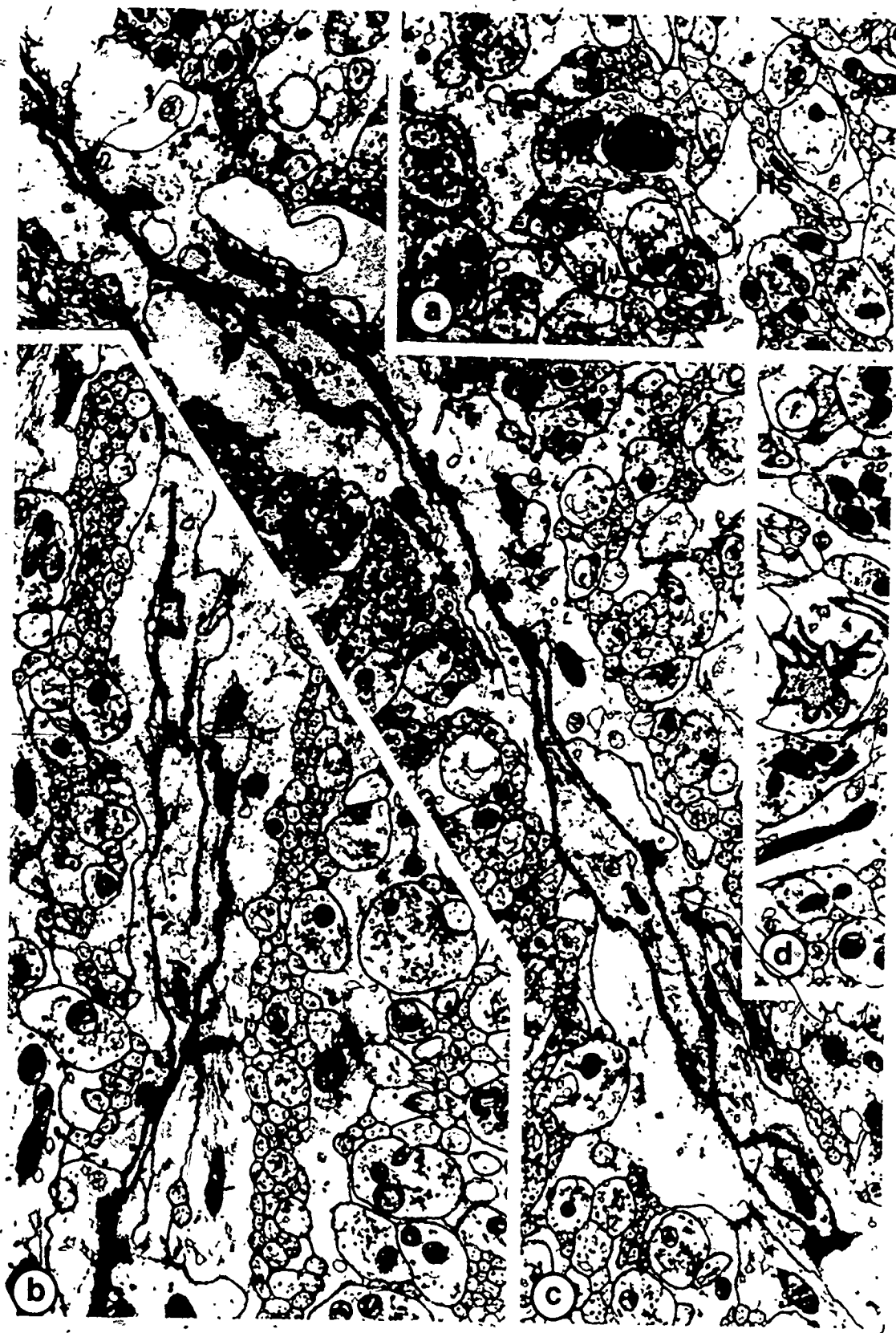


FIGURE 66

Electronmicrographs of the molecular layer following long-term-parallel fiber-deafferentation.

- a,b,c. A CERB L. Three profiles of degenerating terminal (spiny) branchlets. Note the reduction in the number of parallel fiber profiles and the hypertrophied Bergmann glial profiles (Bg) within the molecular layer neuropil. Large expansions of glial profiles are a common feature along the surface of these terminal branchlets and spines (asterisks). Note that many of these spines appear to be separated a considerable distance from the parallel fiber milieu because of this glial covering. The dendritic matrix of these terminal branchlets is markedly increased in electron opacity. 57d p.o. a: X 10,500, b: X 15,833, c: X 22,640.
- d. W CERB L. A degenerating profile of a terminal branchlet. Note the marked loss in the parallel fiber content of the adjacent neuropil and the hypertrophied glia (Bergmann processes) (Bg) which forms a thick sheath around a large portion of this spiny branchlet. 55d p.o. X 11,110.
- e. W CERB L. An electron-dense profile of a degenerating terminal branchlet. Note that the dendritic spine (ds) of this terminal branchlet is ensheathed by a thickened layer of glia. 55d p.o. X 32,500.



FIGURE 67

Electronmicrographs of stellate cells following long-term parallel fiber-deafferentation of the adult rat.

- a. A normal perikaryon from a superficial stellate cell (SC). The nucleus of this cell is slightly lobulated and the cytoplasm contains the usual complement of organelles, the most prominent being the Golgi complex. Note that the soma of this cell bears four synaptic contacts with parallel fiber varicosities (black arrows). X 10,833.
- b. A stellate cell dendrite (Scd). Notice that this dendrite bears three synaptic contacts with parallel fiber varicosities within this short segment (asterisks). X 21,667.
- c. A degenerating soma of a stellate cell. Note that this cell has a slightly lobulated nucleus, a thin cytoplasmic layer and few axosomatic contacts (black arrows). 57d p.o. X 16,304.
- d. A profile of a microglia-like cell found within the molecular layer of the cerebellar cortex. 57d p.o. X 15,000.
- e,f. Profiles of degenerating stellate cell dendrites. These profiles have undergone electron-dense degeneration. Note that the parallel fiber input to these degenerating profiles appears normal. 57d p.o. e: X 15,000, f: X 22,000.

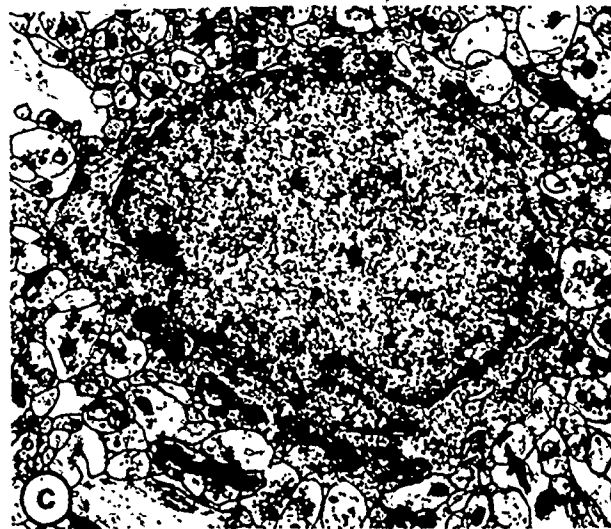
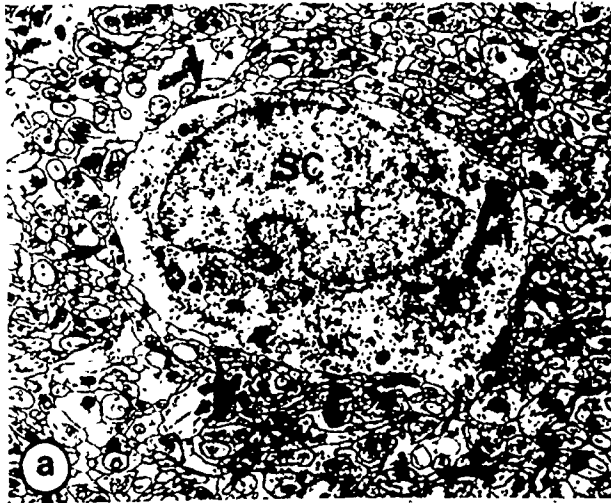


FIGURE 68

Electronmicrographs of dendritic spines along Purkinje cell terminal branchlets following long-term parallel fiber-deafferentation.

- a. A CONT. A terminal branchlet from a Purkinje cell (SpB). This branchlet is partially ensheathed by a covering of Bergmann glia (Bg). Note that three dendritic spines emerge from the shaft of this terminal branchlet (asterisks). One, in particular, forms a synaptic contact with a parallel fiber varicosity (black arrow). X 15,682.

Inset - Golgi-Cox. Note that the dendritic spines form a profuse covering over the surface of the terminal branchlet and most commonly appear clavate in form. X 1,120.

- b,c. W CERB L. Two terminal branchlets. Note that both these branchlets have elongated dendritic spines (Hs). 55d p.o. X 15,682.

Inset - Golgi-Cox. Note the presence of elongated spines within this terminal branchlet field (black arrows). 91d p.o. X 1,120.

- d. W CERB L. Note the lack of a parallel fiber milieu adjacent to this elongated dendritic spine and the hypertrophied glial profile that immediately surrounds it. Notice that this spine receives a synaptic input from a parallel fiber varicosity (Pfv) at approximately its mid-region. 57d p.o. X 16,875.

- e.f. A CERB L. Transverse sections of terminal branchlets from the Purkinje cell dendritic tree. Note the hypertrophied dendritic spines which project from these profiles (asterisks). 57d p.o. X 15,682.

Inset - Golgi-Cox. Note the presence of elongated dendritic spines within this terminal branchlet field (black arrows). 93d p.o. X 1,200.

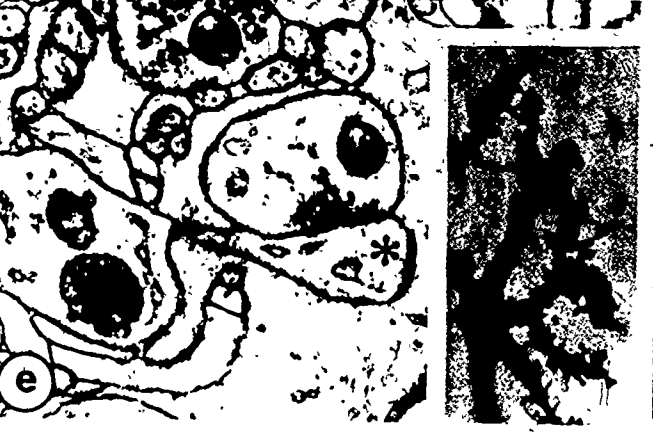
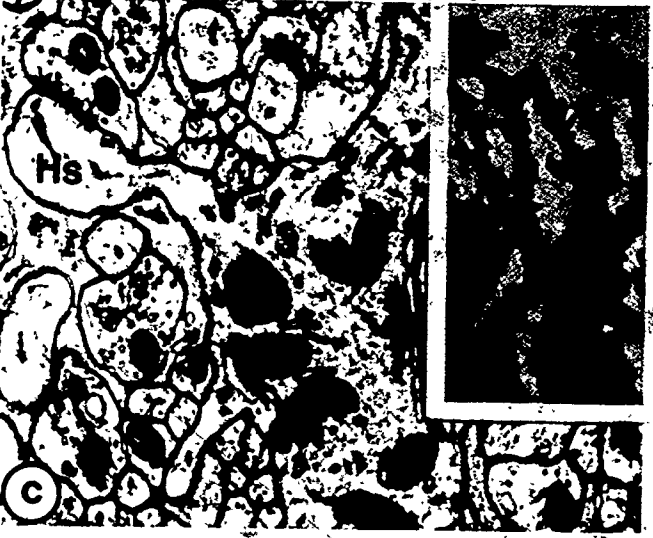




FIGURE 69

A histogram of the length and  
number of Purkinje cell dendritic segments  
in the experimental groups expressed as a  
percentage of the A 3AP.

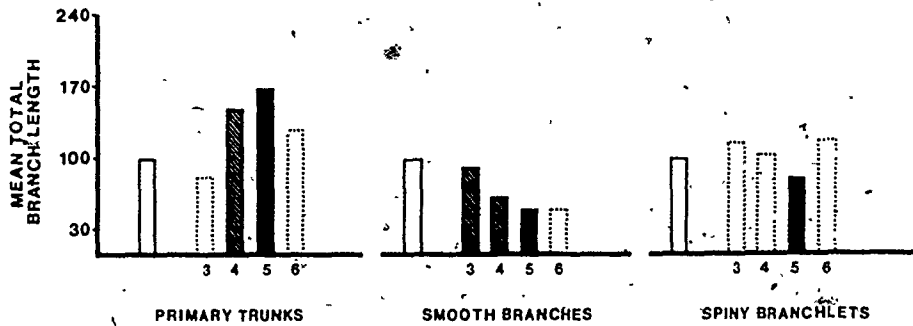
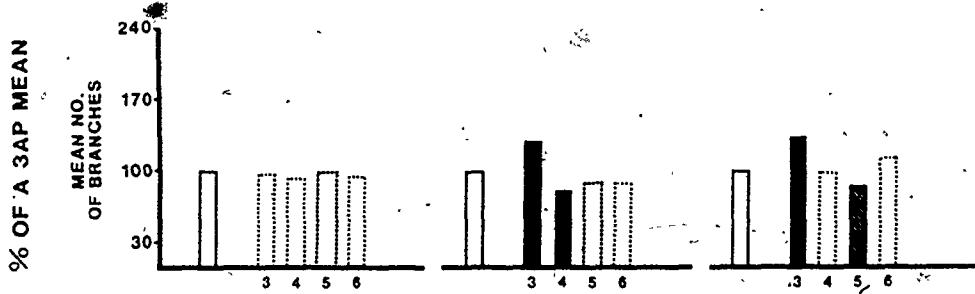
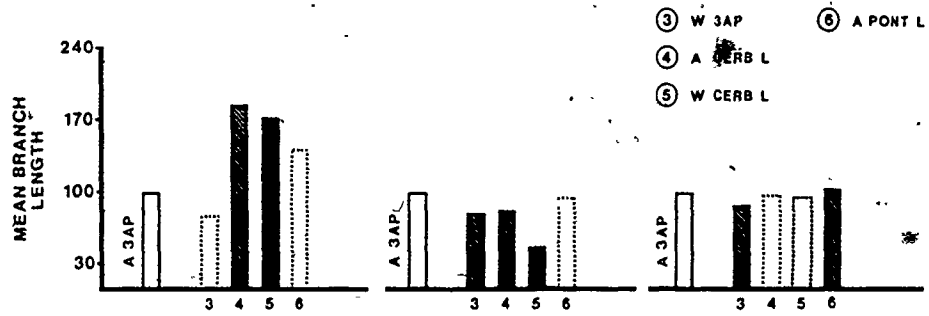


FIGURE 70

A histogram of the length and number of Purkinje cell dendritic segments in the experimental groups expressed as a percentage of the W 3AP.

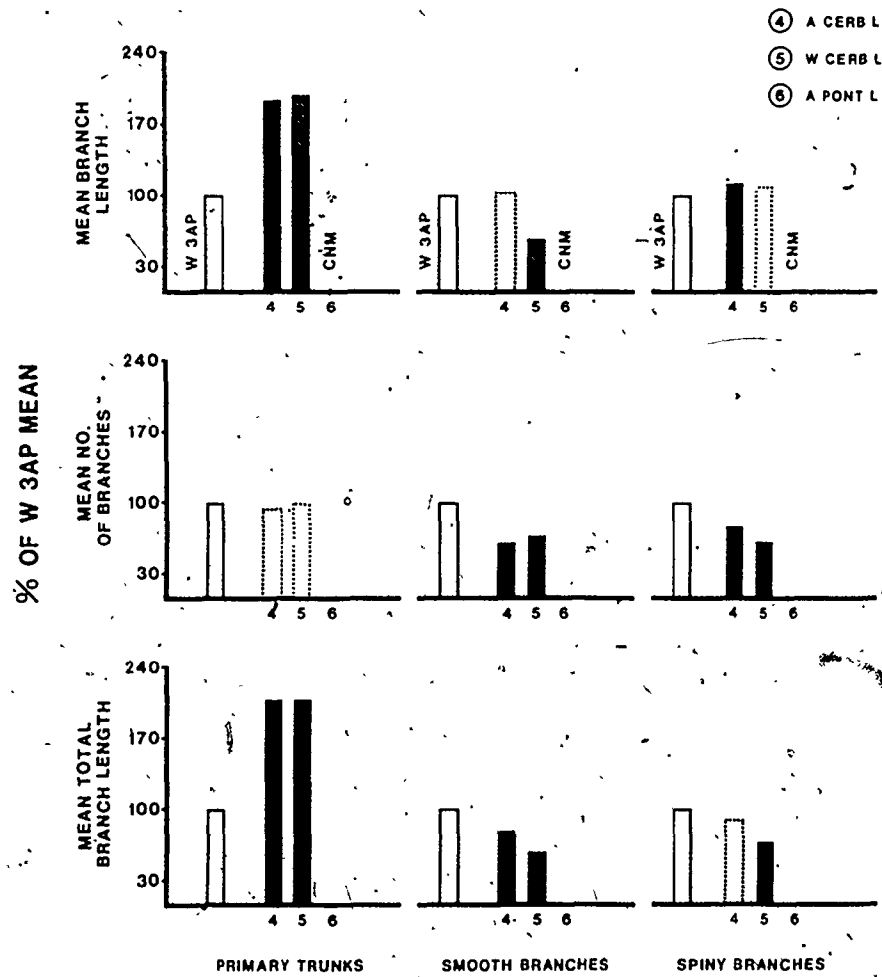


FIGURE 71

A histogram of the length and number of Purkinje cell dendritic segments in the experiment groups expressed as a percentage of the A CERB L.

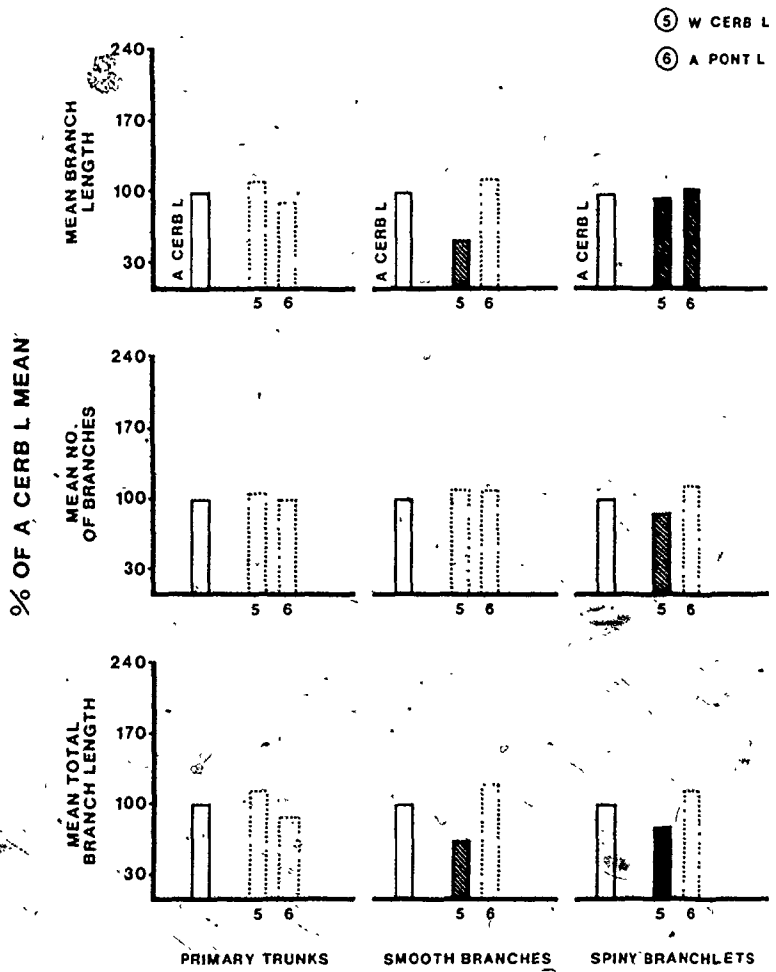
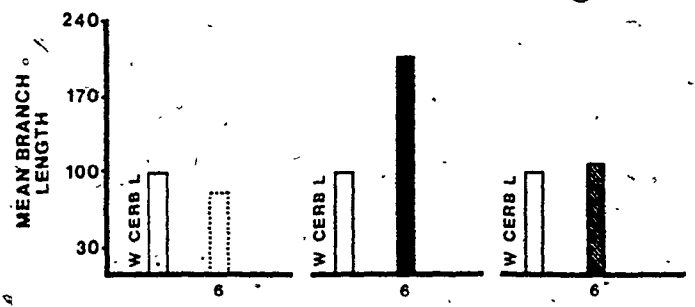


FIGURE 72

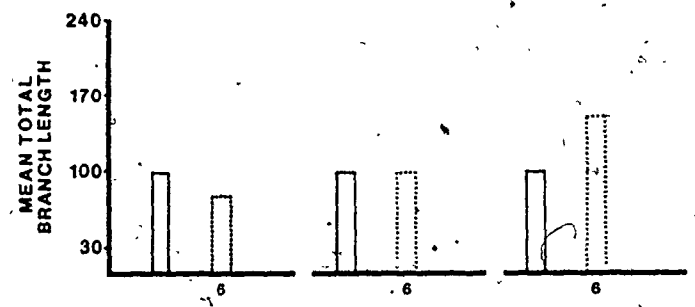
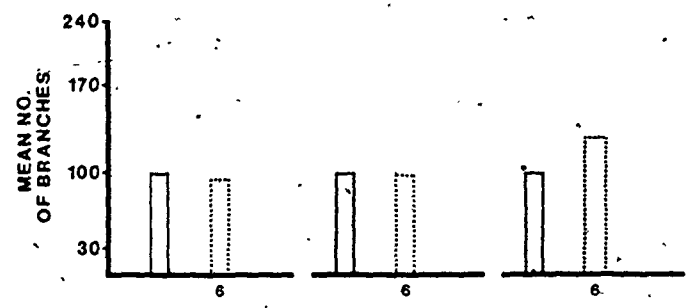
A histogram of the length and  
number of Purkinje cell dendritic segments  
in A PONT L expressed as a percentage of  
the W CERB L.



⑥ A PONT L



% OF W CERB L MEAN



PRIMARY TRUNKS    SMOOTH BRANCHES    SPINY BRANCHLETS



T A B L E S

TABLE 1  
 (2 X 3) FACTORIAL ANOVA  
 Length and number of Purkinje cell dendritic segments in control and experimental groups

Branch type	Group	Mean branch length			Mean no. of branches			Mean total branch length					
		Source of Variation	df	MS	F	Source of Variation	df	MS	F	Source of Variation	df	MS	F
Primary trunks	A CONT	Lesion (A)	2	2,006.66	*7.50	Lesion (A)	2	0.12	0.99	Lesion (A)	2	2,189.89	*7.18
	W CONT	Time (B)	1	273.49	*1.02	Time (B)	1	0.16	1.33	Time (B)	1	152.81	0.50
	A 3AP	(A X B)	2	416.53	1.56	(A X B)	2	0.24	2.09	(A X B)	2	438.20	1.44
	W 3AP	Residual	190	267.38		Residual	190	0.12		Residual	190	305.18	
	A CERB L												
	W CERB L												
Smooth branches	A CONT	Lesion (A)	2	694.34	*5.08	Lesion (A)	2	43.86	**14.01	Lesion (A)	2	27,176.04	*12.24
	W CONT	Time (B)	1	1,043.45	**7.63	Time (B)	1	0.77	0.25	Time (B)	1	13,346.94	**6.01
	A 3AP	(A X B)	2	173.18	1.27	(A X B)	2	18.49	**5.90	(A X B)	2	2,741.86	1.23
	W 3AP	Residual	190	136.73		Residual	190	3.13		Residual	190	2,219.89	
	A CERB L												
	W CERB L												
Spiny branchlets	A CONT	Lesion (A)	2	1.38	0.75	Lesion (A)	2	111,499.57	*38.53	Lesion (A)	2	5,890,000.00	*35.94
	W CONT	Time (B)	1	20.42	*11.03	Time (B)	1	13,626.84	***4.71	Time (B)	1	1,870,000.00	*11.40
	A 3AP	(A X B)	2	2.13	1.15	(A X B)	2	26,468.29	*9.15	(A X B)	2	1,440,000.00	*8.81
	W 3AP	Residual	190	1.85		Residual	190	289.01		Residual	190	164,119.72	
	A CERB L												
	W CERB L												

\*<sup>01</sup> p = .001  
 \*\* p = .01  
 \*\*\* p = .03

TABLE 2  
 (2) ONE WAY ANOVAS  
 Length and number of Purkinje cell dendritic segments in control and experimental groups

Branch type	Group	Mean branch length			Mean total branch length				
		Source of Variation	df	MS	F	Source of Variation	df	MS	F
Primary trunks	A CONT	Among lesion categories	2	922.03	***3.53	Among lesion categories	2	748.84	2.41
	A 3AP	Within lesion categories	114	261.47		Within lesion categories	114	310.05	
	A CERB L	TOTAL	116			TOTAL	116		
	W CONT	Among lesion categories	2	1,370.49	**4.96	Among lesion categories	2	1,658.79	**5.57
	W 3AP	Within lesion categories	76	276.24		Within lesion categories	76	297.88	
	W CERB L	TOTAL	78			TOTAL	78		
Smooth branches	A CONT	Among lesion categories	2	150.06	0.84	Among lesion categories	2	22,521.62	8.72
	A 3AP	Within lesion categories	114	178.78		Within lesion categories	114	2,583.79	
	A CERB L	TOTAL	116			TOTAL	116		
	W CONT	Among lesion categories	2	632.47	*8.59	Among lesion categories	2	9,289.65	**5.55
	W 3AP	Within lesion categories	76	73.65		Within lesion categories	76	1,674.02	
	W CERB L	TOTAL	78			TOTAL	78		

\* p = .001  
 \*\* p = .01  
 \*\*\* p = .05

TABLE 3  
ONE WAY ANOVA

Branch type	Group	Mean branch length			Mean total branch length						
		Source of Variation	df	MS	F	Source of Variation	df	MS	F		
Primary trunks	A CONT	Among lesion categories	6	801.39	**3.06	Among lesion categories	6	0.16	1.42	827.44	**2.78
	A 3AP	Within lesion categories	209	261.93		Within lesion categories	209	0.11		297.90	
	W 3AP	TOTAL	215			TOTAL	215				
	A CERB L										
	W CERB L										
Smooth branches	A CONT	Among lesion categories	6	537.62	*3.91	Among lesion categories	6	23.97	*8.00	12,475.60	*5.76
	A 3AP	Within lesion categories	209	137.35		Within lesion categories	209	2.99		2,165.43	
	W 3AP	TOTAL	215			TOTAL	215				
	A CERB L										
	W CERB L										
Spiny branchlets	A CONT	Among lesion categories	6	4.81	**2.72	Among lesion categories	6	53,193.20	*18.87	2,982,019.72	*18.47
	A 3AP	Within lesion categories	209	1.77		Within lesion categories	209	2,818.36		161,476.71	
	W 3AP	TOTAL	215			TOTAL	215				
	A CERB L										
	W CERB L										

\* P = .001

\*\* P = .01

TABLE 4  
Length and number of Purkinje cell dendritic segments in experimental groups or W CONT compared with the A CONT

Branch type	Group	Mean branch length (um ± S.E.M.)	Percent of A CONT	Confidence Interval <sup>2</sup>	Mean no. of branches (± S.E.M.)	Percent of A CONT	Confidence interval	Mean total branch length (um ± S.E.M.)	Percent of A CONT	Confidence interval	N
Primary trunks	A CONT	41.06 ± 7.20			1.22 ± 0.13			41.83 ± 7.34			27
	W CONT	60.89 ± 10.49	148%		1.05 ± 0.05	86%		60.86 ± 10.49	145%		20
	A 3AP	39.60 ± 6.94	96%		1.09 ± 0.04	89%	84% - 94%	42.54 ± 8.26	102%		43
	W 3AP	30.34 ± 3.71	74%		1.08 ± 0.05	88%		30.80 ± 3.63	74%		26
	A CERB L	**60.80 ± 7.89	145%		**1.04 ± 0.03	85%	80% - 90%	63.68 ± 8.26	152%		47
	W CERB L	**68.43 ± 10.71	167%	83% - 250%	1.09 ± 0.05	89%		72.63 ± 11.26	174%	88% - 295%	33
Smooth branches	A POINT L	55.51 ± 9.37	133%		1.05 ± 0.05	86%	80% - 92%	55.51 ± 9.37	133%		20
	A CONT	59.60 ± 5.00			5.22 ± 0.19			298.97 ± 30.06			27
	W CONT	**54.23 ± 6.09	91%	56% - 126%	**3.40 ± 0.45	83%	63% - 102%	**203.49 ± 33.91	68%	27% - 92%	20
	A 3AP	66.67 ± 5.06	112%		*2.91 ± 0.17	56%	32% - 79%	**207.51 ± 22.31	69%	36% - 103%	43
	W 3AP	**53.06 ± 3.66	89%		**3.77 ± 0.36	73%	38% - 107%	**190.80 ± 18.20	63%	30% - 97%	26
	A CERB L	54.63 ± 6.80	92%		*2.32 ± 0.26	45%	21% - 68%	*150.46 ± 19.94	51%	17% - 84%	47
Spiny branchlets	W CERB L	*30.20 ± 4.71	51%	19% - 82%	*2.57 ± 0.36	49%	17% - 81%	*108.00 ± 19.11	34%	0.9% - 70%	33
	A POINT L	64.00 ± 7.66	107%		*2.55 ± 0.28	49%	20% - 77%	**108.00 ± 19.11	41%	5% - 77%	20
	A CONT	21.29 ± 0.46			186.18 ± 13.89			3,969.46 ± 323.23			27
	W CONT	**19.00 ± 0.51	89%	80% - 98%	**122.30 ± 17.14	65%	34% - 97%	**2,355.94 ± 342.94	60%	27% - 92%	20
	A 3AP	21.17 ± 0.77	99%		*72.93 ± 5.20	39%	20% - 58%	*1,535.63 ± 121.11	42%	18% - 56%	43
	W 3AP	**18.51 ± 0.69	87%	72% - 102%	*97.77 ± 12.66	53%	27% - 78%	*1,786.94 ± 227.94	45%	20% - 70%	26
Spiny branchlets	A CERB L	21.00 ± 0.49	98%		*72.68 ± 8.03	39%	20% - 58%	*1,592.11 ± 165.08	42%	23% - 61%	47
	W CERB L	20.26 ± 0.83	95%		*61.61 ± 6.16	33%	9% - 57%	*1,205.97 ± 128.14	31%	7% - 54%	33
	A POINT L	21.83 ± 0.63	102%		*83.25 ± 10.15	45%	21% - 68%	*1,815.94 ± 234.77	46%	20% - 71%	20

<sup>1</sup> Number of Purkinje cells measured.  
<sup>2</sup> A statistical interval indicating the range of the experimental group (p = 0.01) stated in percentage values of the A CONT mean.  
\* A statistically significant difference between an experimental group or W CONT and the A CONT group at p = 0.01 (Dunnett test).  
\*\* A significant difference at p = 0.05 (Dunnett test).

TABLE 5  
Length and number of Purkinje cell dendritic segments in experimental groups compared with the W CONT

Branch	Group	Mean branch length ( $\mu\text{m} \pm \text{S.E.M.}$ )	Percent of W CONT	Confidence Interval <sup>2</sup>	Mean no. of branches ( $\pm \text{S.E.M.}$ )	Percent of W CONT	Confidence Interval	Mean total branch length ( $\mu\text{m} \pm \text{S.E.M.}$ )	Percent of W CONT	Confidence Interval	N <sup>1</sup>
Primary trunks	W CONT	60.88 $\pm$ 10.49			1.05 $\pm$ 0.05			60.86 $\pm$ 10.49			20
	A 3AP	39.60 $\pm$ 6.94	65%		1.09 $\pm$ 0.04	104%		42.54 $\pm$ 8.26	70%		43
	W 3AP	30.40 $\pm$ 3.71	49%		1.08 $\pm$ 0.05	103%		30.80 $\pm$ 3.63	51%		26
	A CERB L	60.80 $\pm$ 7.89	99%		1.04 $\pm$ 0.03	99%		63.68 $\pm$ 8.26	105%		47
	W CERB L	68.43 $\pm$ 10.71	112%		1.09 $\pm$ 0.05	104%		72.63 $\pm$ 11.26	119%		33
Smooth branches	A POINT L	55.51 $\pm$ 9.37	91%		1.05 $\pm$ 0.05	100%		55.51 $\pm$ 9.37	91%		20
	W CONT	54.23 $\pm$ 6.09			3.40 $\pm$ 0.45			203.49 $\pm$ 33.91			20
	A 3AP	66.57 $\pm$ 5.06	123%		***2.91 $\pm$ 0.17	86%	52% - 119%	***207.51 $\pm$ 22.31	102%	51% - 153%	43
	W 3AP	53.06 $\pm$ 3.66	98%		3.77 $\pm$ 0.36	111%		190.80 $\pm$ 18.20	94%		26
	A CERB L	54.63 $\pm$ 6.80	101%	18% - 93%	***2.32 $\pm$ 0.26	68%	34% - 102%	***150.46 $\pm$ 19.94	74%	23% - 125%	47
Spiny branchlets	W CERB L	**30.20 $\pm$ 4.71	56%		***2.57 $\pm$ 0.36	76%		**108.00 $\pm$ 19.11	53%		33
	A POINT L	64.00 $\pm$ 7.66	118%		***2.55 $\pm$ 0.28	75%	24% - 116%	***108.00 $\pm$ 19.11	61%	8% - 114%	20
	W CONT	19.00 $\pm$ 0.51			122.30 $\pm$ 17.14			2,355.11 $\pm$ 342.94			20
	A 3AP	21.07 $\pm$ 0.77	111%		*72.93 $\pm$ 5.20	60%	29% - 91%	**1,535.63 $\pm$ 121.71	65%	29% - 101%	43
	W 3AP	18.51 $\pm$ 0.69	97%		97.77 $\pm$ 12.66	80%		1,786.94 $\pm$ 227.94	76%		26
Spiny branchlets	A CERB L	21.00 $\pm$ 0.49	110%		*72.68 $\pm$ 8.03	59%	28% - 90%	1,592.11 $\pm$ 165.08	68%	32% - 103%	47
	W CERB L	20.26 $\pm$ 0.83	106%		*61.61 $\pm$ 6.16	51%	12% - 89%	*1,205.97 $\pm$ 128.14	51%	12% - 90%	33
	A POINT L	21.83 $\pm$ 0.63	115%		83.25 $\pm$ 0.15	68%	31% - 105%	1,815.04 $\pm$ 234.77	77%		20

<sup>1</sup> Number of Purkinje cells measured.

<sup>2</sup> A statistical interval indicating the range of the experimental group (p = 0.01) stated in percentage values of the W CONT mean.

\* A statistically significant difference between an experimental group and the W CONT group at p = 0.01 (Dunnett test).

\*\* A significant difference at p = 0.05 (Dunnett test).

\*\*\* A significant difference at p = 0.10 (Dunnett test).

TABLE 6  
Length and number of Purkinje cell dendritic segments in experimental groups compared with the A 3AP

Branch type	Group	Mean branch length ( $\mu\text{m} \pm \text{S.E.M.}$ )	Percent of A 3AP	Confidence interval <sup>1</sup>	Mean no. of branches ( $\pm \text{S.E.M.}$ )	Percent of A 3AP	Confidence interval	Mean total branch length ( $\mu\text{m} \pm \text{S.E.M.}$ )	Percent A 3AP	Confidence interval	N
Primary trunks	A 3AP	39.60 $\pm$ 6.94			1.09 $\pm$ 0.04			42.54 $\pm$ 8.26			43
	W 3AP	30.34 $\pm$ 3.71	77%	14% - 139%	1.08 $\pm$ 0.05	99%	96% - 169%	30.80 $\pm$ 3.63	72%	8% - 136%	26
	A CERB L	**60.80 $\pm$ 7.89	185%	150% - 220%	1.04 $\pm$ 0.03	95%	96%	**63.68 $\pm$ 8.26	149%	102% - 196%	47
	W CERB L	*68.43 $\pm$ 10.71	172%	121% - 223%	1.09 $\pm$ 0.05	100%	96%	*72.63 $\pm$ 11.26	169%	120% - 218%	33
Smooth branches	A PONT L	55.51 $\pm$ 9.37	139%	81% - 297%	1.05 $\pm$ 0.05	96%	96%	55.51 $\pm$ 9.37	125%	67% - 191%	20
	A 3AP	66.57 $\pm$ 5.06			2.91 $\pm$ 0.17			207.51 $\pm$ 22.31			43
	W 3AP	**53.06 $\pm$ 3.66	80%	51% - 108%	*3.77 $\pm$ 0.36	130%	96% - 169%	**190.80 $\pm$ 18.20	92%	35% - 90%	26
	W CERB L	**54.63 $\pm$ 6.80	82%	48% - 116%	*2.32 $\pm$ 0.26	80%	96%	**150.46 $\pm$ 19.94	63%	13% - 91%	47
Spiny branchlets	W CERB L	*30.20 $\pm$ 4.71	46%	17% - 74%	2.57 $\pm$ 0.36	88%	96%	*108.00 $\pm$ 19.11	52%		33
	A PONT L	64.00 $\pm$ 7.66	95%		2.55 $\pm$ 0.28	88%	96%	108.00 $\pm$ 19.11	52%		20
	A 3AP	21.17 $\pm$ 0.77			72.93 $\pm$ 5.20			1,535.63 $\pm$ 121.11			43
	W 3AP	**18.51 $\pm$ 0.69	87%	70% - 104%	*97.77 $\pm$ 12.66	33%	101% - 165%	1,786.94 $\pm$ 227.94	116%		26
Spiny branchlets	A CERB L	21.00 $\pm$ 0.49	92%		72.68 $\pm$ 8.03	99%		1,592.11 $\pm$ 165.08	104%		47
	W CERB L	20.26 $\pm$ 0.83	96%		**61.61 $\pm$ 6.16	85%		*1,205.97 $\pm$ 120.14	78%		33
	A PONT L	**21.83 $\pm$ 0.63	103%		83.25 $\pm$ 10.15	114%		1,815.94 $\pm$ 234.77	118%		20
	A 3AP										

1 Number of Purkinje cells measured.  
 2 A statistical interval indicating the range of the experimental group (0.01) stated in percentage values of the A 3AP mean.  
 \* A statistically significant difference between an experimental group and the A 3AP group at  $p = 0.01$  (Newman-Keuls test).  
 \*\* A significant difference at  $p = 0.05$  (Newman-Keuls test).

TABLE 7  
Length and number of Purkinje cell dendritic segments in experimental groups compared with the W 3AP

Branch type	Group	Mean branch length ( $\mu\text{m} \pm \text{S.E.M.}$ )	Percent of W 3AP	Confidence interval <sup>2</sup>	Mean no. of branches ( $\pm \text{S.E.M.}$ )	Percent of W 3AP	Confidence interval <sup>2</sup>	Mean total branch length ( $\mu\text{m} \pm \text{S.E.M.}$ )	Percent of W 3AP	Confidence interval	N <sup>1</sup>
Primary trunks	W 3AP	30.34 $\pm$ 3.71			1.08 $\pm$ 0.05			30.80 $\pm$ 3.63			26
	A CERB L	*60.80 $\pm$ 7.89	196%	152% - 248%	1.04 $\pm$ 0.03	96%		*63.68 $\pm$ 8.26	208%	162% - 256%	47
	W CERB L	**68.43 $\pm$ 10.71	200%	159% - 249%	1.09 $\pm$ 0.05	101%		**72.63 $\pm$ 11.26	208%	165% - 251%	33
Smooth branches	W 3AP	53.06 $\pm$ 3.66			3.77 $\pm$ 0.36			190.18 $\pm$ 18.20			26
	A CERB L	*54.63 $\pm$ 6.80	103%	26% - 88%	*2.32 $\pm$ 0.26	61%	35% - 87%	*150.80 $\pm$ 19.94	79%	37% - 121%	47
	W CERB L	**30.20 $\pm$ 4.71	57%		*2.57 $\pm$ 0.36	68%	42% - 94%	**108.00 $\pm$ 19.11	57%	19% - 94%	33
Spiny branchlets	W 3AP	18.51 $\pm$ 0.69			97.77 $\pm$ 12.66			1,786.94 $\pm$ 227.94			26
	A CERB L	*21.00 $\pm$ 0.49	113%	101% - 125%	*72.68 $\pm$ 8.03	75%	43% - 106%	1,592.11 $\pm$ 165.08	89%		47
	W CERB L	20.26 $\pm$ 0.83	110%	93% - 126%	*61.61 $\pm$ 6.16	63%	27% - 99%	*1,205.97 $\pm$ 128.14	67%		33

<sup>1</sup> Number of Purkinje cells measured.  
<sup>2</sup> A statistical interval indicating the range of the experimental group (p = 0.01) stated in percentage values of the W 3AP mean.  
\* A statistically significant difference between an experimental group and the W 3AP group at p = 0.01 (Newman-Keuls test).  
\*\* A significant difference at p = 0.05 (Newman-Keuls test).



TABLE 8

Length and number of Purkinje cell dendritic segments in experimental groups compared with the A CERB L

Branch type	Group	Mean branch length ( $\mu\text{m} \pm \text{S.E.M.}$ )	Percent of A CERB L	Confidence interval <sup>2</sup>	Mean no. of branches ( $\pm \text{S.E.M.}$ )	Percent of A CERB L	Confidence interval	Mean total branch length ( $\mu\text{m} \pm \text{S.E.M.}$ )	Percent of A CERB L	Confidence interval	N <sup>1</sup>
Primary trunks	A CERB L	60.80 $\pm$ 7.89			1.04 $\pm$ 0.03			63.68 $\pm$ 8.26			47
	W CERB L	68.43 $\pm$ 10.71	112%		1.09 $\pm$ 0.05	105%		72.63 $\pm$ 11.26	114%	64% - 164%	33
	A PONT L	55.51 $\pm$ 9.37	91%		1.05 $\pm$ 0.05	101%		55.51 $\pm$ 9.37	87%		20
Smooth branches	A CERB L	54.63 $\pm$ 6.80			2.32 $\pm$ 0.26			150.46 $\pm$ 19.94			47
	W CERB L	**30:20 $\pm$ 4.71	55%	12% - 99%	2.57 $\pm$ 0.36	111%		**108.00 $\pm$ 19.11	72%	21% - 122%	33
	A PONT L	64.00 $\pm$ 7.66	117%		2.55 $\pm$ 0.28	110%		108.00 $\pm$ 19.11	120%	69% - 171%	20
Spiny branchlets	A CERB L	21.00 $\pm$ 0.49			72.68 $\pm$ 8.03			1,592.11 $\pm$ 165.08			47
	W CERB L	**20.26 $\pm$ 0.83	104%	91% - 117%	**61.16 $\pm$ 6.16	85%	49% - 120%	*1,205.97 $\pm$ 128.14	76%		33
	A PONT L	**21.83 $\pm$ 0.63	104%		83.25 $\pm$ 10.15	114%		*1,815.94 $\pm$ 234.77	114%		20

<sup>1</sup> Number of Purkinje cells measured.<sup>2</sup> A statistical interval indicating the range of the experimental group ( $p = 0.01$ ) stated in percentage values of the A CERB L mean.\* A statistically significant difference between an experimental group and the A CERB L group at  $p = 0.01$  (Newman-Keuls test).\*\* A significant difference at  $p = 0.05$  (Newman-Keuls test).

TABLE 9  
Length and number of Purkinje cell dendritic segments in A PONT L compared with the W CERB L

Branch type	Group #	Mean branch length ( $\mu\text{m} \pm \text{S.E.M.}$ )	Percent of W CERB L	Confidence interval <sup>2</sup>	Mean no. of branches ( $\pm \text{S.E.M.}$ )	Percent of W CERB L	Confidence interval	Mean total branch length ( $\mu\text{m} \pm \text{S.E.M.}$ )	Percent of W CERB L	Confidence interval	N <sup>1</sup>
Primary trunks	W CERB L	68.43 $\pm$ 10.91			1.09 $\pm$ 0.05			72.63 $\pm$ 11.26			33
	A PONT L	55.51 $\pm$ 9.37	81%		1.05 $\pm$ 0.05	96%		55.51 $\pm$ 9.37	76%	16% - 136%	20
Smooth branches	W CERB L	30.20 $\pm$ 4.71			2.57 $\pm$ 0.35			108.00 $\pm$ 19.11			33
	A PONT L	*64.00 $\pm$ 7.66	212%	177% - 247%	2.55 $\pm$ 0.28	99%		108.00 $\pm$ 19.11	100%	54% - 146%	20
Spiny branchlets	W CERB L	20.26 $\pm$ 0.83			61.61 $\pm$ 6.16			1,205.97 $\pm$ 128.14			33
	A PONT L	**21.83 $\pm$ 0.63	108%		83.25 $\pm$ 10.15	135%	99% - 171%	1,815.94 $\pm$ 234.77	151%		20

<sup>1</sup> Number of Purkinje cells measured.

<sup>2</sup> A statistical interval indicating the range of the experimental group (A PONT L) ( $p = 0.01$ ) stated in percentage values of the W CERB L mean.

\* A statistically significant difference between the experimental group and the W CERB L group at  $p = 0.01$  (Newman-Keuls test).

\*\* A significant difference at  $p = 0.05$  (Newman-Keuls test)

TABLE 10

Length of dendritic appendages along the Purkinje cell dendritic tree of W 3AP compared with the A CONT

GROUP	TYPE	LOCATION	d.f.	F
A CONT	Thorn	Smooth portion of the Pcdt	1	0.758
W 3AP	All	Smooth portion of the Pcdt	32	
A CONT	Thorn	Smooth portion of the Pcdt	1	0.076
W 3AP	Thorn-like	Smooth portion of the Pcdt	23	
A CONT	Thorn	Smooth portion of the Pcdt	1	**5.88
W 3AP	Spine-like	Smooth portion of the Pcdt	17	
A CONT	Spine	Terminal branchlet	1	3.82
W 3AP	Spine-like	Smooth portion of the Pcdt	77	

\*\*p=0.05 (F-statistic for two population means; Ambrose and Donner, 1973)

Pcdt, Purkinje cell dendritic tree

TABLE 11

Length of dendritic appendages along the Purkinje cell dendritic tree of W 3AP compared with the A CONT.

GROUP	TYPE	LOCATION	MEAN LENGTH ( $\mu$ m)	PERCENT OF A CONT	N <sup>1</sup>
A CONT	Thorn	Smooth portion	0.67 0.97		10
	All	Smooth portion of the Pcdt	0.74 0.046	110%	24
W 3AP	Thorn-like	Smooth portion of the Pcdt	0.64 0.064	95%	15
	Spine-like	Smooth portion of the Pcdt	**0.90 0.026	134%	9
A CONT	Spine	Terminal branchlet	1.04 0.026		70
W 3AP	Spine-like	Smooth portion of the Pcdt	0.90 0.026	115%	9

N<sup>1</sup> Number of dendritic appendages measured

\*\* A significant difference between the W 3AP and the A CONT group at  $p=0.05$  (F-statistic for two population means; Ambrose and Donner, 1973)

Pcdt, Purkinje cell dendritic tree

TABLE 12

Length of spines along the Purkinje cell terminal branchlets of  
A and W CERB L compared with the A CONT.

Group	d.f.	F
A CONT	1	* 22.89
W CERB L	120	
A CONT	1	* 24.60
A CERB L	103	
W CERB L	1	2.44
A CERB L	67	

\*  $p = .01$  (F - statistic for two population means;  
Ambrose and Donner, 1973)

TABLE 13

Length of spines along the Purkinje cell terminal branchlets  
of A and W CERB L compared with the A CONT.

Group	Mean Length ( m S.E.M.)	Percent of A CONT	N <sup>1</sup>
A CONT	1.04 0.026		70
W CERB L	*1.25 0.033	120%	34
A CERB L	*1.40 0.089	135%	35
W CERB L	1.25 0.033		34
A CERB L	1.40 0.089	112%	35

N<sup>1</sup> Number of spines measured

\* A significant difference between the experimental group  
and the A CONT group at  $p = 0.01$  (F-statistic for two  
population means; Ambrose and Donner, 1973)

APPENDICES

## ABBREVIATION AND SYMBOLS

## Dependent variables measured

MLPT	mean length of primary trunks
MLSB	mean length of smooth branches
MLSpB	mean length of spiny branchlets
MNPT	mean number of primary trunks
MNSB	mean number of smooth branches
MNSpB	mean number of spiny branchlets
TLPT	total length of primary trunks
TLSB	total length of smooth branches
TLSpB	total length of spiny branchlets
A CONT	untreated adult rat 150 days old
W CONT	untreated weanling rat 21 days old
A 3AP	an adult rat which has been treated with 3-acetylpyridine (3AP) on the 57th day and allowed to survive until reaching the approximate age of the A CONT
W 3AP	a weanling rat which has been treated with 3AP on the 21st day and permitted to survive until reaching the approximate age of the A CONT
A CERB.L	an adult rat which has received a unilateral cerebellar lesion (parasagittal transection of the lateral cerebellar cortex) on the 57th day and allowed to survive until reaching the approximate age of the A CONT
W CERB L	a weanling rat which has received a unilateral cerebellar lesion on the 21st day and permitted to survive until reaching the approximate age of the A CONT
A PONT	an adult rat which has received a contralateral pontine ablation on the 57th day and allowed to survive until reaching the approximate age of the A CONT



- ① the actual value of the dependent variable for the A CONT
- ② the actual value of the dependent variable for the W CONT
- ③ the actual value of the dependent variable for the A 3AP
- ④ the actual value of the dependent variable for the W 3AP
- ⑤ the actual value of the dependent variable for the A CERB L
- ⑥ the actual value of the dependent variable for the W CERB L

AR adult rat

A<sub>V</sub> variable A (lesion type)

B<sub>V</sub> variable B (time of the lesion)

GM grand mean

WR weanling rat

\* indicates a significant variable

open circles indicate the ideal value for each control or experimental group if no interaction exists between the two variables A (lesion) and B (time of the lesion)

solid squares indicate the actual value of the dependent variable for each of the adult groups

solid circles indicate the actual value of the dependent variable for each of the weanling groups

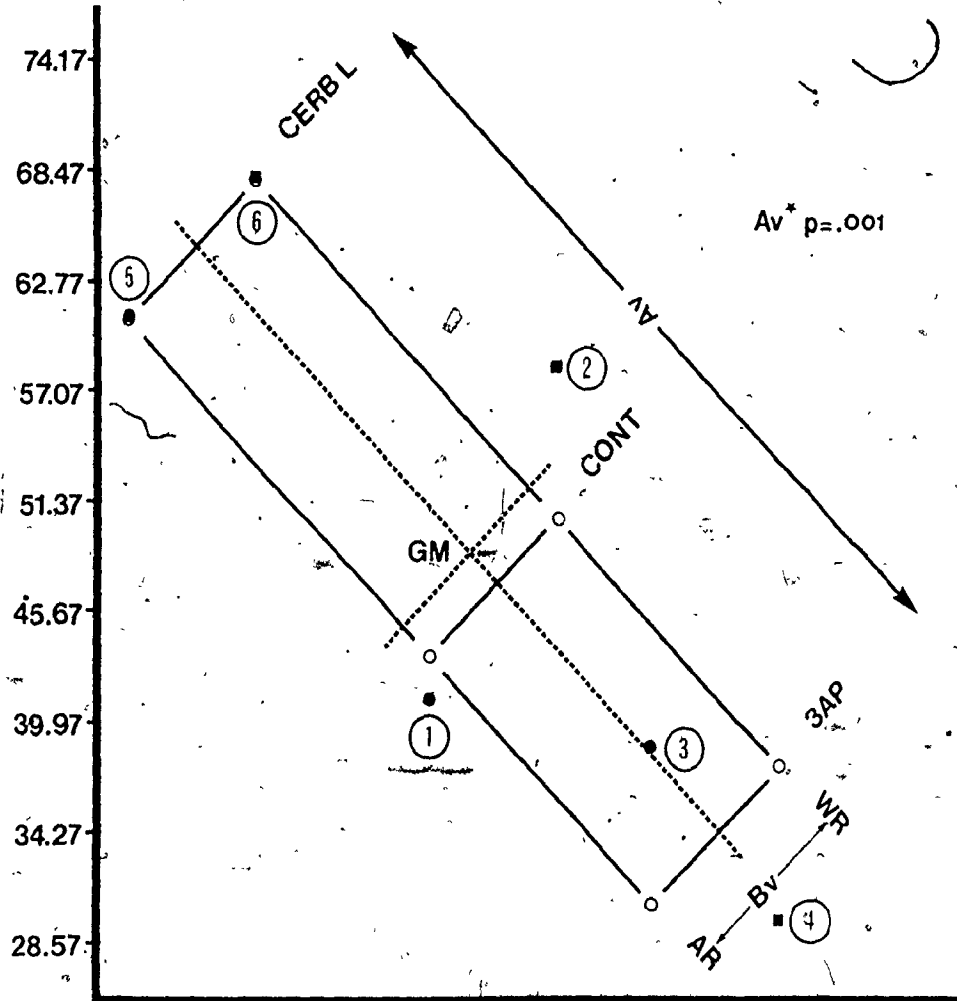
APPENDIX I

A tilted data graph of a 2x3 factorial analysis of variance for the dependent variable MLPT.

		Variable A			MEAN
		NL	3AP	CERB L	
Variable B	AR	41.06	39.60	60.80	47.15
	WR	60.89	30.34	68.43	53.22
	MEAN	50.97	34.97	64.61	

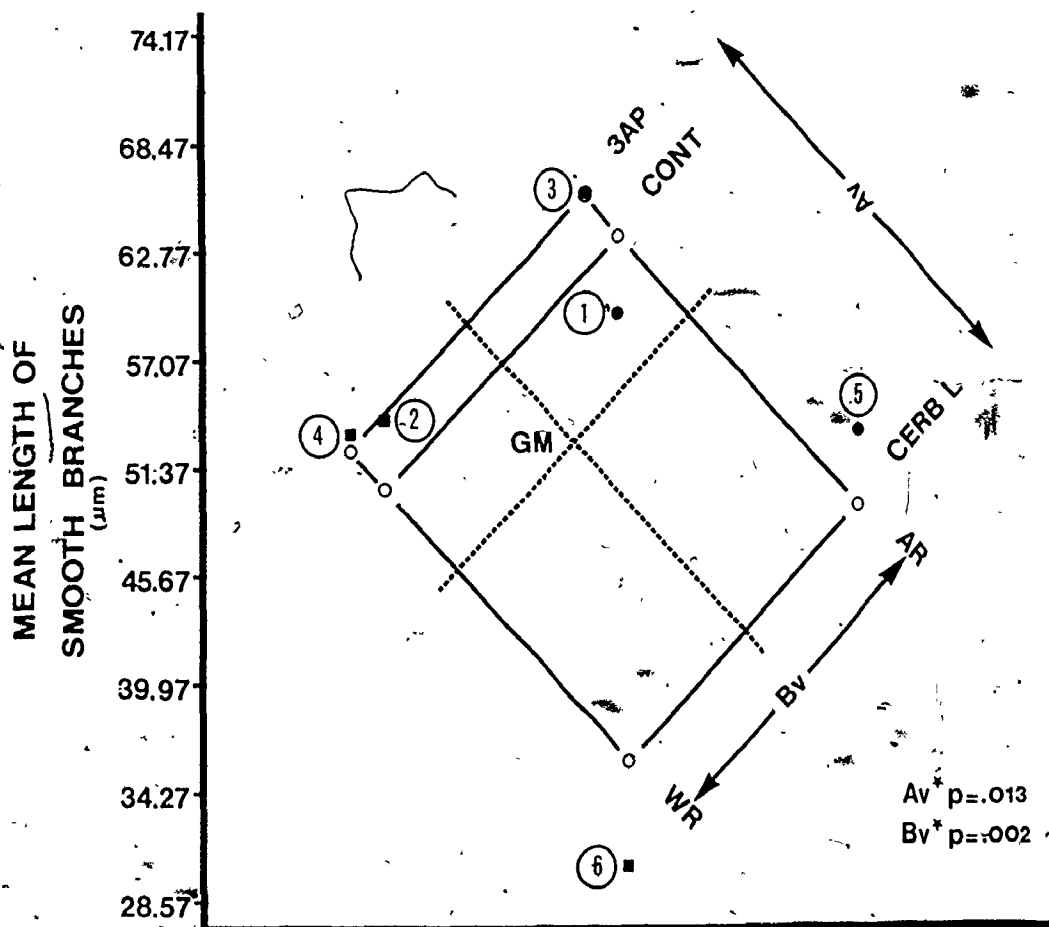
The tilted data graph is a visual representation of a two-way analysis of variance. The vertical scale signifies the range of responses for the dependent variable. The grand mean (GM) for each dependent variable is plotted relative to the vertical scale and approximately mid-way along the horizontal axis. The dashed lines are drawn perpendicular to each other and set at a 45° slant through the grand mean. The three means for the different types of lesions (categories of variable A; i.e. columns) are plotted along one dashed axis while the two means for the different times of deafferentation (categories of variable B; i.e. rows) are plotted along the other dashed axis. Through each plotted point a solid line is drawn perpendicular to the appropriate dashed axis. Each solid line is labeled according to the column or row mean which it signifies (3AP, AR, etc.). This produces a 2x3 grid of lines which serves as the core of the graph. The categories of each variable are ranked automatically from lowest to highest and the effect of each variable is represented as a linear measurement. The six points of intersection produced by such a grid system (open circles) indicate the ideal values for each group if the association between variables A and B is a purely additive effect. The solid squares and circles below or above each of the intersection points denote the actual value obtained for each group mean. The distance between the actual mean and its corresponding value for an additive effect is the interaction term. The sum of squares of these values represents the sum of squares for the interaction of variables A and B.

MEAN LENGTH OF  
PRIMARY TRUNKS  
( $\mu\text{m}$ )



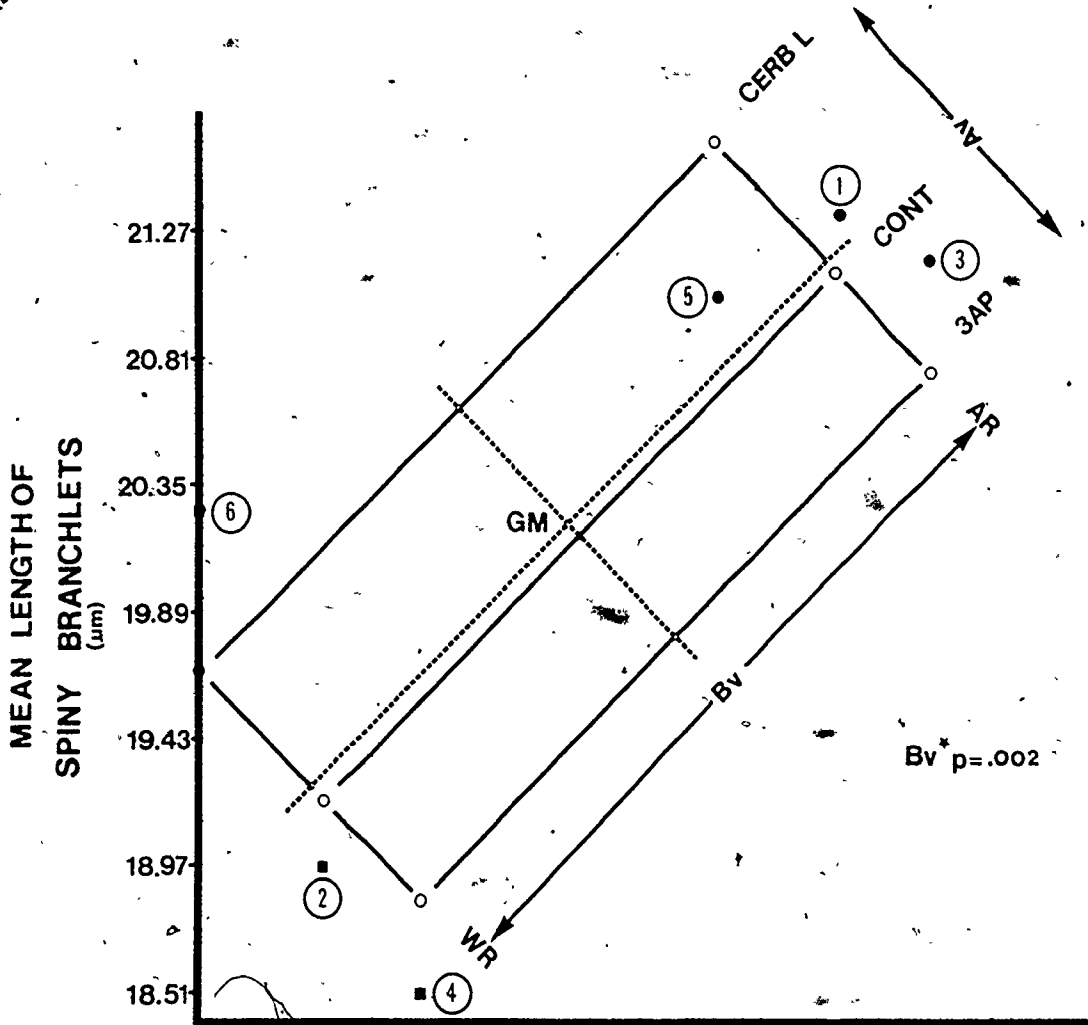
APPENDIX II.

A tilted data graph of a  
2 x 3 factorial analysis of variance  
for the dependent variable MLSB.



APPENDIX III

A tilted data graph of a  
2 x 3 factorial analysis of variance  
for the dependent variable MLSpB.

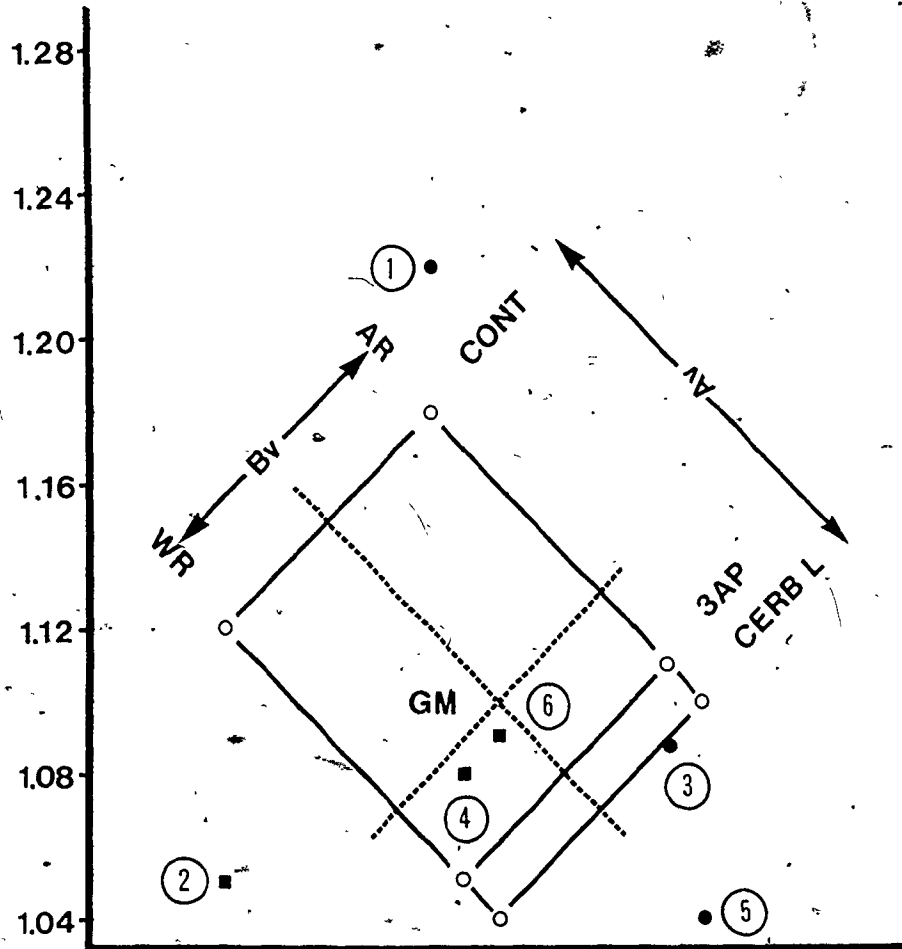


APPENDIX IV

A tilted data graph of a  
2 x 3 factorial analysis of variance  
for the dependent variable MNPT.



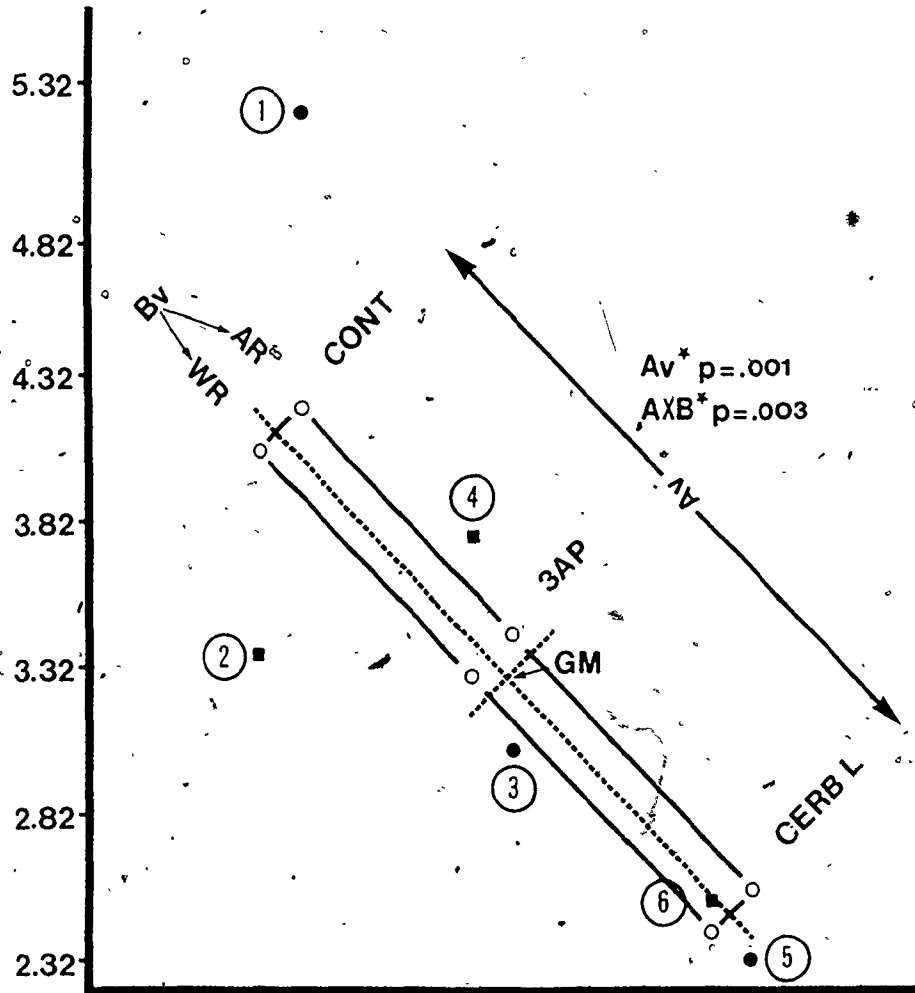
MEAN NO. OF  
PRIMARY TRUNKS



APPENDIX V

A tilted data graph of a  
2 x 3 factorial analysis of variance  
for the dependent variable MNSB.

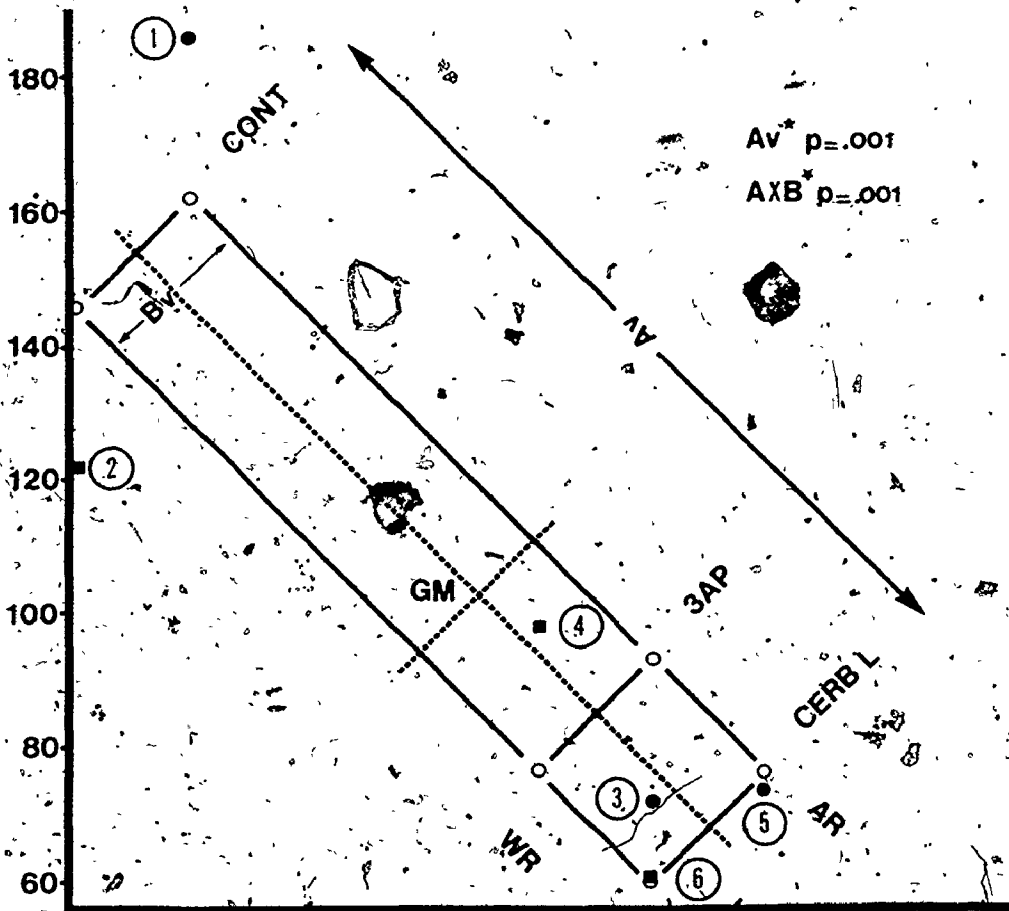
MEAN NO. OF  
SMOOTH BRANCHES



APPENDIX VI

A tilted data graph of a  
2x3 factorial analysis of variance  
for the dependent variable MNSpB.

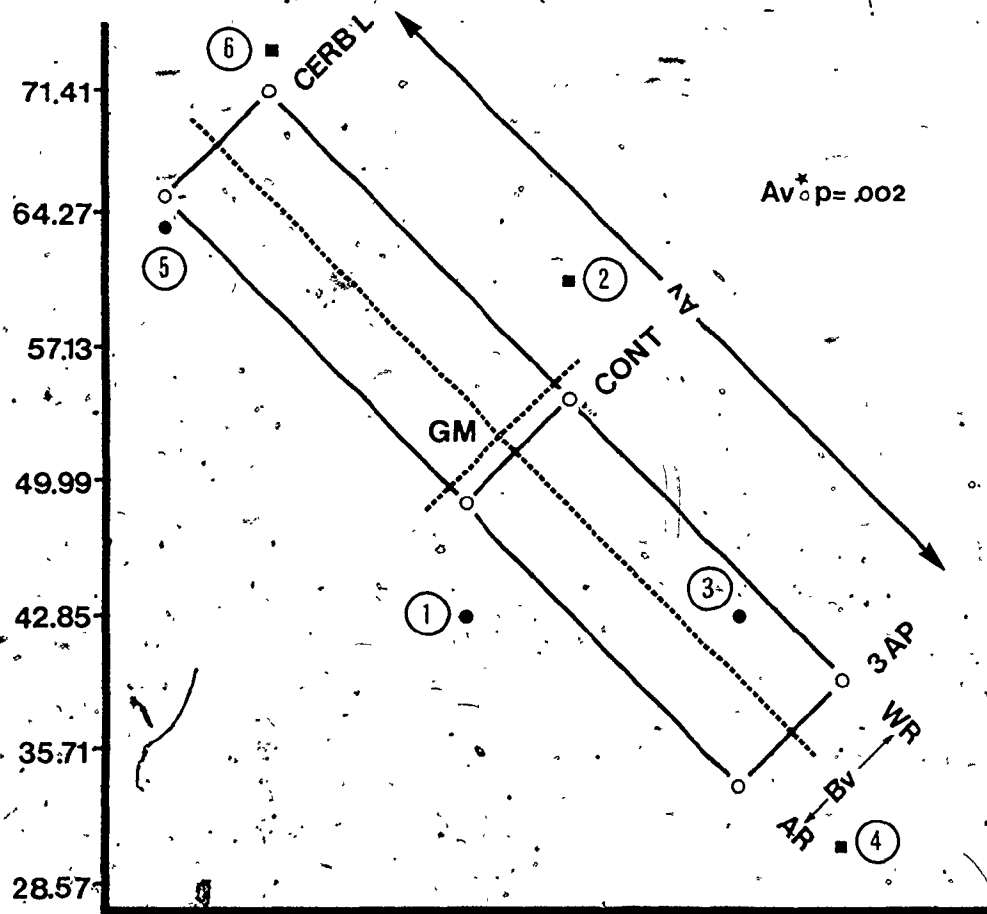
MEAN NO. OF SPINY BRANCHLETS



APPENDIX VII

A tilted data graph of a  
2 x 3 factorial analysis of variance  
for the dependent variable TIPT.

TOTAL LENGTH OF  
PRIMARY TRUNKS  
( $\mu\text{m}$ )

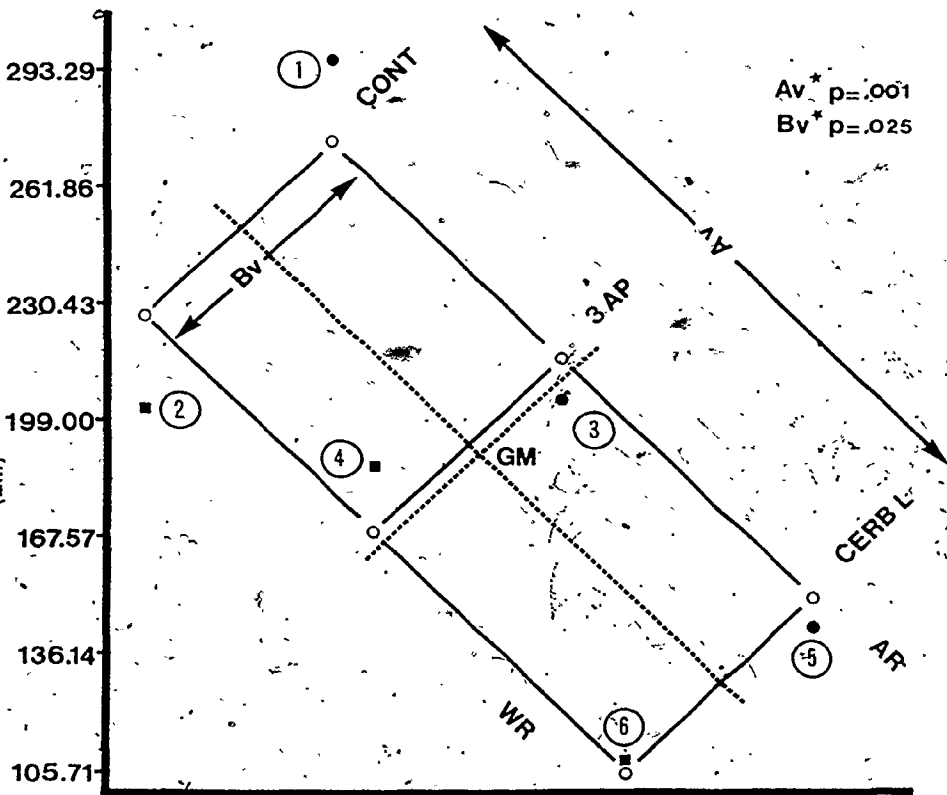


APPENDIX VIII

A tilted data graph of a  
2 x 3 factorial analysis of variance  
for the dependent variable TLSB.

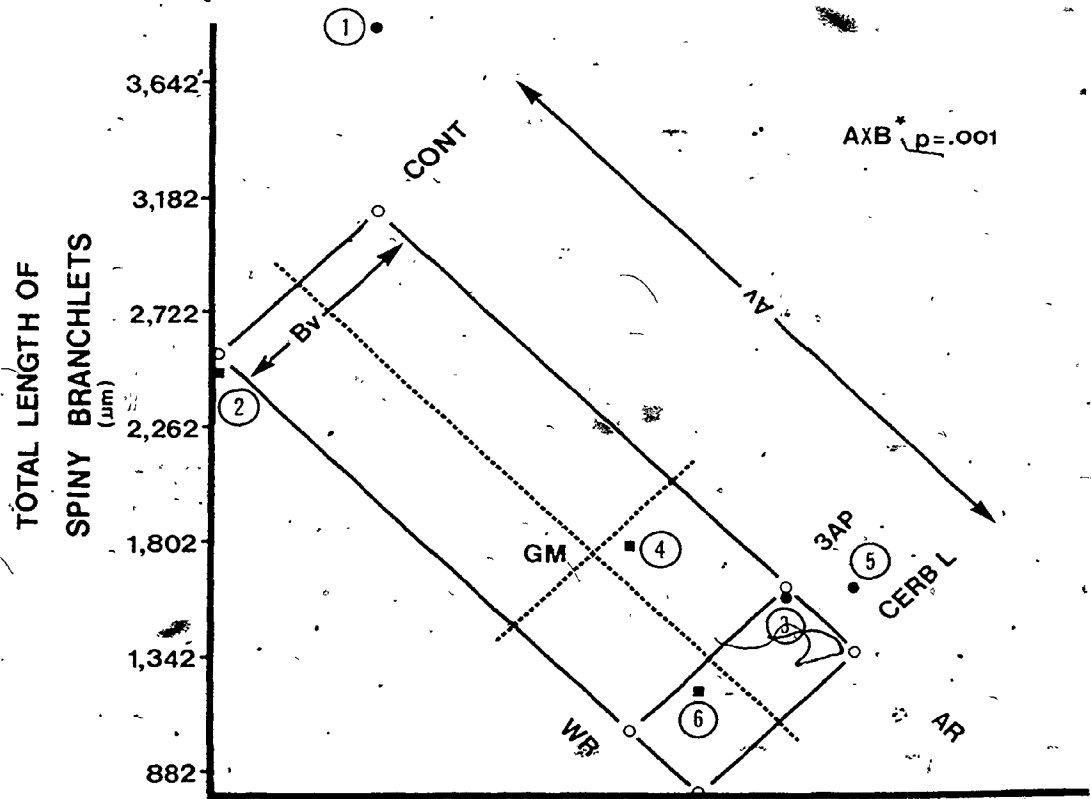


TOTAL LENGTH OF  
SMOOTH BRANCHES  
( $\mu\text{m}$ )



APPENDIX IX

A tilted data graph of a  
2 x 3 factorial analysis of variance  
for the dependent variable TLSpB.



**END**

16.09.82

**FIN**